ABSTRACT

MIXING OF NANOSIZE PARTICLES BY MAGNETICALLY ASSISTED IMPACTION TECHNIQUES

by
James V. Scicolone

Nanoparticles and nanocomposites offer unique properties that arise from their small size, large surface area, and the interactions of phases at their interfaces, and are attractive for their potential to improve performance of drugs, biomaterials, catalysts and other high-value-added materials. However, a major problem in utilizing nanoparticles is that they often lose their high surface area due to grain growth. Creating nanostructured composites where two or more nanosized constituents are intimately mixed can prevent this loss in surface area, but in order to obtain homogeneous mixing, de-agglomeration of the individual nanoparticle constituents is necessary.

Due to high surface area, nano-particles form very large, fractal agglomerates. The structure of these agglomerates can have a large agglomerate composed of sub-agglomerates (SA), which itself consists of primary agglomerates (PA), that contain chain or net like nano-particle structures; typically sub-micron size. Thus the final agglomerate has a hierarchical, fractal structure, and depending upon the forces applied, it could break down to a certain size scale. The agglomerates can be fairly porous and fragile or they could be quite dense, based on primary particle size and its surface energy. Thus depending upon the agglomerate strength at different length scales, one could achieve deagglomeration and subsequent mixing at varying length scale. A better understanding of this can have a major impact on the field of nano-structured materials;

thus the long term objective of this project is to gain fundamental understanding of deagglomeration and mixing of nano-agglomerates.

Dry mixing is in general not effective in achieving desired mixing at nanoscale, whereas wet mixing suffers from different disadvantages like nanomaterial of interest should be insoluble, has to wet the liquid, and involves additional steps of filtration and drying. This research examines the use of environmentally friendly a novel approach based on use of small magnetic particles as mixing media is introduced that achieves a high-degree of mixing at scales of about a micron. The method is tested for binary mixture of alumina/silica and silica/titania. Various parameters such as processing time, size of the magnets, and magnetic particle to powder mixed ratio are considered. Experiments are carried out in batch containers in liquid and dry mediums, as well as a fluidized bed set-up.

Homogeneity of Mixing (HoM), defined as the compliment of the Intensity of Segregation, was evaluated at the micron scale through field-emission scanning electron microscopy (FESEM) and the energy dispersive x-ray spectroscopy (EDS). Secondary electron images, along with elemental mappings, were used to visualize the change in agglomerate sizes. Compositional percent data of each element were obtained through an EDS spatial distribution point analysis and used to obtain quantitative analysis on the homogeneity of the mixture. The effect of magnet impaction on mixing quality was examined on the HoM of binary mixtures. The research shows that HoM improved with magnetically assisted impaction mixing techniques indicating that the HoM depends on the product of processing time with the number of magnets. In a fluidized bed set-up, MAIM not only improved dispersion, but it was also found that the magnetic particles

served to break down the larger agglomerates, to reduce the minimum fluidization velocity, to delay the onset of bubbling, and to convert the fluidization behavior of ABF powder to APF. Thus MAIM techniques may be used to achieve mixing of nano-powders at a desired HoM through adjusting the number of magnets and processing time; and its inherent advantages are its simplicity, an environmentally benign operation, and reduced cost as compared with wet mixing techniques.

MIXING OF NANOSIZE PARTICLES BY MAGNETICALLY ASSISTED IMPACTION TECHNIQUES

by
James V. Scicolone

A Dissertation
Submitted to the Faculty of
New Jersey Institute of Technology
in Partial Fulfillment of the Requirements for the Degree of
Doctor of Philosophy in Materials Science and Engineering

Interdisciplinary Program in Materials Science and Engineering

January 2011

APPROVAL PAGE

MIXING OF NANOSIZE PARTICLES BY MAGNETICALLY ASSISTED IMPACTION TECHNIQUES

James V. Scicolone

Dr. Rajesh N. Dave, Dissertation Advisor — Date
Distinguished Professor of Chemical Engineering, NJIT

Dr. Zafar Iqbal, Committee Member — Date
Research Professor of Chemistry and Environmental Science, NJIT

Dr. Kwabena Narh, Committee Member — Date
Professor of Mechanical Engineering, NJIT

Dr. Somenath Mitra, Committee Member — Date
Professor of Chemistry and Environmental Science, NJIT

Dr. Ecevit Bilgili, Committee Member — Date
Assistant Professor of Chemical Engineering, NJIT

BIOGRAPHICAL SKETCH

Author: James Vincent Scicolone

Degree: Doctor of Philosophy

Date: January 2011

Undergraduate and Graduate Education:

- Doctor of Philosophy in Materials Science and Engineering
  New Jersey Institute of Technology, Newark, NJ, USA, 2011
- Masters of Science in Chemical Engineering,
  New Jersey Institute of Technology, Newark, NJ, USA, 2008
- Bachelor of Science in Chemical Engineering,
  Penn State University, University Park, Pennsylvania, USA, 2005

Major: Materials Science and Engineering

Publications:

James V. Scicolone, Daniel Lepek, Rajesh Davé. Mixing of Nanosized Particles by Magnetically Assisted Fluidization. Powder Technology. In preparation.

James V. Scicolone, Sankaran Sundaresan, Rajesh Davé. Controlling the Homogeneity of Mixing of Nano-particle Blends using Magnetically Assisted Impaction Mixing Process. Journal of Nanoparticle Research. In preparation.

James V. Scicolone, Ajit Mujumdar, Sankaran Sundaresan, Rajesh Davé. Environmentally Benign Dry Mechanical Mixing of Nano-particles using Magnetically Assisted Impaction Mixing Process. Powder Technology. Submitted August 31, 2010.

Ganesh P. Sanganwar, Alexandre Ermoline, James V. Scicolone, Rajesh N. Dave, and Ram B. Gupta., Environmentally Benign Nano-mixing by Sonication in Supercritical CO_2. Journal of Nanoparticle Research, 2009; 11, 405-419.

James V. Scicolone, Peter K. Davis, Ron P. Danner, J. Larry Duda. Solubility and Diffusivity of Solvents by Packed Column Inverse Gas Chromatography. Polymer, 2006; 47, 5364-5370.

Conference Presentations and Poster Sessions:

James V. Scicolone, Ajit Mujumdar, Rajesh Dave, "Magnetically Assisted Mixing Of Nanosized Particles," Graduate Student Poster Competition, ISPE Annual Meeting, San Diego, CA, November 9-10, 2009.

James V. Scicolone, Ajit Mujumdar, Rajesh Dave, "Magnetically Assisted Mixing Of Nanosized Particles," Student Poster Presentation, NSF CMMI Research and Innovation Conference 2009, Honolulu, HI June 22, 2009.

James V. Scicolone, Ajit Mujumdar, Rajesh Dave, "Magnetically Assisted Mixing Of Nanosized Particles," Poster Presentation, ISPE Poster Competition, NJIT, Newark, NJ April 28, 2009.

James V. Scicolone, Ajit Mujumdar, Rajesh Dave, "Magnetically Assisted Mixing Of Nanosized Particles," Poster Presentation, Annual Provost's Student Research Showcase, NJIT, Newark, NJ April 8, 2009.

James V. Scicolone, Ajit Mujumdar, Rajesh Dave, "Comparing Mixing Quality of Nanosized Particles by Environmentally Benign Mixing Techinques," Poster Presentation, AIChE Annual Meeting, Philadelphia, PA, November 17-21, 2008.

James V. Scicolone, Ajit Mujumdar, Rajesh Dave, "Mixing Of Nanosized Particles By Magnetically Assisted Impact Mixing Technique in Dry and Liquid Mediums," AIChE Annual Meeting, Philadelphia, PA, November 17-21, 2008.

James V. Scicolone, Ajit Mujumdar, Rajesh Dave, "Fluidized Bed Mixing Of Nanosized Particles" AIChE Annual Meeting, Philadelphia, PA, November 17-21, 2008.

R. N. Dave, G. Sanganwar, J. V. Scicolone, A. Ermoline, R. B. Gupta, "Nano-mixing by sonication in supercritical and high pressure carbon dioxide," 11th European Meeting on Supercritical Fluids, Barcelona, Spain, pp 1-6, CD-Rom proceedings, May 4-7, 2008.

James V. Scicolone, Rajesh Dave, "Mixing Of Nanosized Particles By Magnetically Assisted Impact Mixing," Poster Presentation, ISPE Poster Compittion, Rutgers University, New Brunswick, NJ April 24, 2008.

James V. Scicolone, Alexandre Ermoline, Ryan Barrow, Rajesh Dave, "Mixing Of Nanoparticles By Magnetically Assisted Impact Mixing Technique," AIChE Annual Meeting, Salt Lake City, UT, November 4-9, 2007.

G. Sanganwar, A. Ermoline, J. Scicolone, R. Gupta, R. Dave, “Environmentally Benign Nanomixing by Sonication in Supercritical CO2,” AIChE Annual Meeting, Salt Lake City, UT, November 4-9, 2007.

J. Scicolone, G. Sanganwar, D. To, A. Ermoline, R. N. Dave, R. B. Gupta, R. Pfeffer, “Deagglomeration and Mixing of Nanoparticles”, Proceedings of Partec 2007 Meeting, paper 36218, pp 1-4, Nuremburg, Germany, March 27-29, 2007.

Scicolone, J.V., Davis, P. K., Danner, R. P., Duda, J. L., "Solubility and Diffusivity of Solvents by Packed Column Inverse Gas Chromatography," ACS 36th MARM, Princeton, NJ, June 8-11, 2003.

This thesis is dedicated to my family and their unending devotion

"One of the symptoms of an approaching nervous breakdown
is the belief that one's work is terribly important."
- Bertrand Russell

ACKNOWLEDGMENT

I would like to express my deepest appreciation to Dr. Rajesh Davé, who not only served as my research supervisor, but also introduced me to the particle field. His valuable knowledge and dedication providing valuable insight, and intuition, but also constantly gave me support, encouragement, and reassurance. I have learned much from his commitment for his students and drive for knowledge. Special thanks are given to Dr. Zafar Iqbal, Dr. Somenath Mitra, Dr. Kwabena Narh, and Dr. Ecevit Biligli for actively participating in my committee.

I would also like to acknowledge the financial support Dr. Rajesh Dave provided for me from the National Science Foundation IGERT Award (DMI-0506722). I would also like to acknowledge the financial support Dr. Robert Pfeffer provided for me from the National Science Foundation NNCS Award (DMI-0210400).

I would like to thank my family: my parents Salvatore and Lori; my brother Michael; my grandparents Geno, Pia, Gioacchino and Vincenza; my aunt Lillie; and my cousins Vivi, John, and Priscilla. Your achievements and sacrifices have molded me into the man I am, and I deeply thank you for all you have done.

I wish to thank Dr. Alexandre Ermoline for his assistance in the laboratory, knowledge, and guidance through this process. Many of my fellow graduate students in the Chemical Engineering Department are deserving of recognition for their support. Finally, I would like to thank Dr. Ganesh Sanganwar, Laila Jallo, and Lauren Beach for their assistance with some of the experiments. Special thanks to my undergraduate research assistant Fernando Rivas for his hard work and tremendous dedication to his research and commitments.

TABLE OF CONTENTS

TABLE OF CONTENTS
(Continued)

Chapter **Page**

TABLE OF CONTENTS
(Continued)

Chapter **Page**

TABLE OF CONTENTS
(Continued)

Chapter **Page**

LIST OF TABLES

LIST OF FIGURES

LIST OF FIGURES
(Continued)

Figures **Page**

LIST OF FIGURES
(Continued)

Figures **Page**

LIST OF FIGURES
(Continued)

Figures **Page**

LIST OF FIGURES
(Continued)

Figures **Page**

LIST OF FIGURES
(Continued)

Figures **Page**

LIST OF FIGURES
(Continued)

Figures **Page**

LIST OF FIGURES
(Continued)

Figures **Page**

LIST OF FIGURES
(Continued)

Figures **Page**

LIST OF FIGURES
(Continued)

Figures **Page**

LIST OF FIGURES
(Continued)

Figures **Page**

LIST OF FIGURES
(Continued)

Figures **Page**

CHAPTER 1

INTRODUCTION

1.1 Introduction to Mixing and Previous Work

1.1.1 Nanopowders Properties and Composites

A particle is defined as a small object that behaves as a whole unit in terms of its transport and properties. It is further classified according to size: in terms of diameter, fine particles cover a range between 100 and 2500 nanometers, while ultrafine particles, on the other hand, are sized between 1 and 100 nanometers. Similar to ultrafine particles, nanoparticles are sized between 1 and 100 nanometers. Nanopowders are formed from agglomerates of nanoparticles. Nanoparticles are of currently of interest as they bridge molecular structures and bulk materials. Bulk materials usually have constant physical properties, however, nanoparticles are observed to have size dependent properties. Therefore, with the use of nanoparticles, the properties of materials can change. This is due to the higher percentage of atoms on the surface of the material in relation to the atoms found in the bulk material. For bulk materials, of particles larger than a few microns, the percentage of atoms is much less signification in relation to the total atoms in the material.

Nano-particles are widely encountered in manufacturing of drugs, foods, cosmetics, catalysts, biochemistry and many other fields of technology. Many paints used for cars, aircrafts or spacecrafts are mainly based on surface modifications by coatings based on ultrafine particles. Powder mixing is an important and extensively

researched area in many industrial sectors such as chemicals, pharmaceuticals, foods, cosmetics, ceramics, fertilizers, detergents, pigments and electronics during the past several decades.

In the past decade, with the advent of availability of a variety of novel nanoscale particles and materials, there has been an increased interest in mixing methods that deal with nanopowders for the purpose of forming nanocomposites.[1,2] However, majority of the mixing research is focused on the non-cohesive and typically smooth, spherical particles limited to the hundreds of micron or millimeter sized particles.[3-11] In the past decade, with the advent of availability of new nano-scale particles and materials, which are becoming popular due to their unique characteristics of small size and large specific surface area, there has been an increased interest in mixing applications that deal with nano-powders in various industrial sectors for the purpose of forming nano-composites.

Unique properties of nano-composites arise from the interaction of different constituents at the interfaces at the nano scale.[12-18] A few of these properties include enhancements in chemical catalysts, wear resistance, oxidation resistance, thermal resistance, and corrosion resistance.[19] However, one major problem that is frequent with nano-powders is that the highly agglomerated particles often lose their high-surface area due to grain growth.[20-24] For example, the shelf life of drug nanoparticles in pharmaceuticals is limited due to the rapid grain growth. Carbon nanotubes highly dispersed in composites have better electrical and thermal properties than agglomerated carbon nanotubes in composites.[25] It has also been shown that burning rates for agglomerate mixtures are significantly lower than more homogeneous mixtures.[26,27] Therefore, grain growth can be prevented by finding ways to properly disperse

nanoparticles in the bulk material, preferably by creating a nanoscale mixture of two or more constituents, or forming a bulk in which the nanoparticles are well dispersed. Mixing of ultra-fine and nano particles at sub-micron scales is one of the most promising approaches for engineering different types of nano-scaled compositions taking advantage of the new functionalities of nano-scale materials. Thus the ability to achieve nano-mixing can open up innovative ways to improve performance of drugs, biomaterials, catalysts, and other high-value added materials.

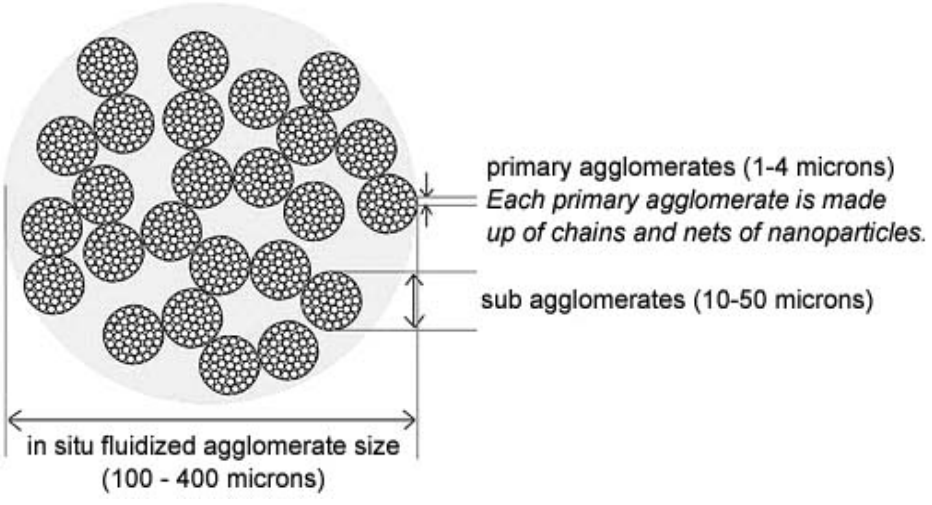

Figure 1.1 An agglomerate of nanoparticles composed of sub agglomerates and primary particles.

However, there are serious challenges faced in handling and homogeneous mixing due to high cohesion and tendency to form large, difficult to break agglomerates that form due to strong inter-particle forces. Figure 1.1 is an example of the composition of an agglomerate of nanoparticles. In fact, conventional methods for powder mixing cannot mix at scales smaller than about a few microns or even hundreds of microns because they fail to break the primary aggregates.[11,28-32] Particle segregation is a process which can hinder powder mixing when solids tend to segregate by the differences in

many properties that include size, density and shape. To prevent segregation, mixing of the powders must occur below the agglomerate scale. Once below the agglomerate scale, the high interparticulate forces resist interparticulate motion leading to segregation. The full potential of a nanocomposite material can only be achieved when the constituent nanoparticles are properly dispersed and mixed – preferably at a nanoscale – and the agglomeration between particles is well controlled.

1.1.2 Nanopowder Mixing

In order to mix on a sub-micron scale, forces and mixing (agitating) motion are required to deagglomerate and then mix the particles at sub-micron scales. Agglomerate breakup can occur by mechanical collisions or by turbulent fluid shearing. Currently, the most popular methods for nanoparticle deagglomeration essentially rely on the shearing of nanoparticle suspensions in organic solvents.[33] Industrial efforts are concentrated towards the wet mixing technique because the solvents can easily wet and penetrate into the agglomerate void spaces, making the process of deagglomeration less tedious.[34] The majority of the mixing operations use batch or semi-batch vessels.[35] There are recent studies on dispersion of nanoparticle agglomerates in liquid media have been carried out in the systems involving high shear stresses such as high shear impeller mixers and high pressure homogenizers.[36-39] However, stirred tank systems can have disadvantages, such as nonuniformity and precipitate agglomeration, which can adversely affect the system.[35]

The solvents, which tend to be organic solvents with surfactants or pH modifiers,[40-45] can be expensive and are harmful to the environment.[35] Also, there are other disadvantages associated with wet mixing processes, such as conditioning steps and downstream drying time. During the drying time, segregation could occur by density

stratification and electrostatic separations which adversely affects the homogeneity of the mixture.

Tumblers, fluidized beds and V-blenders are commonly used in industry as a dry mixing technique; nevertheless, these methods do not create enough forces to deagglomerate.[46] Recently, the deagglomeration and mixing capabilities of different environmentally techniques have been examined; namely, Rapid Expansion of High Pressure and Supercritical Suspensions of nanoparticles,[1-2] sonication of a suspension of nanoparticles in supercritical CO_2,[37-38] Magnetically Assisted Impact Mixing (MAIM),[1,2,48-50] mixing by fluidization assisted by magnets under magnetic field,[20,49,50] and mixing by stirring a supercritical suspension of nanoparticles in supercritical CO_2.[48,49] Recently, the deagglomeration and mixing capabilities of different environmentally techniques have been examined; namely, Rapid Expansion of Supercritical Suspensions of nanoparticles,[1-2] sonication of a suspension of the nanoparticles in supercritical CO_2,[48-50] Magnetically Assisted Impact Mixing (MAIM),[1-2,27-29] mixing by fluidization assisted by magnets under magnetic field,[20,49,50] and mixing by stirring a supercritical suspension of nanoparticles in supercritical CO_2.[48,49]

1.1.3 Fluidization

Fluidization is when a bed of particles is suspended by a fluid flow. The particles in the bed resemble a fluid-like system. When the bed is fluidized, the flow exerts a drag force to counter the weight of the particles. Fluidization is used in industry for mixing, heat transfer, heat exchange, particle coating, drying, adsorption, reactions, etc. The type of fluidization depends on the types of particles used. Geldart[51] classified particles into groups based on their fluidization behavior. This classification is shown Figure 1.2.

Group A particles are fluidized smoothly at velocities greater than the minimum fluidization velocity without bubbles. Group B particles undergo bubbling fluidization, meaning bubbles tend to appear immediately at the minimum fluidization velocity. Group D particles form spouting beds. The group C particles are very difficult to fluidize due to their cohesive properties. Nanoparticles fall under group C fluidization behavior.

Nanoparticle agglomerate fluidization as either agglomerate particle fluidization (APF) or agglomerate bubbling fluidization (ABF).[24] The type of fluidization depends on bulk density and primary particle size. APF particles have a low minimum fluidization velocity, high bed expansion, and homogeneous liquid-like state, while ABF particles have low bed expansions, high minimum fluidization velocity in a bubbling, nonhomogenous, state.[24]

The fluidization of nanoparticle agglomerates tends to channel, lift as a plug, elutriate, and bubble. Conventional fluidization of nanoparticle silica agglomerates were investigated, and they discovered the fluidization was not Geldart group C particles.[24] The group found that the silica particles fluidized smoothly, at low minimum fluidization velocities, with high bed expansions. The nanoparticles form simple, net-like, agglomerates of micron size which form larger complex agglomerates.[24] The larger, porous, agglomerates fall into Geldart group A, which allows them to smoothly fluidize.

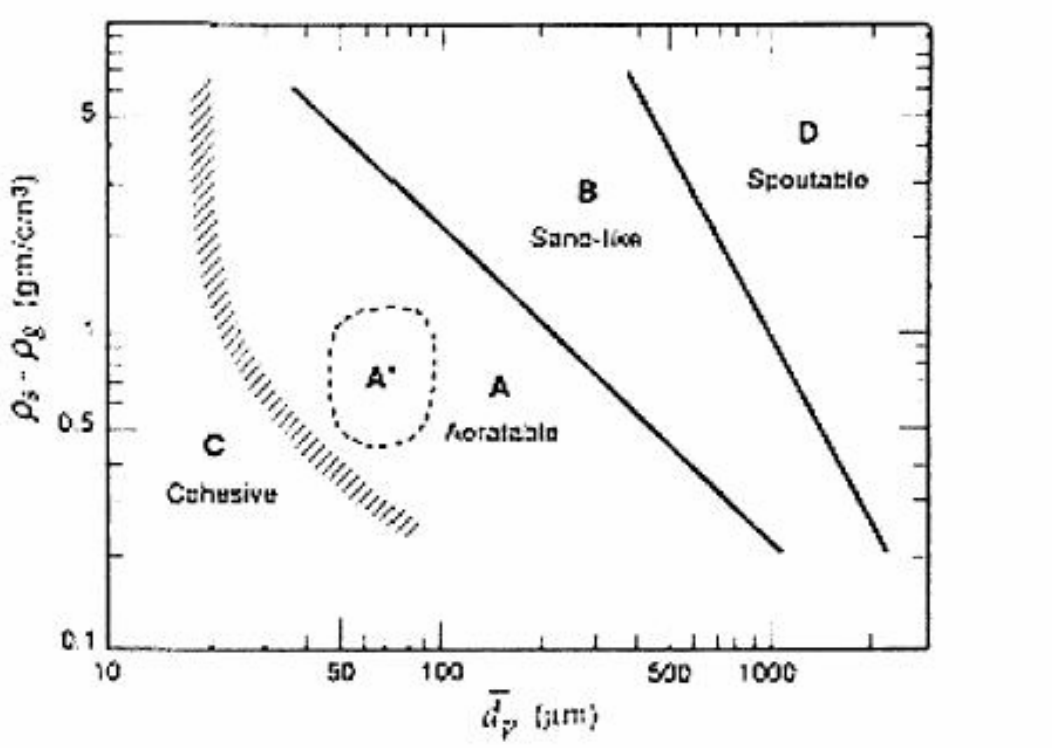

Figure 1.2 Classification of particles by Geldart.[51]

There have been many improvements in the fluidization of group C particles, such as, sound assisted fluidization,[52,53] vibration assisted fluidization,[22,54,55] fluidization in an oscillating magnetic field,[20] and surface modification.[54] In this research, we have expanded experiments on the fluidization of nanoparticle agglomerates using the assistance of magnetic impaction.

It has been reported that magnetically assisted fluidization increases the bed height fourfold and decreases the minimum fluidization velocity required to fluidize the particles.[20] The results also indicated that fluidization can occur with larger, hard to fluidize, agglomerates, as well as, being able to fluidize ABF powders similarly to APF powders.[20] However much of the previous research has involved the fluidization of magnetic particles and not so much on the fluidization of powders assisted by magnetic impaction.[58-67] Nevertheless, it has been observed that the fluidization behavior of

agglomerates of nanoparticles in a mixture with magnetic particles under the influence of an oscillating magnetic field.[20]

Since a major problem in fluidization is the collection of larger agglomerates above the distributor plate, the introduction of magnetic particles serve to break down the larger agglomerates. Given that the magnetic particles are much heavier than the particle bed, they are not fluidized. The particle bed is disrupted by the magnetic particles use of an oscillating magnetic field is used to create movement of magnetic particles. With the magnetic assistance, the bed of nanoparticle agglomerates was smoothly fluidized and the minimum fluidization velocity was appreciatively reduced.[20, 68] In addition, it was noted that channeling or slugging of the bed disappeared and the bed expanded uniformly without bubbles, and with negligible elutriation. An application for the fluidization of nanoparticles includes the fluidization of silica nanoparticles, under reduced pressure conditions, by vibration. The agglomerates of silica are coated with alumina using atomic layer deposition.[69] The results show that individual silica nanoparticles are found to be uniformly coated with alumina.[69] These results open a wide ranges of research options including using nanoparticles as a support for a catalyst by means of coating using atomic layer deposition.

1.2 Scope of Proposed Work

The literature review shows that, while there has been progress in the nanoparticle mixing field, there is still room for improvement. Due to application of nanomaterials in various fields, nanopowders have been selected to study the mixing quality of separate magnetically assisted impaction mixing techniques. Inorganic nanomaterials such as

silica (SiO_2), alumina (Al_2O_3), and titania (TiO_2) have been selected for the projects. Silica has been used in the pharmaceutical industry, coatings, adhesives and many nanocomposites. Titania is used in photo catalytic activities, heat stabilizers and UV protection in the cosmetic industry. Alumina is used in powder coatings, to increase flowability and acts as an antiblocking agent in PET-films. All nanomaterials from inorganic class are donated by Evonik Degussa Inc.

In this work, the impaction of magnetic particles is used in the place of mixing blades, or tumblers, for mixing of nanomaterials. The MAIM process will be batch operations run using sample jars. To prove the effectiveness of the MAIM for both hydrophobic and hydrophilic nanopowders, in-depth studies will be conducted in wet and dry mediums to optimize the mixing process. Since fludized beds are used extensively in industry, MAIM will be used as assistance to the fluidization and mixing in the particle bed. A hydrodynamic study will be performed for different types of fluidizable particles with both hydrophobic and hydrophilic properties. A greater understanding of the fluidization of agglomerates of nanoparticles, and the effects of the fluidization on the quality of mixture, will be obtained by the study of magnetically assisted fluidization.

Since, in industry, mixing is often performed within batch vessels, in a liquid medium, have shown desired results, the first chapter will explore the ability of MAIM process to mix nanoconstituents in liquid mediums. The properties of the solvents are varied in order to obtain better mixture homogeneity. The results collected in this chapter are compared with various mixing methods currently used in industry. The next chapter deals with the batch MAIM mixing as a method for environmentally benign dry mixing. While liquid mixing is favored with fine powders, due to easier handling of the powders,

liquid mixing requires additional steps to condition and then dry/separate the powders. Further magnets and constituents are investigated in order to obtain a more homogeneous mixture. Additional dependencies are also investigated in order to improve mixture homogeneity and the ability to predict mixture homogeneity. The mixture homogeneity results are compared to other published nanoparticle mixing results.

A third experimental chapter is the research results obtained using magnetically assisted fluidized bed mixing (MAFBM). This chapter contains mixing results as well as a detailed study on the fluidization behavior of the agglomerates of nanoparticles in a magnetically assisted fluidization system. Fluidization is a unit operation which is widely used in chemical engineering operations and there are my published works describing the principles, phenomena and applications processes.

The appendix chapters contain additional SEM and TEM images along with summarized research done in collaboration with outside universities. At ETH Zurich, deagglomeration studies of titania nanoparticles is studied. The titania particles, which are created by flame spray pyrolysis at the university, are deagglomerated using a sonic horn and the particles are sized using a NanoSite®. The effect of solvents and surfactants are studied in order to ascertain a system which will produce the most stable suspension.

At the University of Wollongong, particle formation was studied using a spray drying system. Alginate, an anionic polysaccharide, is used as the particle base. To study drug dissolution, the alginate was spray dried with dexamethasone, an anti-inflammatory and immunosuppressant. Using a uv-vis spectrometer, concentration versus time curves are obtained and used to determine methods to best delay the drug's release.

Field Emission Scanning Electron Microscope (FESEM) along with Energy Dispersive X-ray Spectroscopy (EDS) are employed to investigate the mixing effect of different constituents of powders processed in MAIM device. Quantitative analysis of the samples is performed based on the FESEM images and EDS elemental maps by the procedures discussed in the proceeding section. It is noted that this analysis is a significantly improved version of the approaches reported before.[1-2] Effects of magnet-to-sample ratio, processing time, mixture components (i.e., constituents) and the magnet size on the HoM are investigated and discussed in this section. Since the EDS can only examine sample volumes down to the micron size range, transmission electron microscopy (TEM) is used to obtain elemental composition and mappings at the primary particle size range.

CHAPTER 2

EXPERIMENTAL, MATERIALS AND ANALYTICAL METHODOLOGY

2.1 New Jersey Center for Engineered Particulates (NJCEP) Mixing Systems

This section describes the experimental set-ups of devices focused in this dissertation and located at the NJCEP facilities. In addition to the following equipment, rapid expansion of supercritical and high pressure solutions and supercritical stirring are used to compare mixing quality to magnetically assisted impaction mixing methods.

2.1.1 Magnetically Assisted Impaction Mixing (MAIM) System

In magnetically assisted impaction mixing, the different nanopowder components are placed along with magnetized millimeter-sized magnets in a container. The container is placed inside an electro-magnetic coil (7 cm ID and 6 cm height) producing an oscillating magnetic field. The magnetic coil is controlled by a Variac 140V variable transformer connected to alternating current. The magnets undergo rotational and translational motion and promote rearrangements of nano-particles between agglomerates of different materials, potentially mixing them at scales well below the sub-agglomerate (SA) size, and even down to primary agglomerate level.

The magnetic particles promote powder mixing primarily by shear mixing and convection. The rotational motion of the magnets creates many areas of microshear. Shear mixing is a mechanical process that causes slipping along the particle boundaries. Convection mixing occurs when groups of particles and agglomerates collide into other agglomerates. This occurs when the magnetic particles move around the jar and collide

with agglomerates and the sides of the jar. Diffusion mixing, when particles move onto another particle, plays a minor roll in the mixing process as well. Particle segregation is a process which can hinder powder mixing when solids tend to segregate by the differences in many properties that include size, density and shape. To prevent segregation, mixing of the powders must occur below the agglomerate scale. Once below the agglomerate scale, the high interparticulate forces resist interparticulate motion leading to segregation

MAIM studies are carried out in dry conditions along with in liquid suspensions. A fan is connected underneath the coil to prevent any overheating and damaging of the powders. The motivation of this investigation is due to the simplicity of this method and potential low cost and ease of scale-up. A schematic of the MAIM apparatus is shown in Figure 2.1.

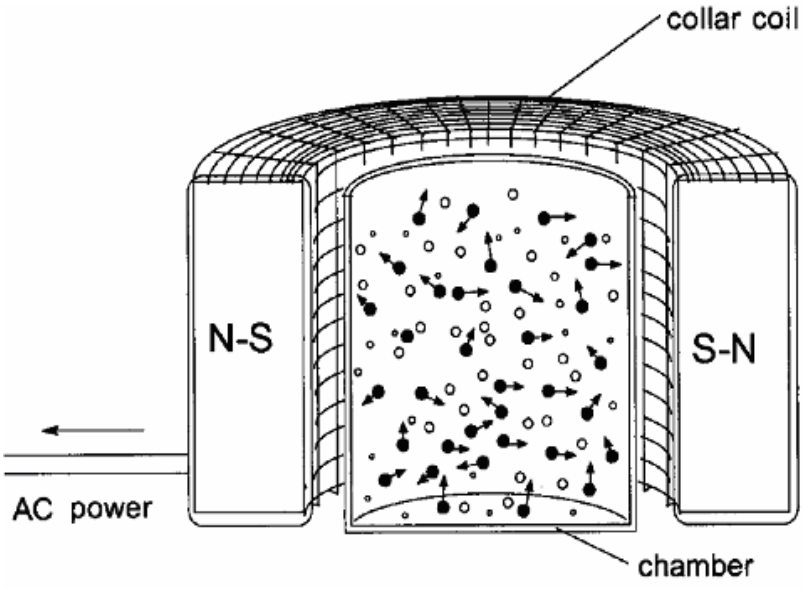

Figure 2.1 Schematic of MAIM setup.

2.1.2 Magnetically Assisted Fluidized Bed (MAFB) System

Fluidization based mixing is carried out in a fluidized bed, which is an industrial method for various types of processing. In conventional fluidization, it is expected that the mixing will be not be at the scale of SA, and may also require a long time. Therefore, various assisted methods such as magnetically assisted fluidization need to be investigated. The fluidized bed is a vertical column 5.06cm in inner diameter and 30.5 cm in height made of acrylic. The porous gas distributor at the base of the column is a sintered steel plate with a thickness of 2 mm and pore size of 20μm. An ultrafine mesh filter is located at the top of the column and over the pressure tap to prevent any agglomerates from elutriating. A digital manometer (Dwyer Instruments, Series 475 Mark III) is used to measure the pressure drop across the fluidized bed. Two electromagnetic coils are situated at opposite sides of the base of the column to generate an oscillating magnetic field. Each coil is regulated by a variable autotransformer (Staco Energy Products Co., Model 3PN1010). Two cooling fans are installed to prevent the coils from overheating.

Humidity can be an issue when working with hydrophilic powders, therefore pure nitrogen gas, N_2, is used as the fluidizing gas. The nitrogen flow rate is controlled by a rotameter (Cole-Parmer PTPE, 150mm). Superficial gas velocity measurements are taken from a flowmeter (Cole-Parmer, Model 32908-71) connected in series. The gas flows into the base region of the column via two inlets to generate a uniform gas field before the distributor. A pressure tap right above the distributor plate, covered with an ultrafine mesh to prevent agglomerates from escaping, is used to obtain the pressure drop

across the particle bed. The pressure at the top of the bed is taken as atmospheric pressure. A schematic of the MAFBM apparatus is shown in Figure 2.2.

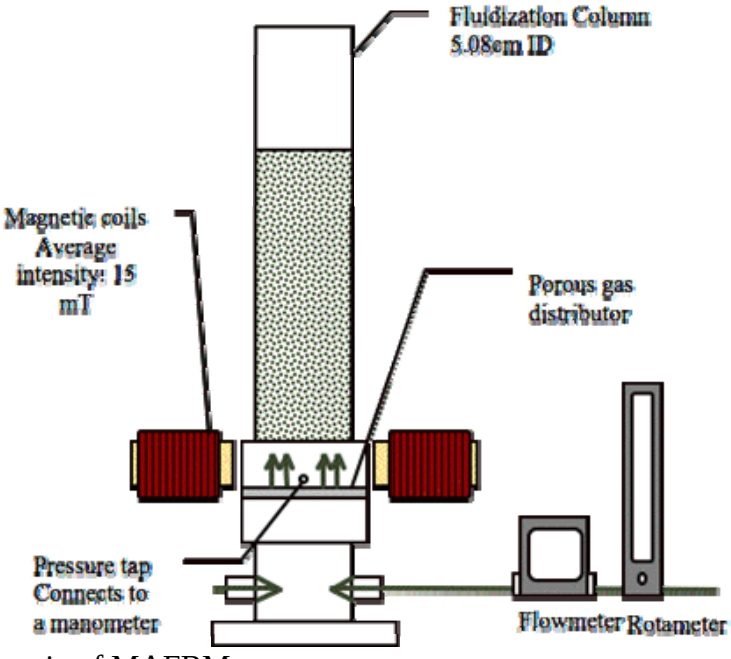

Figure 2.2 Schematic of MAFBM setup.

2.1.3 Liquid Mixing

In order to compare how liquid MAIM mixing compares to conventional wet mixing techniques, impeller blades and a homogenizer are used. The same liquid loading and sample-to-sample weight ratios are used. Pitched impeller blades are used at 300 rpm. The homogenizer (Finemech Precision mechanical components) contains a X 120 hand-held, high speed, drive motor for small volumes. Electronically stabilized speed control for speeds of 11,000 - 33,000 rpm. The shaft used is 17 mm in diameter compatible for low viscosities. For each apparatus, mixing experiments are run at various times to determine trends in mixing.

2.2 Supercritical Sonication in Carbon Dioxide

Mixing of nanoparticles in supercritical carbon dioxide using a sonic horn is investigated by Dr. Ganesh Sanganwar and Dr. Ram Gupta at Auburn University. Results are analyzed at NJCEP facilities and used as a comparison to magnetically assisted impaction mixing methods.

Figure 2.3 shows the schematic diagram of experimental setup used for mixing powders in carbon dioxide. It consists of compressed carbon dioxide gas cylinder, chiller, piston pump (Thar Technology) for pumping CO2, preheated, ultrasonic processor (Sonics and Materials Inc.) producing ultrasonic waves at a frequency of 20 kHz with maximum power capability of 600 W, and a 120 mL stainless steel mixing vessel heated by heating tape. The ultrasonic processor consists of three major components: an ultrasonic power supply, a transducer, and a horn with 0.75 inch tip diameter. Temperature and pressure inside the mixing vessel are measured with a thermocouple and a pressure gauge, and heating tape is controlled by a temperature controller. To prevent the loss of powders during the vessel depressurization, a filter (Fisher Scientific Inc.) at the top exit of the vessel is installed. The ultrasonic processor is designed to deliver constant amplitude, i.e., it automatically adjusts power to maintain constant amplitude during the operation. Therefore, power delivered from the processor depends on the resistance to the movement of horn which is affected by setup and process parameters, such as volume of a mixing vessel, horn size, mixture viscosity, pressurized environment, etc.

All experiments are conducted at constant amplitude, and power is monitored. Nanopowders in weight ratio of 1:1 (100mg:100mg) are loaded into a stainless steel

vessel and then carbon dioxide is introduced. The horn is immersed into the vessel, so that only 100 mL of its volume is available for mixing. Vessel pressure is maintained within ±3.5 9 105 N/m2 and ±0.1 degree C at the start of each experiment. The vessel is heated with the heating tape to 45 degree C in all experiments. After reaching desired pressure and temperature in the vessel, ultrasound is applied for 10 min at particular amplitude to cause mixing. After mixing, the vessel is slowly depressurized to prevent carry over of particles with CO2. Further loss of particle is prevented using the filter at the top exit of the vessel. After complete depressurization, vessel is opened, and powder is collected for analysis.

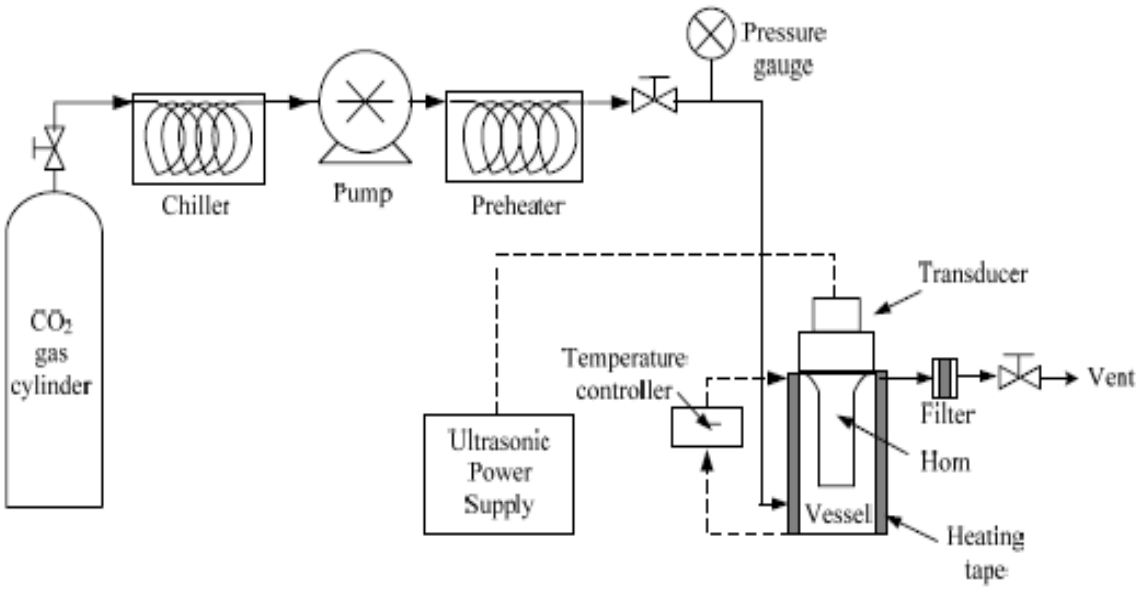

Figure 2.3 Schematic diagram of the experimental setup for mixing nanopowders in carbon dioxide.

2.3 Materials

The inorganic nanopowders used in this work are Aerosil® R974, Aerosil® R972, Aeroxide® Titania P25, Aeroxide® Alumina C, and Aerosil® A200, with primary particle sizes in the range of 12 to 21 nm. They are produced by Evonik Industries, formerly Degussa Corporation, through a pyrogenic process.[1] In pyrolysis, a gas or liquid is pumped through an orifice at high pressure and is burned. At high temperatures, the reaction for this process is:

$$SiCl_4 + O_2 + H_2 \rightarrow SiO_2 + 2HCl \qquad (2.1)$$

The SiCl4 is vaporized and mixed with hydrogen and oxygen. The mixture is then ignited and burned in the combustion chamber. The cooled product is filtered and the product is treated in a de-acidification unit. Generally, the same principle is used in the production of other nanoparticles such as titanium oxide, iron oxide, and alumina oxide. Nanoparticles are said to form hierarchical, fractal structured, porous agglomerates, which have very low density and are irregularly shaped, as shown in the previous chapter as Figure 1.1.

The as-received nanoparticles are in the form of large, soft aggregates; they are sieved (35 mesh) in order to remove agglomerates larger than 500 microns. This sieving also removed hard agglomerates (which may have formed through irreversible sintering), thus erasing the powder storage/consolidation history effects and improving repeatability of all subsequent mixing experiments. In all of the MAIM experiments, the initial volume occupied by the powder in the mixing container is 40 mL for SiO_2 + TiO_2

mixtures and 50mL for SiO_2 + Al_2O_3 mixtures. The initial volume occupied for the MAFB experiments is approximately 115 mL. When the nanopowders are dropped down the column, they aerate causing the increase in volume occupied.

The magnetic particles are barium ferrite ($BaO\text{-}6Fe_2O_3$) permanent magnetic particles (supplied by AVEKA INC) are coated with polyurethane to prevent contamination and to limit the mixture's retention on the particle. The particles are recharged by contacting them with a strong permanent magnet before each experiment. There are three size ranges of 2360 to 1700 microns, 1400 to 850 microns, and 1000 to 600 microns used in these studies. The majority of experiments are carried out with the 1400 to 850 microns magnetic particles.

In all magnetically assisted cases, once the mixing is complete, the magnetic particles are sieved from the nanoparticles. The magnetic particles can be cleaned and reused. Materials are affordable allowing for the process to be scaled up with relative ease.

Table 2.1 Nanoparticle Properties

Material	Primary Particle Size (nm)	Surface Area (m^2/g)	Property
Aerosil® R974	12	200	Hydrophobic
Aeroxide® TiO_2 P25	21	50	Hydrophilic
Aeroxide® Alu C	13	100	Hydrophilic
Aerosil® A200	12	200	Hydrophilic
Aerosil® R972	16	130	Hydrophobic

2.4 Particle Size Analysis

Laser diffraction particle characterization of particles is chosen due to its wide use for many applications. Laser diffraction is obtained by the angle of scatter, and has the advantage of being an automated process. The scattered angle depends on particle size, refractive indexes and the wavelength of the beam. Modeling is used to analyze the scatter and predict a particle size, by assuming all particles are circular in form. The sample has to be a diluted sample because the modeling program cannot detect the differences in the scatter of multiple particles.

First individual dry powders are sized using an Aerosizer. A small sample of nanopowder is placed in a chamber while shear and deagglomeration settings can be adjusted. Samples of silica R974, silica A200 and titania P25 are analyzed under these conditions. The sized particle diameter is plotted versus the particle volume distribution in Figures 2.20 through 2.24. Silica R974 had the highest particle volume distribution of the samples, demonstrating the difficulty in deagglomerating the powder (Figure 2.20). Even under high and peak shear rates, while noticeable minorities of agglomerates are broken down, the majority of the agglomerates remain unchanged (Figure 2.21). Titania P25 (Figure 2.22) showed very little change when changing the shear rates or deagglomeration rates, while silica A200 (Figure 2.23) is the easiest of the three samples to deagglomerate. It is clear, from the silica figures, that the main mechanism for breaking up agglomerates is the shear rate.

The device used to analyze liquid mixtures in this research is a Beckman-Coulter LS 230 (Beckman Coulter Inc., Fullerton, CA, USA). Particle size analysis is collected on the samples from liquid mixing studies, using the LS 230's liquid mode. Since the LS

230 uses Polarized Intensity Differential Scattering, a method used to determine particle sizes below 0.5 microns by using different wavelengths of monochromatic light, particle size data can be collected on particles as small as 0.1 microns in size. Particle size data is collected for LMAIM, homogenizer and sonication techniques versus time to determine the deagglomeration capability of LMAIM technique versus a commercially available homogenizer.

2.5 Mixture Homogeneity Analysis

A LEO 1530 VP Field Emission Scanning Electron Microscope (SEM) equipped with an Oxford UTW X-ray detector is used to obtain qualitative and quantitative analysis of the mixed samples. SEM analysis is used in many industries because its ability to obtain surface characterization and observation of materials. The SEM can magnify images beyond 100,000X and provide resolution of images of a couple nanometers in size.[3] Two 13 millimeter sized tablets are pressed using an International Crystal Laboratory die in a Carver mechanical press with a constant load of 16,000 lb/in^2 to 10,000 lb/in^2 in order to create a uniform packed density. First, a thin coating of electrically conducting carbon is deposited by a vacuum sputter coating onto the sample using a Bal-TEC 020 HR Sputtering Coater. Coating samples prevent the accumulation of static electric fields on the specimen and improves the contrast. Contrast is important for the qualitative analysis of determining agglomerate sizes described later in this chapter.

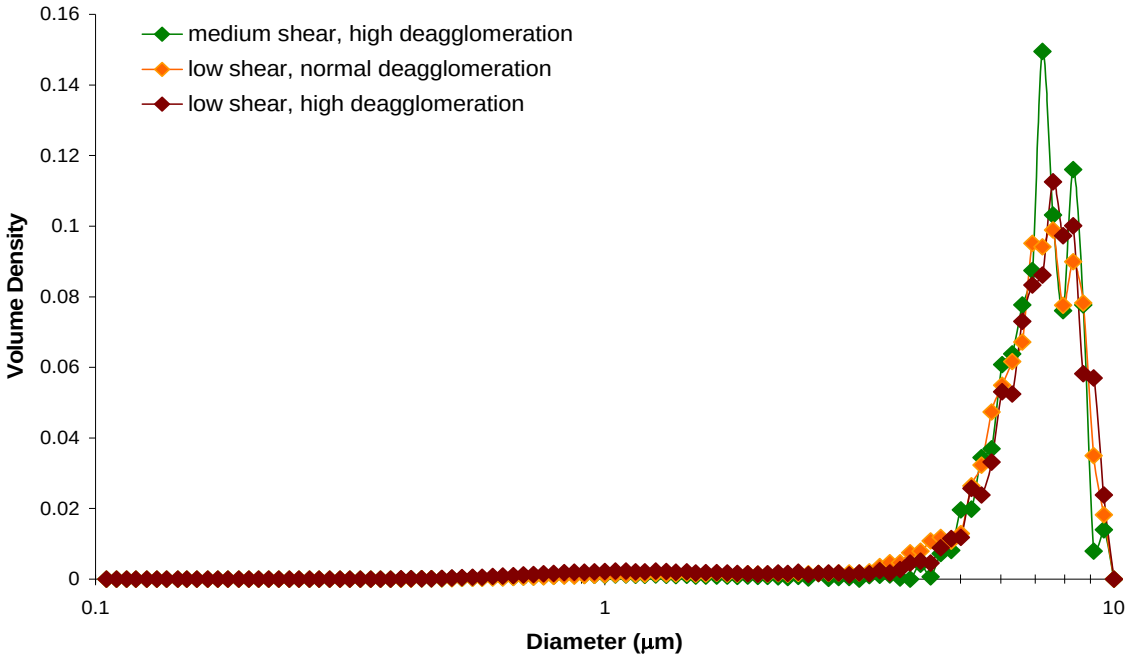

Figure 2.4 Particle volume distribution versus volume density for silica R974 under low or medium shear and high or normal deagglomeration.

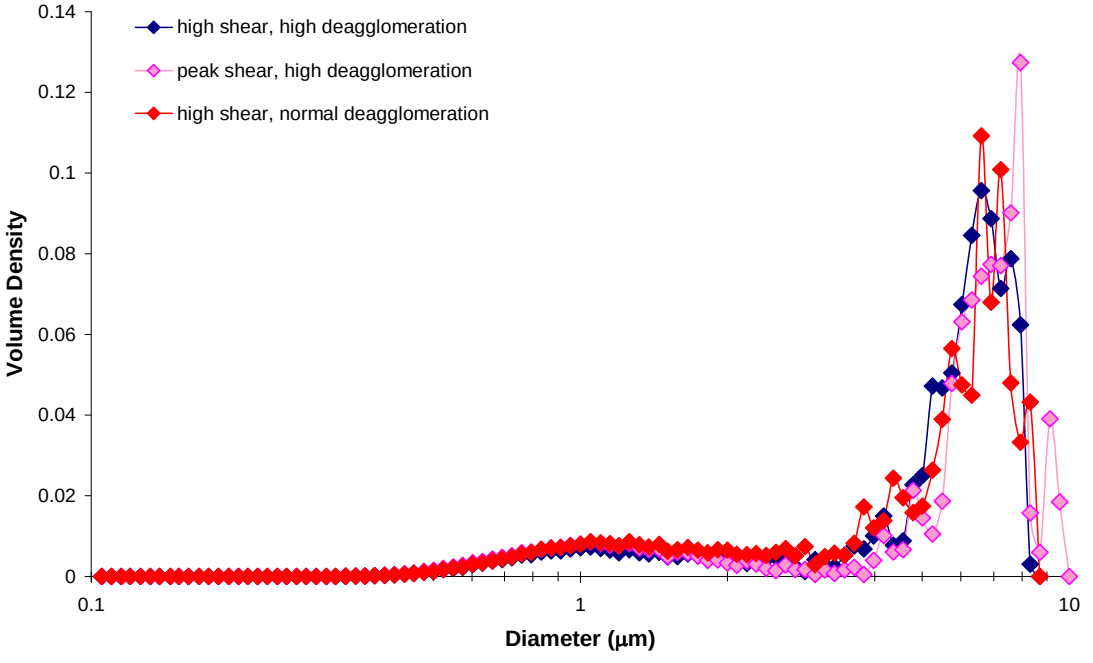

Figure 2.5 Particle volume distribution versus volume density for silica R974 under high or peak shear and high or normal deagglomeration.

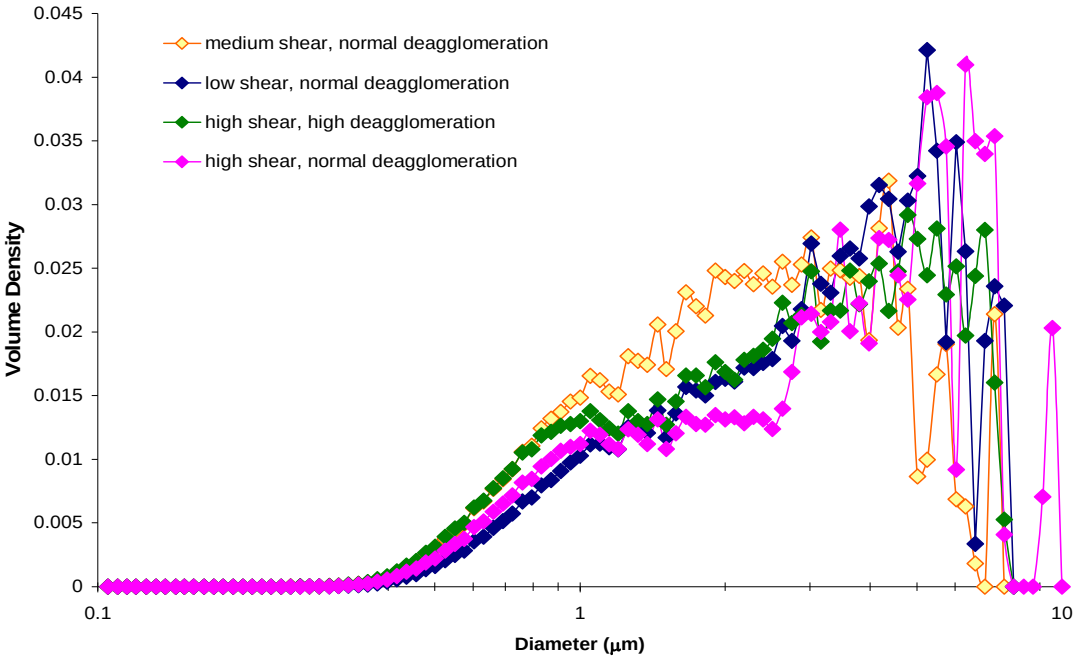

Figure 2.6 Particle volume distribution versus volume density for titania P25 under high, low or medium shear and high or normal deagglomeration.

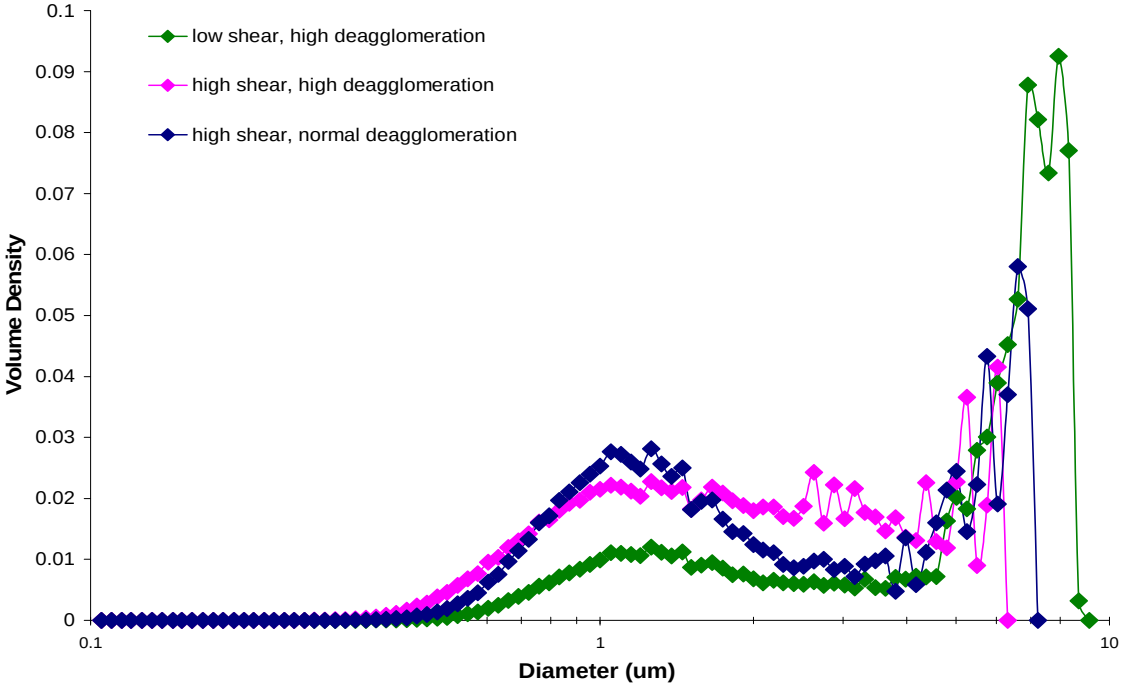

Figure 2.7 Particle volume distribution versus volume density for silica A200 under high or low shear and high or normal deagglomeration.

The area is analyzed by focusing an electron beam, produced by the electron gun, at the desired location. The signal is characterized to obtain an image where topography and composition data can be determined.[3] A study of the EDS and SEM is conducted to figure out the best conditions to analyze the samples. First a magnification needs to be analyzed. Figures 2.4 through 2.8 represent EDS mapping at different magnification levels for a single mixture of alumina Alu C and silica R974 processed by conventional fluidization. The mixture is a very poorly mixed sample since the particles undergo convectional and diffusive mixing while there is no shearing effect. The magnification of 5000x is chosen as the best option. At 5000x large single component agglomerates will not occupy the whole screen which would prevent us from getting an adequate measure of agglomerate size. Also, smaller agglomerates (5 microns) will be visible at 5000x magnification. Two representative areas of 55 μm x 40 μm at 5000 times magnification are chosen randomly on both the tablet surfaces. All samples are analyzed at an accelerating voltage of 15 keV and a working distance of approximately 8 mm.

Mixed samples can be defined into two groups. Ordered mixing is interativeDanckwerts[4] has proposed two concepts for determining the quality of mixture, the scale of segregation and intensity of segregation. The scale of segregation is described in equations 2.2 and 2.3, where *SS* is the scale of segregation (Figure 8.2), *R(r)* is correlation function, ε is a size scale beyond which there is no correlation of domains (it is mixed beyond this size scale), i.e. R(r>=ε)=0, x' and x'' are the concentration at two points (samples) in the mixture separated by distance τ. N is number of sample pair, n is the number of samples taken, σ^2 is the variance and μ is the average. The value of *R(r)* lies between 0 and 1. The values (*R(r)*) close to 1 are found for small values of *r* in an

imperfect mixture. For values of *R(r)* =0, there is a random relation between concentrations at points distant *r* apart.

$$SS = \int_0^{\varepsilon} R(r)dr \tag{2.2}$$

$$R(r) = \frac{(x'-\mu)(x''-\mu)}{(x-\mu)^2}(r) = \frac{1}{N\sigma^2}\sum_{i=1}^{N}(x'-\mu)(x''-\mu)r \tag{2.3}$$

$$\mu = \frac{\sum_i^n x_i}{n} \tag{2.4}$$

$$\sigma^2 = \frac{\left(\sum_i^n |x_i - \mu|^2\right)}{n-1} \tag{2.5}$$

EDS elemental mapping of each of the four analysis sites are used to determine the scale of segregation. Each pixel is approximately calculated to the representative size it covered for the mapping. Using Equation 2.3, with each of the pixel's brightness qualitatively representing the concentration of the particular element at each location, the correlation function is calculated. A few runs are analyzed initially to determine if the

scale of segregation would be a viable analysis tool at our analysis scale. Examples of four of the correlation functions, calculated from four distinct MAIM experiments, appear in Figure 2.8. When looking at correlation function results, most of the data dropped to zero fairly quickly representing a fairly homogeneous system with small agglomerates. In Figure 2.8, the least homogeneous mixture appearing as the slowest trend approaching zero is run for 10 minutes with a 1-2 MSR. A dependence on the amount of magnets and processing time is noticed since when increasing either of these variables, the resultant correlation function approaches zero much quicker. The next step is to take the area under the curve to calculate the scale of segregation. The scale of segregation (SS) is plotted versus time for a 1-2, 2-1 and 5-1 magnet-to-sample ratios in Figure 2.9 and versus the product of time and the number of magnets in Figure 2.10

As for the results from the correlation function, the SS results showed very little difference in the results from 2-1 MSR and 5-1 MSR. The 1-2 MSR showed the clearest trend line of the experiments. These results indicate that with higher magnet-to-sample ratios, the mixtures created are too homogeneous. Most of the SS values have reached the limits and fall below the size of the pixel. In Figure 2.10 a clear trend is visible when SS is plotted versus time and the number of magnets. For poorer mixtures, such as the results from the 1-2 MSR, and analyzed at the same settings, the scale of segregation would provide clear trends to help distinguish mixture homogeneity. Since the magnetically assisted mixing methods produced much better mixing results, another analysis method is needed.

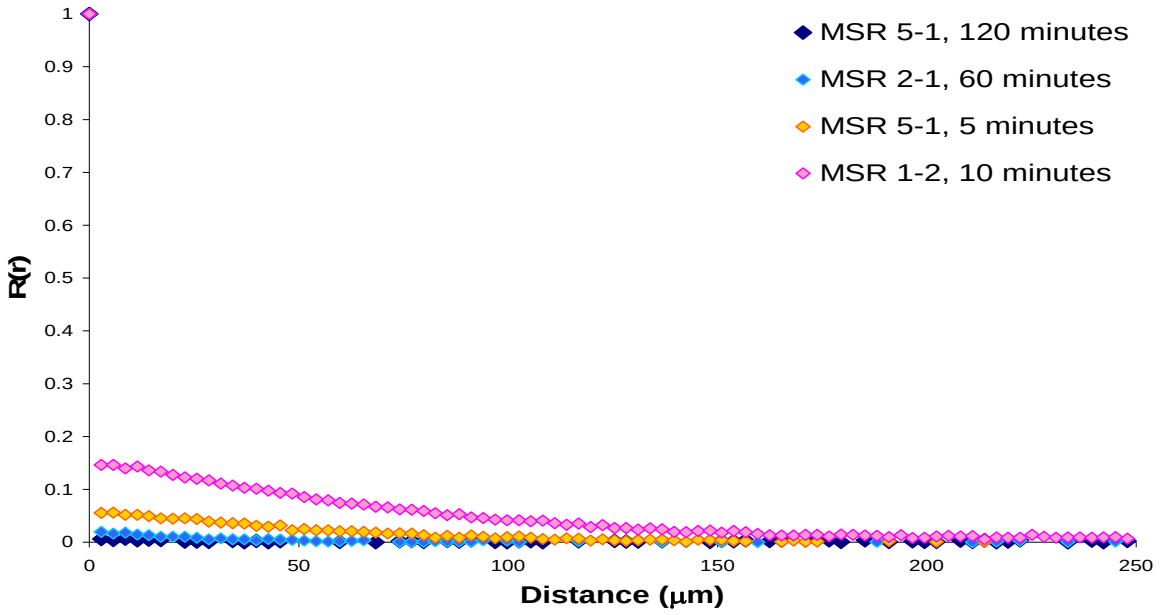

Figure 2.8 Correlation function calculations from MAIM R974 silica - P25 titania mixtures with 5-1, 2-1 and 1-2 magnet-to-sample ratios (MSR) run for specific processing times.

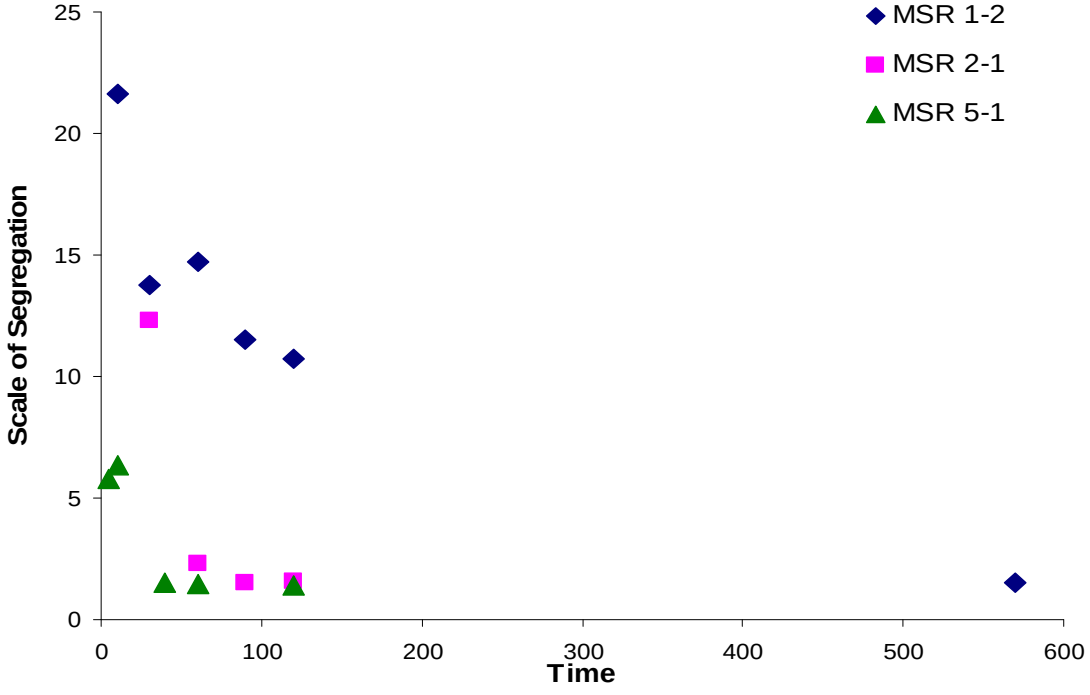

Figure 2.9 Scale of Segregation versus Time from MAIM R974 silica - P25 titania mixtures run with 5-1, 2-1 and 1-2 magnet-to-sample ratios (MSR) for at a specific processing times.

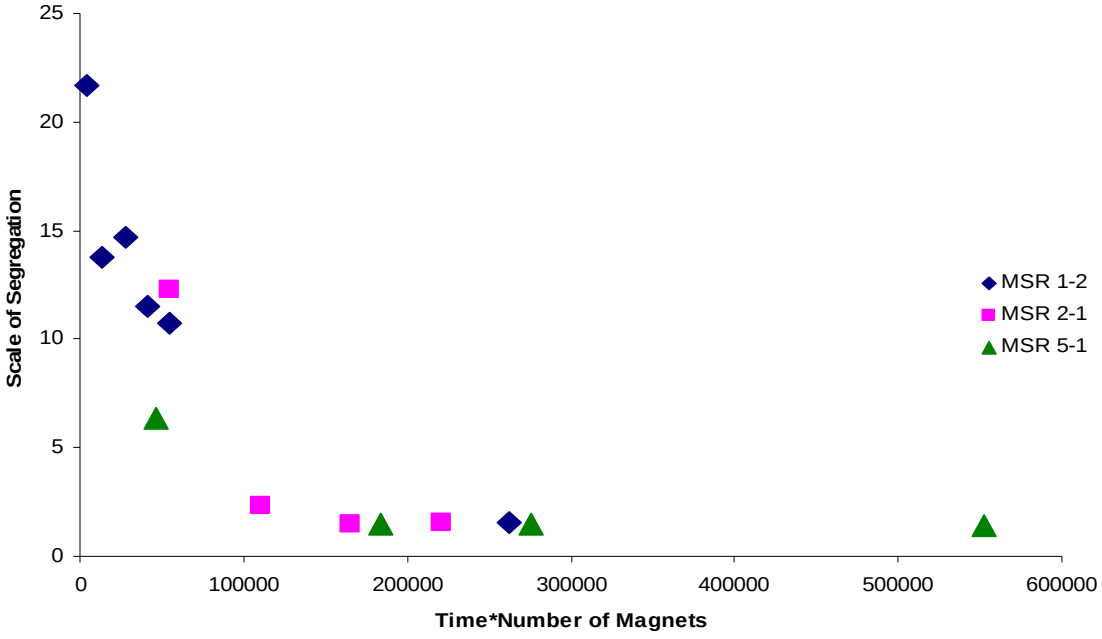

Figure 2.10 Scale of Segregation versus Time*Number of Magnets from MAIM R974 silica - P25 titania mixtures run with 5-1, 2-1 and 1-2 magnet-to-sample ratios (MSR) for at a specific processing times.

The scale of segregation reflects only the size of segregation and does not comment on the intensity of segregation. The Intensity of Segregation similarly, does not have an association with size but only reflects the concentration difference between constituents. Figure 2.11 shows a simplistic relationship between SS and Intensity of Segregation using black and white grids to represent particle distribution within the sample

Using the point analysis option for the EDS, normalized compound compositional data can be obtained at points with a diameter of under 3 microns with a representative area under 7 microns. The size of the point does not change with a change in magnification. Therefore, with the magnification chosen, the point dwell time and number of points need to be determined. A 10 by 10 point grid is chosen to supply significant data to cover the screen area. The dwell time of the point analysis has to be

long enough to obtain an equilibrium value while not sacrificing too much time. A location is chosen and analyzed multiple times with various dwell times. The compositional data is plotted versus time in Figure 2.9. It is apparent that after a time of approximately 10 seconds, the compound percent value does not vary too much.

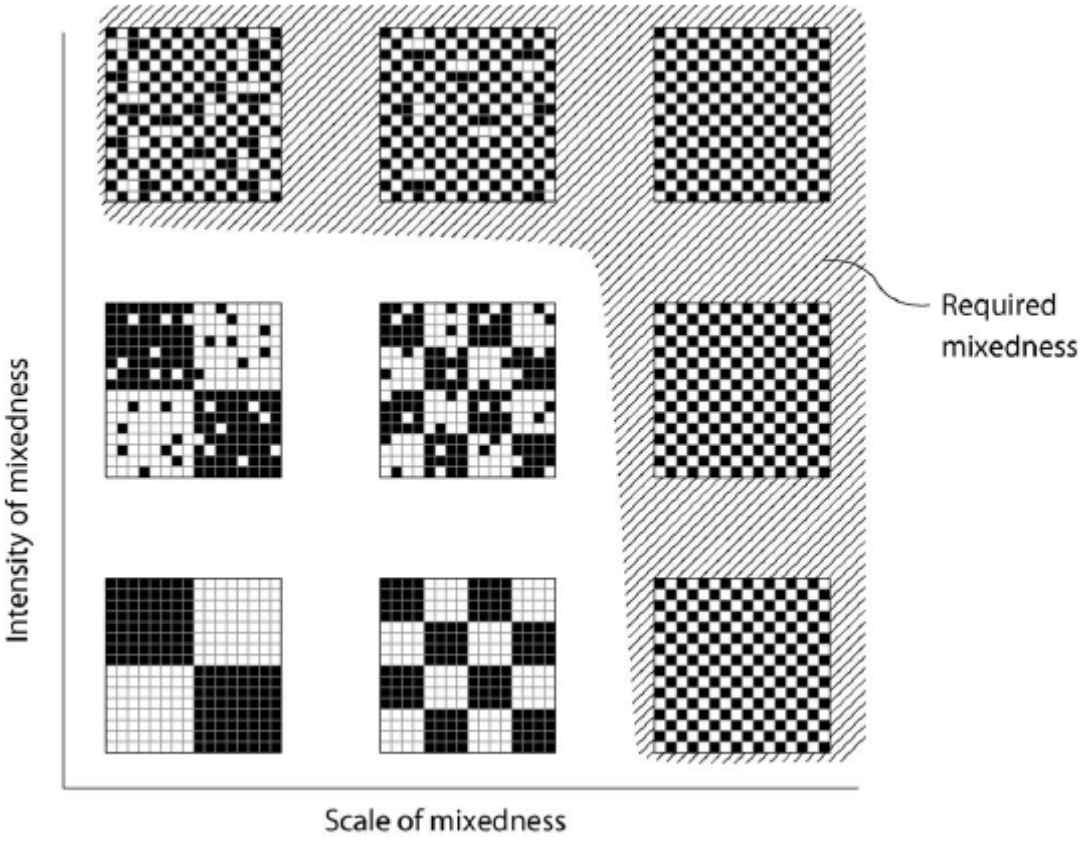

Figure 2.11 A schematic representation of mixing according to Dankwerts.[4] Intensity of mixedness is interchangeable to the homogeneity of mixing.

Source: van Herk D, Castano P, Quaglia M, Kreutzer M, Makkee M, Moulijn J. Avoiding segregation during the loading of a catalyst-inert powder mixture in a packed micro-bed. Applied Catalysis A: General, 2009; 365, 110-121

From the 100 points, arranged in a 10 x 10 grid, for each of the four areas, four-hundred total points of compositional data is obtained for each mixture. The data

collected is used to calculate the average concentration of the constituents (μ_a and μ_b) and variance (σ^2).

As a basis to compare the mixture homogeneity, the Homogeneity of Mixing, which is the compliment of the Intensity of Segregation, a dimensionless number, is employed in this work. Intensity of Segregation, the second concept developed by Danckwerts,[4] is calculated by dividing the variance by the two mean values of each component compound percent (Equation 2.6). The Intensity of Segregation for a perfect random mixture would be approaching 0, while for completely unmixed mixtures it would be approaching 1. Conversely, the HoM (Equation 2.7) for a perfect random mixture would be approaching 1, while for completely unmixed mixtures it would be approaching 0.

$$I = \frac{\sigma^2}{\mu_a \cdot \mu_b} \tag{2.4}$$

$$HoM = 1 - \frac{\sigma^2}{\mu_a \cdot \mu_b} \tag{2.5}$$

As the homogeneity of the mixture increases, visible changes on the FESEM (secondary electron) and EDS images are evident. For poor mixtures, there are large agglomerate regions of single elements that are easily visible on both the FESEM and EDS images. The images from mixtures of silica Aerosil® R974 and Aeroxide® Titania P25 are used due to the large distance in atomic number. Higher atomic number elements

appear brighter the secondary electron (SE) images, therefore, the changes in the agglomerate sizes are noticed by the differences in the contrast.

An example of a poor mixture is presented in Figure 2.9. As mixture homogeneity increases, the visible agglomerate regions decrease in size as shown in Figures 2.9 through 2.13. Figure 2.13 shows a well-mixed sample; where there are no visible agglomerates on either the FESEM or EDS images. These images in Figure 2.13 do not necessarily imply that there is mixing at the primary particle level, but that the mixing is at or below the detection level of the EDS. It should be noted that while the image shown can be magnified beyond 5000X, no improved quantitative data can be obtained at a higher magnification because the resolution of the EDS detection does not improve beyond 5000X. Additional SEM and EDS images for the silica R974 and titania P25 mixtures, along with the calculated values of intensity of segregation for the image, can be found in Appendix A. Also included in Appendix A are a few backscattered images of mixtures containing silica R974 and titania P25. Backscatter detection is temporarily explored as a possible method for analyzing agglomerate sizes since the backscattered electrons penetrate further into the tablet than secondary electrons but not as far as the x-rays used for EDS. In order to obtain clear distinctions between constituents when using backscatter detection, the two constituents must have a large difference in atomic to visibly appear difference by contrast levels. Therefore backscatter imagery can not be used for mixtures of silica and alumina since the z-contrast is not large enough.

The FESEM and EDS images of a mixture can be quantified to estimate the HoM for that mixture. Based on those values and an analysis of corresponding EDS images by

using imaging technique, one can deduce a qualitative relationship between HoM and approximate agglomerate sizes as shown in Table 2.2. It is noted that such a relationship is relative and only applicable to the results of this specific work and the procedures followed. As can be seen from Table 2.2, as the HoM increases, there is a corresponding decrease in the agglomerate size. All values of the HoM above 0.9985 indicate excellent mixing even though one cannot estimate the agglomerate size which is below the detection limit.

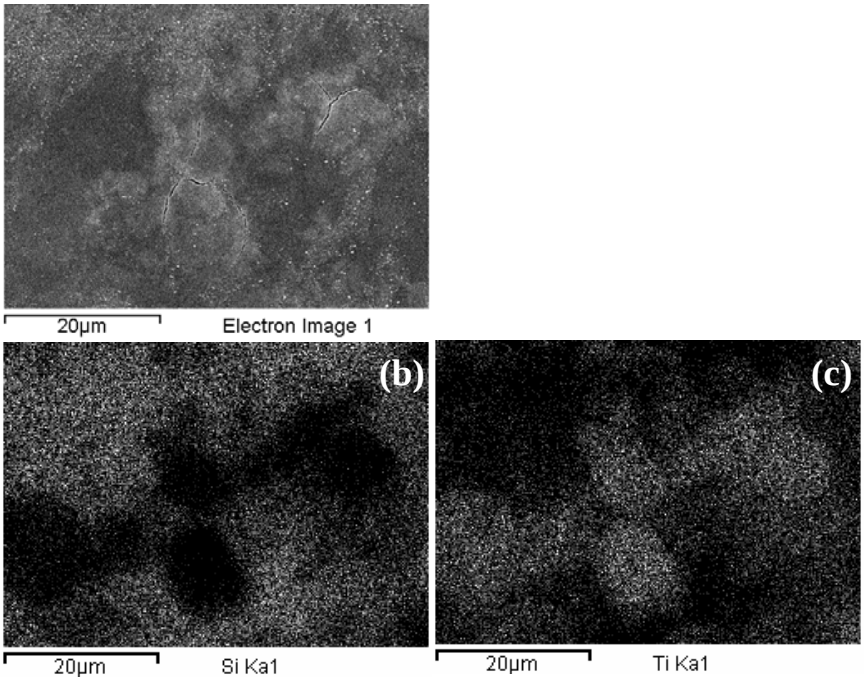

Figure 2.12 FESEM and EDS images for poorly-mixed (SiO2+TiO2) sample (1:2 MSR, 5 minutes, 1400-850 µm magnet size). (a) SE image, (b) Si elemental mapping, (c) Ti elemental mapping.

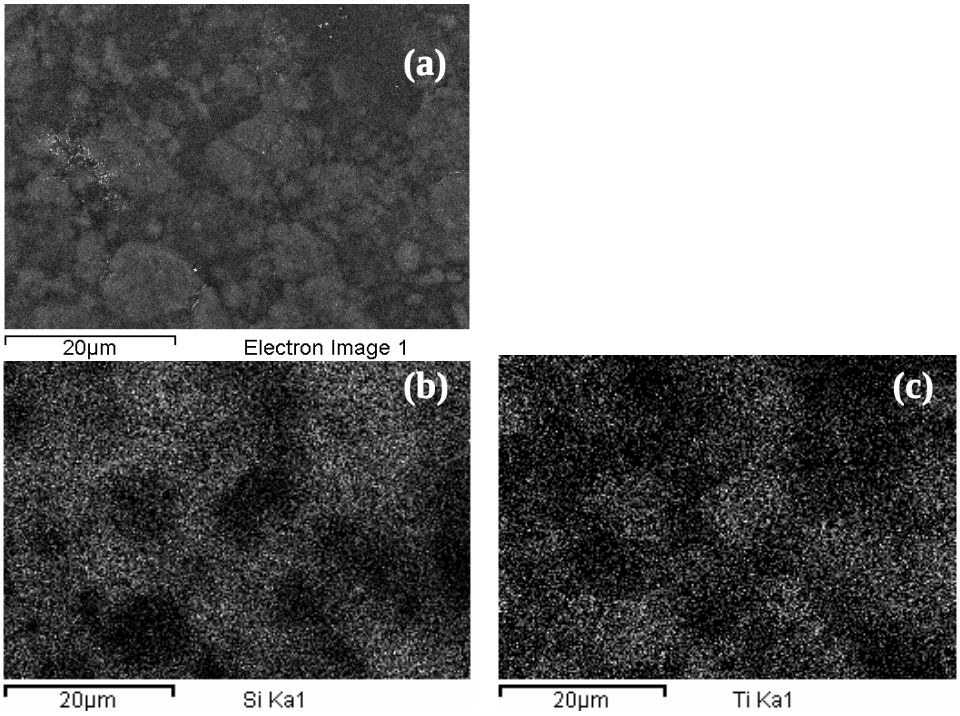

Figure 2.13 FESEM and EDS images for (SiO2+TiO2) sample (1:2 MSR, 10 minutes, 1400-850 µm magnet size). (a) SE image, (b) Si elemental mapping, (c) Ti elemental mapping.

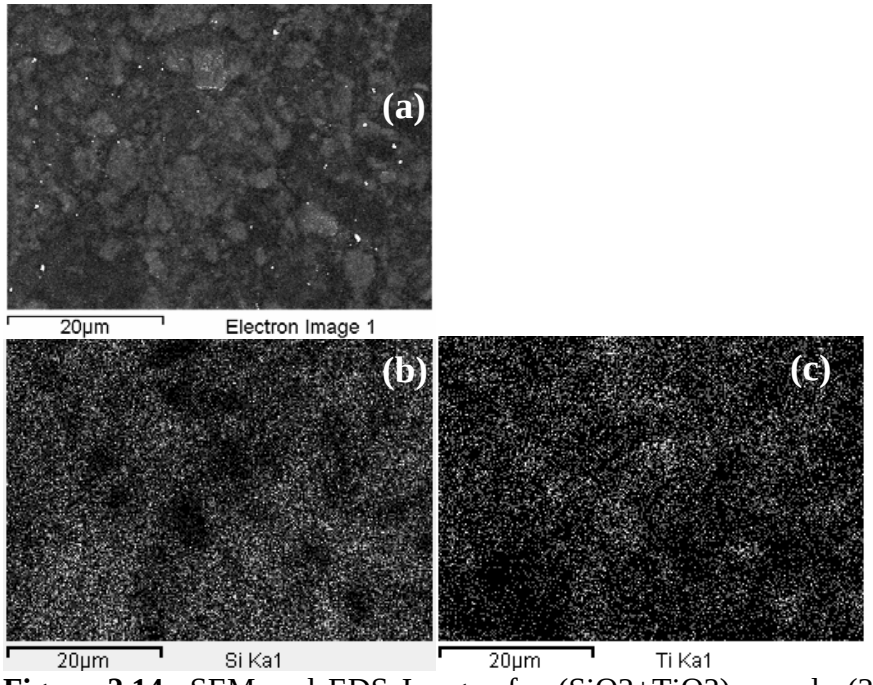

Figure 2.14 SEM and EDS Images for (SiO2+TiO2) sample (2:1 MSR, 10 minutes, 1400-850 µm magnet size). (a) SE image, (b) Si elemental mapping, (c) Ti elemental mapping.

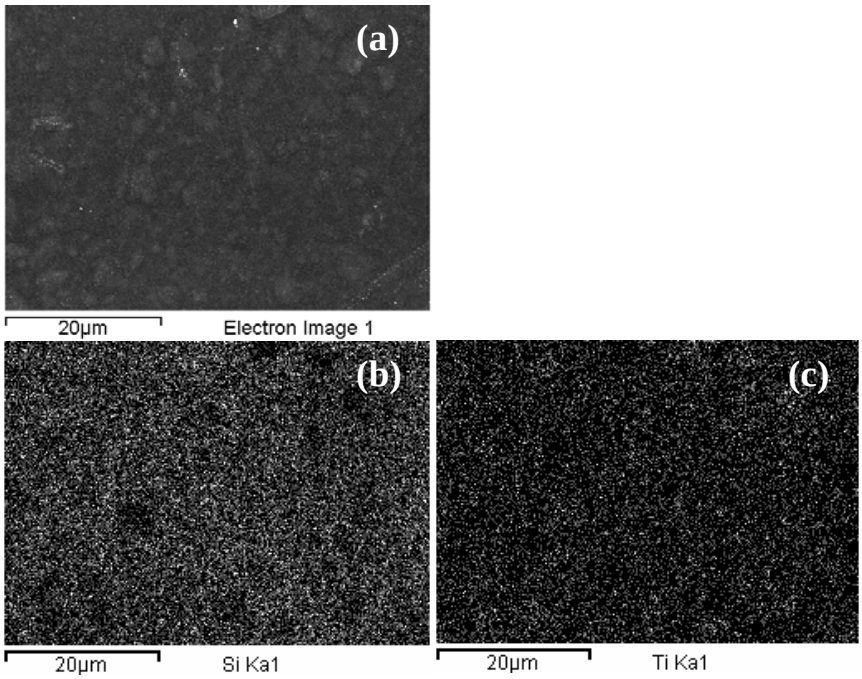

Figure 2.15 SEM and EDS Images for (SiO2+TiO2) sample (5:1 MSR, 10 minutes, 1400-850 µm magnet size). (a) SE image, (b) Si elemental mapping, (c) Ti elemental mapping.

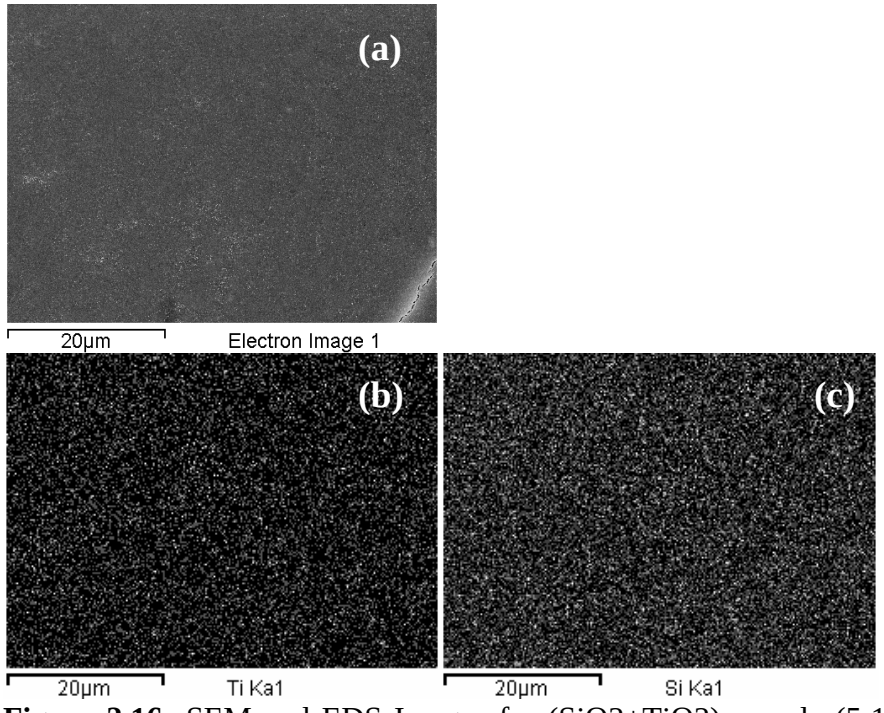

Figure 2.16 SEM and EDS Images for (SiO2+TiO2) sample (5:1 MSR, 120 minutes, 1400-850 µm magnet size). (a) SE image, (b) Si elemental mapping, (c) Ti elemental mapping.

Table 2.2 Comparison Between Homogeneity of Mixing and Agglomerate Size

Homogeneity of Mixing	**Approximate Agglomerate size (microns) (Estimated from image)**	
	FESEM	**EDS**
0.5316	45	40
0.7259	20	30
0.8034	10	15
0.8736	15	15
0.9223	7	7
0.9872	< 5	5
0.9985	Below analysis level	

2.6 Transmission Electron Microscopy

Since the EDS-SEM is limited to compositional analysis within the scale of 1-3 microns, transmission electron microscopy is used to analyze mixtures on the nanometer scale. Two TEM models are used to analyze samples: (a) JEOL 2010F TEM with a 2Kx2K GATAN imaging filter (GIF) electron energy loss spectrometer (EELS) and energy filtered transmission electron microscopy (EFTEM) is used to image nanoparticles and (b) LEO 1530 VP Field Emission Scanning Electron Microscope equipped with an Oxford UTW X-ray detector using a beam energy of 15kV and a Zeiss Libra120 EFTEM equipped with a LaB6 filament using a beam energy of 120 kV are used to image the nanoparticle mixtures. Panels (a) and (b) in Figures 2.15 and 2.17 show electron energy loss spectroscopy (EELS) zero-loss and energy filtered transmission electron microscopy (EFTEM), respectively, for two different mixtures, and illustrate good mixing achieved through MAIM. The difference between the images is that for EFTEM, a slit is inserted to collect electron energies in a certain range. The bright areas on the Ti elemental mapping represent the titania in the mixture, while the particles that appear in the zero loss image (2.15a and 2.17a) but not in EFTEM images (2.15b and 2.17b) are the silica particles. The TEM images clearly show that mixing on the scale of primary particles may be achieved using magnetically assisted mixing methods, which would be not possible with conventional dry mixing techniques. While Figure 2.15 and 2.17 correspond to different mixtures magnet-to-sample weight ratios and different processing times, they have the same value for the product of processing time and number of magnets per unit mass of the sample. Figures 2.16 and 2.18 are the EELS spectrum of silica and titania particles within an agglomerate for respective Figures 2.15 and 2.17.

Comparable quality of mixing (down to sub-micron scale) is obtained in both cases, providing evidence for the suggestion that the product of processing time and number of magnets per unit mass of the sample may be the crucial process parameter. In the next few sections, details of these experimental results are discussed. Additional TEM images for the silica R974 and titania P25 mixtures and silica A200 and titania P25 can be found in Appendix B.

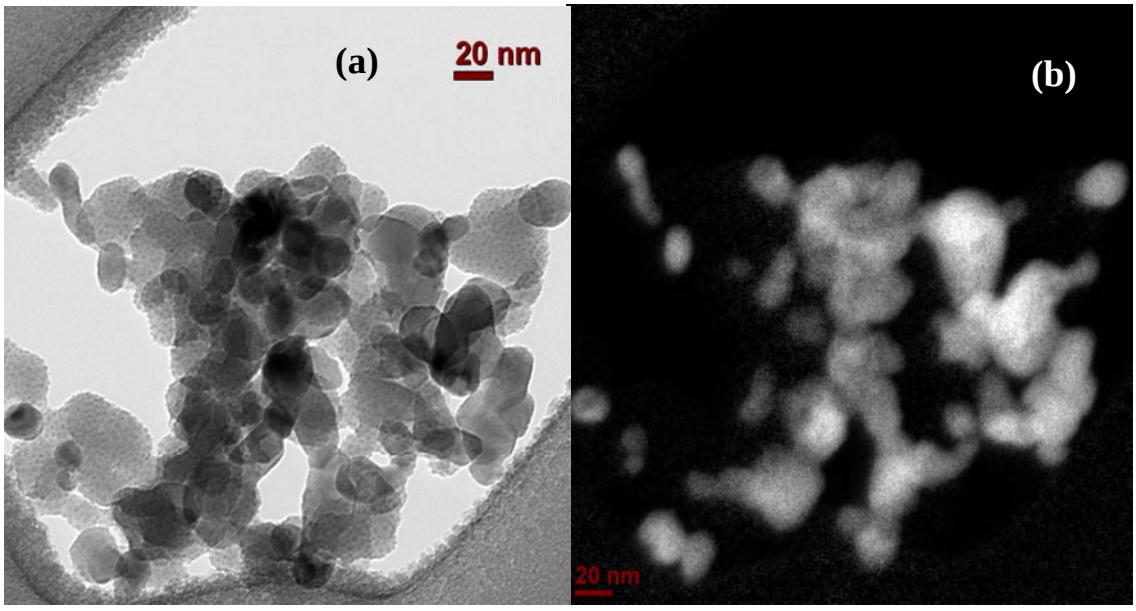

Figure 2.17 (a) EFTEM zero-loss image for well-mixed (SiO2+TiO2) sample (10:1 MSR, 60 minutes, 1400-850 µm magnet size) and the corresponding (b) Ti elemental mapping.

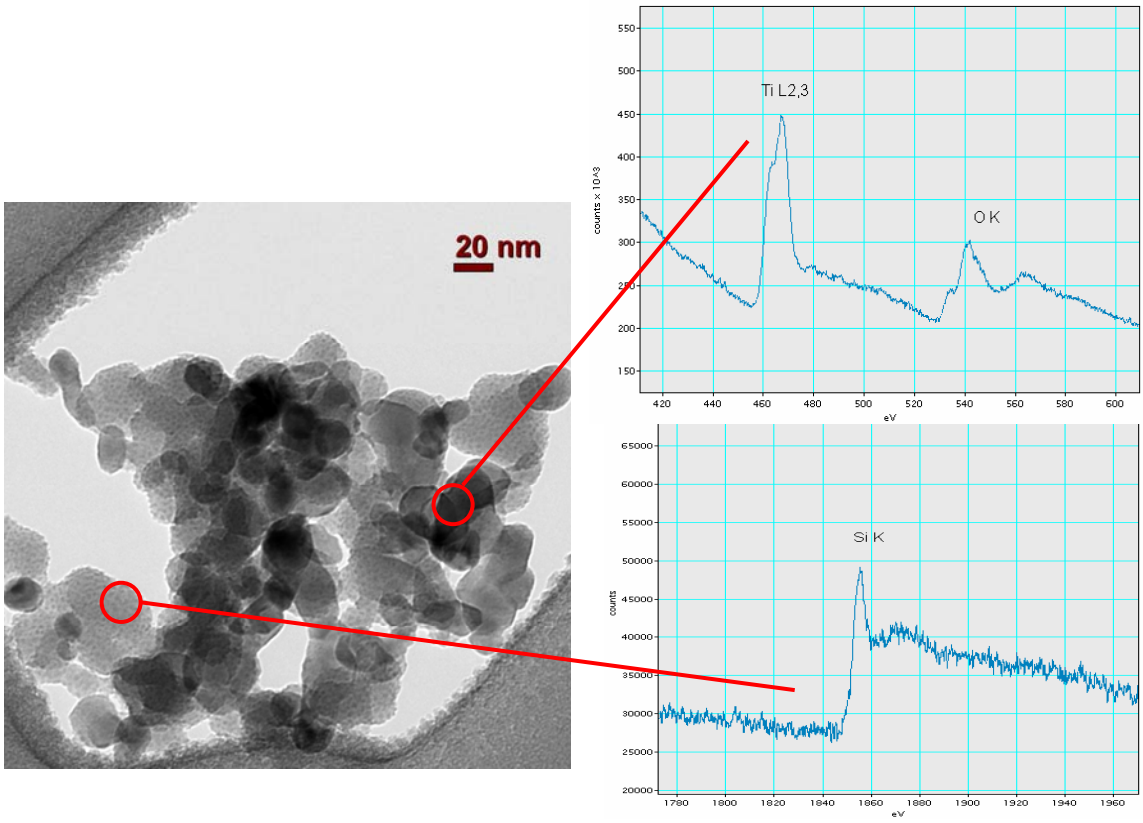

Figure 2.18 EELS spectrum of an agglomerate of silica R974 and titania P25 showing the ionization edges around 455, 530 and 1850 eV, corresponding to the $L_{2,3}$ ionization edge of Ti and the K-shell ionization edges of oxygen and Si, respectively.

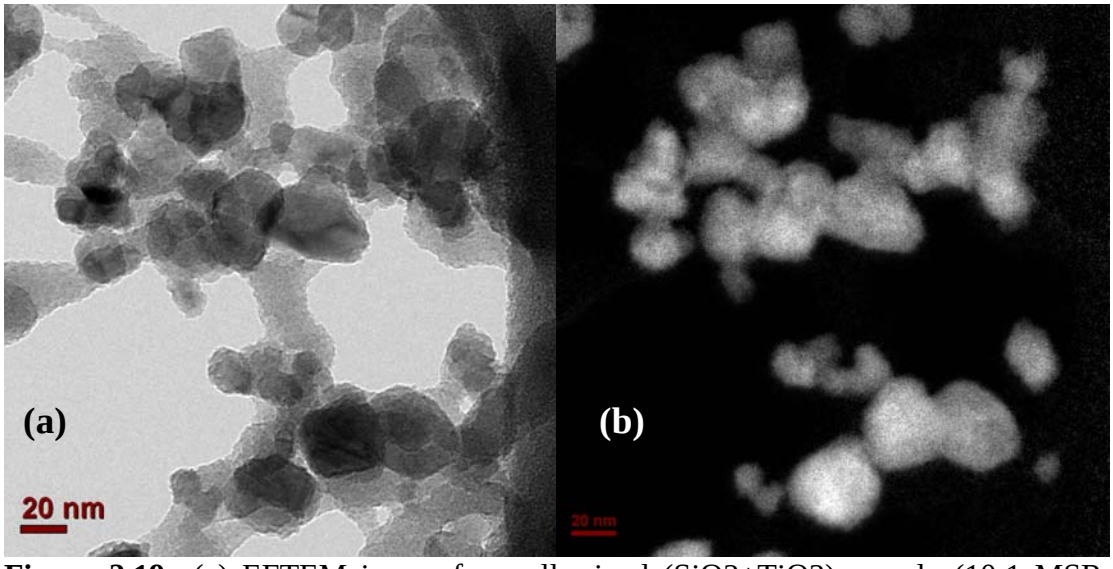

Figure 2.19 (a) EFTEM image for well-mixed (SiO2+TiO2) sample (10:1 MSR, 60 minutes, 1400-850 µm magnet size) and the corresponding (b) Ti elemental mapping.

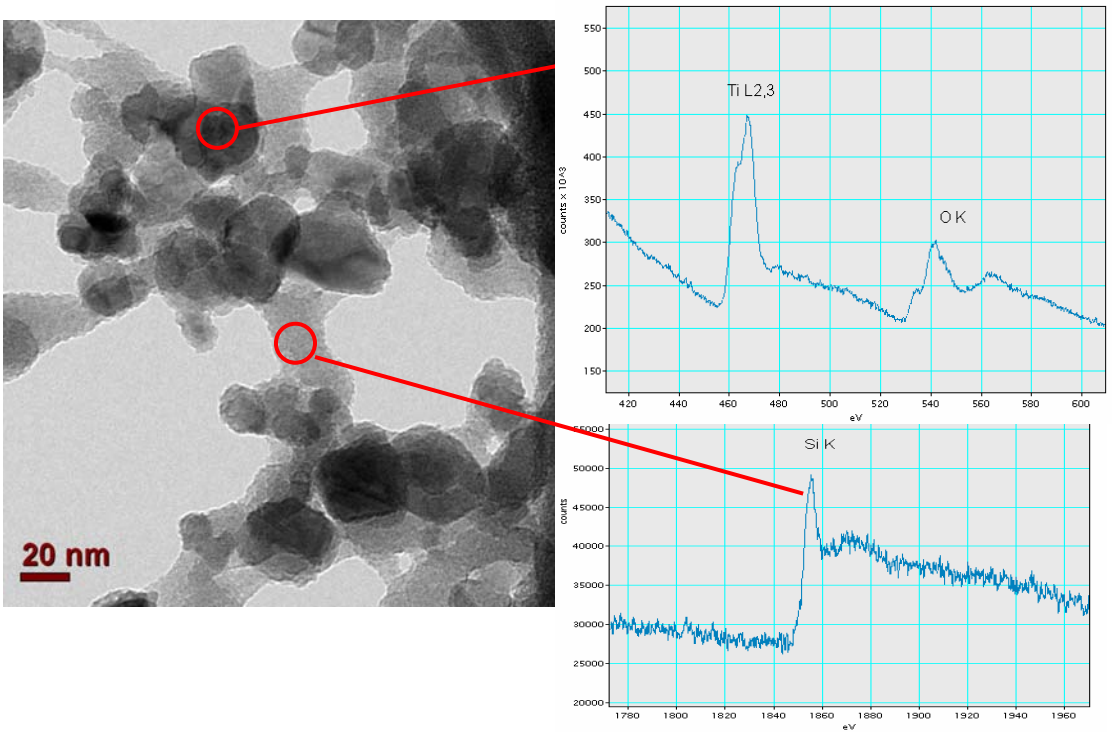

Figure 2.20 EELS spectrum of an agglomerate of silica R974 and titania P25 showing the ionization edges around 455, 530 and 1850 eV, corresponding to the $L_{2,3}$ ionization edge of Ti and the K-shell ionization edges of oxygen and Si, respectively.

CHAPTER 3

MAGNETICALLY ASSISTED IMPACTION MIXING OF NANOSIZED PARTICLES IN LIQUID SUSPENSIONS

Previous magnetically assisted impaction mixing studies are performed as dry systems[1,2]. Many industrial and pharmaceutical mixing processes are performed as liquid suspensions, usually expensive solvents that are harmful to the environment. Liquid magnetically assisted impaction mixing (LMAIM) is an environmentally benign and unique mixing technique that uses magnets to collide with agglomerates. In this study variables are studied to optimize the process to obtain submicron deagglomeration and mixing. Mixing quality obtained is compared to homogenizer and sonication mixing. Before carrying out experiments at various conditions, a preliminary study is performed on the effect of magnet-to-sample ratio on Homogeneity of Mixing.

Initial system optimizations are carried out. First step is to determine an adequate volume of solution. Two grams of nanopowders are added to 30, 60, 130 and 200 mL of deionized water and 4 grams of magnets are added. The experiments are carried out for 15 minutes. 30mL of water was not enough because the mixture turned into a paste and was too viscous for the magnetic particles to move around. For 130 and 200 mL volumes, the nanopowders in suspension formed two layers. The lower layer contained higher concentration of the nanopowders while the upper layer is very dilute. It was determined that the lower layer is where the magnetic shearing occurs and by having too much liquid volume would leave mixtures with a lower Homogeneity of Mixing value. It is determined that 60mL of solvent would be adequate to dilute the two grams of powder, while keeping the powders in a single, high concentration volume. The next step was to

determine powder loading. Experiments are run with 1 and 2 grams of nanopowder loading. A 5:1 magnet-to-sample weight ratio (MSR) is used for both loading. Three processing times, 30 60 and 120 minutes, are investigated. The Homogeneity of Mixing is calculated using the EDS compositional point analysis. The results indicated that a higher powder loading provided better results than the lower concentration.

3.1 Homogeneity of Mixing versus Time

In order to study the effect of processing time, nano-powders Aerosil® silica A200 and Aeroxide® titania P25 are processed for different magnet-to-sample ratios in water for the MAIM device. Processing times of 5 through 240 minutes are plotted with various magnet-to-sample ratios of 1:2, 1:1, 2:1, 5:1 and 10:1, and the results are shown in Figure 3.1 as Homogeneity of Mixing versus Time. It is observed that as processing time increases, there is an increase in the Homogeneity of Mixing, leading to a better mixture. It should be pointed out that the lines connecting the points in the figures are for the sake of visual clarity. As with the magnet-to-sample ratio, when there is an increase in the processing time, there are more interactions of the moving and rotating magnets with the agglomerates of nanoparticles promoting deagglomeration and mixing.

Homogeneity of Mixing versus time multiplied by the magnet-to-sample ratio is plotted as shown in Figure 3.2 for the magnet-to-sample ratios of 1:2, 1:1, 2:1, 5:1, and 10:1 and a magnet size range of 1400-850 microns for SiO_2/TiO_2 mixtures. The same data is also shown versus time times the number of magnets in Figure 3.3. These transformations of the data from Figure 3.1 results in a collapse of the multiple curves, and a single trend is evident for all the values of magnet-to-sample mass ratios. Since

both trends hold true for the data in this chapter, the data in the next sections are presented as Homogeneity of Mixing versus time multiplied by the number of magnets.

In order to test the reproducibility of the data obtained, ANOVA with replication technique is used for the present study.[3] Results indicated that there is no significant statistical difference between the two selected test runs for the samples with higher magnets to sample weight ratio as well as for the longer processing time.

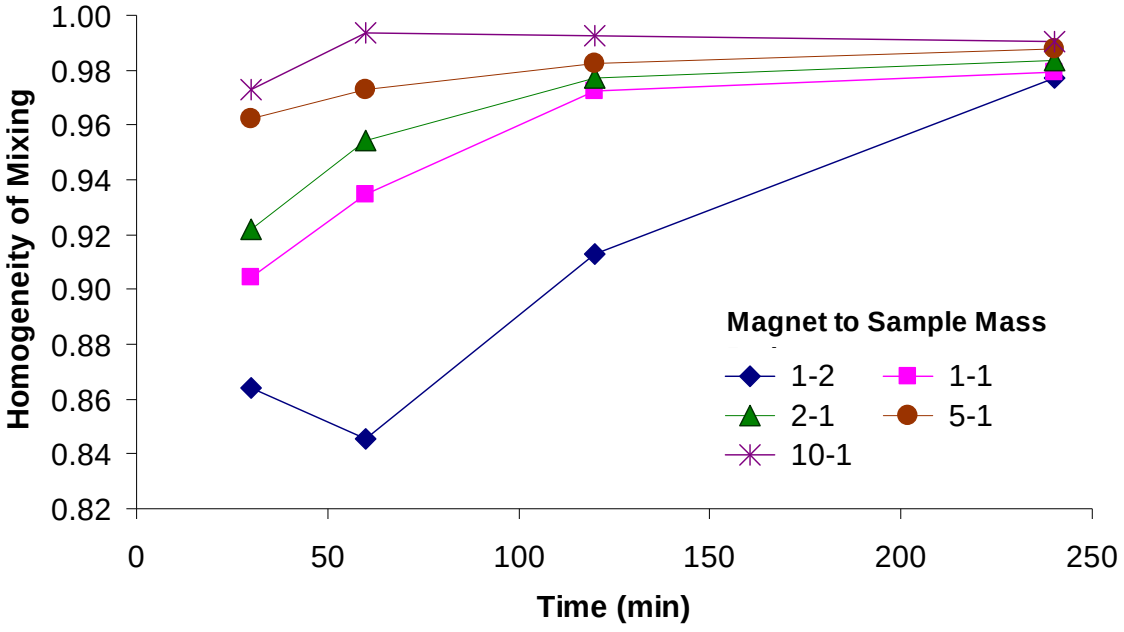

Figure 3.1 Homogeneity of Mixing versus time for various mixing times and magnet-to-sample ratio for SiO2/TiO2 mixtures and a magnet size range of 1400-850 microns.

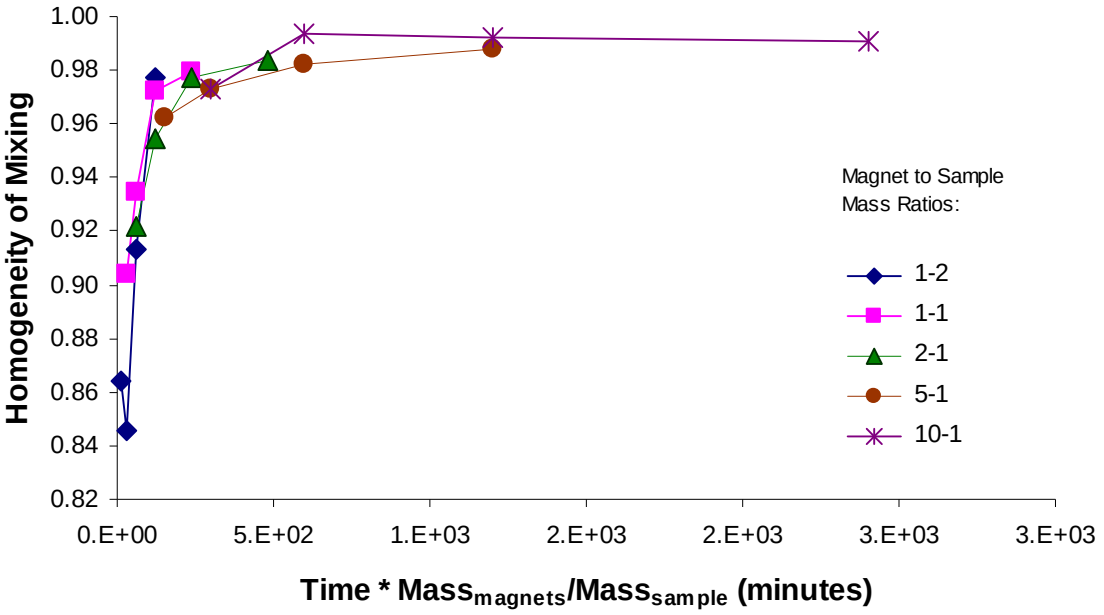

Figure 3.2 Homogeneity of Mixing versus time*magnet-to-sample ratio for SiO2/TiO2 mixtures and a magnet size range of 1400-850 microns.

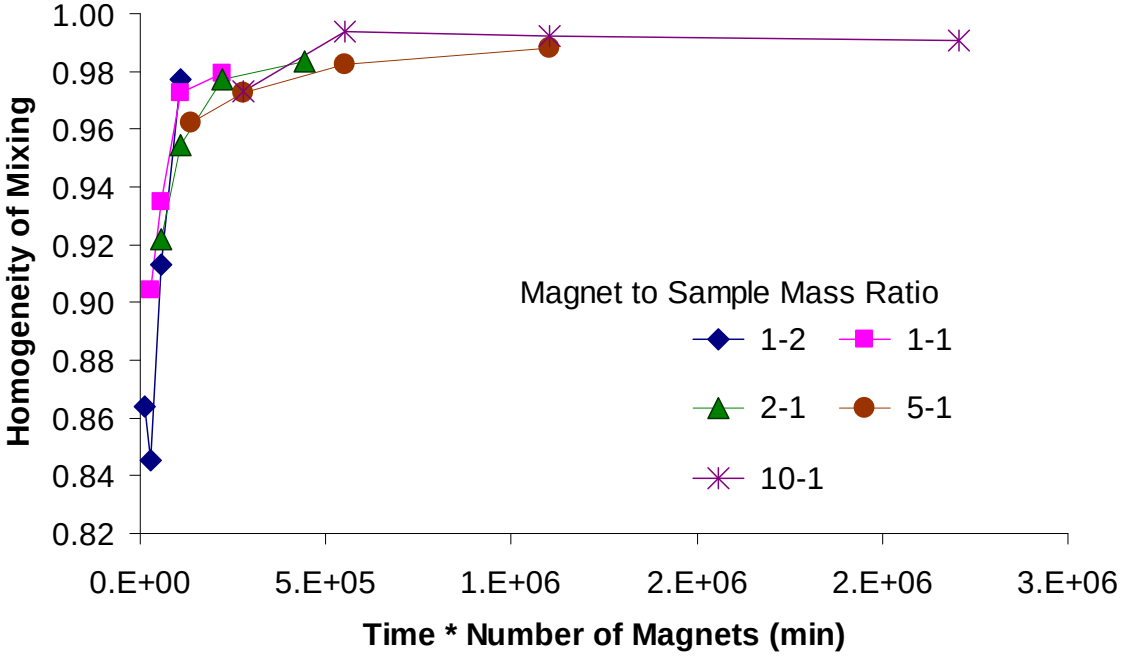

Figure 3.3 Homogeneity of Mixing versus time*number of magnets for SiO2/TiO2 mixtures and a magnet size range of 1400-850 microns.

The results obtained so far suggest that the main process control factor for the mixing quality is related to total number of collisions per mass of nano-powder mixture. To be more general when the magnet sizes vary in different experiments, the control factor for the number of collisions is expected to be the amount of magnets per the mass of the powder sample. That means that the main process control factor for the mixing quality is related to total number of collisions per mass of nano-powder sample, which is proportional to the processing time multiplied by the number of magnets used for a given mass of powder sample. The number of magnets present in the mixture is estimated by counting the magnets per gram for a given magnet size range. Thus the hypothesis is proved and that the Homogeneity of Mixing increases as the product of the amount of magnets with time increases.

3.2 Homogeneity of Mixing versus Drying Technique

In wet mixing, drying time can be a very important process. It can be time consuming and costly in the production line. In the initial experiments, processed samples are dried overnight in an oven at 150 ºC. During this time, the solids would fall out of suspension leaving a dilute layer above and a denser layer below. Using EDS analysis, the dilute surface layer had a higher concentration of titania than silica. It is to be noted that while the titania stayed suspended longer, the surface layer is very dilute that the majority of the titania is located in the dense lower layer. During this drying time, segregation could occur by density stratification and electrostatic separations which would adversely affect the homogeneity of the mixture. To avoid the separation that occurs during drying, samples are filtered out of suspension. The magnets are sieved out first and the powders

are collected from suspension using filter paper. A vacuum is attached to expedite the filtration. The remaining moist sample is further dried in a safety hood or in an oven. The Homogeneity of Mixing for vacuum filtered results are compared with the oven dried results in Figure 3.4. While the vacuum filtration process expedited the drying time, the results show no negligible differences in the mixing homogeneity. Since there is no difference, the settling of the nanoparticles during the oven drying does not play a major role in the mixing homogeneity. The rest of the experiments in the chapter, unless otherwise stated, are dried in the oven.

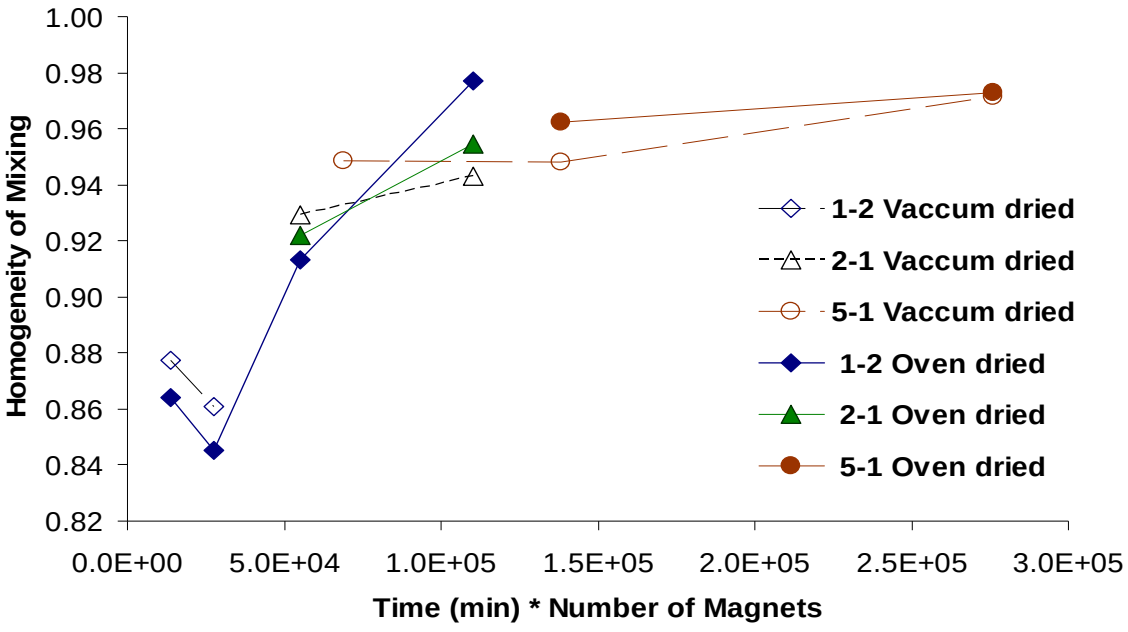

Figure 3.4 Homogeneity of Mixing versus time*number of magnets for separate drying techniques for SiO2/TiO2 mixtures and a magnet size range of 1400-850 microns.

3.3 Homogeneity of Mixing versus Liquid Medium

The goal of the research is to use an environmentally benign technique that can perform as well, or better, than current mixing techniques. Mixing in water removes the necessity of using harmful and expensive organic liquids. By testing different solvents, the dependence on viscosity on mixing homogeneity can be obtained. An advantage of using other solvents besides water is that hydrophobic powders can also be mixing constituents. Besides water (1 centipoise, 1g/mL), mixtures containing solvents of methanol (0.59 cP, 0.7918 g/mL), acetone (0.32 cP, 0.7925g/mL) and hexane (0.29 cP, 0.6548 g/mL) are examined in this section. The Homogeneity of Mixing versus time and the number of magnets for the different solvents are shown in Figure 3.5. Mixtures of silica A200 and titania P25, both hydrophilic, are used in these experiments. The results show no significant difference for the polar solvents (acetone, methanol and water). The hexane results provided slightly lower values of Homogeneity of Mixing for low values of time and number of magnets, but with higher times and number of magnets, the hexane performed similarly to the results from the other solvents. This could be due to the fact that hexane is nonpolar.and the constituents are hydrophilic. During storage, the particles could undergo moisture adsorption, from the atmosphere, creating liquid bridges and moisture coatings. Since the hexane is nonpolar, it will not be able to penetrate the water and preventing the agglomerates from becoming saturated. Overall, not much difference is observed between solvents promoting the benefit of magnetically assisted mixing as an environmentally benign mixing method.

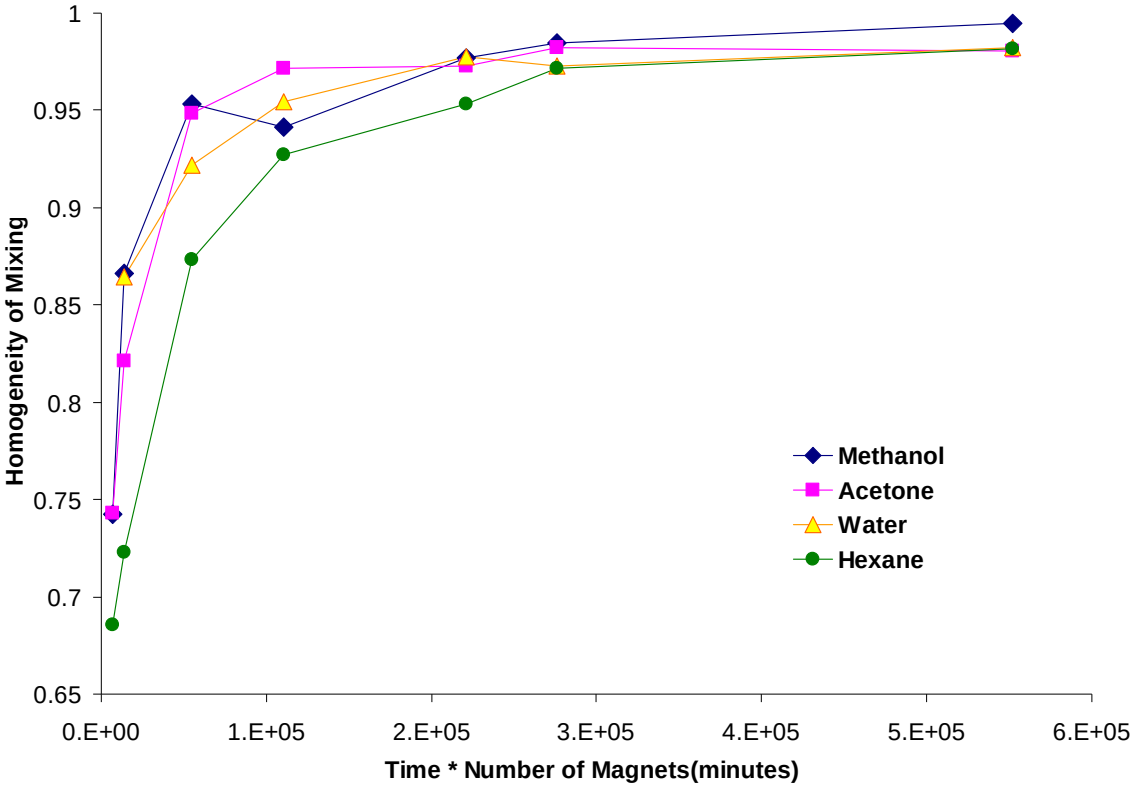

Figure 3.5 Homogeneity of Mixing versus time*number of magnets for different liquid mediums for SiO2/TiO2 mixtures and a magnet size range of 1400-850 microns. Magnet-to-sample ratio 2-1.

3.4 Effect of pH and Surfactant Concentration on Homogeneity of Mixing

According to DLVO (Derjaguin Landau Verwey Overbeek) theory, when nanopowders are suspended in solution, they form larger agglomerates due to Brownian motion collisions. Eventually the agglomerates grow large enough where they settle. The individual particles can only remain in suspension if there is a mechanism to prevent them from adhering. By this determination, another method to maintain particles in suspension longer is to alter the pH and add a surfactant. Metal oxides usually have a hydroxide outer layer which is amphoteric. When altering the pH, the particles will become charged and repel the each other. Equations 3.1 and 3.2 represent the two

reactions which take place in acid and basic solutions, respectively. 1 molar of NaOH solution is added to the suspension to raise the pH from 4, normal pH of suspension, to a more basic pH, and HCl is added to make the suspension more acidic. Homogeneity of Mixing results are compared for pH values from 2 through 13, including 6.5 and 7.5, for a magnet-to-sample ratio of 2-1 and a processing time of 60 minutes (Figure 3.6).

$$M\text{-}OH + H^{+} \rightarrow MOH_2^{+}$$

$$M\text{-}OH + OH^{-} \rightarrow M\text{-}O^{-} + H_2O \qquad (3.2)$$

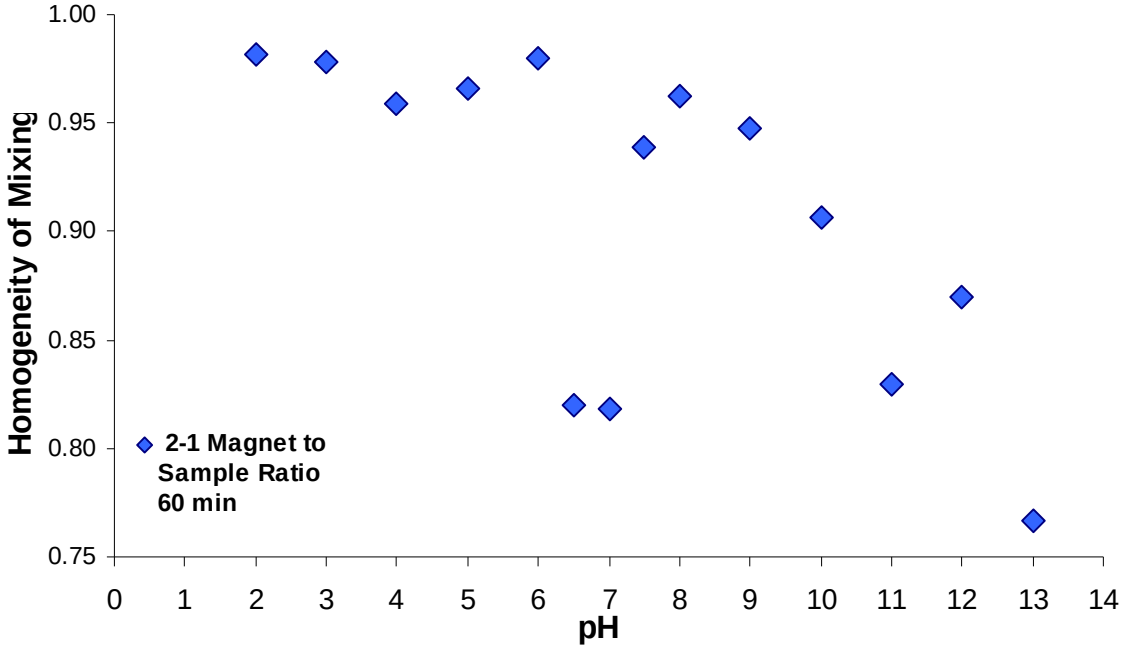

Figure 3.6 Homogeneity of Mixing versus pH for SiO2/TiO2 mixtures run with a 2-1 magnet-to-sample ratio, processed for 60 minutes with magnet of size range 1400-850 microns.

The results show that higher values of Homogeneity of Mixing are obtained at more acidic pH values, while the more basic values showed a much lower value for HoM. At the pH values of 6.5 and 7, a lower value for HoM is also obtained. Since all charges are neutral at pH of 7, no surface charges are present to repel the individual particles, resulting in larger agglomerates in suspension. The agglomeration causes poorer mixtures. All the Homogeneity of Mixing versus pH results are obtained by oven drying the samples overnight. To further investigate the settling effect of the suspension at different pH values, the samples are vacuum dried at pH values of 2, 4, 6, and 7. The results in Figure 3.7 are run with a 2-1 magnet-to-sample ratio for 60 minutes.

While no significant difference is shown for the previous drying study, all the results except pH 7 showed approximately 0.015 increases in HoM. The results are repeated for 5-1 magnet-to-sample ratio and vacuum drying in Figure 3.8. The same trend as 2-1 is observed with 5-1; however, as expected, higher HoM values are obtained with the 5-1 samples.

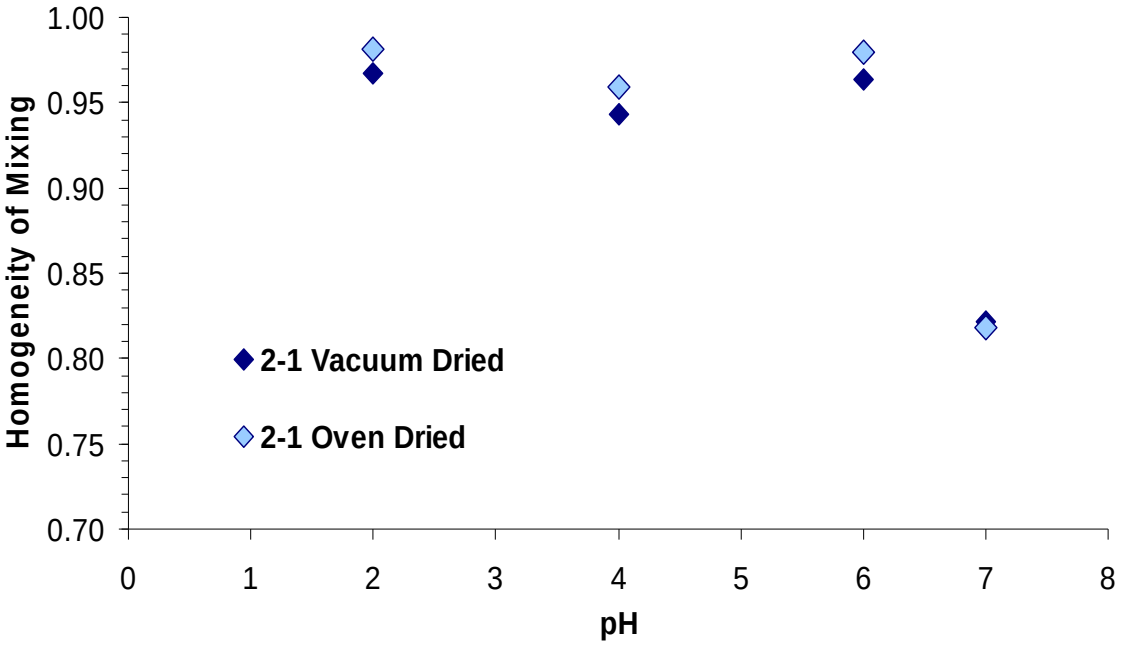

Figure 3.7 Homogeneity of Mixing versus pH for different drying methods with SiO2/TiO2 mixtures and a magnet size range of 1400-850 microns. Samples run with a magnet-to-sample ratio of 2-1 for 60 minutes.

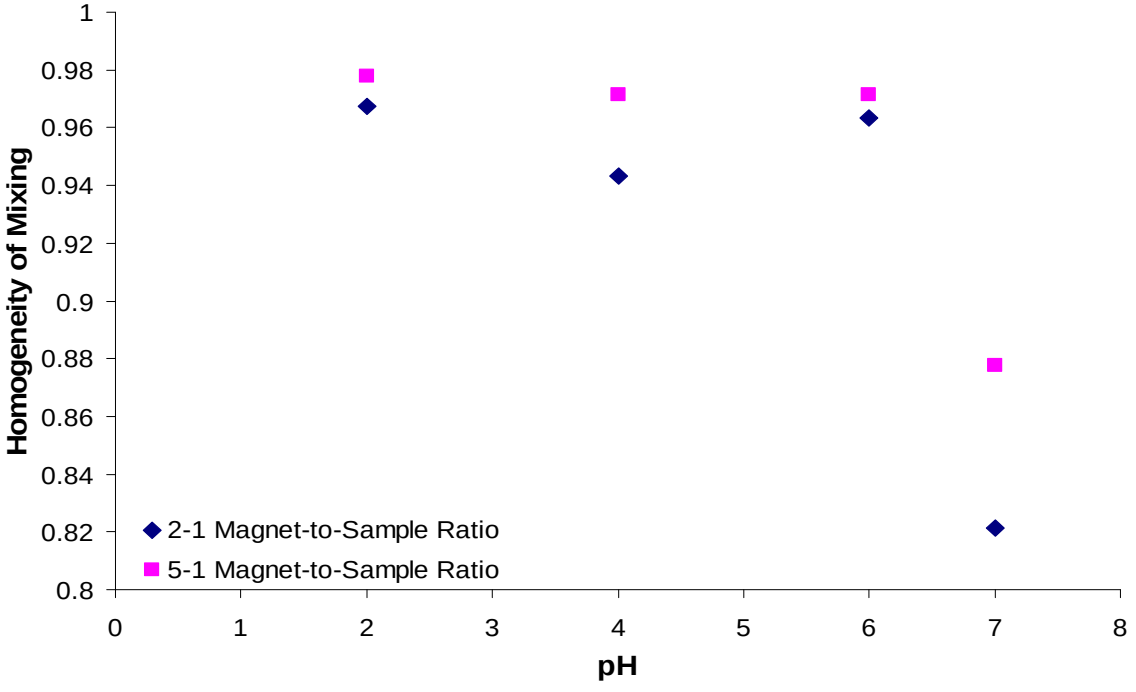

Figure 3.8 Homogeneity of Mixing versus pH for SiO2/TiO2 mixtures and a magnet size range of 1400-850 microns. Samples are vacuum dried and run with 2-1 or 5-1 magnet-to-sample ratio and 60 minutes processing time.

To determine the sizes of particles in solution, particle size analysis is performed on individual constituents in solution at different pH values prior to MAIM processing, Table 3.1. The titania dispersed into solution with less agitation than the silica and remained in suspension longer and the particle size analysis shows that the titania disperses in finer agglomerates (around 1 micron) allowing it to remain suspended longer. In suspension the silica formed agglomerates of 39 microns and higher. The silica is processed with a 5-1 magnet-to-sample ratio for 60 minutes at pH values of 4, 7 and 11. In all cases the agglomerate sizes are reduced below a micron in size. The samples are tested again the following day, and while the agglomerates remain fairly constant at pH values of 4 and 11, at pH 7 the agglomerates grew in size over 25 microns. The particle size analysis proves that at a pH of 7, if the constituents remain in suspension for extended periods of time, large agglomerates will form promoting poorer mixing.

Table 3.1 Particle Size Analysis on of Silica and Titania

pH	P25 TiO_2 (before MAIM)	A200 SiO_2 (before MAIM)	A200 SiO_2 (after MAIM)	A200 SiO_2 (24 hrs after MAIM)
2	0.976	39.64	-	-
4	1.921	43.56	0.599	0.733
6	1.93	46.96	-	-
7	1.287	49.32	0.466	25.65
8	1.953	46.19	-	-
11	0.723	45.01	0.509	0.401

Adding a surfactant to lower the surface tension of the liquid and allowing samples to remain disperse is another option that may help obtain higher Homogeneity of Mixing values. In the study, polysorbate 80 (Tween 80) is used as a surfactant to try keep particles segregated during and after mixing. Tween 80 is added for different percentages of the critical micelle concentration (CMC). The CMC point, 100%, is the concentration of surfactant where micelles are spontaneously formed. The critical micelle concentration for Tween 80 is 0.012mM. HoM data is analyzed using CMC values of 25 and 100percent and comparing the results to mixtures without surfactant added. Tween 80 is added at the beginning of the process. Another run is performed by adding 100% CMC at the last 5 minutes of the process when much of the deagglomeration has occurred and there is still time to disperse the surfactant. The Homogeneity of Mixing results, Figure 3.9, show negligible change at low pH values. The best improvement in Homogeneity of Mixing is obtained at pH 7 when adding 100% CMC toward the end of the process. pH 7 is also the point where 25% and 100% of the CMC show lower HoM values. At the pH of 10, 100% CMC showed significant improvement for both added at the beginning and toward the end of the process.

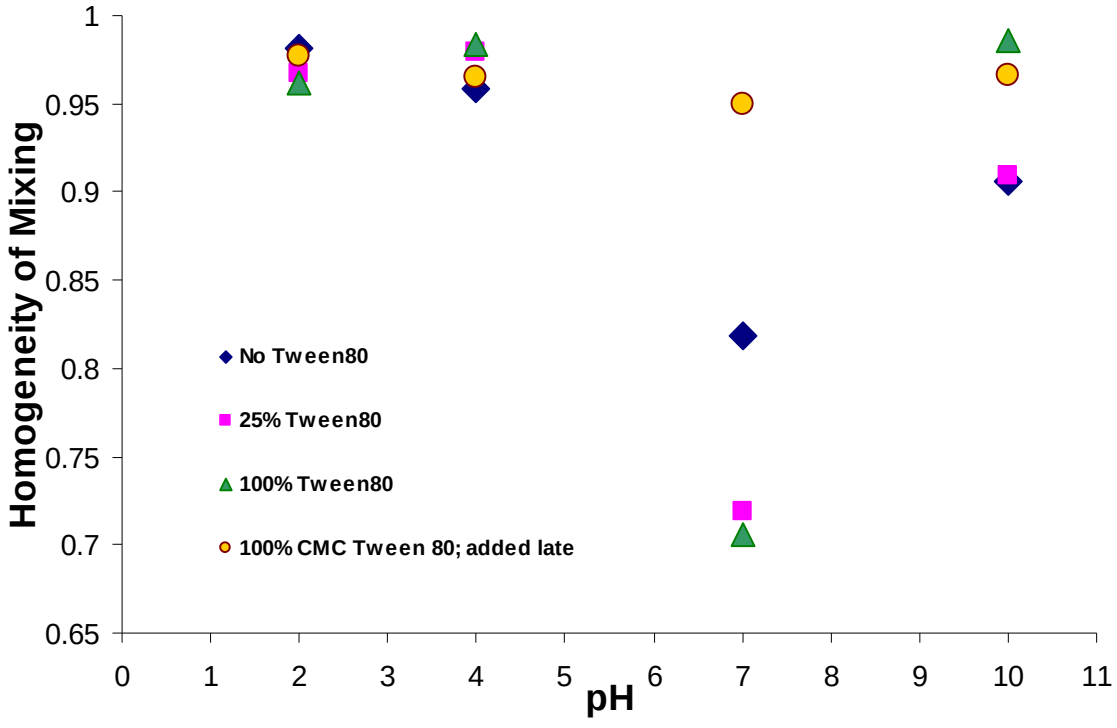

Figure 3.9 Homogeneity of Mixing versus time*pH for different CMC percents of Tween 80 for SiO2/TiO2 mixtures and a magnet size range of 1400-850 microns. Run at a magnet-to-sample ratio of 2-1 and 60 minute processing time.

3.5 Homogeneity of Mixing versus Magnetic Field Strength

In order to study the effect of the magnet field, nano-powders are processed for different magnetic field strengths. The field strength is altered by using a Variac controller to change the voltage. Processing times of 10, 30 and 60 minutes and magnet-to-sample ratios of 5-1 and 2-1 are used in the experiments. Magnetic field strengths of 18.7 (39V) is chosen to compare with the data collected at 43.6 (98V) mT. With higher field strengths the magnetic particles should undergo faster translational motion and impact agglomerates with more force. The higher force should create more deagglomeration and homogeneity in the mixing; however, when the coils overheat, an internal controller is triggered to turn off the coils. Initially, all settings run constantly, but eventually enter a

phase of repeated off-on cycle. The higher voltage settings, stronger magnetic fields, enter the repeat cycle sooner than the low voltage settings. It should be noted that this off-on cycle occurs when a container with magnetic particles is placed in the coil. Without magnetic particles the coils have remained on for 2 hours in some attempts.

Since recording field strength data with magnetic particles present in the system could damage the probe, collecting accurate field strength measurements has been difficult. In this study, which used processing times up to an hour, the 18.7mT field strength setting did not reach the repeat off-on cycle in this study. So a comparison of an intermittent field strength of 43.6 mT is compared to a constant field strength of 18.7 mT. Once the field strength is accurately collected, an averaged value of magnetic field strength will be used to represent the data. The resultant Homogeneity of Mixing versus time multiplied by the number of magnets for the different magnet field strengths is presented in Figure 3.10. It is visible that for the same field strengths, the different magnet-to-sample ratios can be represented by a single trend line. It is evident that a lower field strength run constantly will achieve better mixing than a higher field strength run intermittently. The next step in the study is to take into account the actual processing time, run time. It is determined that when a magnetic field strength of 43.6mT is generated, the field remains on for approximately 56% of the time. In the time frame for this study, the 18.7mT magnetic field remained on constantly. When taking into account the correction to the processing time, the two trends previously obtained in Figure 3.11 collapse into a single trend (Figure 3.12). So from the data, there is no significant difference when operating at a field strength of 18.7mT through a strength of 43.6mT.

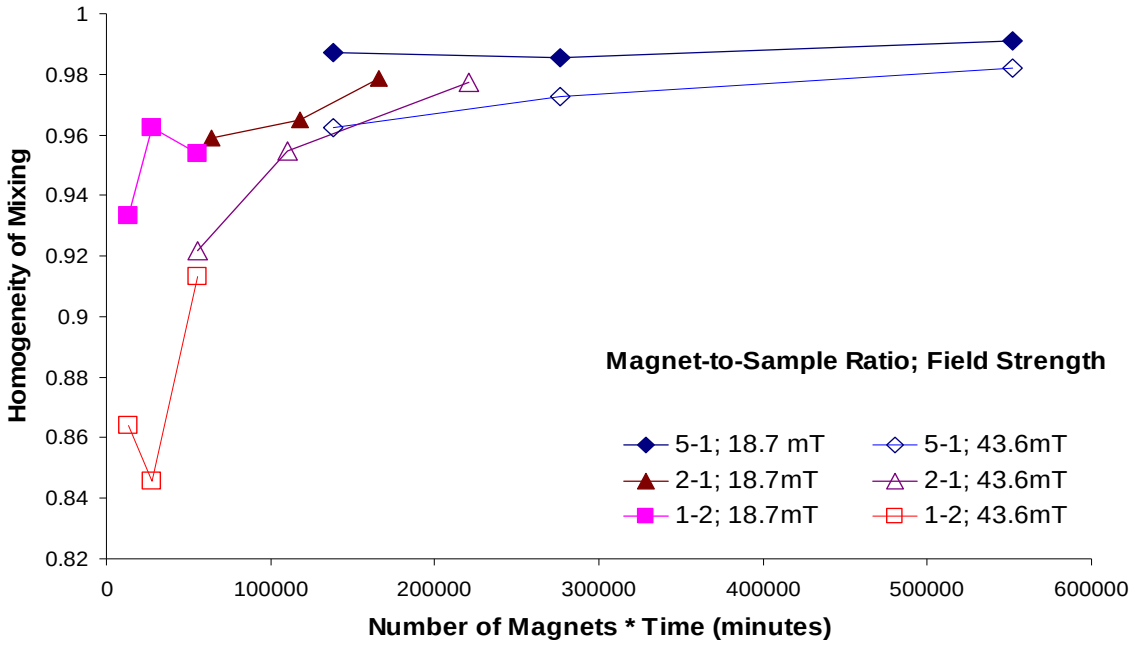

Figure 3.10 Homogeneity of Mixing versus time*number of magnets for magnet-to-sample mass ratios of 1-2, 2-1, and 5-1 with a magnet size range of 1400-850 microns for magnetic field strengths of alternating 43.6 mT and constant 18.7mT.

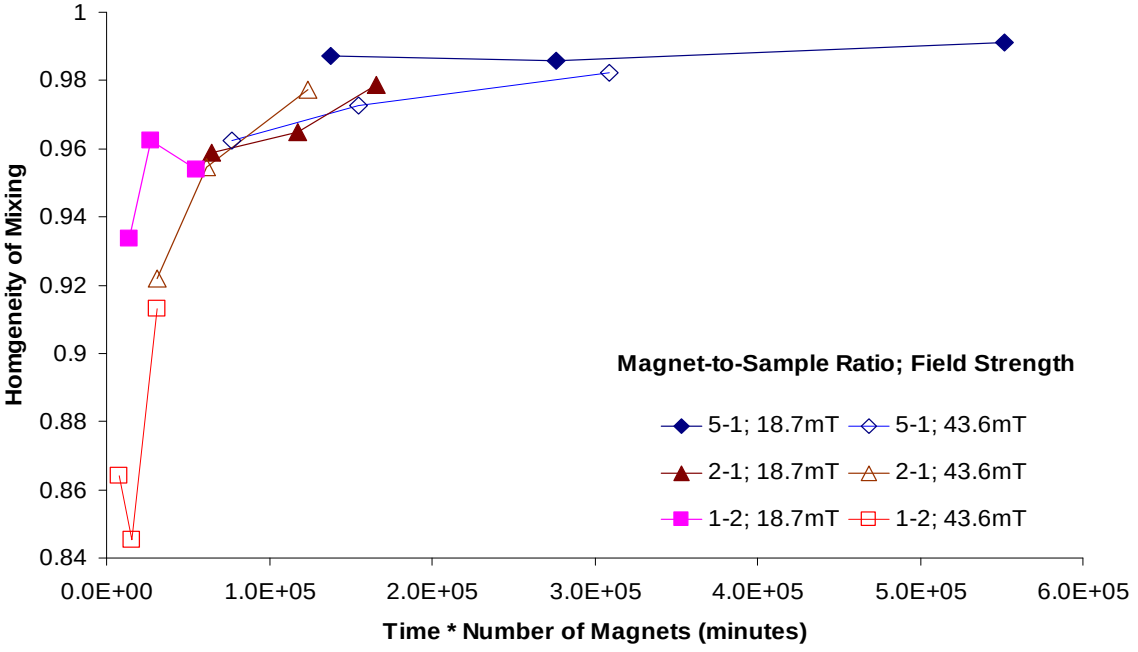

Figure 3.11 Homogeneity of Mixing versus run time*number of magnets for magnet-to-sample mass ratios of 1-2, 2-1, and 5-1 with a magnet size range of 1400-850 microns for magnetic field strengths of 43.6 mT and constant 18.7mT.

3.6 Comparison of liquid MAIM with Other Mixing Methods

A systematic study of the deagglomeration of the SiO2 – TiO2 suspensions, dispersed in deionized water, versus time. The liquid systems compared are magnetic impaction, homogenizer and sonication. Particle size analysis is completed at set time intervals for two individual setting for each of the mixing techniques, Figure 3.13. The results show that sonication is the best instrument for deagglomeration. Since ultrasonic sonication has shown such promising results to deagglomerate nanoparticles in suspension,[4-7] much attention is focused on sonication research. The sonication and homogenizer deagglomerate only two a certain scale until it reaches a plateauing effect. The plateau is reached within 30 minutes of deagglomeration. The magnetic assisted impaction method showed the least deagglomeration power of the three methods. After an hour of processing, a definite plateau is not reached. Visually, the suspensions undergo more intense macro operation for the homogenizer and the sonication. Since the magnetic particles create microshear areas, there may only be enough shearing forces momentarily break the agglomerates and mix them, however to keep the particles in a deagglomerated form, additional shearing would be required.

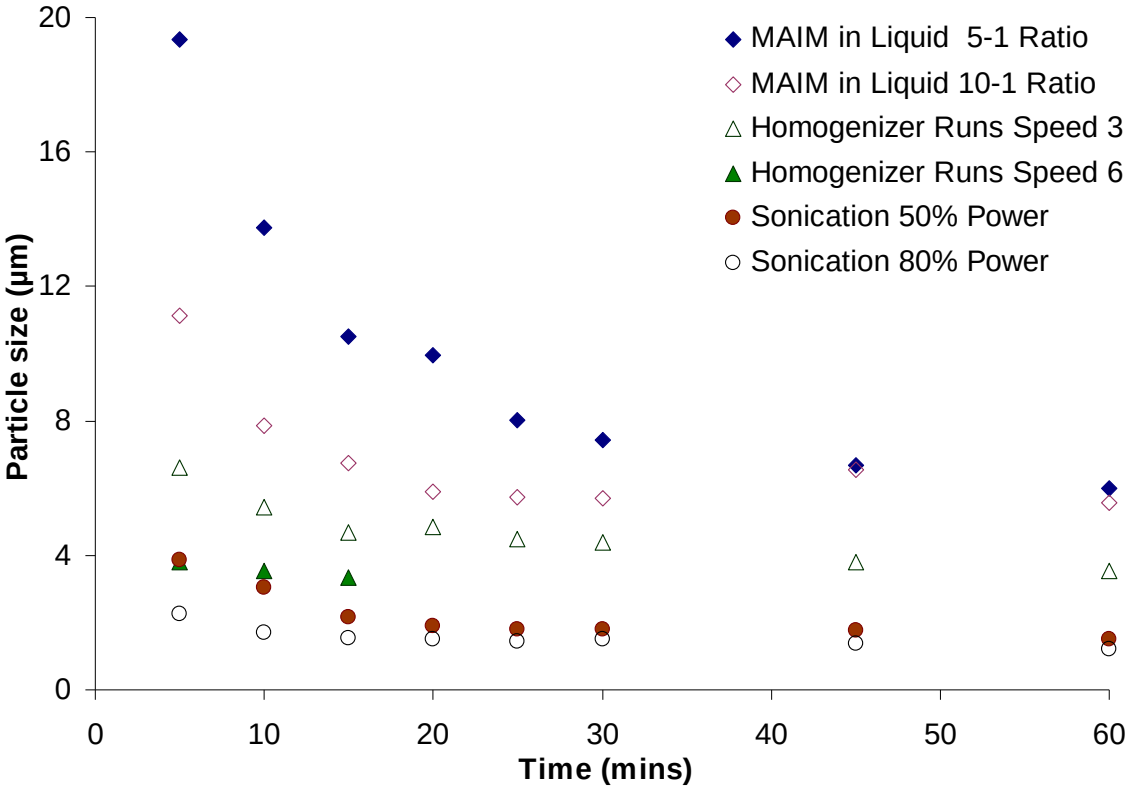

Figure 3.12 Particle size versus time of mixtures of silica A200 and titania P25 for different liquid mixing processes.

A systematic study to compare the Homogeneity of Mixing obtained from LMAIM is compared to mixing results obtained using pitched impeller blades, a homogenizer and a sonic horn. For the homogenizer and the sonic horn, two different power settings will be used to for multiple times. The pitched impeller blade runs at 300 rpm in an unbaffled system. Since these techniques are currently used in industry, obtaining comparable results in mixture homogeneity is an important step to validate the LMAIM process and is the purpose of this section. Impeller blade mixing provided the worst results of the methods. The results are very comparable to magnetically assisted mixing with a magnet-to-sample ratio of 1:2. The homogenizer speed settings of 3 and 4, to rpm, results compared similarly to magnetically assisted with a 10:1 MSR. There

seems to be slight increases in mixing quality for each increase in revolutions per minute. Sonication provided the best mixing results of the different methods examined. The Homogeneity of Mixing does not seem to change much from 50% amplitude to 80%. The quality of mixing obtained by sonication after 30 minutes is similar to the homogenizer (rpm) and the magnetically assisted mixing of 10:1 MSR run for 60 minutes. These results indicate that magnetically assisted impaction mixing in liquid mediums can provide similar mixing results to those of techniques currently used in industry.

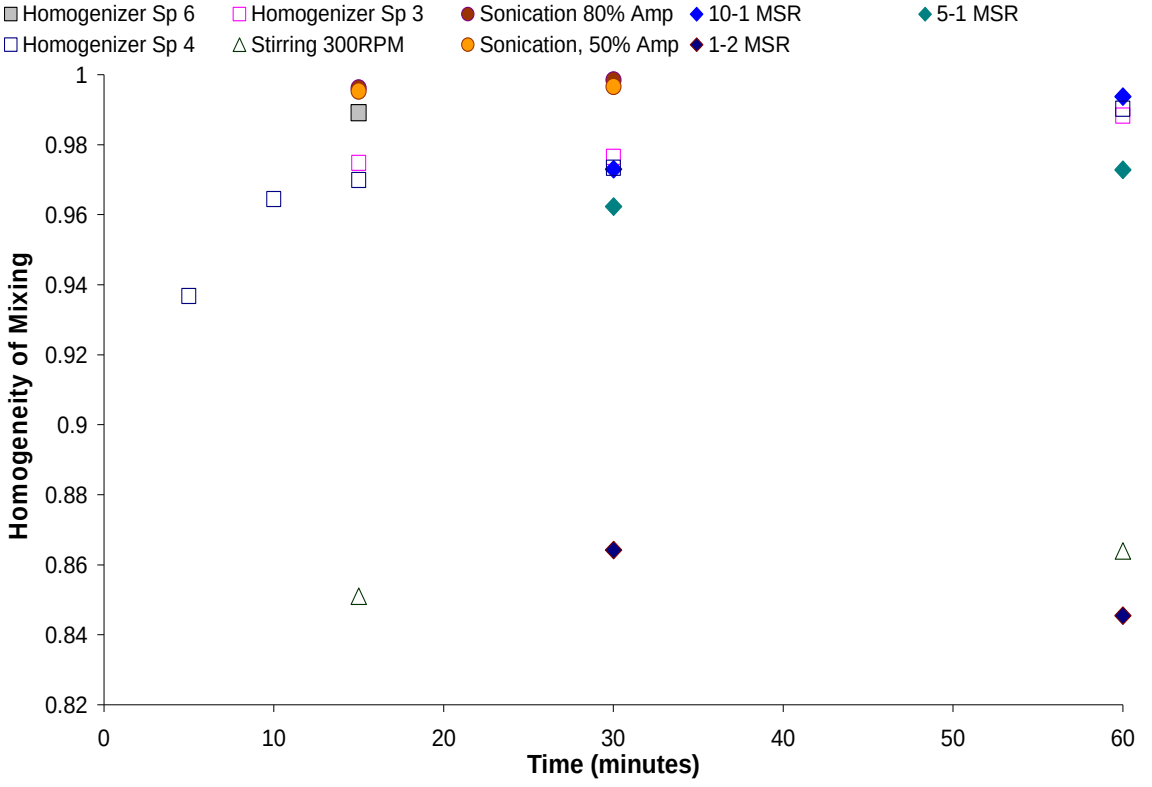

Figure 3.13 Homogeneity of Mixing versus time for the various aqueous mixing methods.

3.7 Summary of Results

Magnetically Assisted Impaction Mixing, in liquid mediums, has shown to be an effective, environmentally benign dry method to mix nanoparticles. The TEM results, although limited, indicate that optimized operating conditions could achieve mixing at sub-agglomerates down to nanoscale. Longer processing times and/or higher magnet to powder ratios led to better mixing. It is found that as magnet-to-sample ratios increased, the Homogeneity of Mixing increased, suggesting improved mixing. For the same magnet-to-sample ratios, processing time is studied from thirty minutes up to two-hundred-forty minutes. As processing time is increased, Homogeneity of Mixing is found to increase for all magnet-to-sample ratios. For a long enough processing time, all magnet-to-sample ratios, even the lowest ratio of 1:2, created a homogeneous mixture.

Magnet size ranges of 2360 to 1700 microns and 1000 to 600 microns are also studied to compare to the data obtained from the magnet size range of 1400 to 850 microns. It is evident from all the results, including the varying of the magnet size range, that the main process control variable is the product of time with the number of magnets per powder mass, and increase in that within the ranges studied significantly improves the homogeneity of the mixture.

MAIM technique can be further improved by optimizing the liquid system. By altering pH and adding surfactant the Homogeneity of Mixing can be further improved. For the nano-mixture of Aerosil A200 SiO_2 and Aeroxide TiO_2 P25, an acidic medium provided more homogeneous mixing results than basic conditions. It is also noted that when surfactant is added during the mixing process, the overall homogeneity of the mixture improves.

The results clearly suggest viability of MAIM in liquid mediums to industrial applications requiring nanocomposite powders. While deagglomeration results show that MAIM results do not reach the level obtained by using homogenizer or ultrasonic horn. However Homogeneity of Mixing results show that mixture homogeneity obtained from MAIM is similar to that of the homogenizer and it can reach the same level of homogeneity as using an ultrasonic horn. Results also show that unlike previous reports stating ineffectiveness of MAIM for nanoparticle mixing, MAIM may be used to achieve not only mixing quality as good as other environmentally benign methods but also a desired level of mixing, i.e., Homogeneity of Mixing, through adjusting the number of magnets and processing time. The MAIM process is simple, and a potentially scalable method that can be used on a wide variety of nano-materials.

CHAPTER 4

ENVIRONMENTALLY BENIGN MAGNETICALLY ASSISTED IMPACTION MIXING OF NANOSIZED PARTICLES

While LMAIM showed promising results, drying steps, adding surfactants, altering the pH, or using solvents, add extra steps, and expenses, to the mixing process. In this chapter, MAIM is explored as a novel, environmentally benign, dry mixing technique, and the process is further optimized.

4.1 Overview

The focus of this research is on the Magnetically Assisted Impaction Mixing techniques, which is an environmentally benign dry mixing technique that does not require any solvents, conditioning steps, or subsequent drying time. In MAIM, a magnetic field is created from the surrounding electromagnetic coil and the magnetic particles undergo agitation. The magnetic particles undergo rotational and translational motion, inside the container, creating a fluidized state for the nanoparticles. Magnetic particles collide with the agglomerates of nanoparticles, and other magnetic particles or the walls of the container, transferring the energy from the generated momentum. It is believed that the collisions between magnetic particles and the agglomerates, under appropriate operating conditions, should contain enough energy to deagglomerate the nanoparticle agglomerates and promote mixing.[1]

4.2 Homogeneity of Mixing Versus Magnet-to-Sample Weight Ratio

First operating parameter of importance is the loading of magnets versus the nano-powders. Its influence is examined as a function of the processing time. Magnet-to-sample ratio is the weight of the magnets to the total weight of the nanoparticles. One gram of each of the two nano-particle constituents is measured and combined with magnets corresponding to the selected value of the magnet-to-sample ratio. Previous research [2, 3] used magnet-to-sample weight ratios of 12:1, processed for 15 minutes[3], and 3:1, processed for 30 minute[2], and had determined the mixture qualities is poor. In the present work, experiments are carried out with magnet-to-sample weight ratios of 10:1, 5:1, 2:1, and 1:2. Mixing times of 30, 20, and 10 minutes are used initially to study the general trend of the results for four magnet-to-sample ratios.

The results (Figure 4.1) show that for a set mixing time, increasing the magnet-to-sample ratio (while keeping the average size of the magnet the same) increases the Homogeneity of Mixing, i.e., improves mixing. Clearly, an increase in the number of magnets per unit mass of the sample would result in an increase in the interaction between the magnets and the agglomerates of nanoparticles promoting deagglomeration and mixing; such interactions as collisions or exposure of the agglomerates to shear field set up by the spinning magnets. The Homogeneity of Mixing for a processing time of 30 minutes is consistently higher than those for processing times of 10 and 20 minutes for all magnet-to-sample weight ratios; the Homogeneity of Mixing values for 10 and 20 minutes are not significantly different for the lower magnet-to-sample weight ratios, but a definite trend is seen at the higher ratios, i.e. 5:1 and 10:1. These results are in general agreement with the previous results [2, 3]. However, the trend seen in Figure 4.1

suggests that higher processing time (which is not considered in previous studies) could lead to further increase in the Homogeneity of Mixing. In the next sub-section, those results are presented.

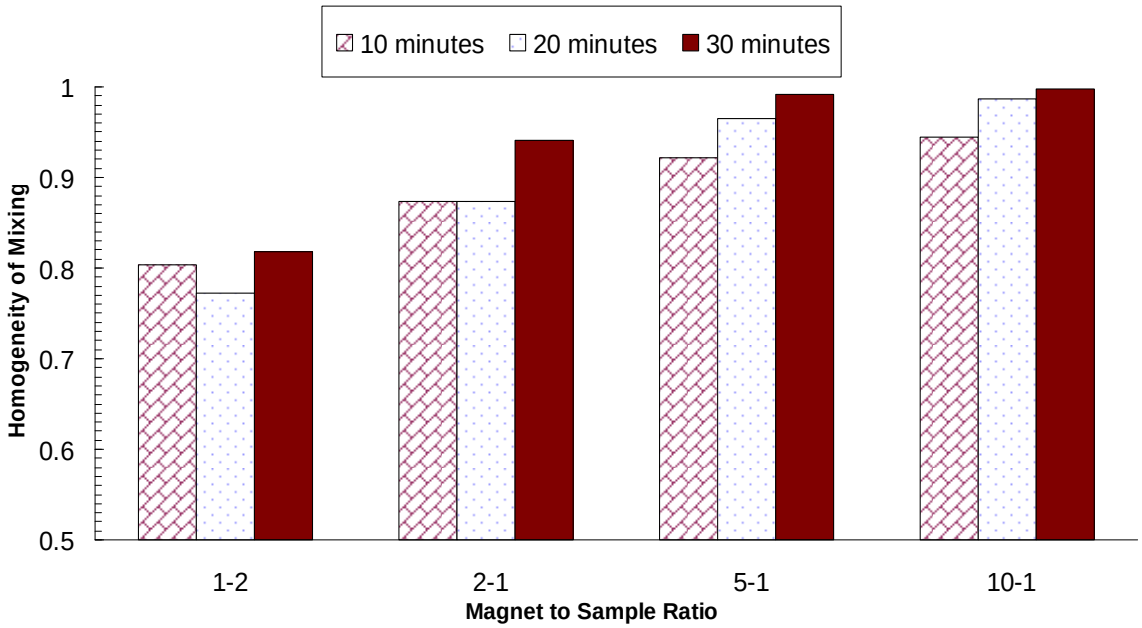

Figure 4.1 Homogeneity of Mixing versus magnet-to-sample ratio for SiO2/TiO2 mixtures and a magnet size range of 1400-850 microns.

4.3 Homogeneity of Mixing Versus Time

In order to study the effect of processing time, nano-powders of Aerosil® silica R974 and Aeroxide® titania P25 are processed for different magnet-to-sample ratios in MAIM device. Processing times of 5 through 570 minutes are examined with various magnet-to-sample ratios of 1:2, 1:1, 2:1, 5:1 and 10:1, and the results are shown in Figure 4.2 as Homogeneity of Mixing versus Time. It is observed that as processing time increases, there is an increase in the Homogeneity of Mixing, leading to a better mixture. After 120 minutes, all magnet-to-sample ratios other than 1:1 or 1:2 reach very high values of the

Homogeneity of Mixing. Therefore, for 1:2 magnet-to-sample ratios, mixing times of 240, 360, and 570 minutes and for 1:1 mixing times of 240 and 360 minutes are examined. The results show that with a long enough processing time, even a 1:2 magnet-to-sample ratio can produce a rather well-mixed sample, similar to the higher magnet-to-sample ratios. It should be pointed out that the lines connecting the points in the figures are for the sake of visual clarity. As with the magnet-to-sample ratio, when there is an increase in the processing time, there are more interactions of the moving and rotating magnets with the agglomerates of nanoparticles promoting deagglomeration and mixing.

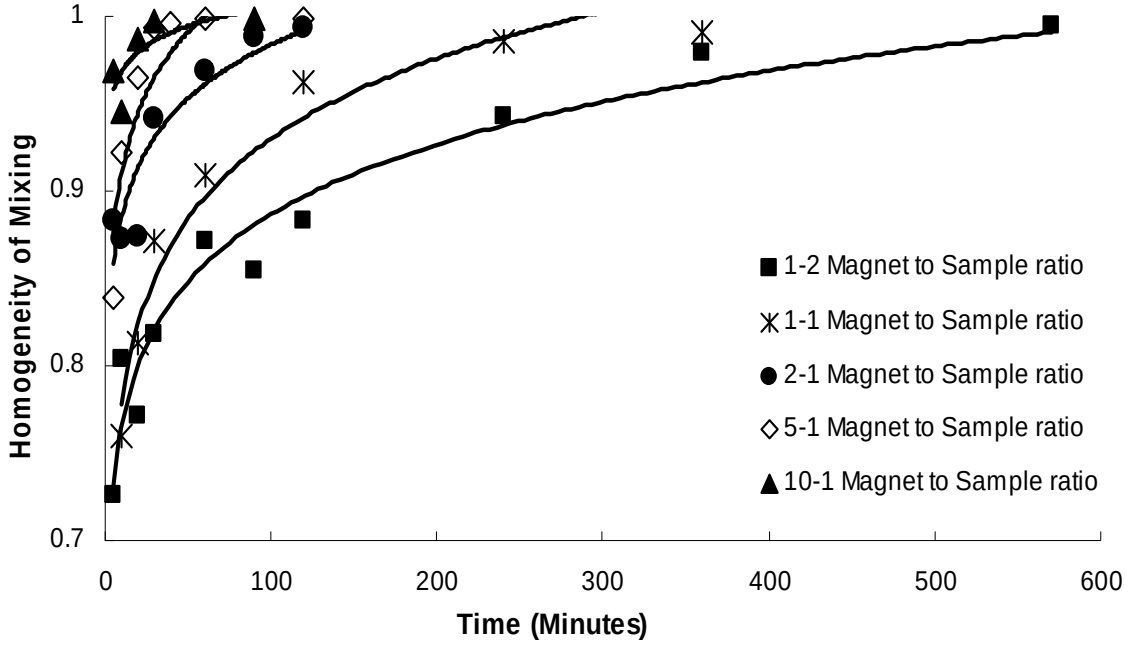

Figure 4.2 Homogeneity of Mixing versus time for various mixing times for SiO2/TiO2 mixtures and a magnet size range of 1400-850 microns.

Homogeneity of Mixing versus time multiplied by the magnet-to-sample ratio is plotted as shown in Figure 4.3 for the magnet-to-sample ratios of 1:2, 1:1, 2:1, 5:1, and 10:1 and a magnet size range of 1400-850 microns for SiO_2/TiO_2 mixtures. This

transformation of data from Figure 4.3 results in a collapse of the multiple curves, and a single trend is evident for all the values of magnet-to-sample mass ratios. The same collapse is also seen if the abscissa is the product of the number of magnets and processing time, Figure 4.4. Thus, the hypothesis introduced in liquid MAIM, that the Homogeneity of Mixing increases as the product of the number of magnets and time increases, is proven to work in a dry system as well as for liquid mediums.

As for liquid MAIM, in order to test the reproducibility of the data obtained, ANOVA with replication technique is used for the present study.[1] Results indicated that there is no significant statistical difference between the two selected test runs for the samples with higher magnets to sample weight ratio as well as for the longer processing time.

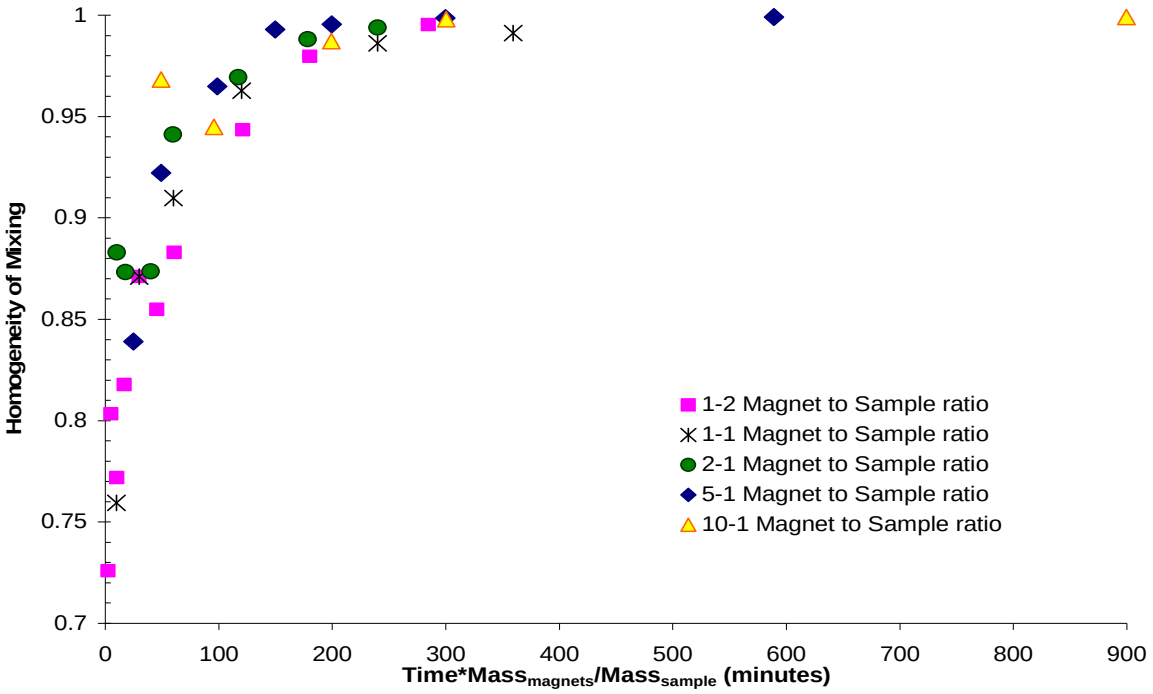

Figure 4.3 Homogeneity of Mixing (HoM) versus time*magnet-to-sample ratio for SiO2/TiO2 mixtures and a magnet size range of 1400-850 microns.

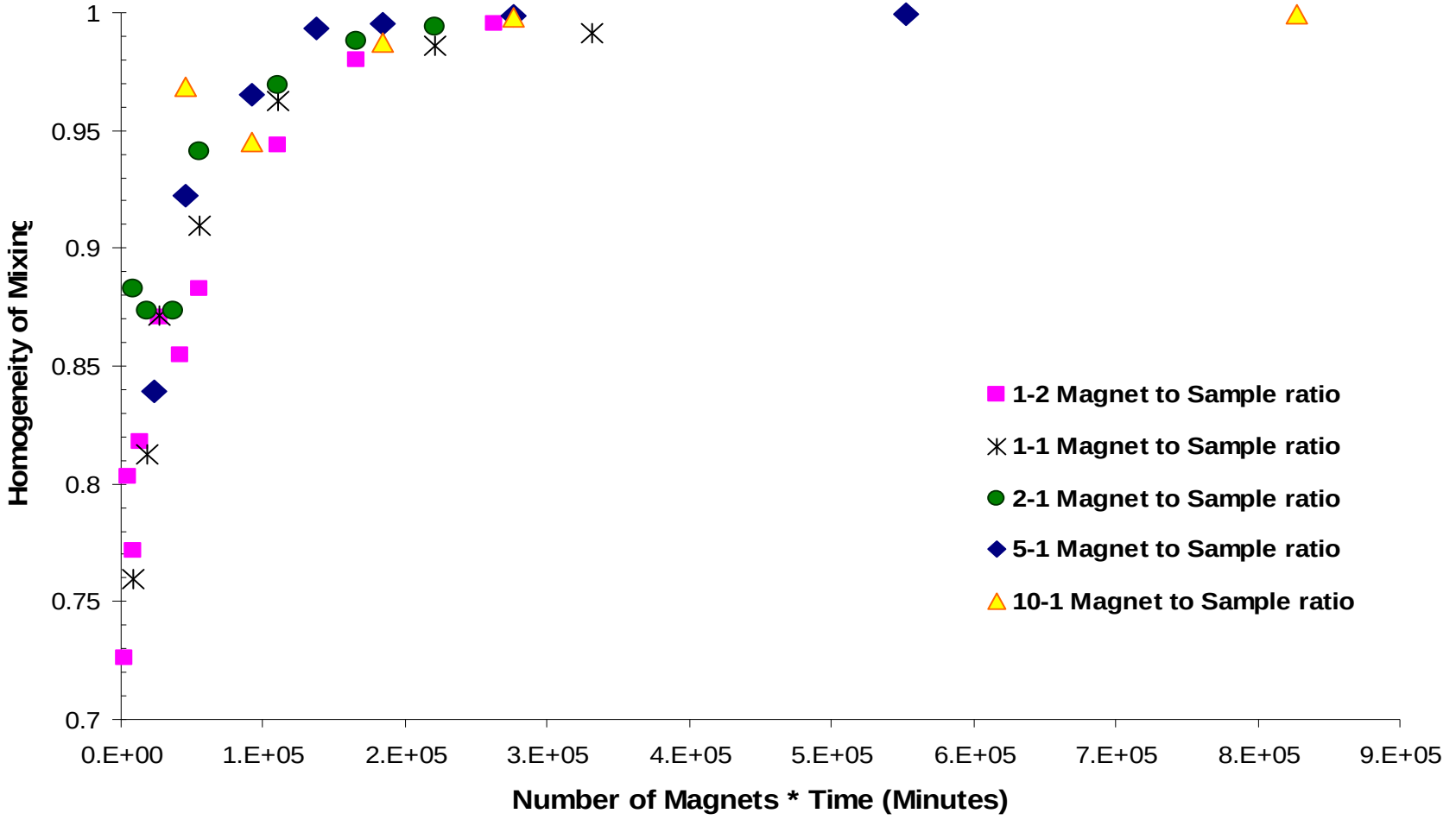

Figure 4.4 Homogeneity of Mixing (HoM) versus time*number of magnets ratio for SiO2/TiO2 mixtures and a magnet size range of 1400-850 microns

It is noted that with high magnet-to-sample ratios (such as 10:1), as the processing time gets longer, the nano-powder bed gets compacted and forms a packed bed, having reduced mobility. Such caking effect is due to the excessive amount of the magnetic particles which tend to force the nano-powders to get compressed at the bottom of the container. The caking effect is a common problem when handling dry nanopowders due to the very cohesive nature of the constituents. Due to the caking effect, the 10:1 magnet-to-sample ratio is not further investigated in the subsequent case studies. Nonetheless, the results clearly indicate the general trend of mixing, which implies that the higher rate of collisions promote faster mixing.

Table 4.1 Standard Deviation and Relative Standard Deviation Versus Increasing Time and Number of Magnets

Time*Number of Magnets (minutes)	Homogeneity of Mixing	Standard Deviation	Relative Standard Deviation
1150	0.7489	2.07E-02	2.76%
2300	0.8039	2.26E-02	2.81%
13800	0.8753	1.69E-02	1.93%
55201	0.9699	9.84E-03	1.01%
92002	0.9887	9.83E-04	0.10%
138002	0.9984	6.80E-04	0.07%
138002	0.9987	3.54E-04	0.04%
276005	0.9993	6.70E-05	0.01%

Instead of providing the error bars, which would not be visible due to the very low standard deviations obtained for increased values of the time*number of magnets, standard deviations and relative standard deviation (RSD) are provided of selected points along the trend in Table 4.1. Here, the RSD is an indicator for the reproducibility of the results and not of the quality of mixing. Table 4.1 shows that when increasing the

time*number of magnets, there is a significant decrease in the RSD of the points demonstrating a higher reproducibility of the data.

4.4 Homogeneity of Mixing Versus Magnet Size

Three magnet size ranges are broadly classified here as large, medium, and small categories. Size range from 2360 microns to 1700 microns is used as large magnets. The medium magnets, which are used in the most experiments, have a size range from 1400 microns to 850 microns. The small magnets are in the range of 1000 microns to 600 microns. Magnet-to-sample mass ratios of 1:2, 2:1, and 5:1 are used for investigating the effect of magnet size on the Homogeneity of Mixing. The purpose of the study is to determine if smaller magnets will carry enough forces to break up agglomerates, or by increasing the mass of the magnets, will the increased mass of each individual magnet play a larger role in the mixing.

The results of the different magnet sizes are shown in Figure 4.5 as Homogeneity of Mixing versus time multiplied by the magnet-to-sample ratio (MSR). From Figure 4.5, the Homogeneity of Mixing data no longer collapses onto a single trend, but a separation in the data occurs in groups. The data is separated by magnet size and plotted in Figures 4.6 through 4.8. The figures show that for each magnet size range, there is a particular trend. The Homogeneity of Mixing data is now plotted versus the product of time and the number of magnets, Figure 4.9. It is clear from the plot that the Homogeneity of Mixing for all the different operating conditions (i.e. for different magnet-to-sample ratios as well as the magnet sizes) converge to follow a single trend, continuing to prove the hypothesis.

The results obtained so far suggest that the main process control factor for the mixing quality is related to total number of collisions. To be more general when the magnet sizes vary in different experiments, the control factor for the number of collisions is expected to be the number of magnets and not necessarily the mass of the magnet powder sample. That reasoning is based on previously reported numerical simulations results.[2] The results mean that the main process control factor for the mixing quality is related to total number of collisions, which is proportional to the processing time multiplied by the number of magnets used for a given mass of powder sample. The number of magnets present in the mixture is estimated by counting the magnets per gram for a given magnet size range. Thus the hypothesis is proved and that the Homogeneity of Mixing increases as the product of the number of magnets with time increases. To further understand dependencies on the Homogeneity of Mixing, jar size and powder loading are studied in Appendix C.

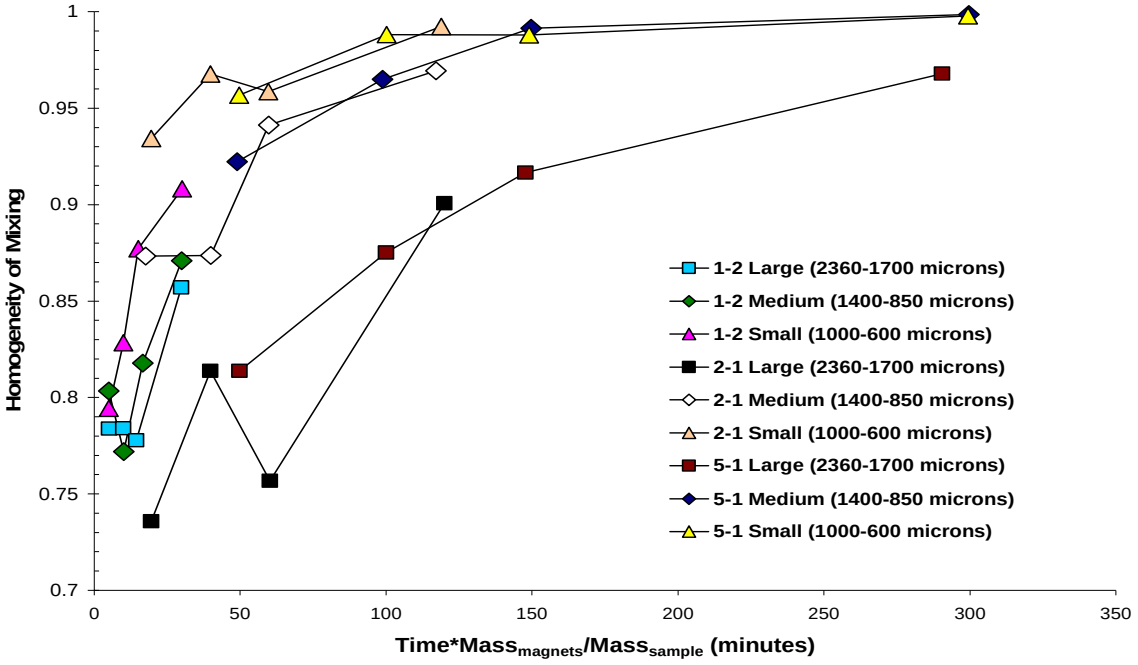

Figure 4.5 Homogeneity of Mixing for the magnet-to-sample ratios of 1:2, 2:1, and 5:1 with a magnet size range of 2360-1700, 1400-850 and 1000-600 microns for SiO2/TiO2 mixture shown versus time*magnet-to-sample ratio.

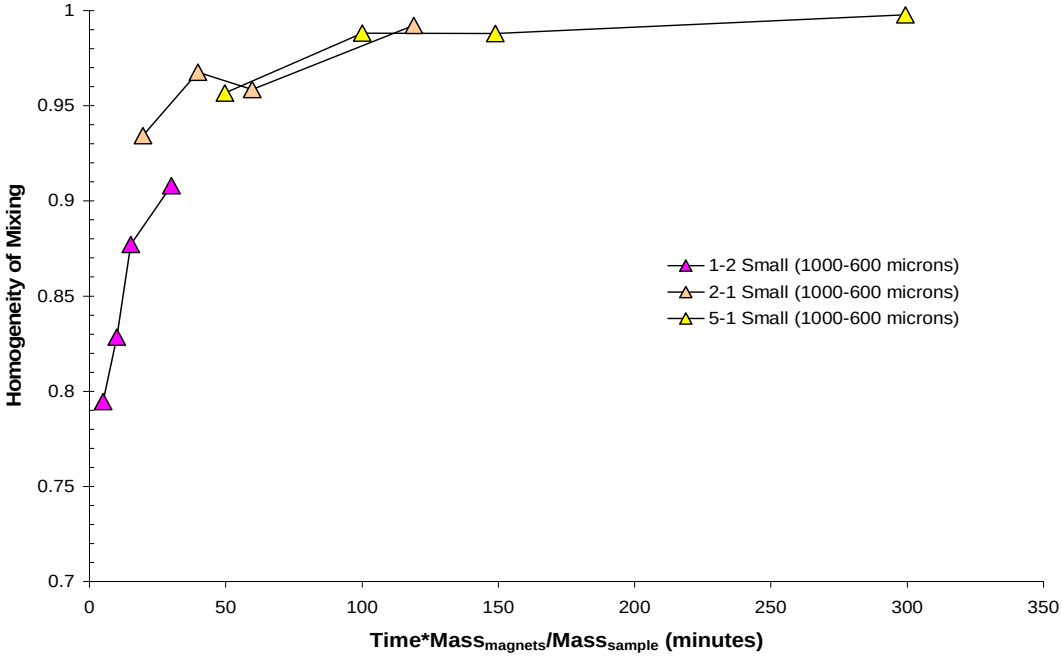

Figure 4.6 Homogeneity of Mixing for the magnet-to-sample ratios of 1:2, 2:1, and 5:1 with a magnet size range of 1000-600 microns for SiO2/TiO2 mixture shown versus time*magnet-to-sample ratio.

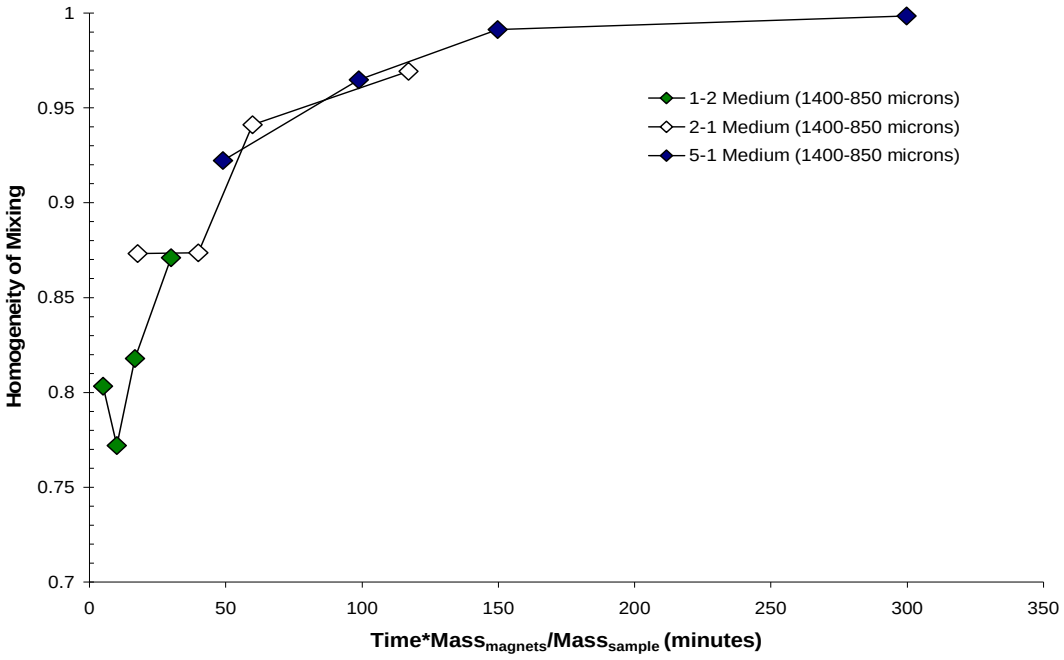

Figure 4.7 Homogeneity of Mixing for the magnet-to-sample ratios of 1:2, 2:1, and 5:1 with a magnet size range of 1400-850 microns for SiO2/TiO2 mixture shown versus time*magnet-to-sample ratio.

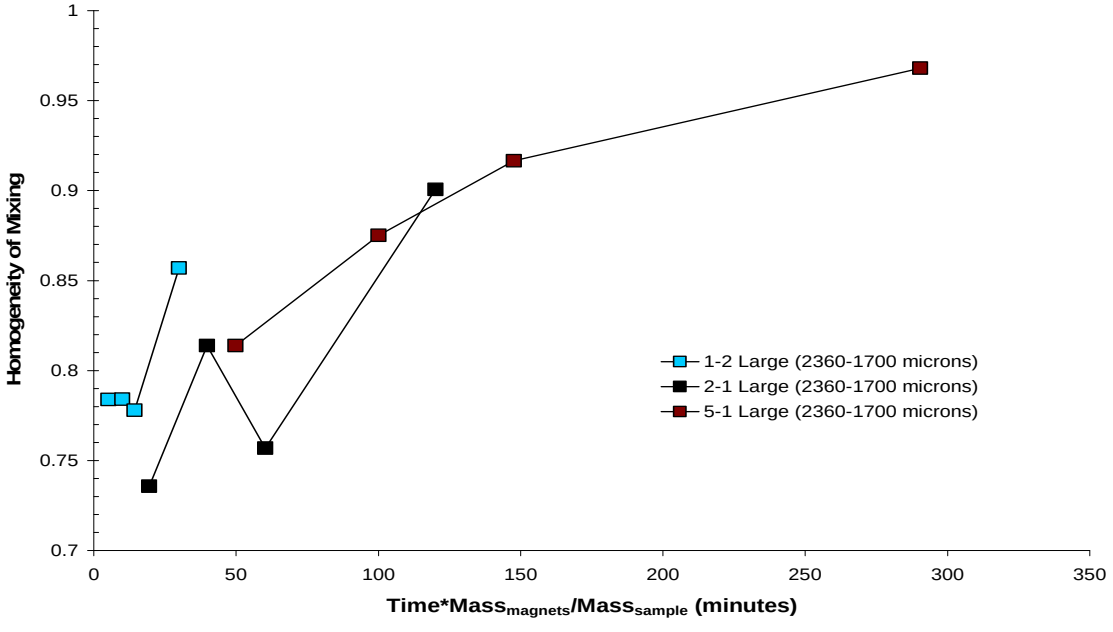

Figure 4.8 Homogeneity of Mixing for the magnet-to-sample ratios of 1:2, 2:1, and 5:1 with a magnet size range of 2360-1700 microns for SiO2/TiO2 mixture shown versus time*magnet-to-sample ratio.

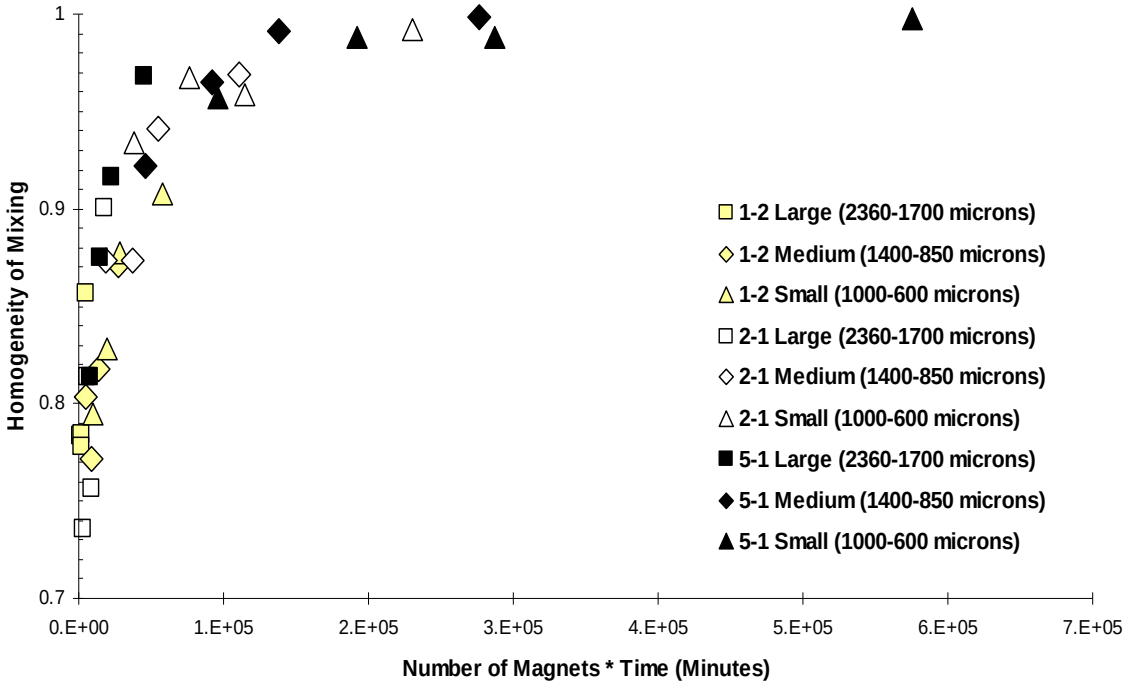

Figure 4.9 Homogeneity of Mixing for the magnet-to-sample ratios of 1:2, 2:1, and 5:1 with a magnet size range of 2360-1700, 1400-850 and 1000-600 microns for SiO2/TiO2 mixture shown versus time*number of magnets.

4.5 Homogeneity of Mixing Versus Mixture Components

The results so far are with respect to one specific mixture. Next, the effect of different constituents of nano-powders on the Homogeneity of Mixing is analyzed. In addition to the mixtures of Aerosil® R974 + Aeroxide® titania P25, the mixtures of Aerosil® R974 + Aeroxide® alumina Alu C and Aerosil® A200 + Aeroxide® titania P25 are processed in the MAIM device and characterized for the estimation of Homogeneity of Mixing. Magnet-to-sample weight ratios of 5:1, 2:1, and 1:2 are studied. The resultant Homogeneity of Mixing versus time multiplied by the number of magnets in the sample mass is presented in Figure 4.10 for both the types of mixtures. Although the trends observed are similar for the different samples of the same magnet-to-sample weight ratio, the Alumina-Silica mixture is found to have a higher Homogeneity of Mixing as

compared to Titania-Silica mixture. This result indicates that the MAIM method is effective for the type of particles utilized, i.e., metal oxides, and that the controlling process variable is the product of time with number of magnets per mass of sample. When dry powder mixing using MAIM of silica Aerosil A200 and titania Aeroxide P25 is compared to mixing in liquid mediums, Chapter 3, the dry mixing produced higher values for Homogeneity of Mixing, indicating more homogeneous mixing.

Since the Alumina-Silica mixture shows better mixing, it is possible that the deagglomeration of alumina is easier than titania, which is similar to what is observed in the previous work.[2] On the other hand, it is also possible that the X-rays generated from the EDS propagate inside the two mixture mediums in different ways, thereby changing the sampling volume analyzed. The volume analyzed by the EDS changes the value of Homogeneity of Mixing as it is higher for larger sampling volumes. One method to determine how X-ray propagation changes between different sample mediums is to calculate the depth of X-ray production, which is estimated by the Anderson–Hasler expression as illustrated below in equation 4.1.

$$R = \frac{0.0064\left(E_0^{1.68} - E_c^{1.68}\right)}{\rho} \tag{4.1}$$

R is the depth of X-ray generation (μm), E_o is the electron beam energy (keV), and ρ is the sample density (1.96 g/cm^3). E_c is the critical ionization energy (keV), K-edge can be used. K-edge energy is 4.965 keV for Ti and 1.560 keV for Al[2]. Therefore, the X-ray generation depth is 0.262 μm and 0.301μm, for Ti and Al, respectively. Therefore, this could have a minor impact on the results observed.

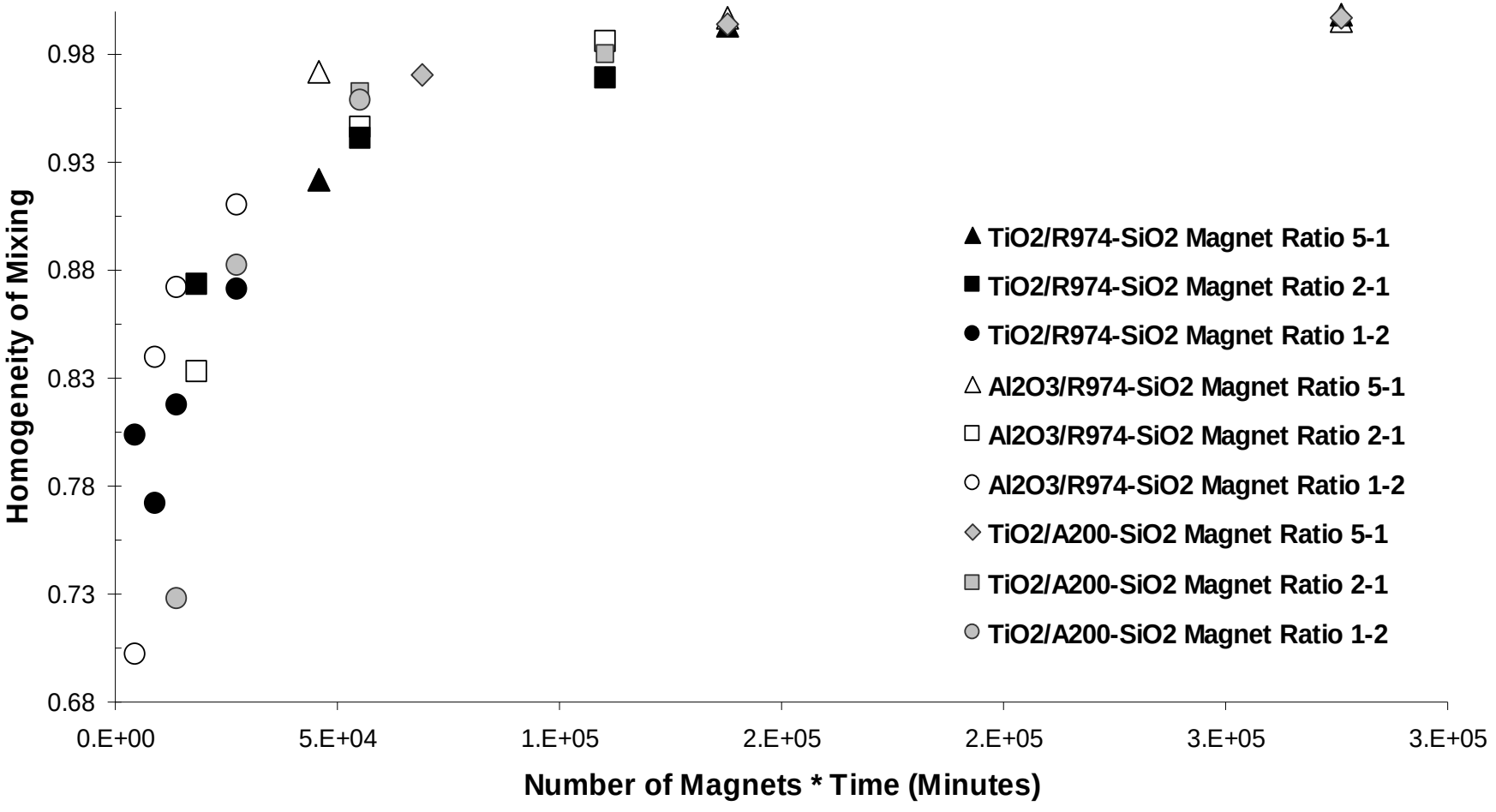

Figure 4.10 Homogeneity of Mixing versus time*number of magnets for magnet-to-sample mass ratios of 1:2, 2:1, and 5:1 with a magnet size range of 1400-850 microns for SiO2(R974)/TiO2, SiO2(R974)/Al2O3 and SiO2(A200)/TiO2 mixtures.

4.6 Summarizing the Effect of Multiple Factors on the Homogeneity of Mixing

All the results from multiple factors, namely, the effect of magnet to powder mass ratio (Figure 4.4), the magnet size (Figure 4.9), and the mixture constituents (Figure 4.10), may be summarized in a single plot as shown in Figure 4.11. While there is the expected scatter, for example, arising from the different constituents that may be explained due to the x-ray propagation in the different materials, the figure indicates an overall pattern of behavior. The main trend which is a function of time*number of magnets, indicates that there are multiple factors that allow for tuning the quality of mixing of the nanoconstituents for ceramic powders similar to those studied here.

4.7 Homogeneity of Mixing Versus Magnetic Field Strength

In order to study the effect of the magnet field in a dry system, nano-powders are processed for different magnetic field strengths. The field strength is altered by using a Variac controller to change the voltage. Processing times of 10, 30 and 60 minutes and magnet-to-sample ratios of 5-1 and 2-1 are used in the experiments. Magnetic field strengths of 18.7 (39V) and 37.4 (84V) mT are chosen to compare with the data collected at 43.6 (98V) mT. With higher field strengths the magnetic particles should undergo faster translational motion and impact agglomerates with more force. The higher force should create more deagglomeration and homogeneity in the mixing; however, as noted for the LMAIM process, when the magnetic coils overheat, an internal controller is triggered to turn off the coils.

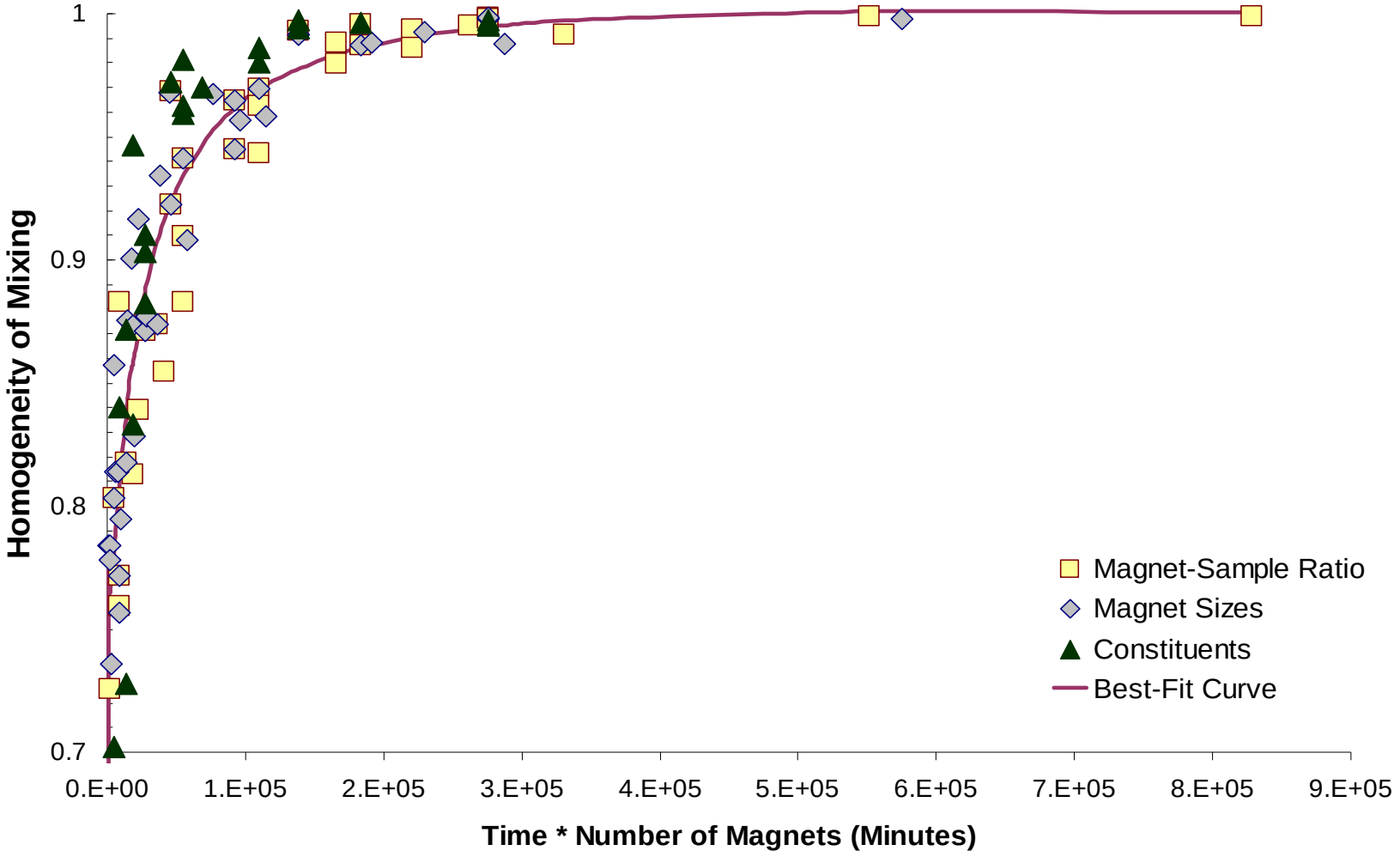

Figure 4.11 Homogeneity of Mixing versus time*number of magnets for MAIM data from Figures 4.4, 4.9 and 4.10is plotted with a best-fitted curve.

Initially all settings run constantly, but eventually the settings enter a phase of repeated off-on cycle. The higher voltage settings, stronger magnetic fields, enter the repeat cycle sooner than the low voltage settings. It should be noted that this off-on cycle occurs when a container with magnetic particles is placed in the coil. Without magnetic particles the coils have remained on for 2 hours in some attempts. Since recording field strength data with magnetic particles present in the system could damage the probe, collecting accurate field strength measurements has been difficult. In this study, which has processing times up to an hour, the 18.7 mT field strength setting did not reach the repeat off-on cycle in this 1 hour study. Once the field strength is accurately collected, an averaged value of magnetic field strength will be used to represent the data.

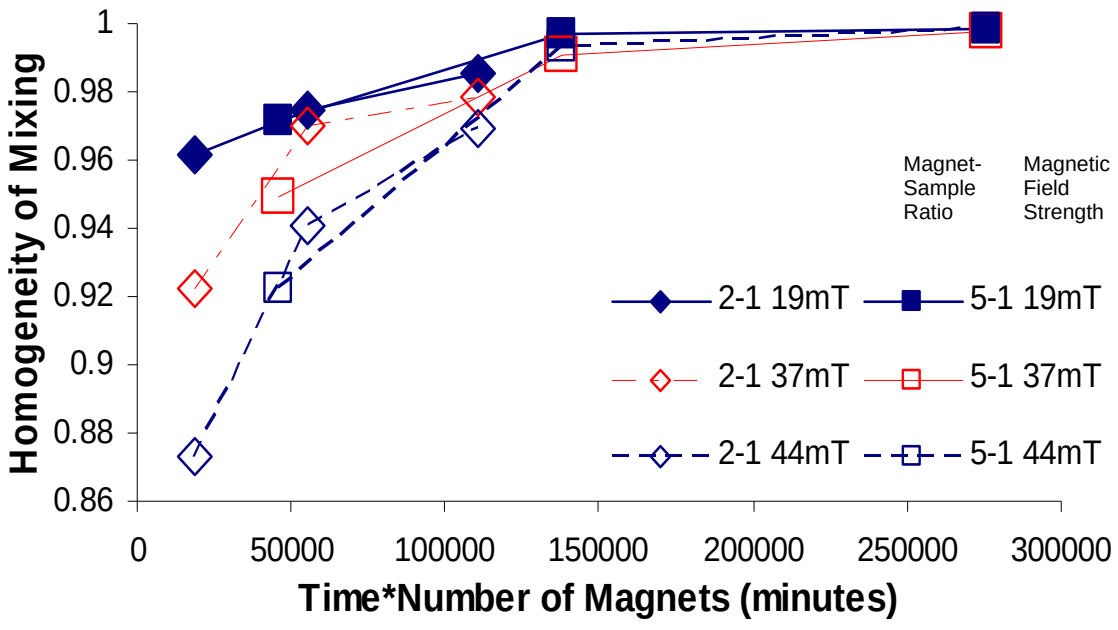

Figure 4.12 Homogeneity of Mixing versus time*number of magnets for magnet-to-sample mass ratios of 2:1, and 5:1 with a magnet size range of 1400-850 microns for magnetic field strengths generated at 18.7 mT, 37.4 mT and 43.6 mT.

The resultant Homogeneity of Mixing versus time multiplied by the number of magnets for the different magnet field strengths is presented in Figure 4.12. It is visible that for the same field strengths, the different magnet-to-sample ratios can be represented by a single trend line. It is evident that a lower field strength run constantly will achieve better mixing than a higher field strength run intermittently. However, after a long enough processing time, 1 hour, for the 5-1 magnet-to-sample ratio, the Homogeneity of Mixing is approximately the same.

To take into account the actual processing time, run time, since the fields of 43.6 and 37mT do not run constantly, changes to the times are made. It is determined that when a magnetic field strength of 43.6mT is generated, the field remains on for approximately 56% of the time, while a field strength of 37mT remains on for approximately 20 minutes and remains on about 82% of the time. In the time frame for this study, the 18.7mT magnetic field remained on constantly. Since the actual processing time for the 43.6mT data 10, 30, 60 represent times closer to 5, 15 and 30 minutes, the 120 minute (approximately 60 minutes of actual processing time) is added to complete the trend at relatively same times. When taking into account the true processing time, the trends previously obtained collapse into a single trend (Figure 4.13). Therefore, similar to the results from the LMAIM, there is no significant difference when operating at field strengths of 18.7mT through 43.6mT.

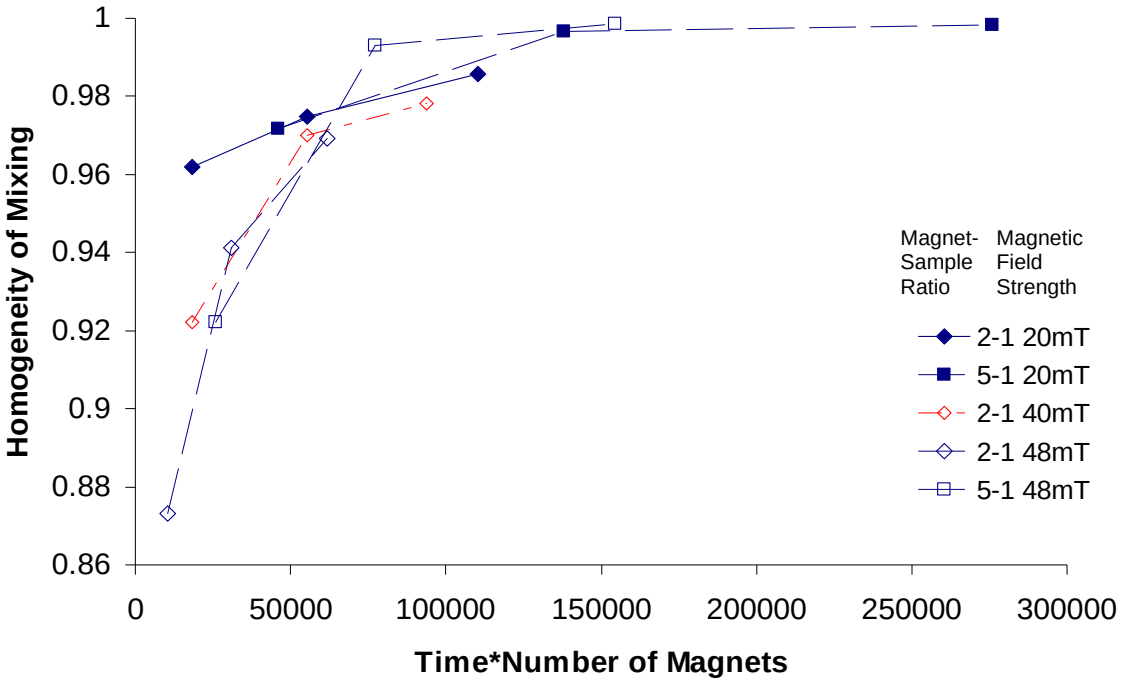

Figure 4.13 Homogeneity of Mixing versus time*number of magnets for magnet-to-sample mass ratios of 2:1, and 5:1 with a magnet size range of 1400-850 microns for magnetic field strengths generated at 18.7 mT, 37.4 mT and 43.6 mT.

4.8 Component to Component Weight Ratio

In the previous studies, the component to component weight ratio is a one to one ratio. With each component being fifty percent of the mixture, it is easier to see how the agglomerates break down with the mixing process. However, in most real world applications, mixing is rarely one to one. Since the Homogeneity of Mixing, a compliment of Intensity of Segregation developed by Danckwerts, is a variance divided by both component concentrations, the dimensionless number can be interchanged with any component to component weight ratio system. In this section silica R974 and titania P25 are mixed at a ten to one weight ratio. The samples are run with 5-1, 2-1 and 1-2 magnet-to-sample weight ratios in order to form a trend line. In Figure 4.14, the 10:1 weight to weight ratio results are plotted with the data from Figure 4.11. The 10:1

component to component weight ratio data follows a similar trend line in comparison with the data collected from fifty-fifty mixtures. This information further demonstrates the overall effectiveness of magnetically assisted impaction mixing as a novel, environmentally friendly, nanomixing device.

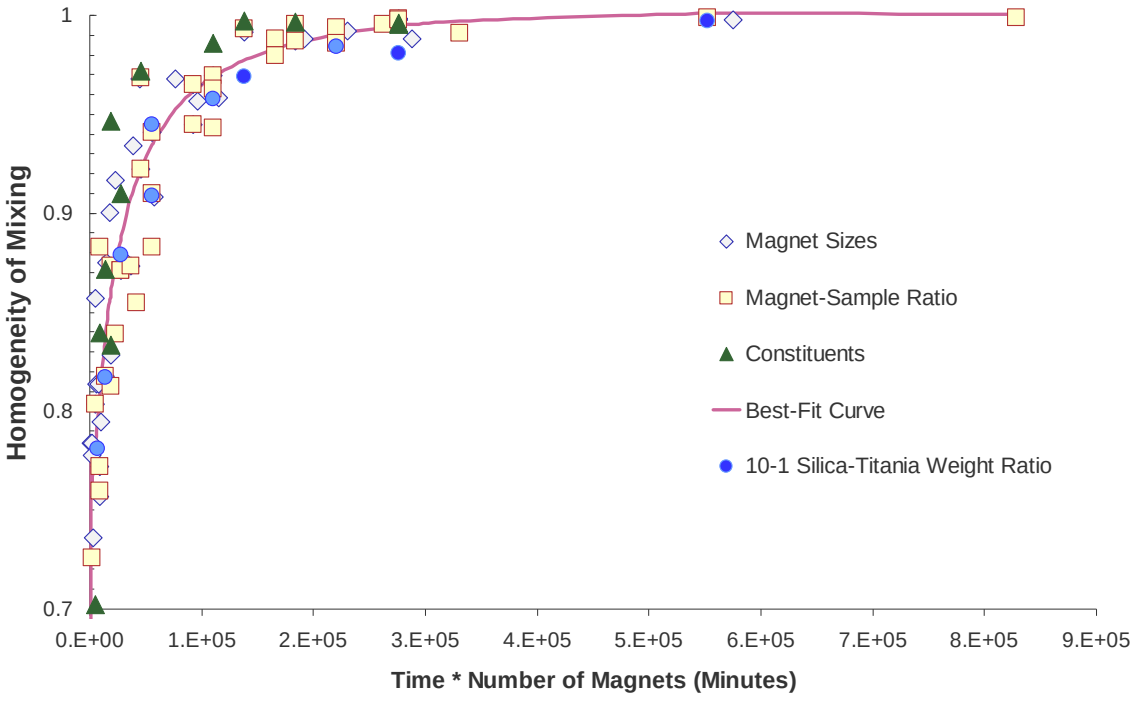

Figure 4.14 Homogeneity of Mixing versus time*number of magnets for magnet-to-sample mass ratios of 1:2, 2:1 and 5:1 with a magnet size range of 1400-850 microns for a silica R974 to titania P25 weight ratio of 10-1.

4.9 Comparison of MAIM with Other Mixing Methods

The Homogeneity of Mixing values of several mixing methods are compared to MAIM in Figure 4.15. To enhance the clarity in differences in the best methods, Figure 4.15 is presented on a modified homogeneity of mixing axis in Figure 4.16. Two previously unpublished mixing methods compared are fluidized bed and supercritical carbon dioxide stirred mixing. For the fluidized bed set up, the powders are charged in the column and

nitrogen gas flow is introduced through a distributor at the bottom of the column. The particle bed expanded with the flow, behaving similarly to a liquid, and mixed the powders. Fluidized bed mixing provided poor mixing because of the lack of strong shear required to cause deagglomeration. Mixing is achieved on the order of tens of microns, the size of agglomerates, and after three hours of fluidization, large agglomerates remained throughout the mixture and resulted in the poor Homogeneity of Mixing values. For supercritical carbon dioxide stirred mixing, powders are charged in a vessel and the pressure and temperature are increased to achieve supercritical conditions. An impeller rotating at 2000 rpm for 30 minutes at 1200 psi is used to create shear within the mixture to break agglomerates and promote mixing. The results show an improvement over fluidized bed mixing but are significantly poorer than the results obtained through MAIM with a 5-1 magnet to powder weight ratio processed for 120 minutes.

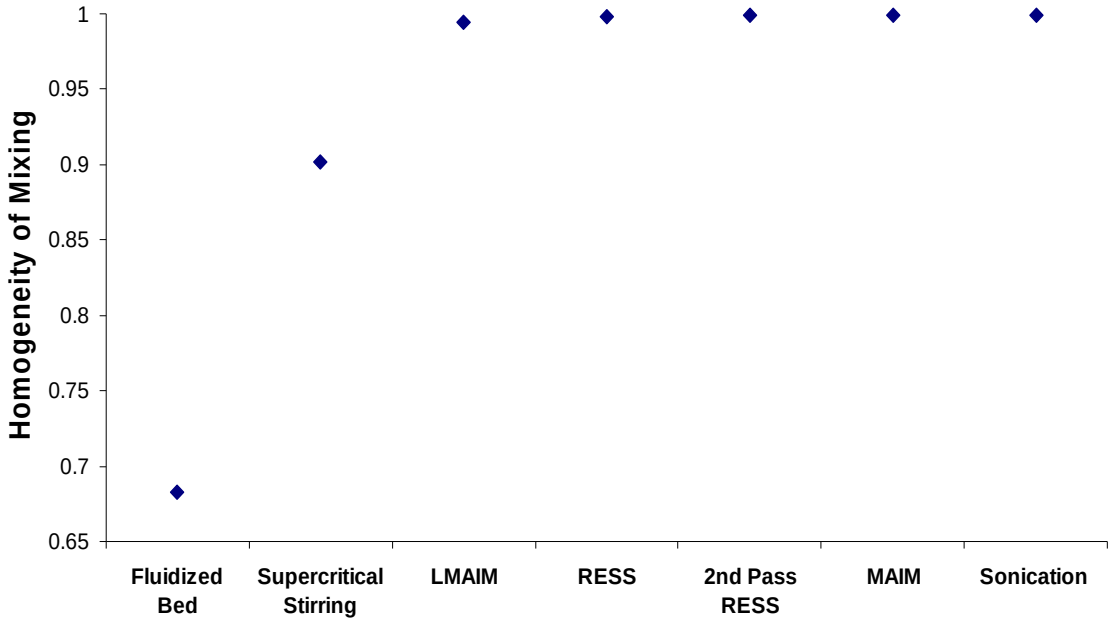

Figure 4.15 Typical, well-mixed, results obtained for Homogeneity of Mixing for various mixing methods.

Homogeneity of Mixing values are also compared against other recently published mixing techniques including rapid expansion of high pressure suspensions (REHPS)[2,3,6] and sonication in supercritical carbon dioxide.[7] For REHPS processes, powders are charged in a vessel and brought to supercritical conditions. After allowing the system to stabilize, the suspension is quickly released through a nozzle with an inner diameter of 256 microns. The rapid release creates high shearing, breaks up the agglomerates, and promotes the mixing on the submicron scale.[6]

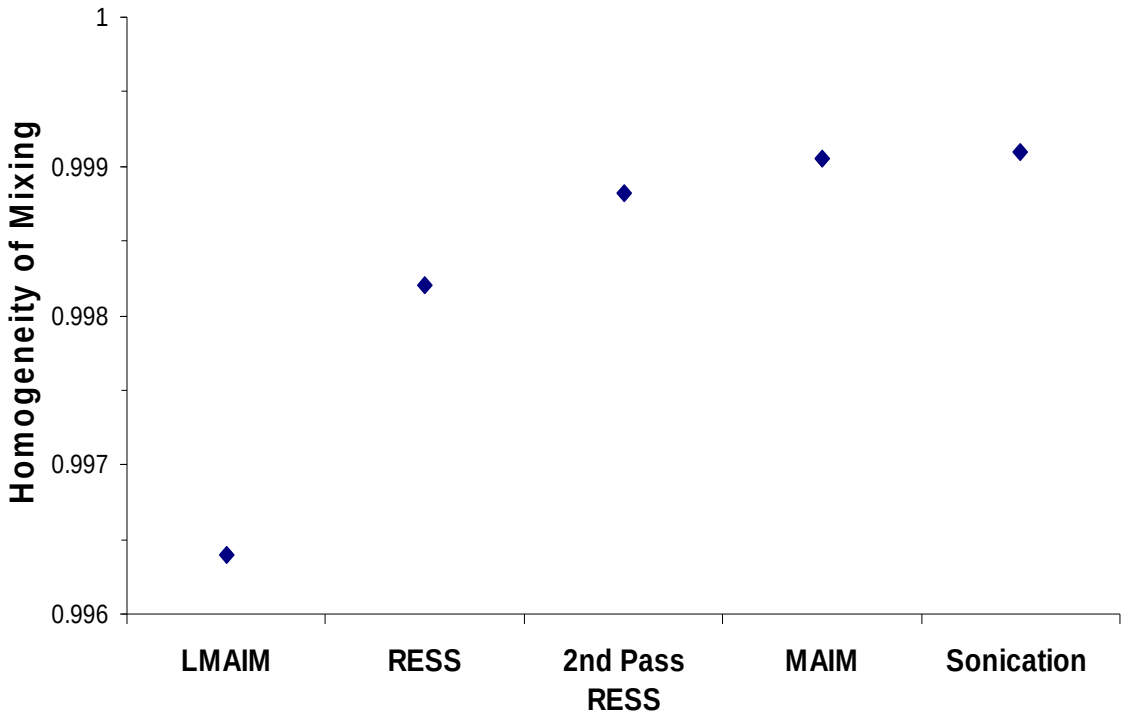

Figure 4.16 Focused Homogeneity of Mixing results for LMAIM, RESS, MAIM and sonication.

In supercritical sonication, the powders are charged in a vessel and filled with carbon dioxide. The system is brought to supercritical conditions. Once stabilized, a sonic horn, inside the chamber, is turned on creating sonic waves through the carbon

dioxide. The sonic waves break the agglomerates and promote mixing on the nanometer scale.[7] From the Homogeneity of Mixing results, it can be observed that the MAIM method can produce mixing on the same scale as sonication in supercritical carbon dioxide, and slightly better than what is obtained for the REHPS method. The MAIM comparison to sonication appears in Figure 4.17 for mixtures of silica R974-titania P25 and silica R972-alumina Alu C.

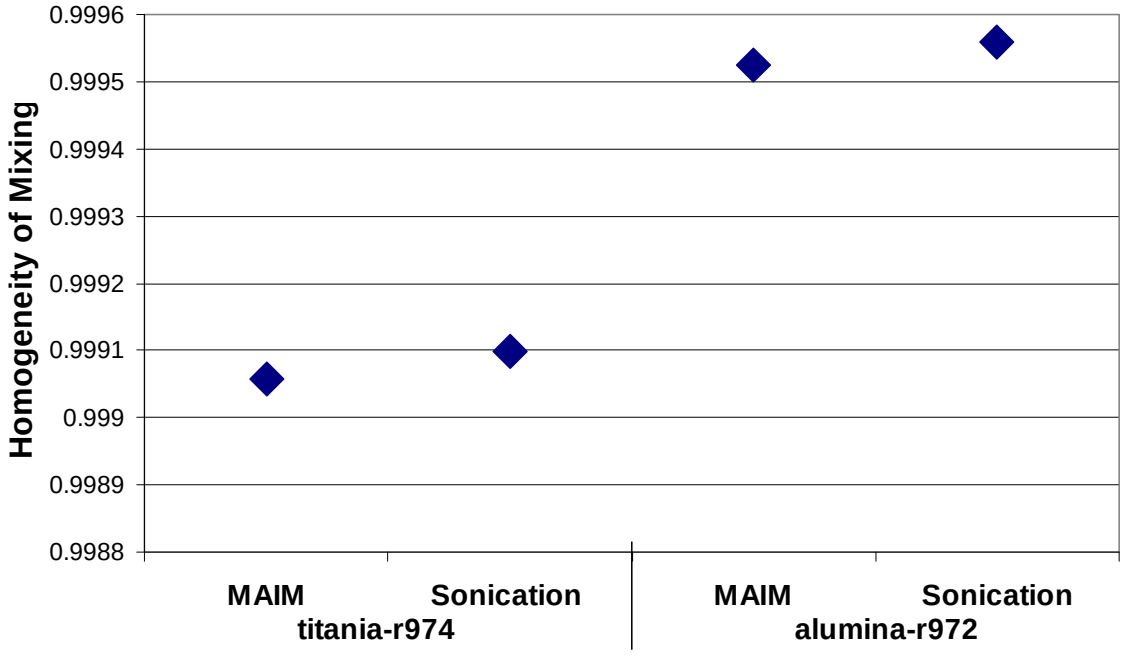

Figure 4.17 Homogeneity of mixing for MAIM and supercritical sonication for mixtures of silica R974-titania P25 and silica R972-alumina Alu C.

4.10 Summary of Results

Magnetically Assisted Impaction Mixing is shown to be an effective, environmentally benign dry method to mix nanoparticles. The TEM results, although limited, indicate that optimized operating conditions could achieve mixing at sub-micron down to nanoscale. Longer processing times and/or higher magnet to powder ratios led to better mixing. It is

found that as magnet-to-sample ratios increased, the Homogeneity of Mixing increased, suggesting improved mixing. For the same magnet-to-sample ratios, processing time is studied from five minutes up to five-hundred-seventy minutes. As processing time is increased, Homogeneity of Mixing is found to increase for all magnet-to-sample ratios. For a long enough processing time, all magnet-to-sample ratios, even the lowest ratio of 1:2, created a homogeneous mixture. Magnet size ranges of 2360 to 1700 microns and 1000 to 600 microns are also studied to compare to the data obtained from the magnet size range of 1400 to 850 microns. It is evident from all the results, including the varying of the magnet size range, that the main process control variable is the product of time with the number of magnets per powder mass, and increase in that within the ranges studied significantly improves the homogeneity of the mixture.

Mixtures of silica Aerosil® R974/alumina Aeroxide® Alu C and silica Aerosil® A200/titania Aeroxide® P25 are also considered in addition to the mixtures of silica Aerosil® R974 and titania Aeroxide® P25. While more studies would be needed to determine the effectiveness of the MAIM as a function of the constituents, in this research, mixtures of metal oxides are well-mixed down to the primary particle scale, as shown by TEM analysis. At the same conditions silica R974 and alumina Alu C resulted in a slightly more homogeneous mixture than the silica R974 and Titania P25. When dry powder mixing using MAIM is compared to mixing in liquid mediums, Chapter 3, dry mixing produced higher values for Homogeneity of Mixing, indicating more homogeneous mixing. While handling of nanopowders in a liquid suspension is easier than dry powder, the end result will produce a less homogeneous mixture.

The results clearly suggest viability of MAIM to many industrial applications requiring nanocomposite powders. Results also show that unlike previous reports stating ineffectiveness of MAIM for nanoparticle mixing, MAIM may be used to achieve not only mixing quality as good as other environmentally benign methods but also a desired level of mixing, i.e., Homogeneity of Mixing, through adjusting the number of magnets and processing time. The MAIM process is simple, and a potentially scalable method that can be used on a wide variety of nano-materials.

CHAPTER 5

MAGNETICALLY ASSISTED FLUIDIZATION AND MIXING OF NANOSIZED PARTICLES

This chapter studies the fluidization behavior and mixing of magnetically assisted fluidized bed mixing. The results address the fluidized bed behavior, effect of bed composition, effect of the amount of magnets and the gas velocity on the bed stability and the homogeneity of the powders.

In this project, the mixing of nano-powders in an environmentally benign fluidized bed system is explored. The objective of this study is to explore the homogeneity of nanoparticle mixtures obtained using various types of fluidize bed systems, and determining what variables will improve mixing quality and why. The fluidized bed systems studied are conventional versus magnetically assisted fluidized bed systems. All of the fluidized bed methods are environmentally benign dry mixing techniques. The characterization of the resulting nanoparticle mixtures are conducted using Scanning Electron Microscope (SEM) equipped with Energy Dispersive X-ray Spectroscopy (EDS).

5.1 Introduction

Gas-solid fluidization is currently used extensively in industry for dispersing particulates for reactions, particle coating, granulation, foods, catalysts, drugs manufacturing, drying and mixing. Unlike large particulates (greater than a few microns), nanoparticles do not fluidize as individual particles because they form larger agglomerates. These

agglomerates are hierarchically fractal structured and very porous. Most fluidization of particles can be classified using Geldart's classifications[1]; however, due to the nanoparticles cohesive nature, nanoparticles can fluidize very differently. At low gas velocities, gas channels through the bed and creates spouting of the powder. At high superficial velocities, vigorous bubbling and powder elutriation is observed.

Wang et al.[2] studied nanoparticle fluidization, and they classified the fluidization behavior as either agglomerate particulate fluidization (APF) or agglomerate bubbling fluidization (ABF). APF fluidization is smooth bed expansion and lacking bubbles, while ABF fluidization is characterized as having very little bed expansion and many bubbles. The group also found that the nanoparticles required high gas velocities in order to reach a minimum fluidization state.

In response, much research has been devoted into the field of modifying the fluidization state by adding additional assistance. The use of sound waves[3-5], vibration,[6,7] magnetic,[8-11] and jet[12] are a few methods implemented to enhance the fluidization of nanoparticles. In all of the cases, the assistance provided improved fluidization by reducing the minimum fluidization velocity required to reach a steady state. The assisted methods break up the clusters of agglomerates and help distribute the gas flow in order to hinder the formation of bubbles. Magnetic assisted showed the most promise because not only are nanoparticles fluidized, the work showed larger clusters (>500 μm) can be fluidized in a nanoparticle bed.[8,11] Additionally the magnetic particles provided enough agitation that powders that normally fell in the category of ABF are able to be fluidized similar to APF powders.

Magnets in the size range of 1400 to 850 microns are used at magnet-to-sample weight ratios of 5:1, 4:1, 3:1, 2:1, 1:1 and 1:2. Two magnetic coils are placed at opposite locations on the column, directly above the distributor plate, producing a field strength of approximately 15 mT.

5.2 Hydrodynamic Study of the Fluidization Behavior

5.2.1 Fluidization of Pure Nanopowders

Aerosil® SiO_2 R972, Aerosil® SiO_2 R974, Aeroxide® Al_2O_3 Alu C, and Aeroxide® TiO_2 P25 powders are fluidized at high velocities and de-fluidized (decreasing gas velocity) to obtain fluidization measurements of pressure drop and bed height. The behavior of the bed during fluidization is also noted. Elutriation of particles is observed at velocities greater than 1.32 cm/s.

The SiO_2 powders exhibited typical APF behavior, such as quick and uniform bed expansion. No bubbling is observed within the bed during fluidization. The bed remained expanded even at low velocities with minimal fluctuation of the bed height. TiO_2 exhibited ABF behavior. Its fluidization behavior is characterized by bubbling, channeling, and vigorous spouting. There is limited bed expansion even at higher superficial gas velocities. Al_2O_3 exhibited both types of fluidization behaviors. The Al_2O_3 bed height tended to fluctuate with a maximum range of 6cm.When expanded, fluidization is smooth and the bed is relatively uniform. However, when the bed height fluctuated to lower heights – there is bubbling and spouting within the unstable bed. At lower gas velocities, there is greater channeling and frequent collapse of the bed.

Figure 5.1 is the reduced pressure drop curves for the de-fluidization of the four nanopowders. Fluctuations in the pressure drop readings are largely due to the bubbling and channeling behavior in the beds. The observed U_{mf} for SiO_2 is ~0.5cm/s. Figure 5.2 is a comparison of the bed expansion ratio among the fluidization of pure nanopowders. SiO_2 R974 demonstrated the greatest bed expansion, i.e. it reached approximately 5 times its original bed height. Bed expansion is high and immediate even at low velocities for SiO_2 powders. Significant bed expansion for Al_2O_3 occurred at higher velocities. Even at velocities of 5.5cm/s, the TiO_2 bed only reached 1.21 times its original bed height.

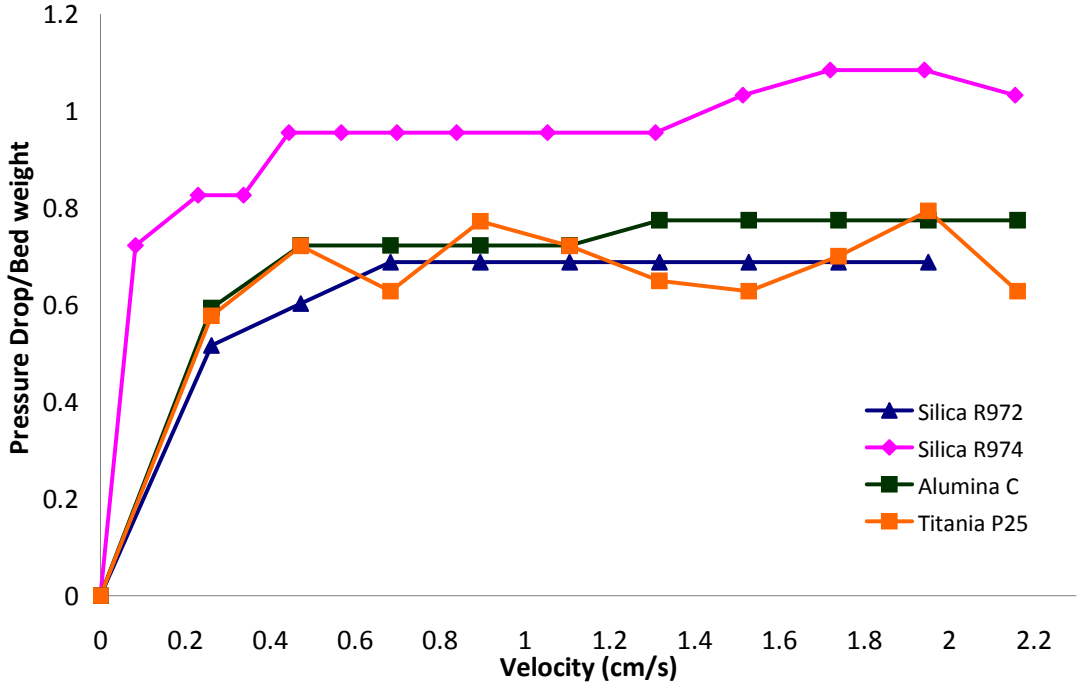

Figure 5.1 The reduced pressure drop of pure nanopowders measured by de-fluidizing the particle bed.

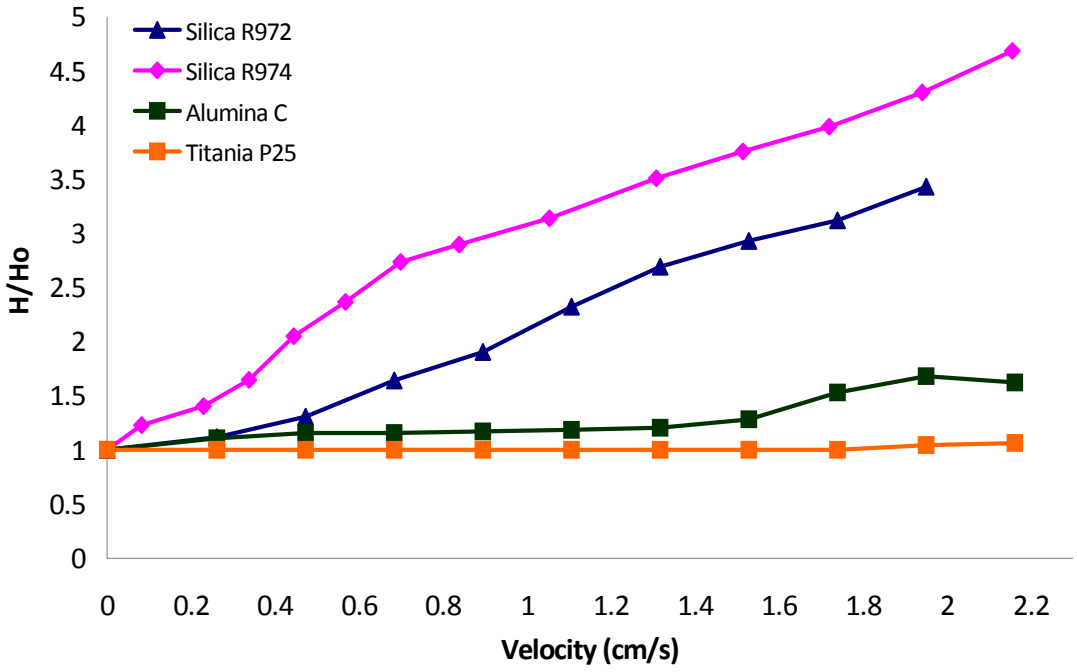

Figure 5.2 The reduced bed height of pure nanopowders measured by de-fluidizing the particle bed.

5.2.2 Fluidization of Nanoparticle Mixtures

SiO_2 R974 and Al_2O_3 Alu C mixtures of different weight ratios (1:1, 1:2, and 2:1) are fluidized and fluidization measurements are taken at decreasing gas velocity. Hysteresis is observed between fluidization (increasing velocity) and de-fluidization (decreasing velocity) of the nanopowder mixtures. Fluidization of the bed mixture required additional particle rearrangement of both the SiO_2 and Al_2O_3 nanopowders. In fluidizing the bed, misleading pressure drop readings are made at lower gas velocities because of plug formation and channeling behavior. When all samples are de-fluidized, they had mixed at high velocities prior to de-fluidizing. De-fluidization experiments yielded greater consistency.

Similar reduced bed height and reduced pressure drop curves are obtained for the nanopowder mixtures at different SiO_2 to Al_2O_3 weight ratios. There is less expansion at

higher velocities for the mixture of lowest SiO_2 to Al_2O_3 ratio (1:1). The reduced bed expansion of the various mixtures fell between the reduced bed expansions of the pure samples. By increasing the percentage of a particular constituent, the mixture behaved closer to the pure powder's expansion.

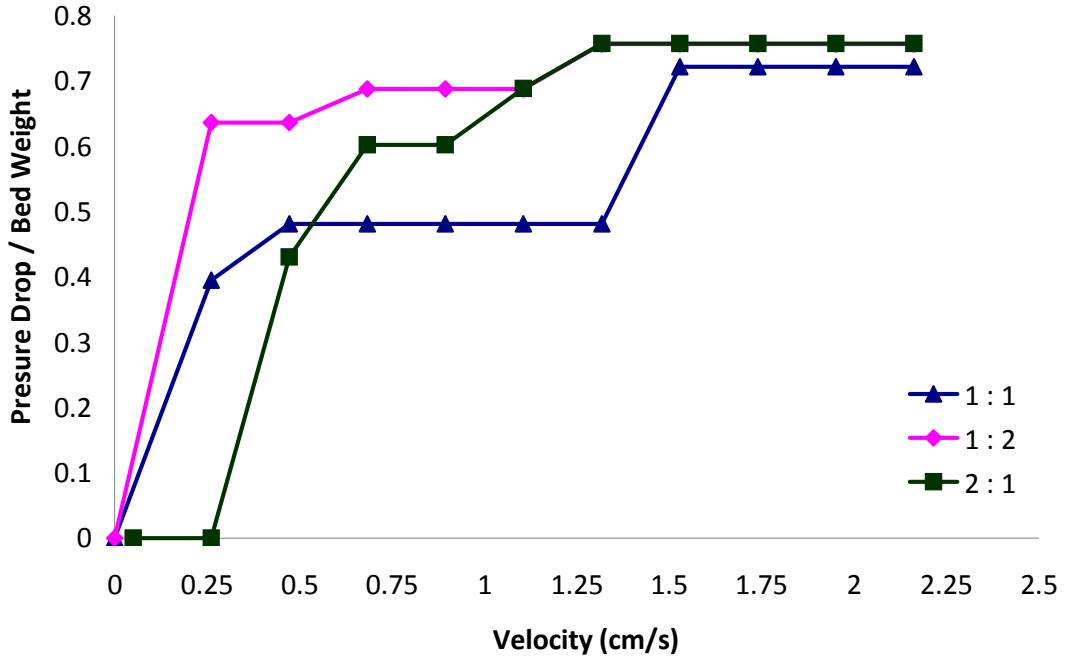

Figure 5.3 Reduced pressure drop of mixtures of SiO_2 R974 to Al_2O_3 Alu C at different weight ratios measured by de-fluidizing particle bed.

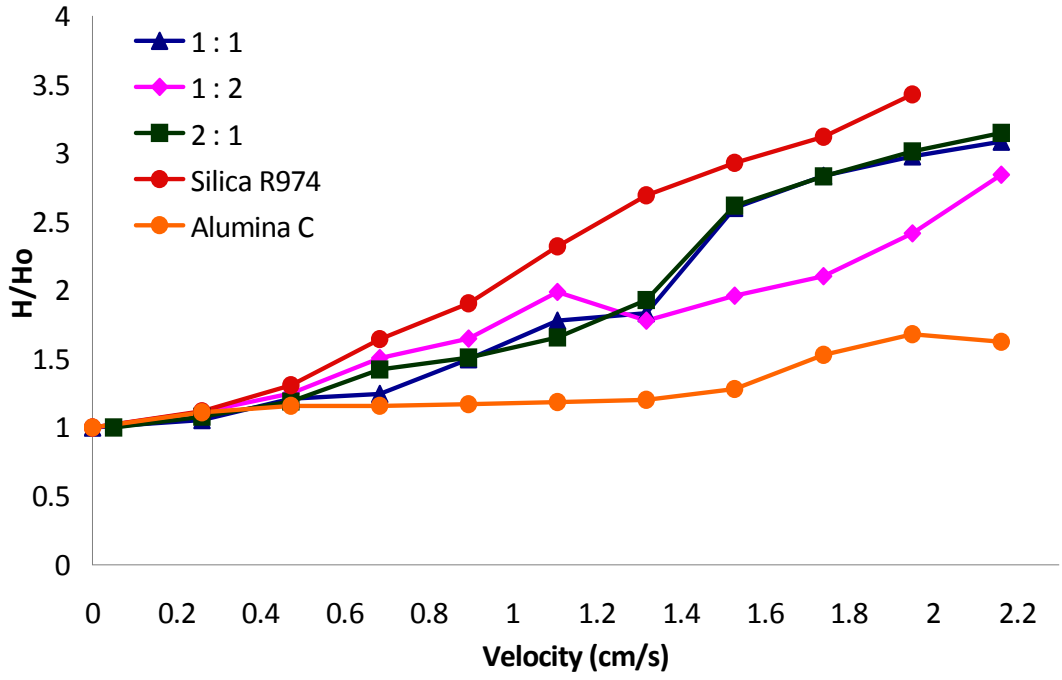

Figure 5.4 Reduced bed height of pure nanopowders and mixtures of SiO_2 R974 to Al_2O_3 Alu C at different weight ratios measured by de-fluidizing particle bed.

5.2.3 Magnetically Assisted Fluidized Bed Mixing of Pure Nanopowders

Magnetic particles located above the distributor underwent rotational and translational motion to rearrange the bed structure and disrupt channeling. The collisions also provided enough kinetic energy to break up agglomerates to mix the nanoparticles on a sub-agglomerate scale. The magnetic particles are removed and the remaining nanopowder is re-fluidized without magnets. The behavior of the nanoparticle bed during re-fluidization is noted.

Immediate expansion of the bed occurred when the oscillating magnetic field is switched on. When the SiO_2 R974 bed is fluidized, the entire bed is in motion and appeared to be uniform throughout. The reduced bed height appeared to be a linear function of the superficial gas velocity. Fluidization under magnetic excitation resulted in twice the bed expansion of fluidization alone at the same velocity. When SiO_2 powder

is re-fluidized in the absence of magnets, the particle bed reached similar bed height ratios as did during fluidization without magnetic excitation. However, bed behavior during fluidization involved bubbling and channeling.

Magnetically assisted fluidization of Al_2O_3 did not achieve as high bed expansion ratios as magnetically assisted fluidization of SiO_2. However, at same velocities, it also resulted in twice the bed expansion of fluidization of Al_2O_3 without magnetic assistance. The fluidized bed for Al_2O_3 is less uniform – greater bed density occupied the upper region of the column. The addition of magnetic particles stabilized the fluidized bed by maintaining expansion and minimizing height fluctuations. The Al_2O_3 bed after fluidization is denser and refluidization is difficult. The particle bed tended to form channels and spout vigorously.

5.2.4 Magnetically Assisted Fluidized Bed Mixing of Mixtures

Fluidized bed mixing with the aid of an oscillating magnetic field is performed on mixtures of the following SiO_2 R974 and Al_2O_3 weight ratios: 1:1, 1:2, and 2:1. The bed behavior of the mixtures under magnetic excitation is similar to the behavior observed in the magnetically assisted fluidized bed mixing of the pure nanopowders.

The results for the defluidization of the mixtures, with or without magnetic assistance, showed that the 1:2 silica to alumina mixtures had the lowest bed expansion ratio. This may be due to the higher concentration of Al_2O_3 in the sample mixture since Al_2O_3 expands less. The pressure drop readings during defluidization are stable. After magnetic processing, there is greater difficulty in refluidizing the mixtures and expanding the particle bed without magnets.

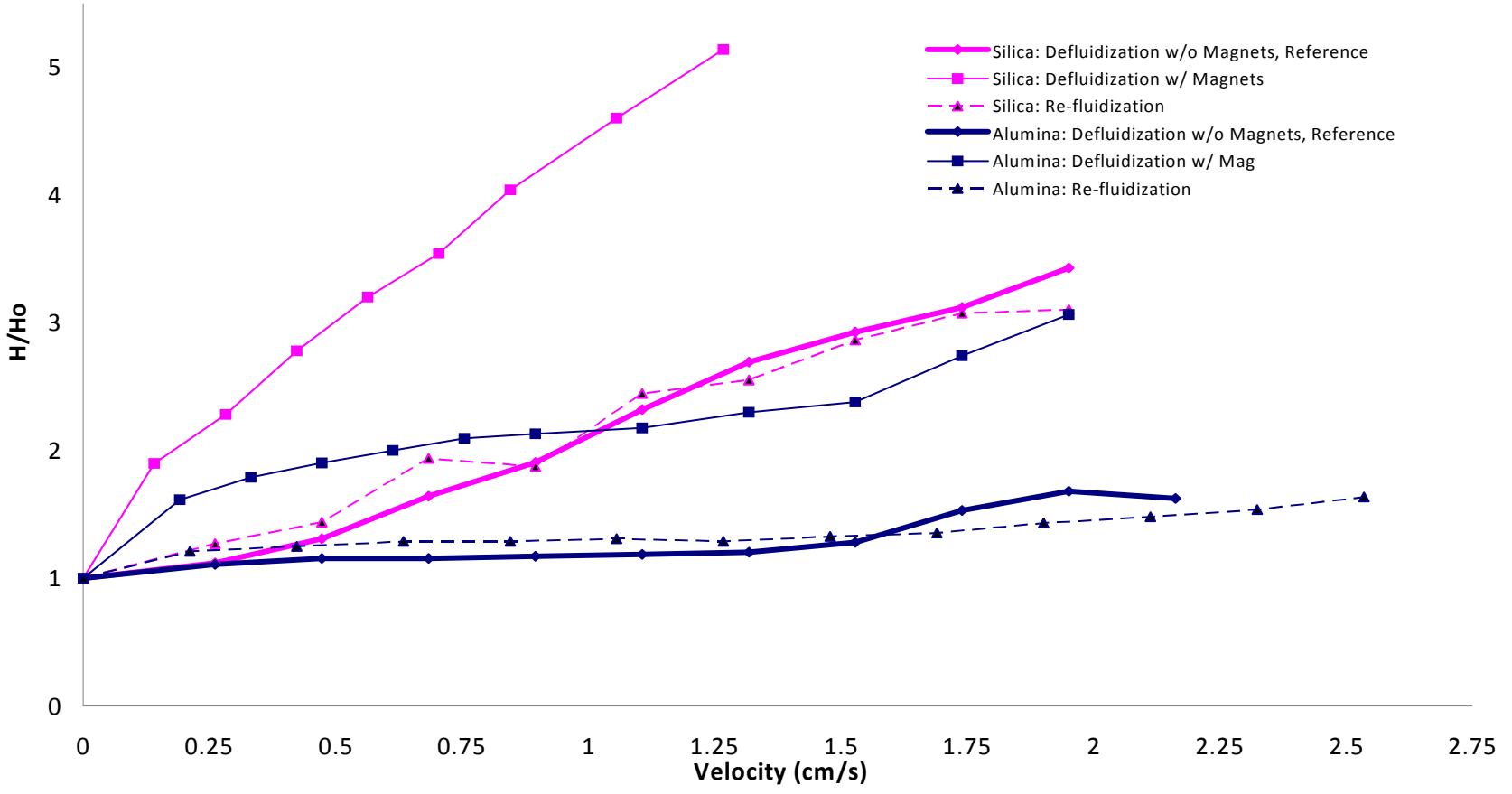

Figure 5.5 Comparison of the reduced bed height for fluidized bed mixing, magnetically assisted fluidization, and refluidization of pure nanopowders: SiO_2 R974 and Al_2O_3 Alu C.

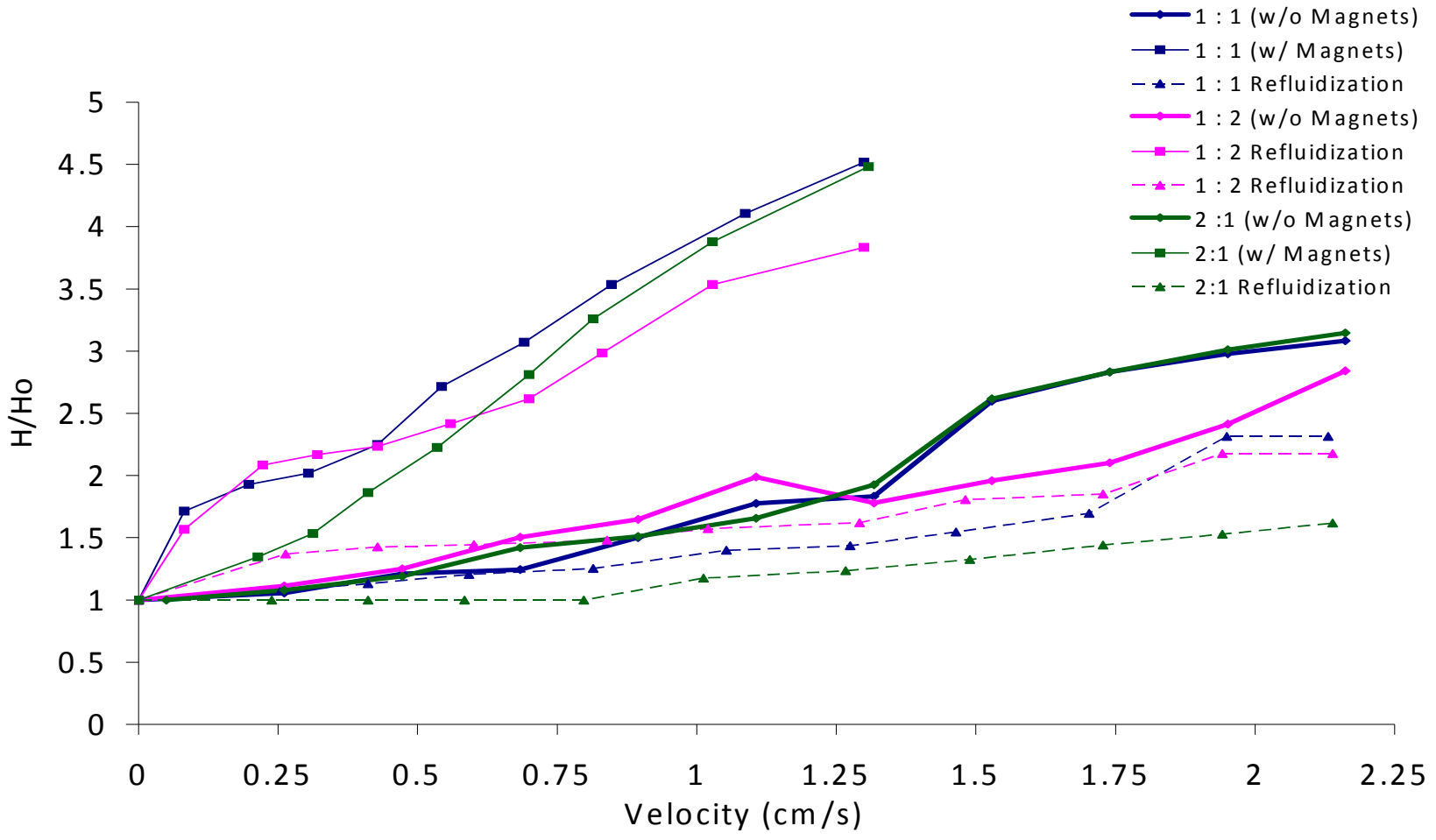

Figure 5.6 Comparison of the reduced bed height for fluidized bed mixing, magnetically assisted fluidized bed mixing, and refluidization of mixtures of SiO_2 R974 to Al_2O_3 Alu C at different weight ratios.

5.2.5 The Effects of Magnet-to-Sample Weight Ratio and Process Time on Magnetically Assisted Fluidization of Nanopowders

The effect of processing time on fluidization behavior is studied for SiO_2 R974, SiO_2 R974 and Al_2O_3 Alu C. The bed maintained its expansion at approximately 2 times its original bed height for unassisted R974 fluidization. During a 2-1 magnet-to-sample ratio magnetically assisted fluidization, the bed expanded to 4 times its original bed height and began to decline after 30 minutes of fluidizing. Fluctuations in the bed height also occurred during the fluidization of pure Al_2O_3 without magnets. Unlike pure SiO_2 R974, the height of the Al_2O_3 bed decreased and the bed expansion reduced over time. Occasionally the bed collapsed completely and vibration is needed to rearrange the bed to incite fluidization. For Al_2O_3 with magnetic assistance, the bed height began to decline immediately after fluidization. The results for R974 and Alu C appear in Figure 5.7.

The effect of processing time on bed height is also determined for nanopowder mixtures fluidized with or without magnetic assistance, Figure 5.8. For the SiO_2 and Al_2O_3 mixtures, an increased ratio of SiO_2 to Al_2O_3 yielded higher maximum bed expansion ratios. However, mixture samples with greater SiO_2 to Al_2O_3 concentration had a greater rate of decrease in bed height.

To compare the differences in the reduction of bed height over time between the pure and mixtures, experiments are carried out with silica R974 and alumina Alu C. The experiments are carried out with magnet-to-sample ratios of 1:1 and 4:1, Figures 5.9 and 5.10 respectively. Alumina continues to show the least bed expansion and the greatest rate of decrease in bed height. Silica showed the slowest rate of decrease in bed height versus processing time. The 1:1 weight ratio of silica to alumina had the highest initial

bed expansion but had a rate of decrease in bed height fell between that of the pure runs of alumina and silica.

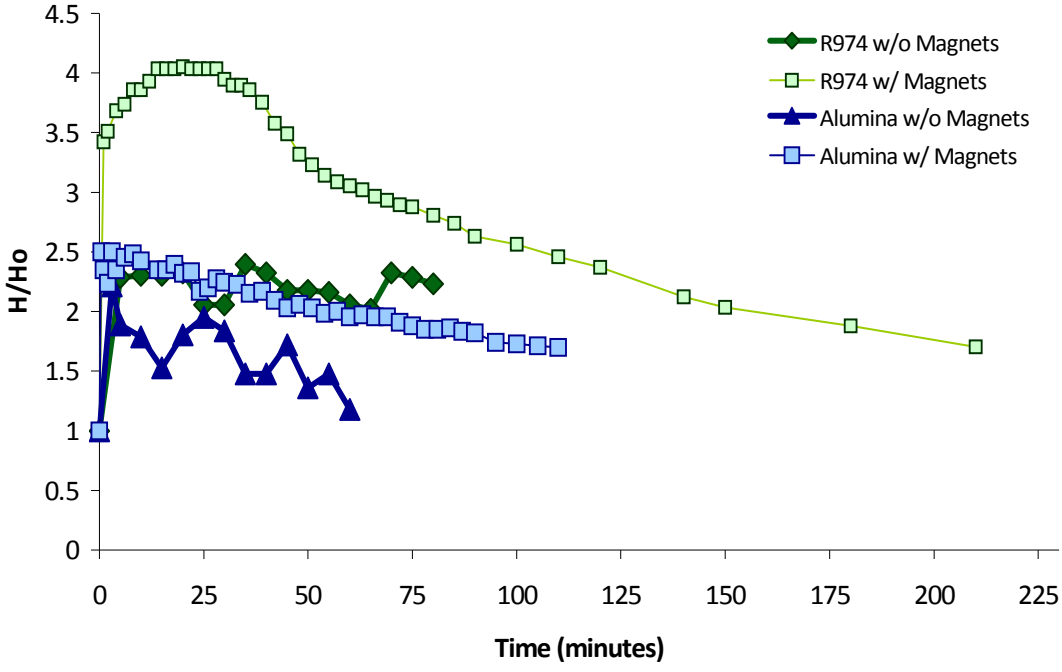

Figure 5.7 The reduced bed height of pure nanopowders (SiO_2 R974 and Al_2O_3 Alu C) fluidized over time. Velocity of 1.95cm/s (without magnetic assistance) and 1.32cm/s (with 2-1 magnet-to-sample weight ratio).

In order to determine if there is vertical segregation within the two component systems, the concentrations of the constituents at the top of the expanded bed is compared versus time. Since the alumina and silica are not distinguishable by the naked eye, SEM stubs with adhesive tape are lower into the column brushing the top of the column. The agglomerates that adhere to the tape are analyzed using SEM and EDS. SEM images, elemental maps and the concentrations of the constituents are collected at various locations and times for 1:1 silica to alumina weight ratios run with 1-1 and 4-1 magnet to sample ratios (Figures 5.11 to 5.13). When looking at the SEM images, the agglomerate

sizes decrease with processing time. The SEM images help prove the concept that the magnetic particles break up the agglomerates in the impaction zone and distribute the smaller agglomerates to the top of the bed. The last SEM and EDS images show that the agglomerates are no longer made up of individual constituents, but are a mixture of both samples. These images show that after a period of time, the mixing takes place on a subagglomerate scale. Figures 5.14 and 5.15 show the composition percentages of the two components at the surface of the bed versus time. After the powders are poured into the column, there is a higher concentration of silica present at the top of the bed. For both cases, as processing time increased, the amounts of silica and alumina came closer to the theoretical 50/50 ratio with some fluctuation.

To determine the effect of magnet-to-sample ratio on the rate of bed reduction, magnet-to-sample ratios of 5:1, 4:1, 3:1, 2:1, 1:1 and 1:2 are investigated for velocities of 2.85 and 3.36 cm/s, Figures 5.16 and 5.17. The reduction in bed height over time increases with the increase in magnet weight. In both cases, the 3:1 magnet-to-sample ratio had the most rapid decrease, while 4:1 and 5:1 are only slightly slower. With a velocity of 2.85 cm/s, the beds had an initial expansion approximately 3.5 times the initial height, while with velocity 3.36 cm/s, the bed expanded to 5 times the initial height. The respective reduced pressure drops appear in Figure 5.18. The reduced pressures drops remained near the value of 1 until the very end of the runs. At the end of the experiments, since the bed height is very diminished, the magnets start to compact the powders trapping some of the powder, and magnets, in a cake on the distributor plate. At this point, the reduced pressure drop decreases below 1. If the powders are all conditioned in the same manor, the experiments are very reproducible, Figure 5.19 and

Figure 5.20. Powders reach a higher fluidized height when the powders are fluidized soon after sieving; however, if the powders are left in storage, particles form larger agglomerates and do not reach the same fluidized bed height. Run 3 on Figure 5.20 is run a couple weeks after runs 1 and 2. As seen in the data, the bed height did not expand as high as the previous runs; however, the rate of decline is very similar.

The decline in the bed height over time in a magnetically assisted fluidized bed may be due to several factors. Therefore the bed mixture is more compacted after magnetic processing. The porosity of the agglomerates may be affected by the processing with magnets during fluidization. Since the magnetic particles are located at the base of the particle bed above the gas distributor, the collisions between the particles caused some caking of the nanopowder which can obstruct the N_2 gas flow.

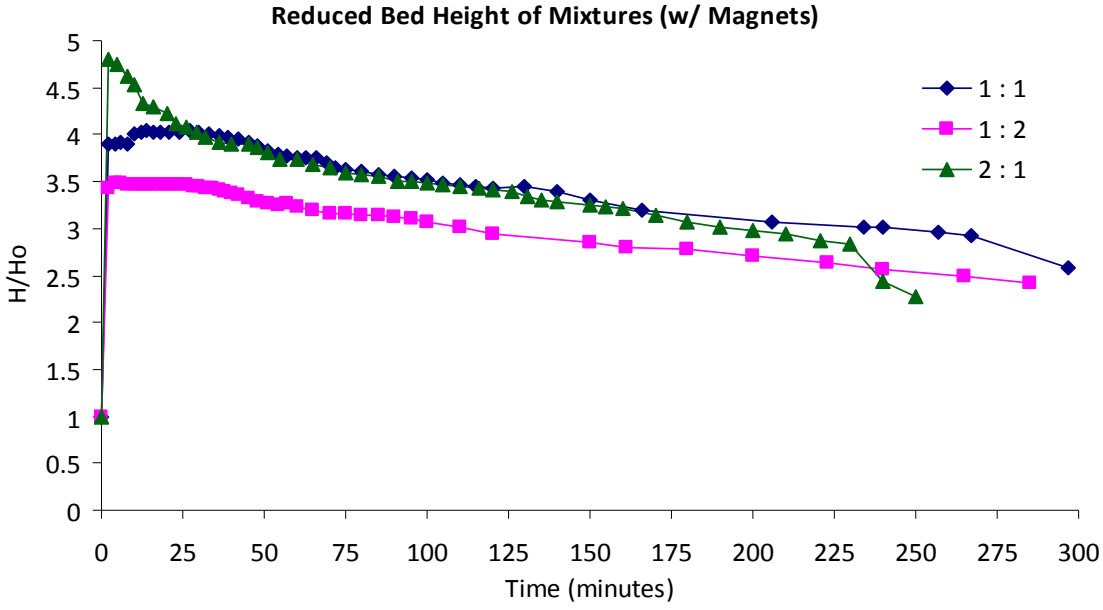

Figure 5.8 The reduced bed height versus time for mixtures of R974 SiO_2 and Al_2O_3 Alu C at 1:1, 1:2 and 2:1 weight-to-weight ratio. Nitrogen velocity of 1.32cm/s.

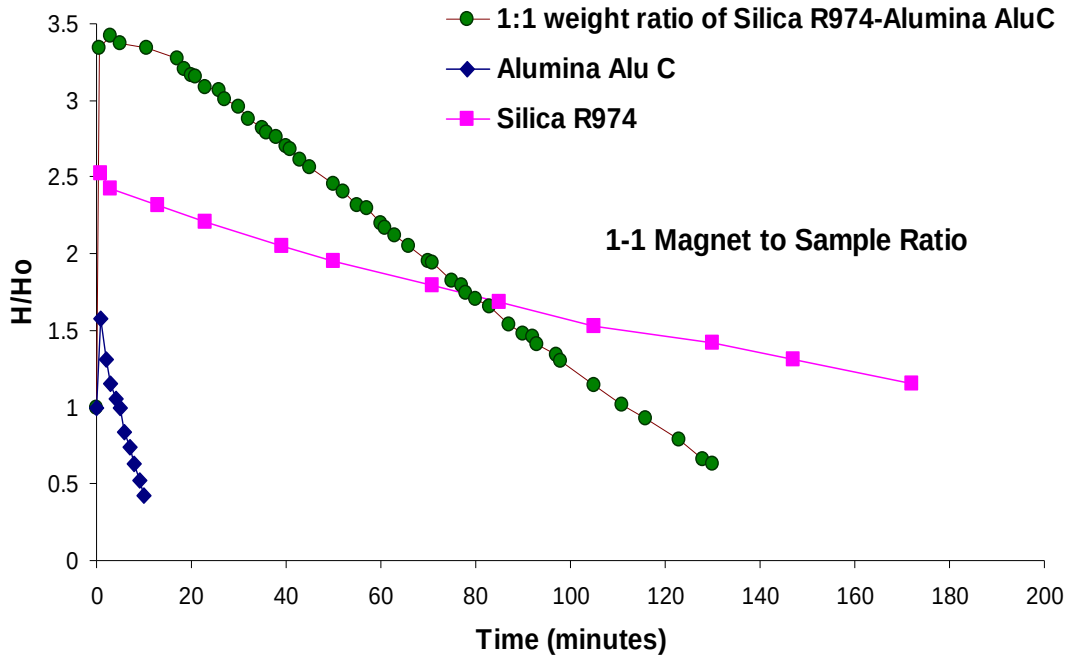

Figure 5.9 The reduced bed height of R974, Alu C and a mixture of 1:1 weight ratio of R974 and Alu C. Magnet-to-sample weight ratio of 1-1.

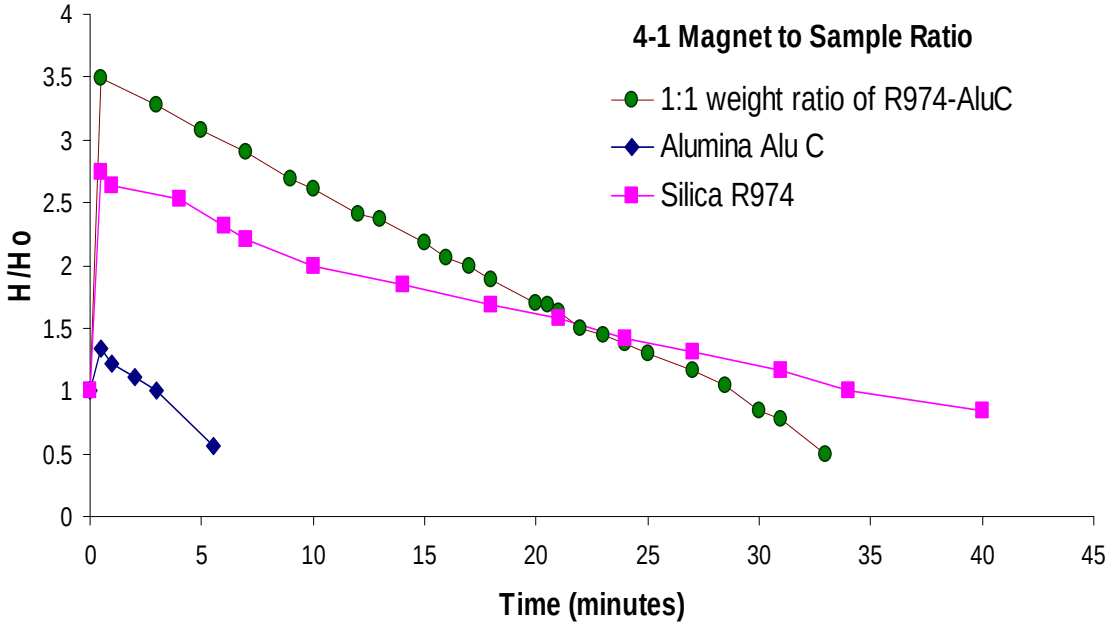

Figure 5.10 The reduced bed height of R974, Alu C and a mixture of 1:1 weight ratio of R974 and Alu C. Magnet-to-sample weight ratio of 4-1.

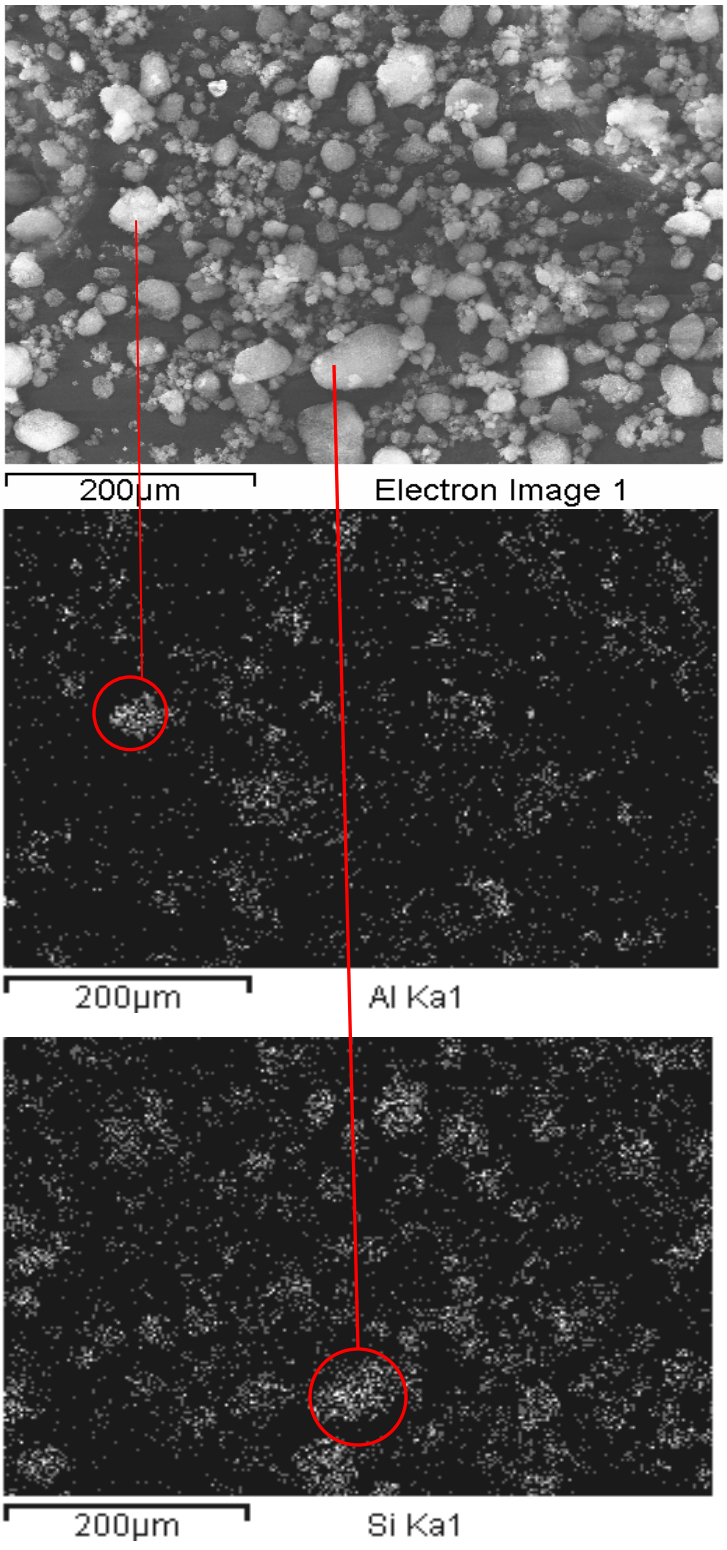

Figure 5.11 SEM image (top), aluminum map (middle) and silica map (bottom) for 4-1 magnet-to-sample ratio of a 1:1 alumina to silica ratio. Processing time of 5 minutes.

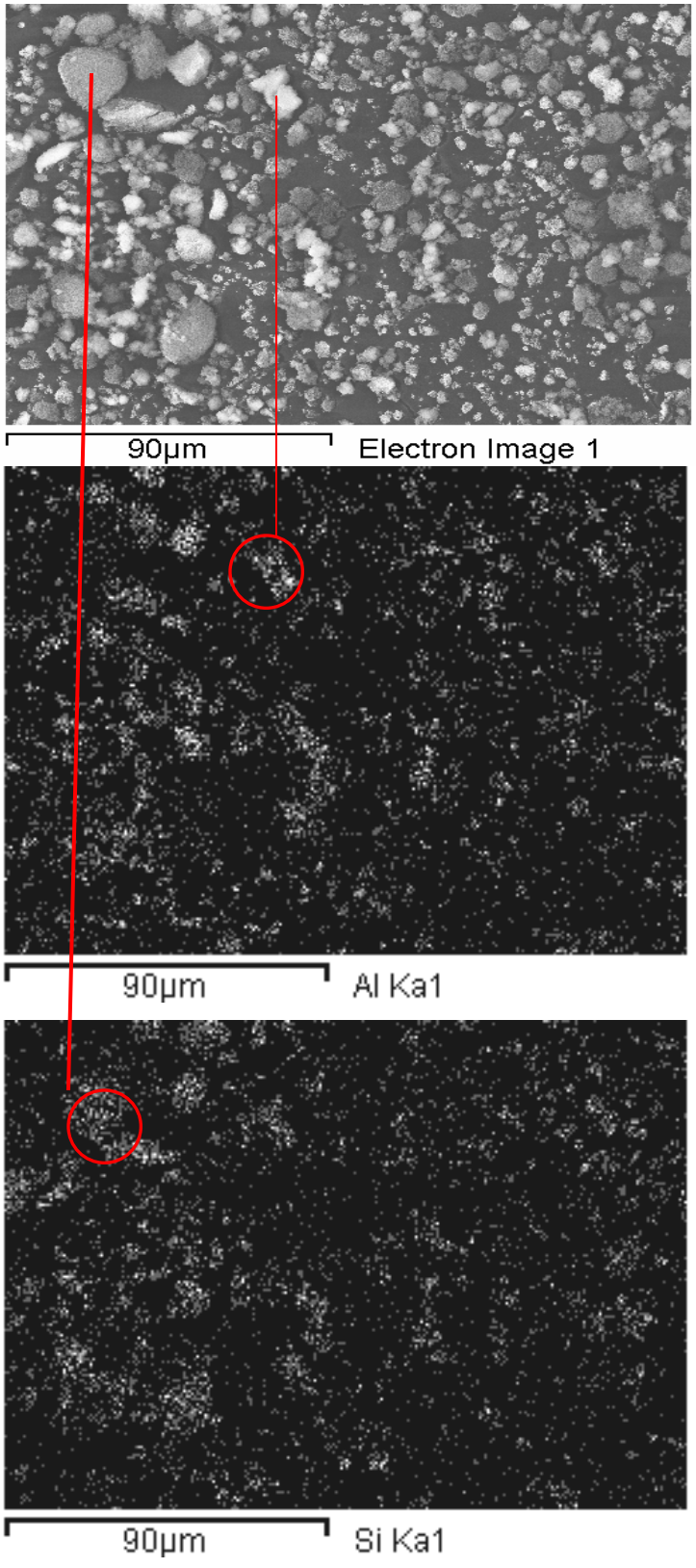

Figure 5.12 SEM image (top), aluminum map (middle) and silica map (bottom) for 4-1 magnet-to-sample ratio of a 1:1 alumina to silica ratio. Processing time of 20 minutes.

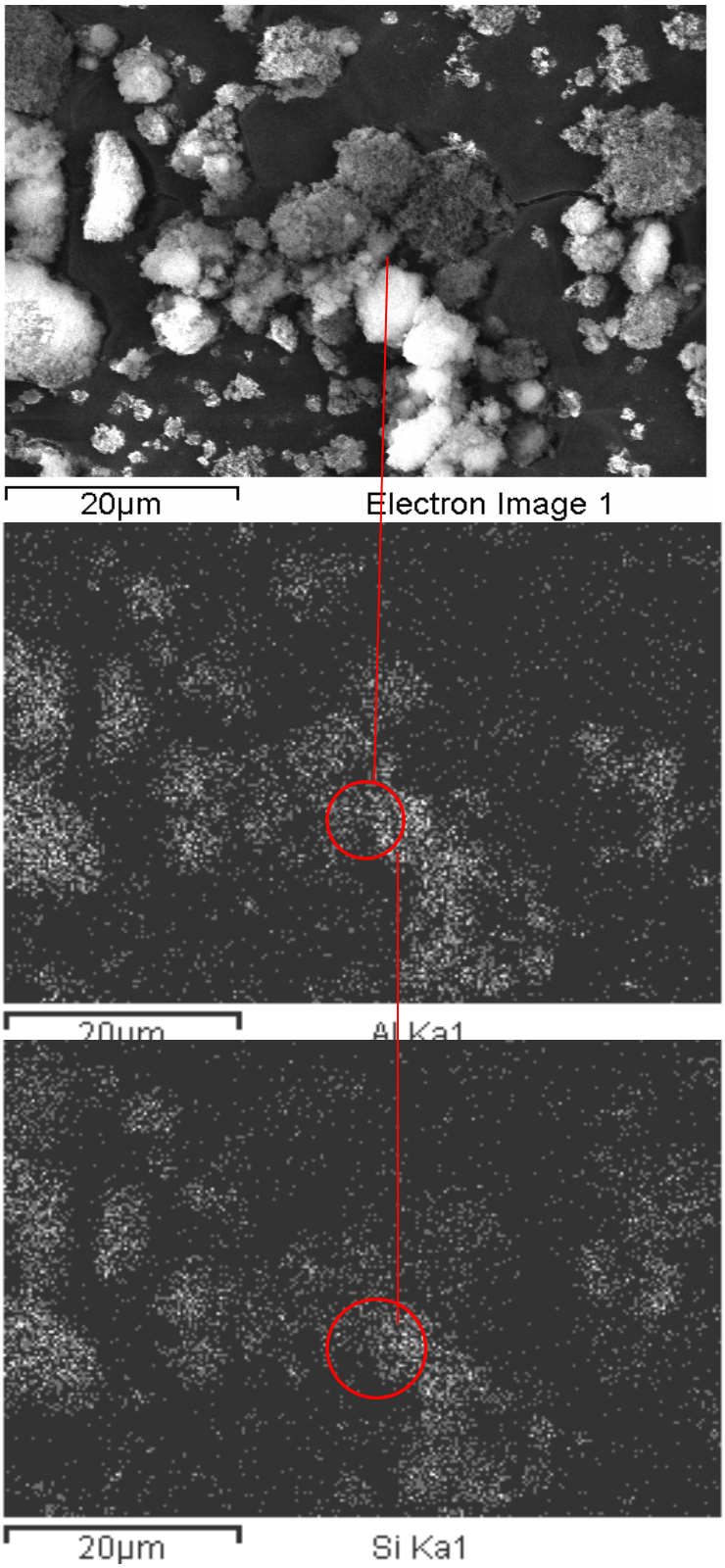

Figure 5.13 SEM image (top), aluminum map (middle) and silica map (bottom) for 4-1 magnet-to-sample ratio of a 1:1 alumina to silica ratio. Processing time of 30 minutes.

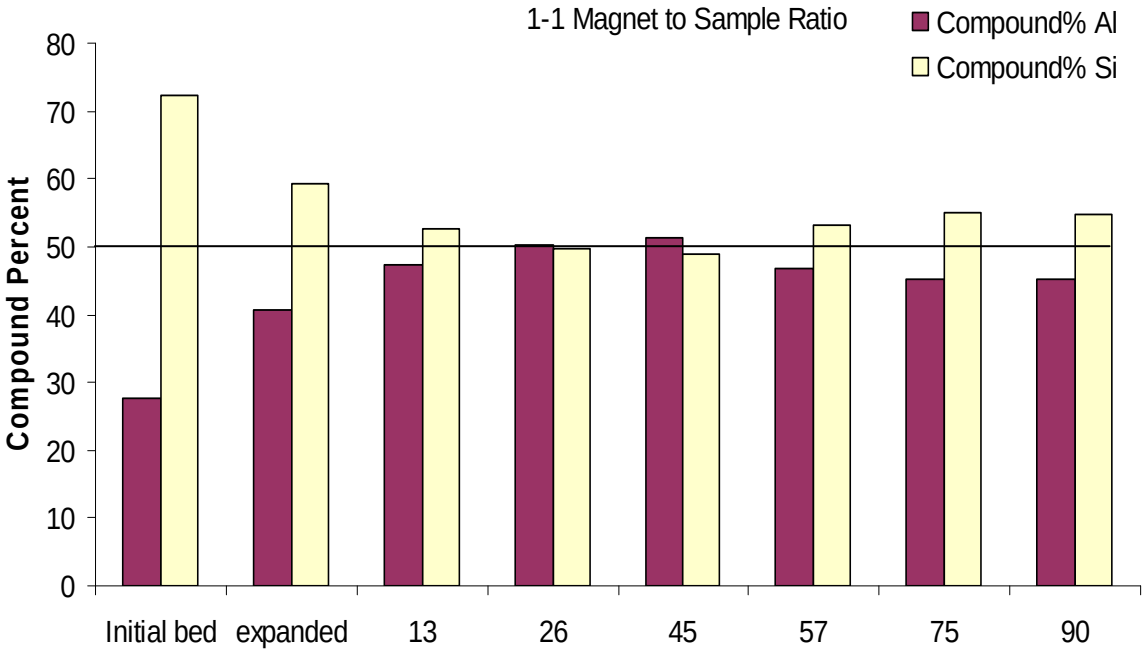

Figure 5.14 The concentration of constituents (silica and alumina), at the surface of the fluidize bed, versus time. Samples collected at a 1-1 magnet to sample ratio.

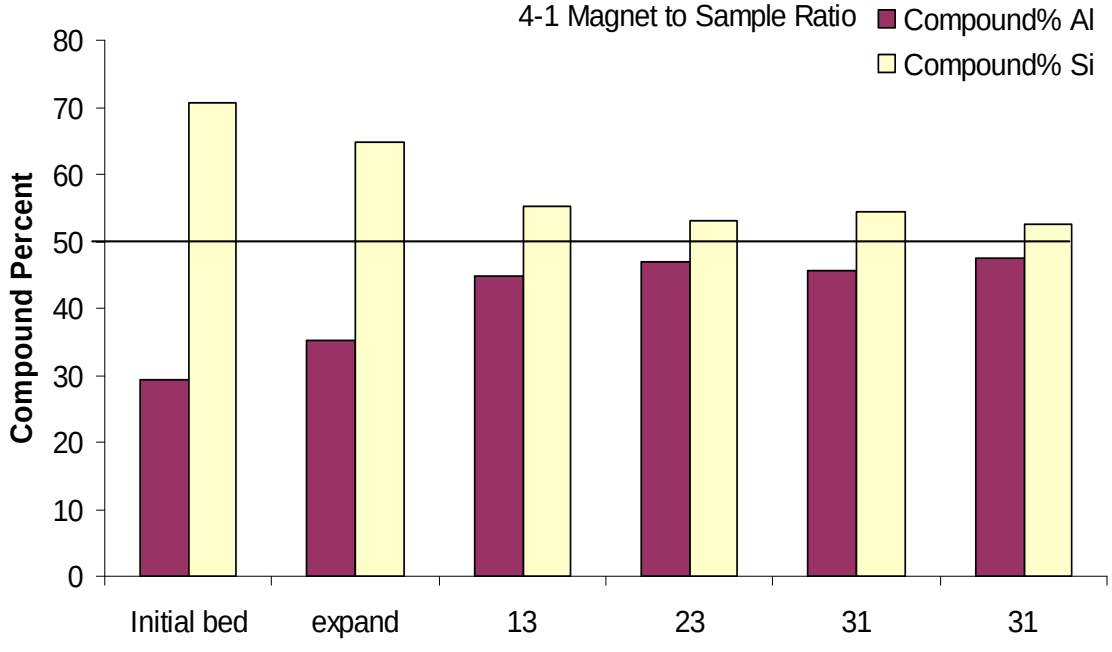

Figure 5.15 The concentration of constituents (silica and alumina), at the surface of the fluidize bed, versus time. Samples collected at a 4-1 magnet to sample ratio.

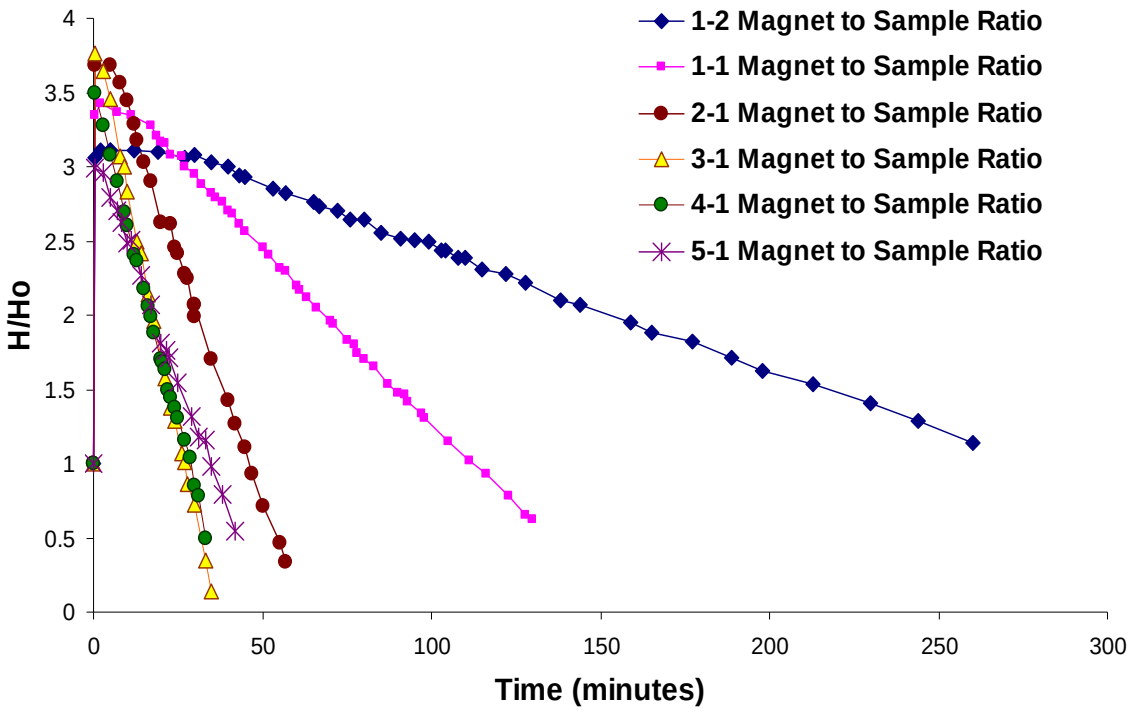

Figure 5.16 The reduced bed height of 1:1 mixtures of R974 and Alu C for magnet-to-sample weight ratios of 5:1, 4:1, 3:1, 2:1, 1:1 and 1:2. Velocity 2.85cm/s.

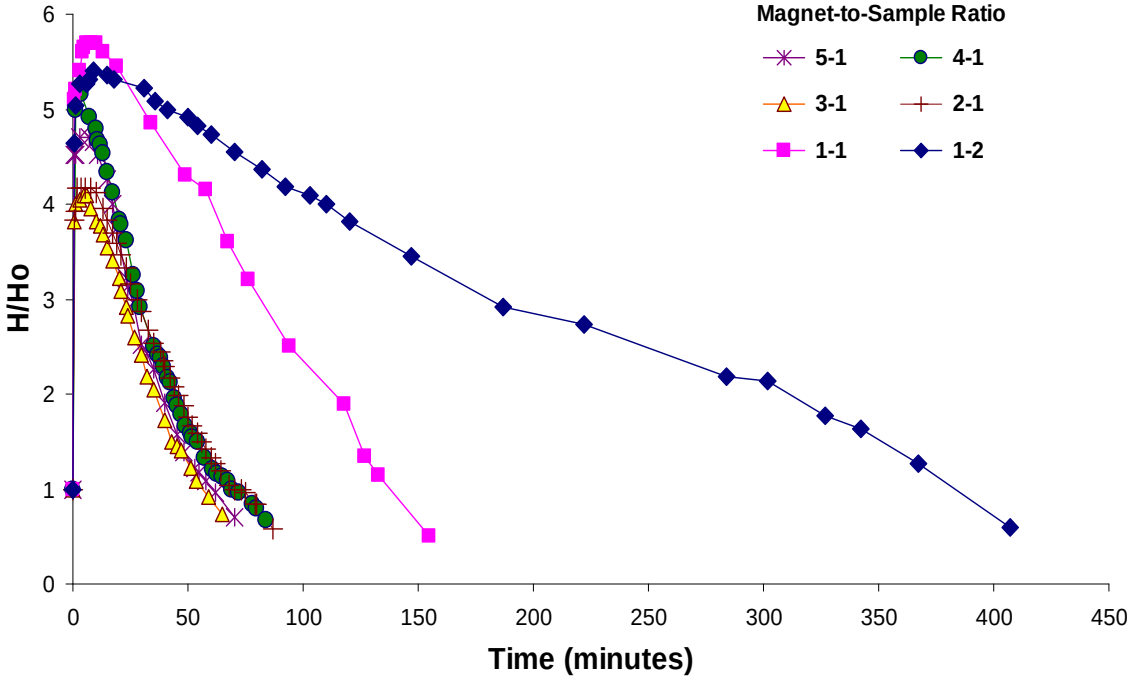

Figure 5.17 The reduced bed height of 1:1 mixtures of R974 and Alu C for magnet-to-sample weight ratios of 5:1, 4:1, 3:1, 2:1, 1:1 and 1:2. Velocity 3.36cm/s.

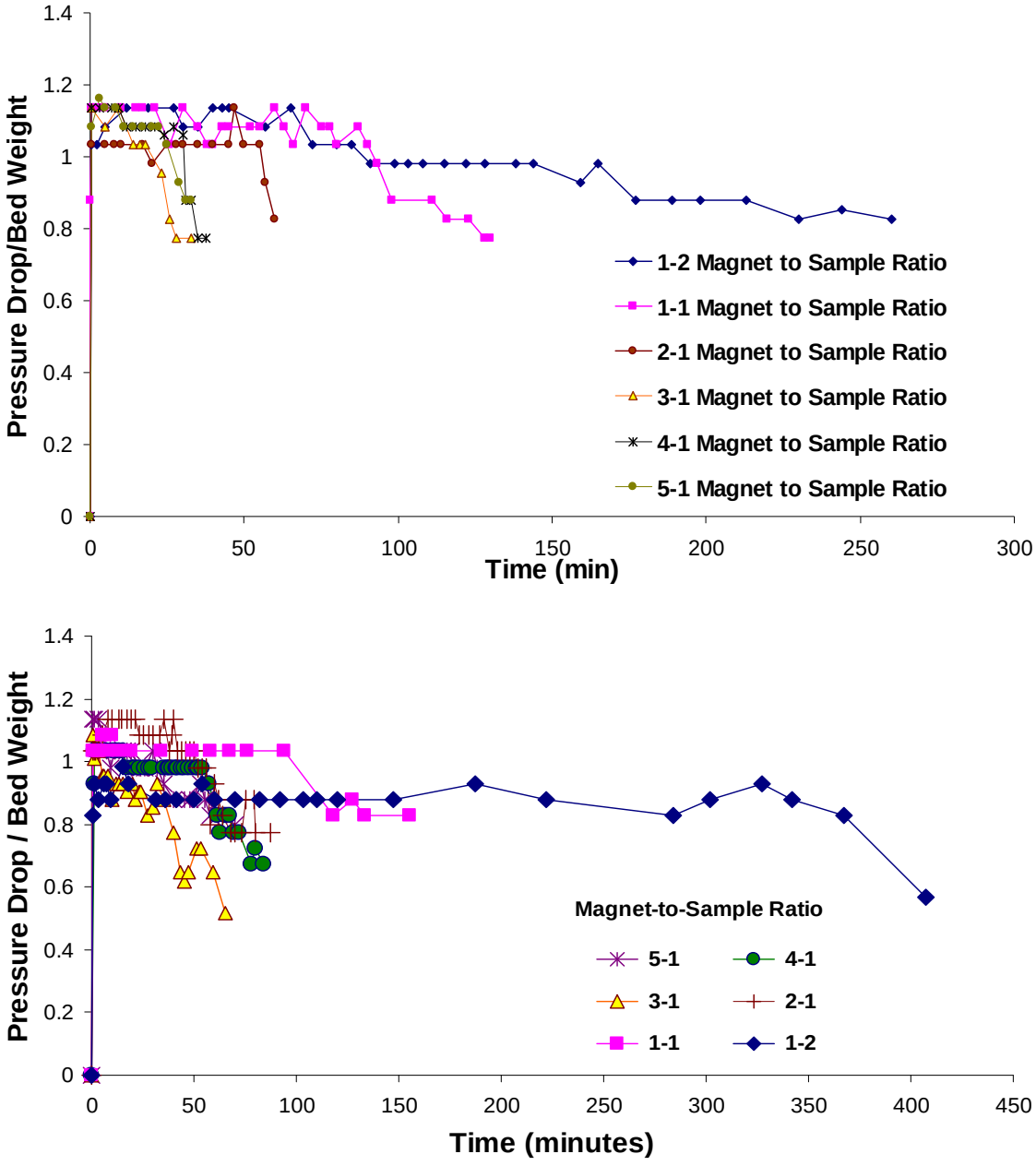

Figure 5.18 The reduced pressure drop of 1:1 mixtures of R974 and Alu C for magnet-to-sample weight ratios of 5:1, 4:1, 3:1, 2:1, 1:1 and 1:2. Velocity 2.85 cm/s (top) and 3.36 cm/s (bottom).

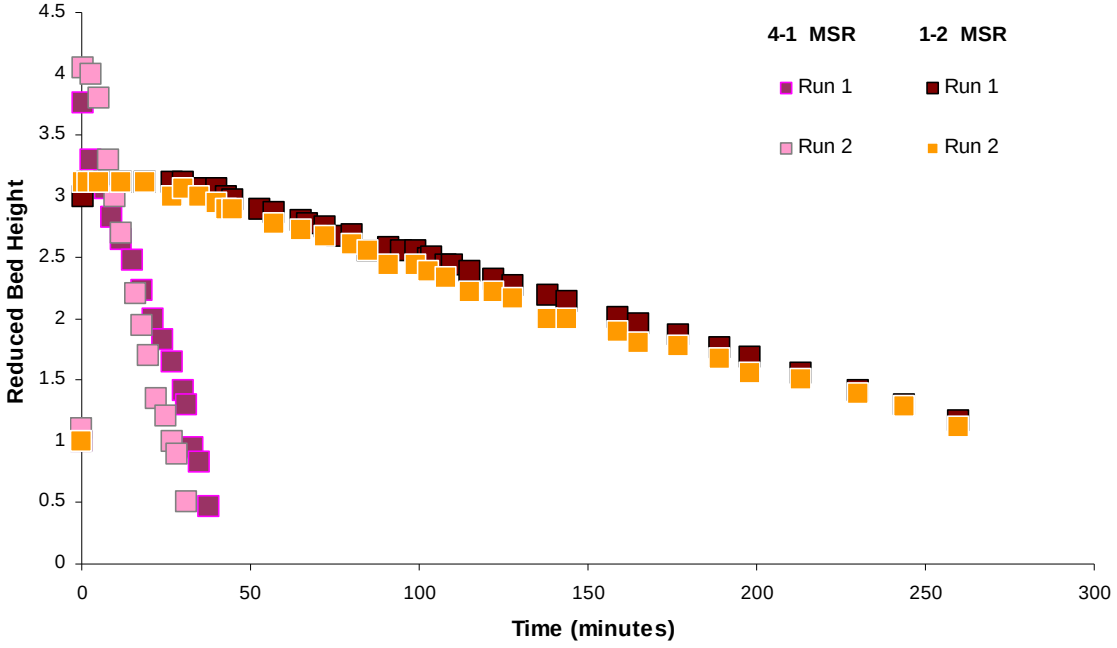

Figure 5.19 Reproduced experiments for reduced bed height versus time for 4-1 and 1-2 magnet-to-sample ratios.

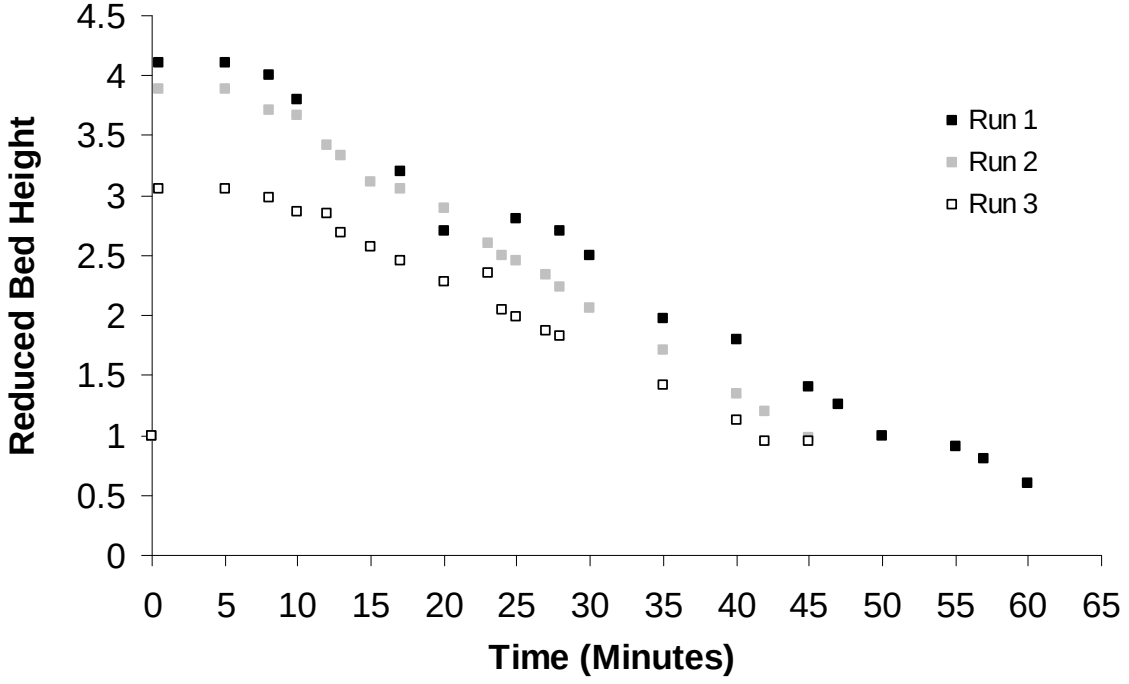

Figure 5.20 Reproduced experiments for reduced bed height versus time for 2-1 magnet-to-sample ratio.

5.2.6 Effect of Magnet Size on the Magnetically Assisted Fluidization of Nanopowders

Three magnet size ranges are broadly classified here as large, medium, and small categories. Size range from 2360 microns to 1700 microns is used as large magnets. The medium magnets, which are used in the most experiments, have a size range from 1400 microns to 850 microns. The small magnets are in the range of 1000 microns to 600 microns. Magnet-to-sample mass ratios of 1:1 and 4:1 are used to investigate the effect of magnet size on the rate of decrease in bed height. The purpose of the study is to determine if smaller magnets will carry enough forces to break up agglomerates, or by increasing the mass of the magnets, will the increased mass of each individual magnet play a larger role in the mixing.

The results of the different magnet sizes are shown in Figure 4.21 and 4.22 as reduced bed height versus time. From the figure, it appears that the number of magnets plays a significant role in the rate of the bed height decline. The smaller magnets caused the bed to decline at an accelerated rate than for the medium magnets and the large magnets slowed the rate of decline. The bed height data is then plotted versus the product of time and the number of magnets, similar to MAIM and LMAIM processes. The decline in bed height data did not form a singular curve like in earlier magnetically assisted mixing techniques, Figures 4.23 and 4.24. The results do show similar rates of bed decline versus the product of time and number of magnets. The results indicate that the rate of bed decline can be controlled by the number of magnets present in the system, not by the size of the magnets. However the bed expansion depends on other properties, such as preconditioning of the powders and how the powder properties are changing with processing.

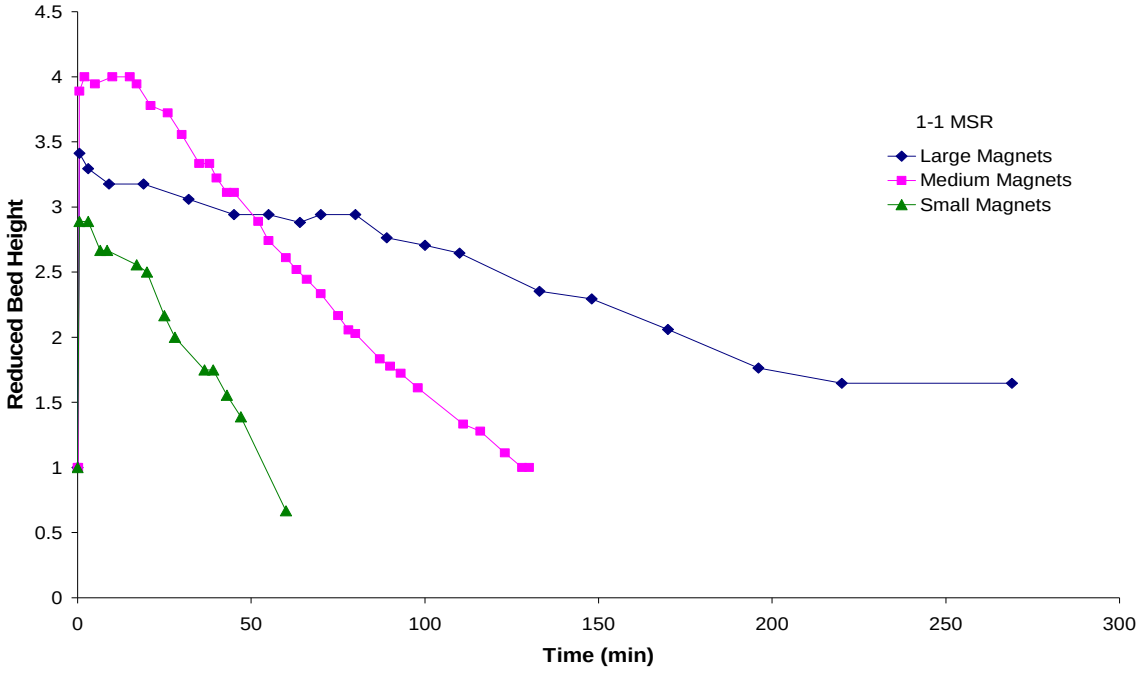

Figure 5.21 Reduced bed height versus time for the size ranges of 2360-1700 (large), 1400-850 (medium) and 1000-600 (small) microns for SiO2/Al2O3 mixture. Run with a 1:1 magnet-to-sample ratio.

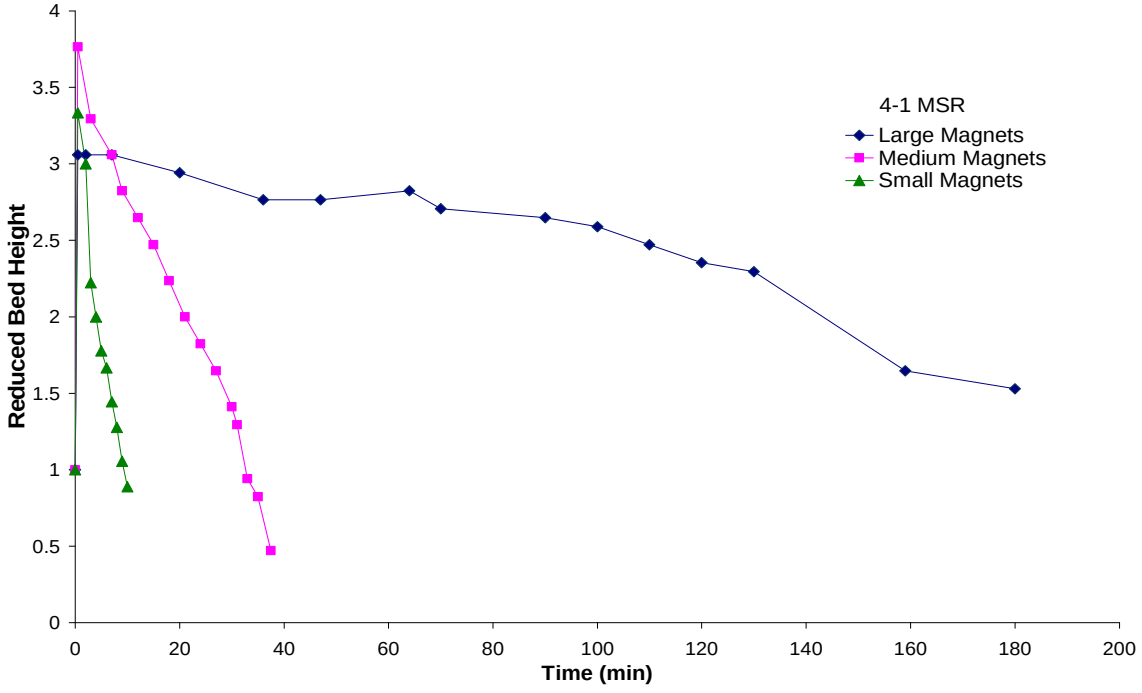

Figure 5.22 Reduced bed height versus time for the size ranges of 2360-1700 (large), 1400-850 (medium) and 1000-600 (small) microns for SiO2/Al2O3 mixture. Run with a 4:1 magnet-to-sample ratio.

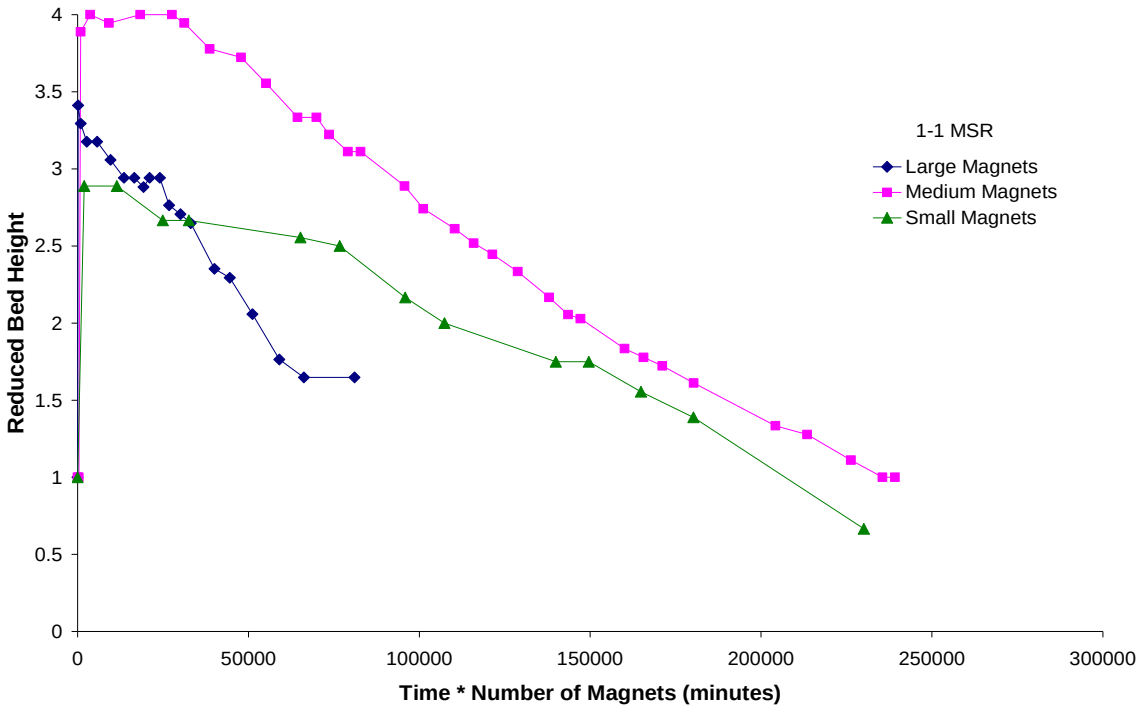

Figure 5.23 Reduced bed height versus time * number of magnets for the size ranges of 2360-1700 (large), 1400-850 (medium) and 1000-600 (small) microns for SiO2/Al2O3 mixture. Run with a 1:1 magnet-to-sample ratio.

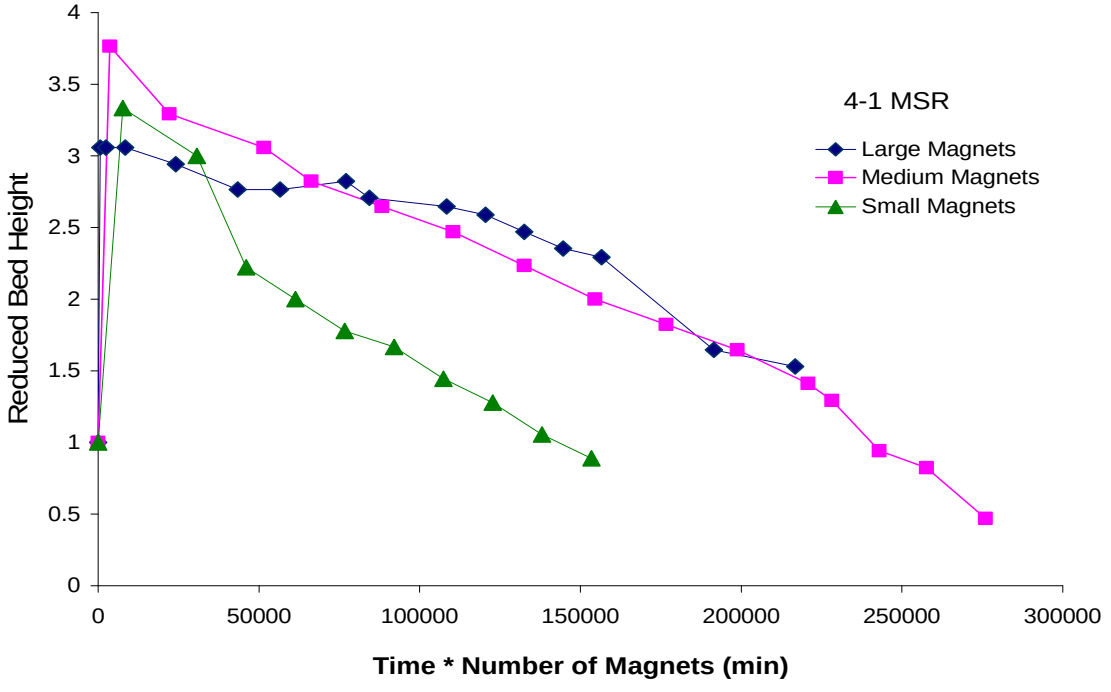

Figure 5.24 Reduced bed height versus time * number of magnets for the size ranges of 2360-1700 (large), 1400-850 (medium) and 1000-600 (small) microns for SiO2/Al2O3 mixture. Run with a 4:1 magnet-to-sample ratio.

5.2.7 Reducing Electrostatic Effects

Among the cohesive forces, nanoparticles form larger agglomerates due to liquid bridges and electrostatic effects. It is unsure how much electrostatic forces play a role with the decrease in bed height. Extensive research on the effect of electrostatic charge on the behavior of fluidized beds has been done by Park et al,[15] who showed that electrostatic charge is dissipated by increasing the relative humidity of the fluidizing air. Mehrani et al.[16] suggested that most of the electrostatic charges generated in a fluidized bed are due to the entrained particles that leave the bed, which results in buildup of a net charge inside of the fluidized bed. Quevedo et. al.[17] found that electrostatic charges can be removed by bubbling the gas flow through an ethyl alcohol-water solution. The alcohol vapor dissipates the charge buildup.

The gas flow is bubbled through water, ethanol or 50/50 mixture of water to ethanol. The relative humidity increased up to 73%. The reduced bed height versus time data is compared to the bed decline for dry gas flows. All systems are run with 3:1 magnet-to-sample weight ratio. The results, figures 5.25 and 5.26, show no significant difference in the rate of bed decline versus bubbling solution.

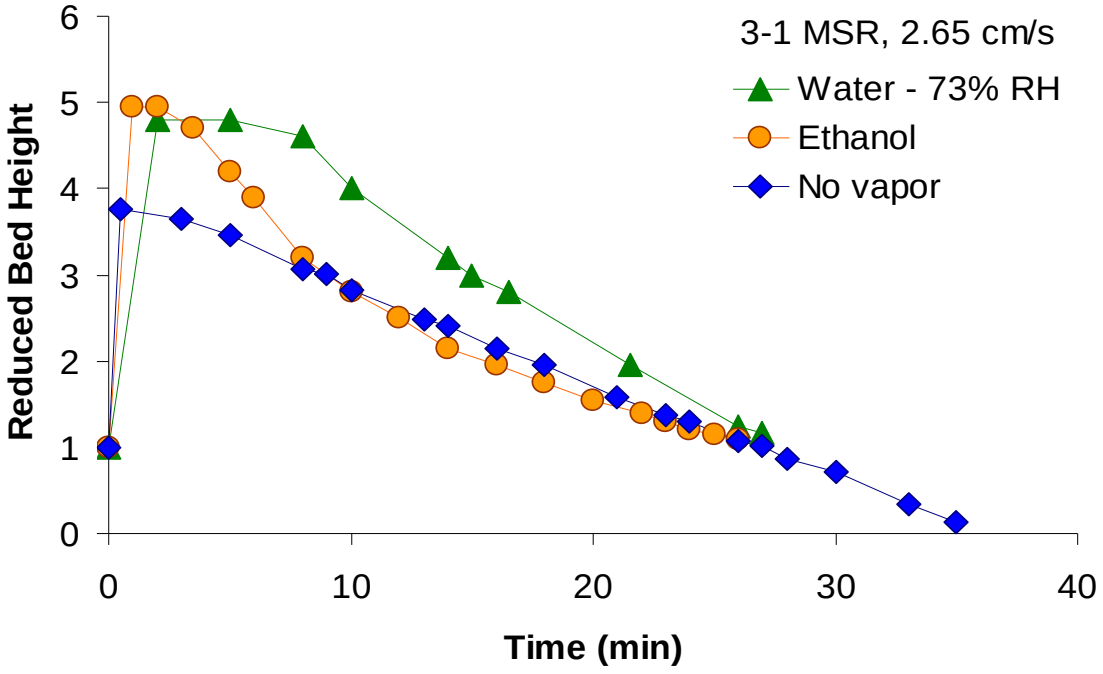

Figure 5.25 Reduced bed height versus time for systems where the dry gas flow is compared with gas flow bubbled through water and ethanol. 3:1 magnet-to-sample ratio.

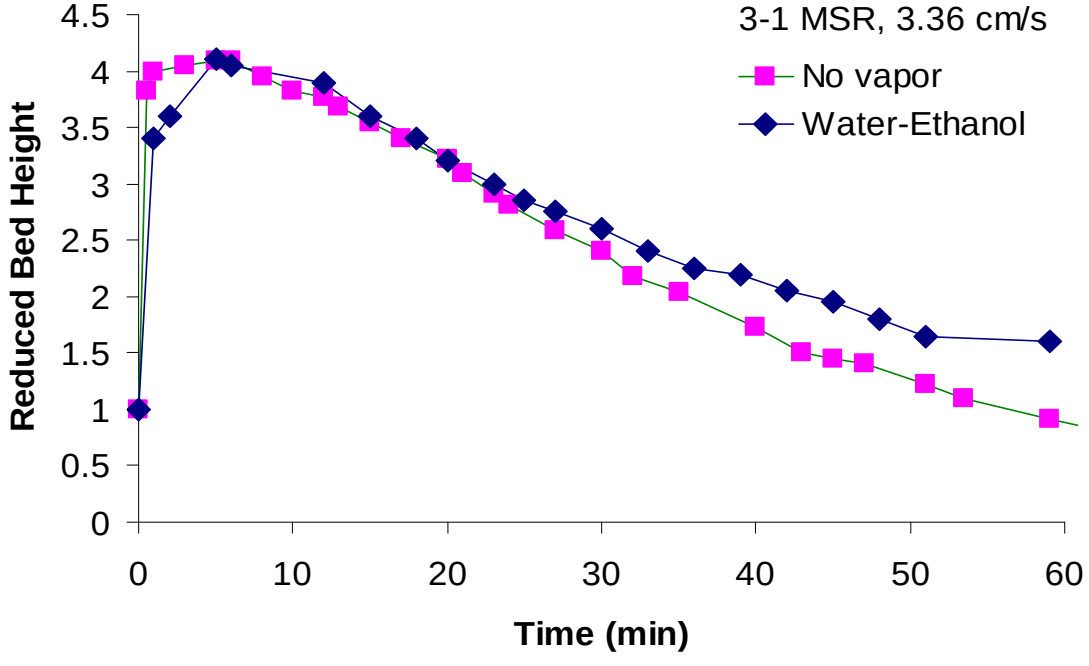

Figure 5.26 Reduced bed height versus time for systems where the dry gas flow is compared with gas flow bubbled through a 50/50 mixture of water and ethanol. 3:1 magnet-to-sample ratio.

5.2.8 Changes in Powder Bed Properties

Since trying to control electrostatic effects did not seem to have much effect on the rate of bed decline, a closer look at the powders before and after magnetically assisted fludized bed mixing is explored. After processing, the final settled bed height is always less than the initial bed height. By comparing the mass of powder before and after mixing, the loss of powder (either by elution or coating on the column) did not match with the change in bed volume. The ratio of settled bed height at time "t", $h_o(t)$, by the starting bed height, h_o, is presented versus time, Figure 5.27.

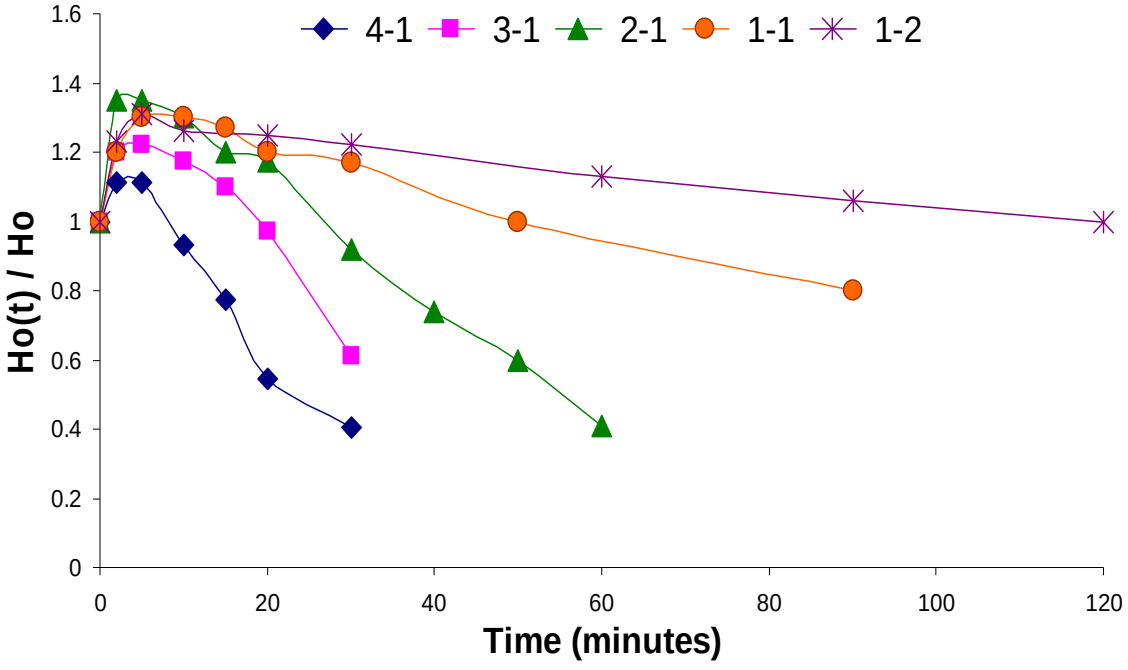

Figure 5.27 The change in the settled bed height versus processing time.

The results indicate that the settled bed height, height of the bed when without gas flow, initially expands with magnetically assisted fluidization processing. This is due to the largest agglomerates being broken down first and being dispersed within the bed. The number of smaller agglomerates increases and the total volume and surface area of

powders increases. After the first moments of expansion, the settled bed height starts to decrease in height. The more magnets present increases the rate of decrease in the settled bed height. The decrease can be caused by a combination of effects. With the shearing taking places in the impaction zone, the voidage of the agglomerates are decreasing, creating denser powders. The densities of the powders are measured before and after magnetically assisted fluidization mixing, Table 5.1. The powder densities increase with increasing processing time and magnet-to-sample ratio. The denser powders will change the behavior of the fluidized powders from APF to ABF. ABF fluidization requires higher flow rates and less bed expansion is achieved. Another contributing factor to the bed decrease can be due to the weight of the magnets compacting the powders into a cake at the distributor.

Table 5.1 Change in Bulk Density of SiO2 – Al2O3 Mixtures Obtained From MAFB

Magnet to Sample Ratio	Time (mins)	Initial Bulk ρ (g/mL)	Final Bulk ρ (g/mL)	Final ρ/Initial ρ
1-2	260	0.044	0.091	2.092
1-1	45	0.039	0.041	1.057
	123	0.041	0.098	2.378
	130	0.044	0.118	2.698
2-1	30	0.044	0.058	1.325
	60	0.044	0.173	3.957
3-1	30	0.041	0.146	3.541
	35	0.039	0.208	5.300
4-1	30	0.039	0.142	3.605
	37.5	0.046	0.157	3.402
5-1	33	0.039	0.120	3.046
	54	0.044	0.141	3.227

5.2.9 Maintenance of Constant Bed Height Throughout Processing

By maintaining constant bed height, the percentage of the bed falling within the impaction zone, the volume percent where the magnets are colliding with the powder, can be controlled. Using this method, velocity versus time data is collected while maintaining the bed height. All experiments, unless otherwise stated, are run with a 3:1 magnet-to-sample ratio and 1:1 component-to-component ratio. Two versions of the

constant bed height experiments are designed. The first runs maintained a constant bed height from start to finish. Two grams of both alumina and silica, and twelve grams of magnets, are added to the column. Three separate reduced bed heights, the ratio of expanded bed height to the initial height of the bed, of 3.5, 3 and 1.9 are maintained, Figure 5.28. Larger initial gas velocities are required to maintain higher reduced bed heights. For the first moments, the bed heights remain fairly constant before slight changes to the velocity are required. After a given processing time, longer times required for the larger reduced bed height values, velocity changes are required more frequently and the rate of velocity increase also increased. The most changes in velocity occurred with the lowest reduced bed height of 1.9, while the reduced bed height of 3.5 remained fluidized the longest. This is due to the fact that a higher percent of the powder is in the impaction zone which is enacting change on the structure of the agglomerates. The collisions and shearing is occurring on more agglomerates and decreasing their size and creating denser powder faster than for the larger reduced bed heights. Upon reaching high gas velocities, around 7 cm/s, the smooth fluidization turned into a bubbling fluidization and the powders started to elute from the top of the bed. Elutriation becomes a problem when the powders have been deagglomerated to a small enough size where gravity will be insufficient to keep the particles buoyant versus the high velocity required to maintain a constant height. Once it is noticed that large amount of powder is starting to carry to the top of the column, the experiments are ended. It should be noted that, once the bubbling occurs, if the velocity is lowered, the bubbling stops and the powders fluidize smoothly at a lower bed height.

The next step is to determine the velocity profiles for the other magnet-to-sample ratios (MSR). A reduced bed height of 2 is chosen and the velocities are collected for 4:1, 2:1, 1:1 and 1:2 are added to the previously collected 3:1 data. The results indicate that a greater rate of increase in gas velocity is required for the higher MSR, Figure 5.29. To determine if there is a dependency on the number of magnets present in the bed, the results are plotted versus "time*number of magnets" and "time*magnet-to-sample ratio," Figures 5.30 and 5.31, respectively. There seems like there is some dependency on the amount of magnets present in the system, nevertheless there are more contributing factors that need to be taken into account.

For the next part of the study, the silica-alumina, 1:1, mixture is fluidized up to a reduced bed height of 4 and the bed is allowed to decline. At a specific reduced bed height (approximately 3.5, 3 and 2) the bed height is maintained until the onset of particle elutriation, Figure 5.32. Experiments are all run with a 3:1 MSR. When comparing the velocity profiles from Figure 5.32 to Figure 5.28, there seems to be a very similar trend in the velocity profile once the bed height is maintained at a fixed height. Runs of single component systems, pure silica and pure alumina, are also compared in Figure 5.33 and 5.34, respectively. As with previous fluidization results, the silica remained fluidized much longer than the mixture and the alumina is the first of the beds to decline. An example of reproducible velocity and height versus time data are plotted in Figure 5.35 for a silica-alumina mixture, with a 3:1 MSR, fluidized to a reduced bed height of 4 and fixed at a reduced bed height of 3.

The densities of the powders are calculated, Table 5.2, and the results show similar densities between the constant bed height and the corresponding decline then

fixed bed height data. The higher densities are collected from experiments with lower fixed bed heights. These data points are reproducible, assuming that the powders are conditioned similarly.

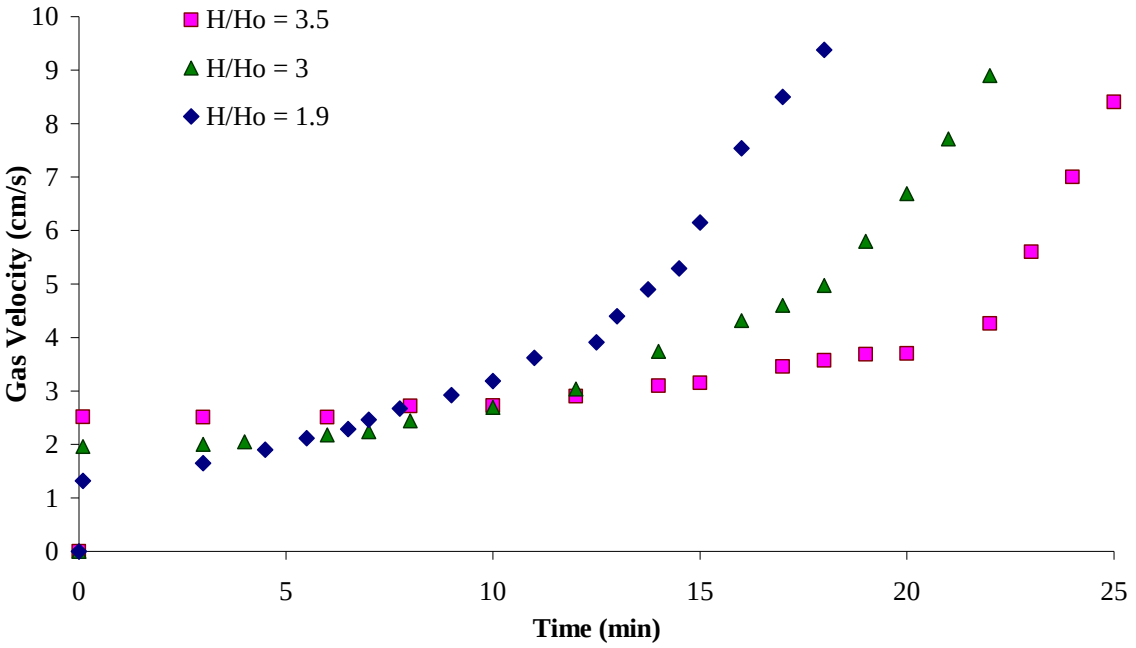

Figure 5.28 Maintaining a constant height from start (left) and maintaining the height after the bed has started its decline (right).

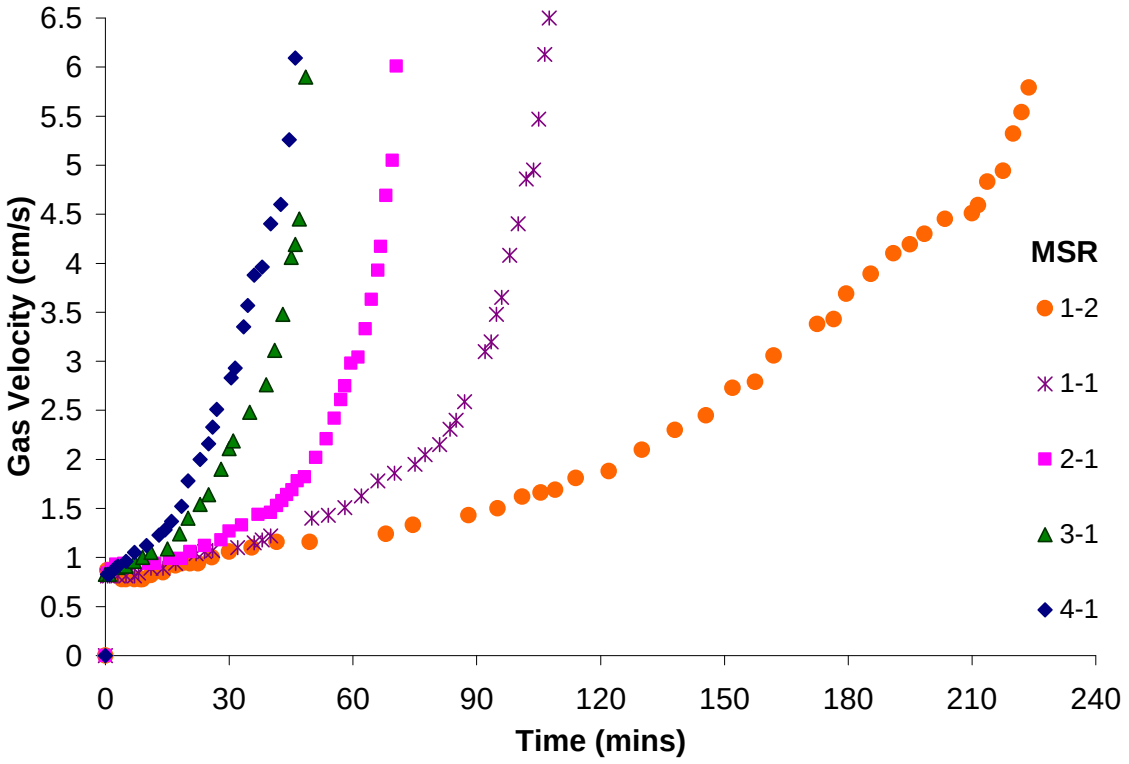

Figure 5.29 Gas velocity versus time while maintaining a constant reduced bed height of 2. Run with various magnet-to-sample ratios (MSR).

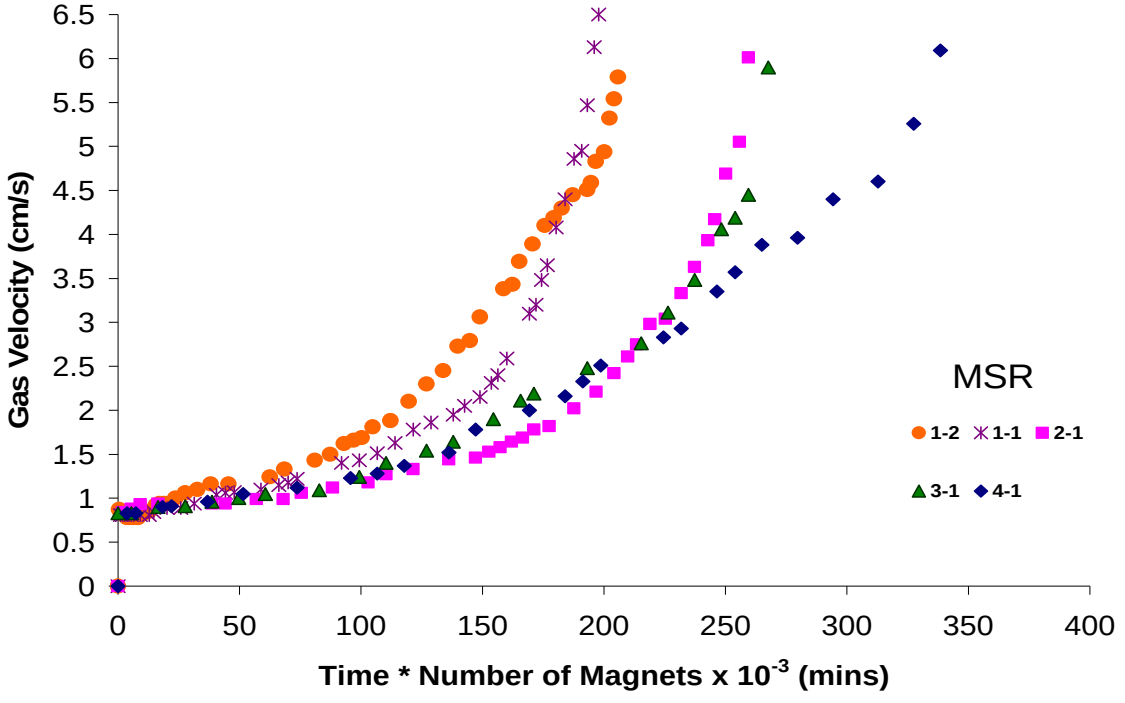

Figure 5.30 Gas velocity versus time * number of magnets while maintaining a constant reduced bed height of 2. Run with various magnet-to-sample ratios (MSR).

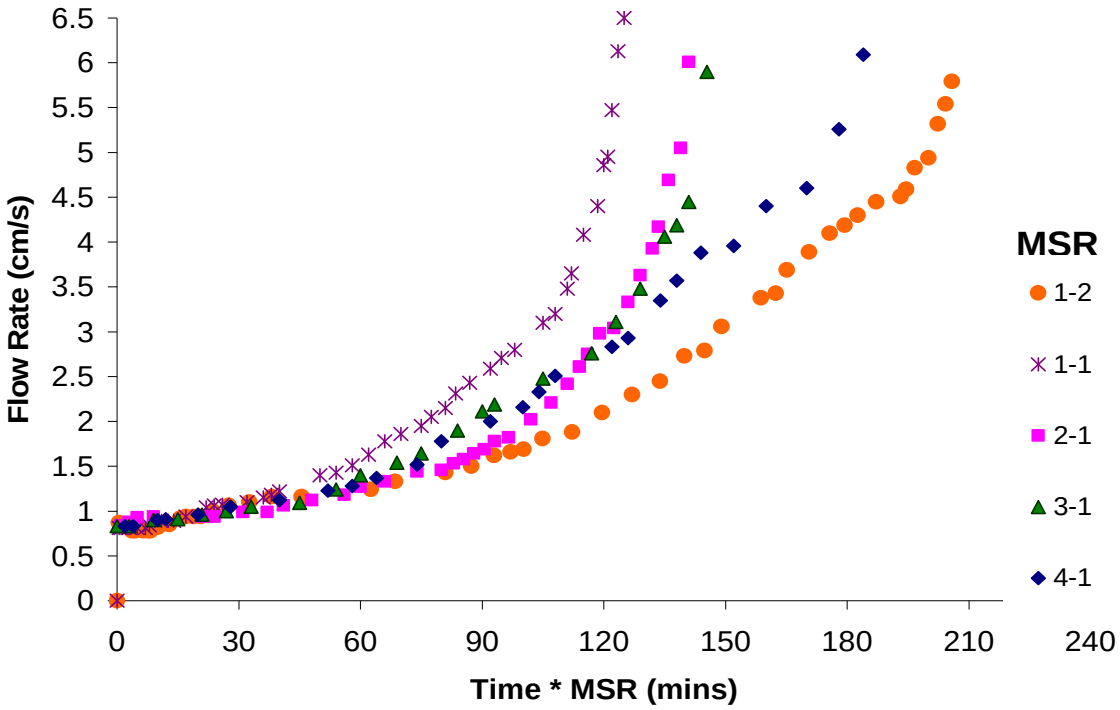

Figure 5.31 Gas velocity versus time * number of magnets while maintaining a constant reduced bed height of 2. Run with various magnet-to-sample ratios (MSR).

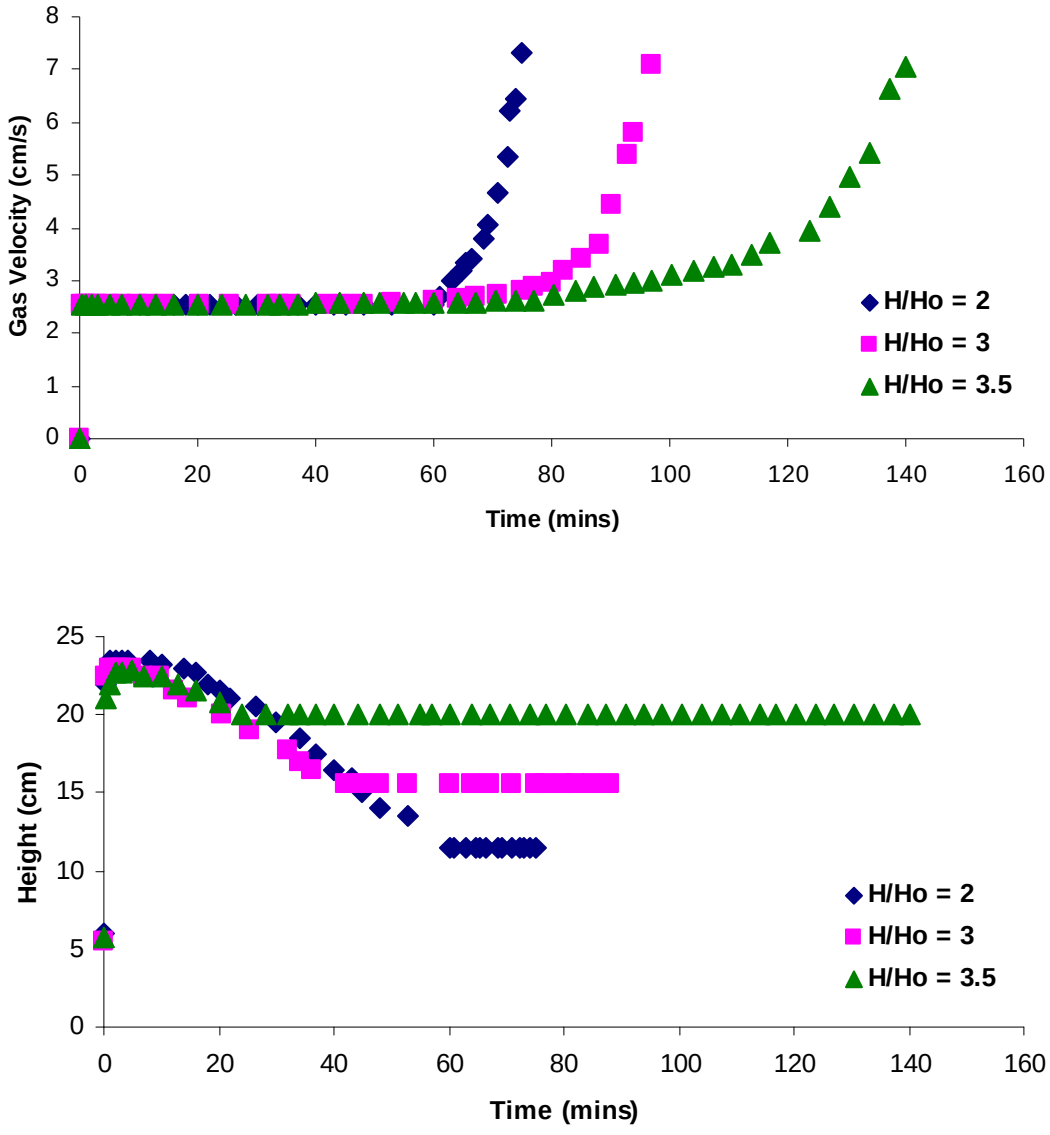

Figure 5.32 Silica-alumina mixtures with a 3:1 MSR are fluidized up to a reduced bed height of 4 and the bed is allowed to naturally decline with processing time. At a specific reduced bed height (approximately 3.5, 3 and 2) the bed height is maintained until the onset of particle elutriation. Top: Gas velocity versus time. Bottom: Bed Height versus time.

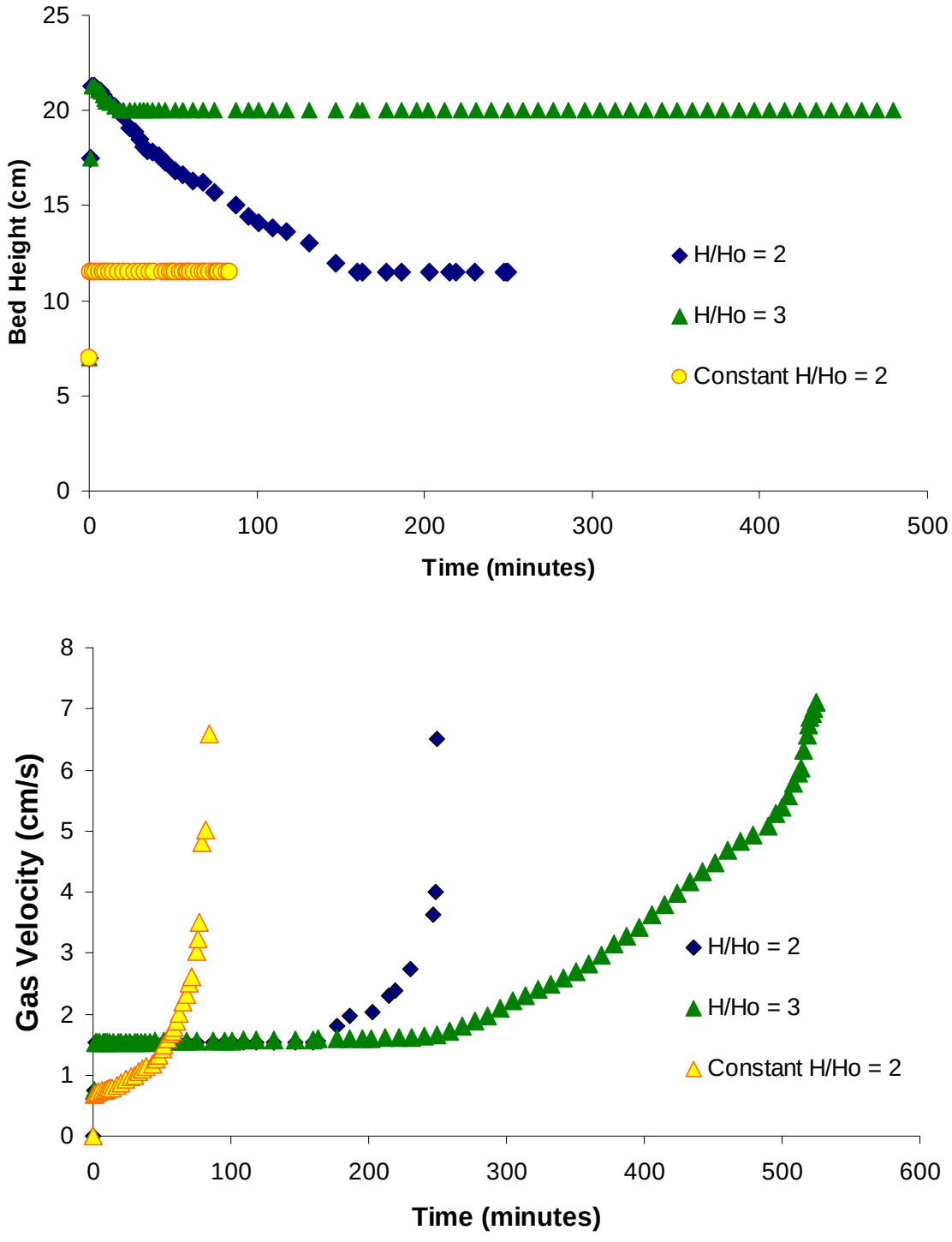

Figure 5.33 Pure silica with a 3:1 MSR are fluidized up to a reduced bed height of 4 and the bed is allowed to naturally decline with processing time. At a specific reduced bed height (approximately 3.5, 3 and 2) the bed height is maintained until the onset of particle elutriation.

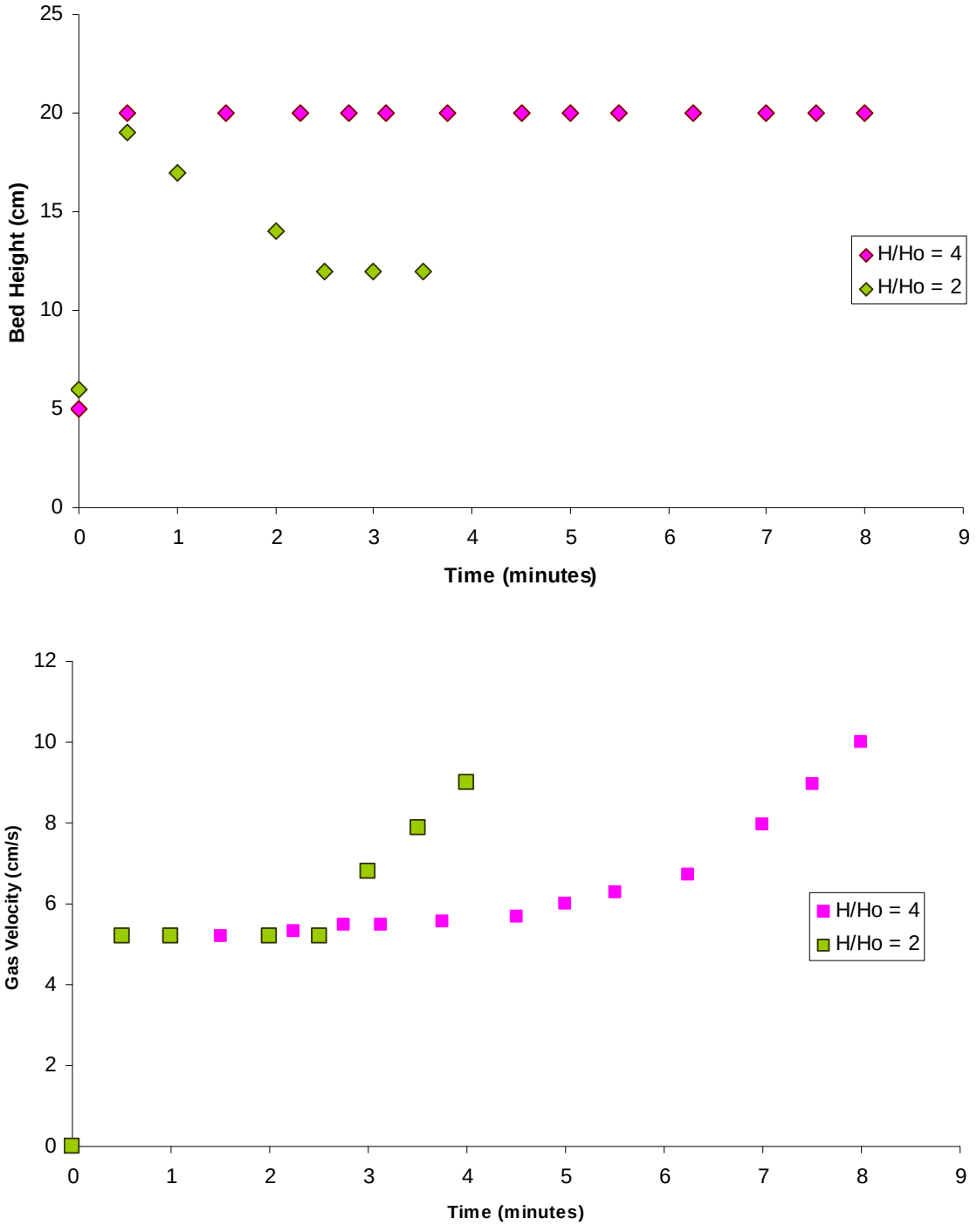

Figure 5.34 Pure alumina mixtures with a 3:1 MSR are fluidized up to a reduced bed height of 4 and the bed is allowed to naturally decline with processing time. At a specific reduced bed height (approximately 3.5, 3 and 2) the bed height is maintained until the onset of particle elutriation.

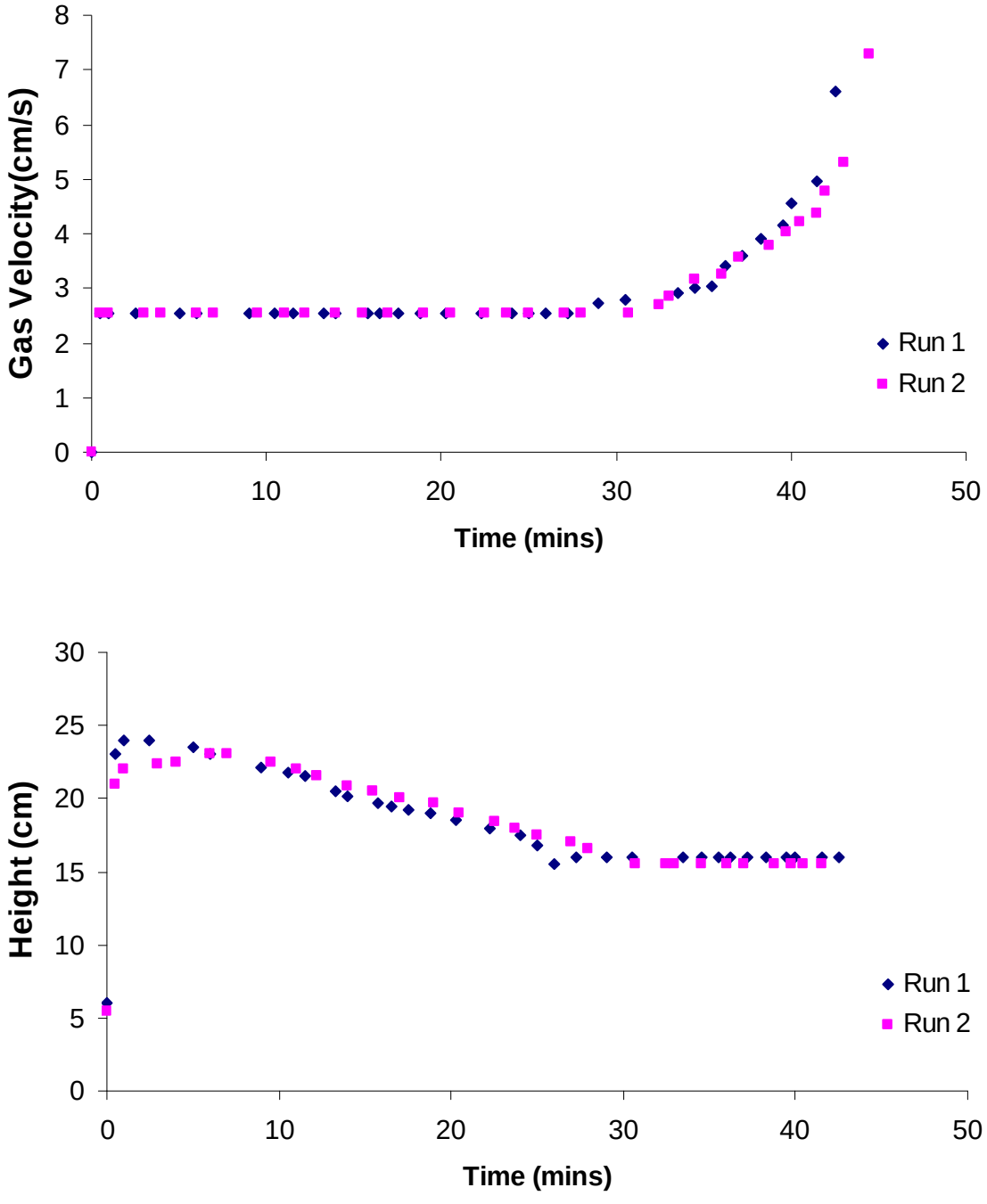

Figure 5.35 Example of the reproducibility of MAFB 3:1 MSR experiments. Fluidized bed allowed to naturally decline, then held at a constant bed height by increasing the velocity. Top: Velocity versus time profile. Bottom: Bed height versus time.

Table 5.2 Change in Bulk Density of SiO2-Al2O3 Mixtures Obtained From MAFB Velocity Profile Study

MSR	Fluidization Method	Density g/mL
3-1	Constant 20cm	0.058
3-1	Declined then fixed 20cm	0.061
3-1	Constant 16cm	0.078
3-1	Decline then fixed 16cm	0.070
3-1	Constant 11.5cm	0.091
3-1	Decline then fixed 11.5cm	0.108
1-1	Constant 11.5cm	0.078
2-1	Constant 11.5cm	0.101
4-1	Constant 11.5cm	0.102

5.3 Homogeneity of Mixing Versus Time

In order to study the effect of processing time, the nano-powders mixtures of silica R974 and alumina Alu C are processed for different magnet-to-sample ratios (5:1, 4:1, 3:1, 2:1, 1:1 and 1:2) and various times up to when the expanded bed height reduces to a value below the initial bed height. Results are shown in Figure 5.36 as Homogeneity of Mixing versus time for a velocity of 2.85 cm/s. It is observed that as either the processing time or the MSR increases, there is an increase in the Homogeneity of Mixing, leading to a better mixture. It should be pointed out that the lines connecting the points in the figures are for the sake of visual clarity. As with the magnet-to-sample ratio, when there is an increase in the processing time, there are more interactions of the moving and rotating magnets with the agglomerates of nanoparticles promoting deagglomeration and mixing.

Homogeneity of Mixing versus time multiplied by the number of magnets is plotted in Figure 5.37. This transformation of the data from Figure 5.36 results in a collapse of the multiple curves, and, as with the other magnetically assisted mixing methods, a single trend is evident for all the values of magnet-to-sample mass ratios. The Homogeneity of Mixing results from Figure 5.37, gas velocity of 2.85 cm/s, is compared to results collected at a faster gas velocity of 3.36 cm/s, Figure 5.38. A similar trend line is obtained to the slower gas velocity is collected with the velocity of 3.36 cm/s. The results show that with a higher gas velocity, a less homogeneous mixture is obtained versus time and the number of magnets. This is because, with the higher velocity, a larger bed height is attained and a smaller percent of the powder is in the impaction zone. The impaction zone is the area where magnetic particles undergo rotational and translational motion creating enough shear to break up agglomerates and assist the fluidization. The total number of magnet-magnet, magnet-wall, and magnet-powder collisions are increased with the increase of magnet-to-sample ratio and processing time. As a result, a better mixture is obtained. From the experimental studies, it is believed that the MAFBM technique can be scaled up while avoiding potential slow downs.

Homogeneity of Mixing results obtained from maintenance of a constant bed height are compared in Table 5.3. Similar to the trend of density increase, fluidized beds which are held at similar constant bed heights produced similar results. Higher values of Homogeneity of Mixing are obtained for the bed heights with lower constant bed heights. As with the other fluidize bed studies, when a higher percentage of powders are located in the impaction zone, great values of HoM are obtained.

Finally the Homogeneity of Mixing results obtained from MAFB mixing are compared to previous results collected in the dissertation, Figure 5.39. The results show that MAFB can obtain more homogeneous mixtures than conventional methods as well as magnetically assisted impaction mixing in liquid mediums. A major side effect that will accompany higher values of Homogeneity of Mixing is that the processing required to create a more homogeneous sample will result in a large amount of powders forming a cake at the bottom of the bed.

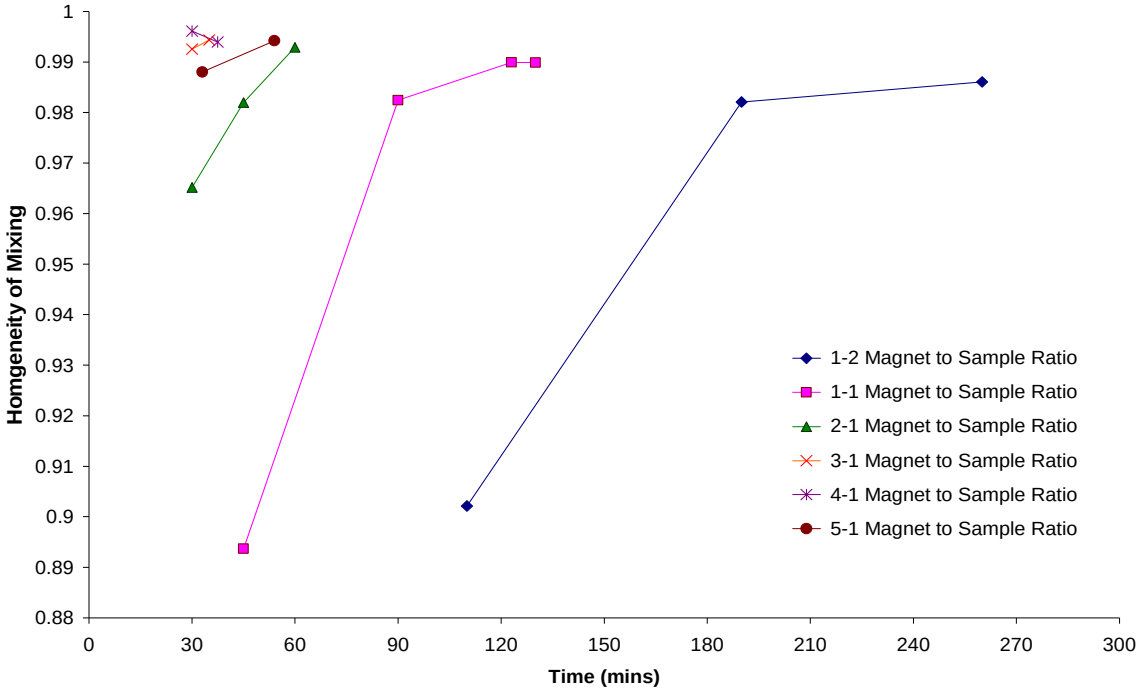

Figure 5.36 Homogeneity of Mixing versus time for various mixing times for SiO2/Al2O3 mixtures and a magnet size range of 1400-850 microns.

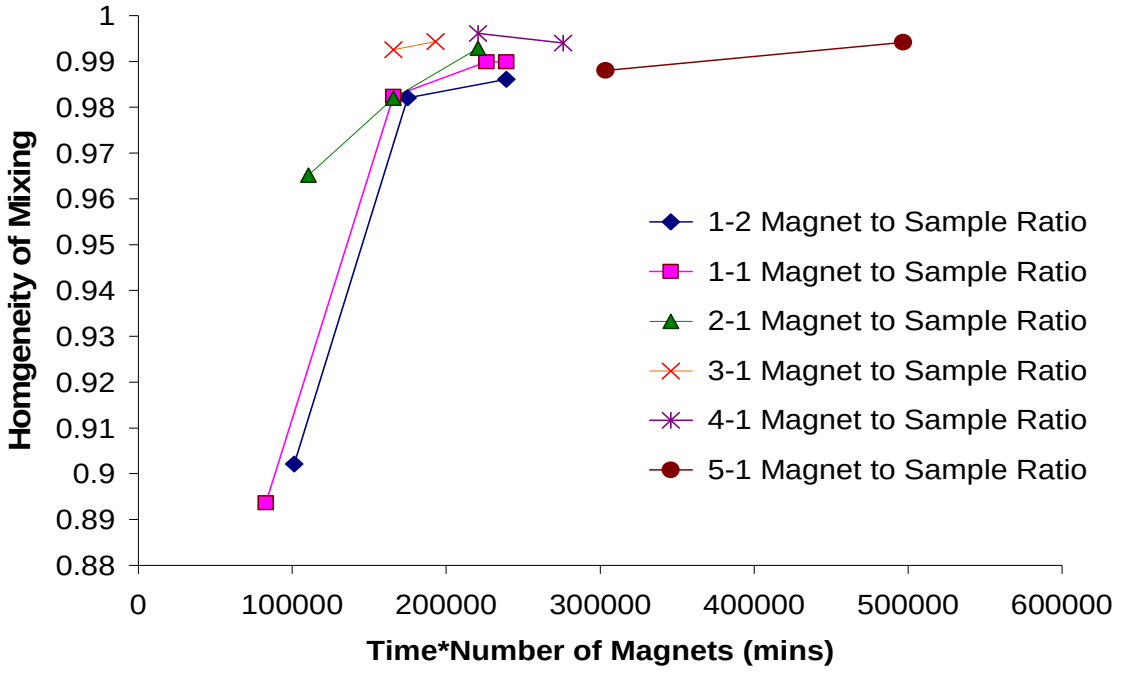

Figure 5.37 The Homogeneity of Mixing for 1:1 mixtures of R974 and Alu C for magnet-to-sample weight ratios of 5:1, 4:1, 3:1, 2:1, 1:1 and 1:2. Velocity is 2.85 cm/s.

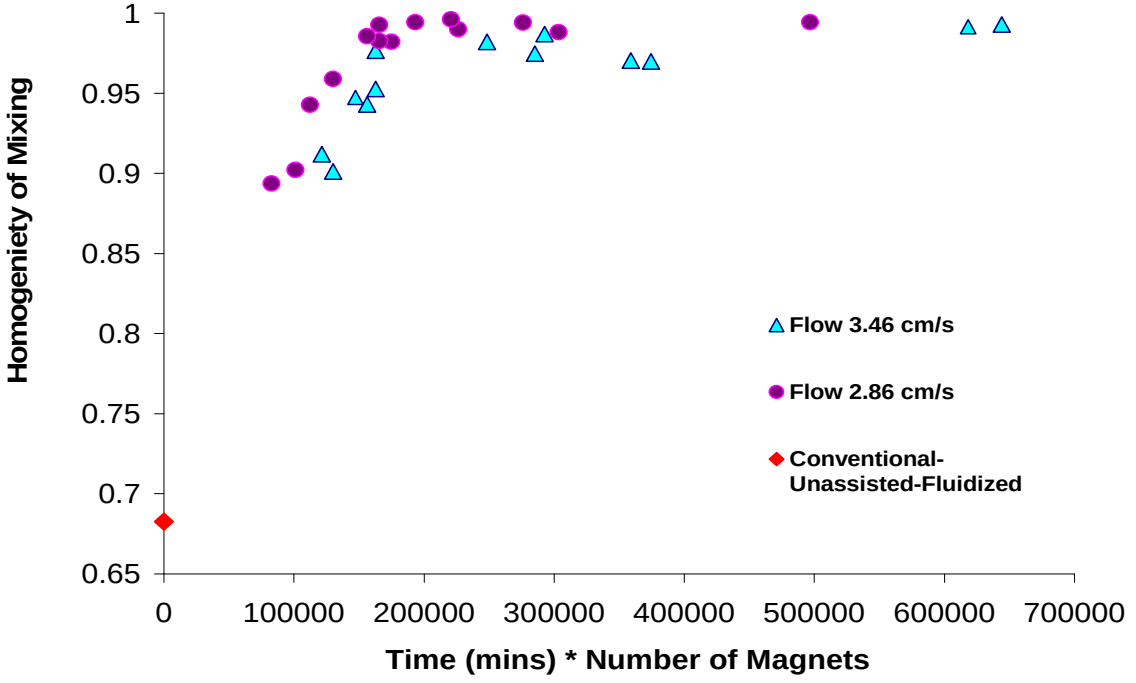

Figure 5.38 The Homogeneity of Mixing for 1:1 mixtures of R974 and Alu C for magnet-to-sample weight ratios of 5:1, 4:1, 3:1, 2:1, 1:1 and 1:2. Velocities of 2.85 cm/s and 3.36 cm/s.

Table 5.3 Homogeneity of Mixing Versus Constant Bed Height and Declined Then Held Fixed for MAFB Mixing with 4:1, 3:1 and 2:1 MSR

MSR	Fluidization Method	Homogeneity of Mixing
3-1	Constant 20cm	0.9034
3-1	Declined then fixed 20cm	0.9085
3-1	Constant 16cm	0.9410
3-1	Decline then fixed 15cm	0.9619
3-1	Constant 11.5cm	0.9583
3-1	Decline then fixed 11.5cm	0.9633
2-1	Constant 11.5cm	0.9481
4-1	Constant 11.5cm	0.9815

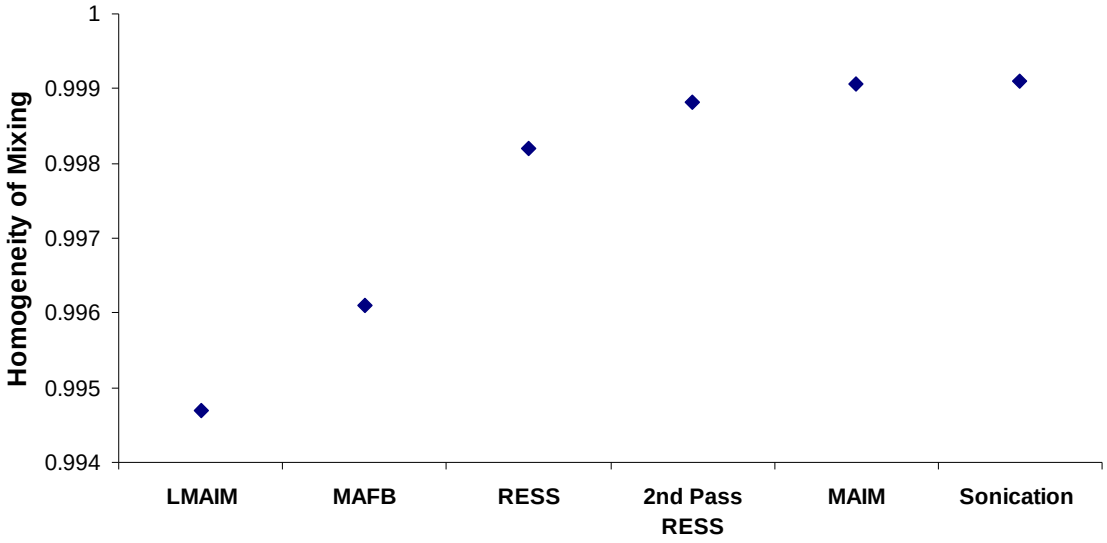

Figure 5.39 The Homogeneity of Mixing for various mixing methods.

5.4 Conclusion

Hysteresis is observed in the pressure drop and bed height measurements for fluidization and de-fluidization of the particle bed. Because de-fluidization yielded greater consistency and produced more accurate values, de-fluidization is used to obtain all fluidization measurements of pressure drop and bed height in this study. In the de-

fluidization studies, SiO_2 nanopowders demonstrated APF behavior: high bed expansions and smooth fluidization at low superficial gas velocities. TiO_2 and Al_2O_3 particles are harder to disperse and fluidize. The bed is unstable with bubbling and channeling behavior, characteristic of ABF.

A magnetically assisted fluidized bed facilitated fluidization and lowered minimum fluidization velocity. Greater bed expansion is observed for a fluidized bed with magnetic assistance than a fluidized bed without. The addition of these magnetic particles stabilized the bed height and minimized particle elutriation. The refluidization of the magnetically processed SiO_2 powder achieved similar results as fluidization of SiO_2 without magnetic assistance. The magnetic assistance of SiO_2 R974 and Al_2O_3 Alu C mixtures produced smaller agglomerates and greater dispersion of the nanoparticles. Mixtures with greater SiO2 concentration reached higher bed expansion ratios but they also declined at a greater rate.

The results indicate that the settled bed height, height of the bed when without gas flow, initially expands with magnetically assisted fluidization processing. This is due to the largest agglomerates being broken down first and being dispersed within the bed. The number of smaller agglomerates increases and the total volume and surface area of powders increases. After the first moments of expansion, the settled bed height starts to decrease in height. The more magnets present increases the rate of decrease in the settled bed height. The decrease can be caused by a combination of effects. With the shearing taking places in the impaction zone, the voidage of the agglomerates are decreasing, creating denser powders. The powder densities increase with increasing processing time and magnet-to-sample ratio. The denser powders will change the behavior of the

fluidized powders from APF to ABF. ABF fluidization requires higher flow rates and less bed expansion is achieved. Another contributing factor to the bed decrease can be due to the weight of the magnets compacting the powders into a cake at the distributor.

The rate of bed height decline may be in relation to homogeneity of mixtures after magnetic processing. For the mixtures of SiO_2 and Al_2O_3 at different weight ratios, the homogeneity of the different mixtures increased for greater rate of collapse. In addition, if the bed height is maintained during magnetic excitation by increasing the velocity over time, the higher flow can prevent caking, allowing the powder to remain fluidized longer.

It is found that with longer processing times and/or higher magnet-to-powder ratios led to an increase in the Homogeneity of Mixing, suggesting improved mixture homogeneity. As processing time is increased, Homogeneity of Mixing is found to increase for all magnet-to-sample ratios. For a long enough processing time, all magnet-to-sample ratios, even the lowest ratio of 1:2, created a homogeneous mixture. When studying the results from with different velocity profiles, it is evident that higher Homogeneity of Mixing results are obtained when a larger percentage of the powder is located within the impaction zone. Besides the amount of magnets, another major factor driving the improvement of mixing quality, and powder density, is the percent of powders in the impaction zone.

Besides simply creating a homogeneous mixture, a potential application for the MAFB mixing would be in the area of coating micron sized powder with a nanopowder mixture through MAFB. If a fluidized bed height is maintained until the bed starts to become unstable and powders are eluting from the top of the bed, the powders can be siphoned off and directed into a coating process, or the larger size powder can be added

to the system and coated within the bed. The quality of the coating can be controlled by the height at which the bed is maintained.

CHAPTER 6

SUMMARY OF CONTRIBUTIONS

This dissertation has primarily focused on the topic of magnetically assisted impaction mixing of nanosized particles. The research is in particle technology: having to deagglomerate nanopowders, agglomerates of nanoparticles, and successfully mix the nanoparticles on the primary particle scale. All the experiments are run using nanoparticles with size ranges from 12 to 21 nanometers.

Most nanoparticle mixing systems are performed in solvents because using solvents can help to penetrate agglomerates, allowing for the dissipation of interparticle changers, and making mixing of nanoparticles easier. Another benefit is that nanopowders are easier, and safer, to handle. When working with magnetically assisted impaction mixing in liquid solvents, longer processing times and/or higher magnet to powder ratios led to better mixing. It is found that as magnet-to-sample ratios increased, the Homogeneity of Mixing increased, suggesting improved mixing. An acidic solution, and the addition of Tween 80 during processing, improved Homogeneity of Mixing results.

While handling nanopowders is easier when in liquid, additional processing steps and costs need to be included into the set up. As processing time is increased, Homogeneity of Mixing is found to increase for all magnet-to-sample ratios. For a long enough processing time, all magnet-to-sample ratios, even the lowest ratio of 1:2, created a homogeneous mixture. Magnet size ranges of 2360 to 1700 microns and 1000 to 600 microns are also studied to compare to the data obtained from the magnet size range of

1400 to 850 microns. It is evident from all the results, including the varying of the magnet size range, that the main process control variable is the product of time with the number of magnets per powder mass, and increase in that within the ranges studied significantly improves the homogeneity of the mixture.

When dry powder mixing using MAIM is compared to mixing in liquid mediums, Chapter 3, dry mixing produced higher values for Homogeneity of Mixing, indicating more homogeneous mixing. While handling of nanopowders in a liquid suspension is easier than dry powder, the end result will produce a less homogeneous mixture.

Magnetically assisted fluidized bed facilitated fluidization and lowered minimum fluidization velocity. Greater bed expansion was observed for a fluidized bed with magnetic assistance than a fluidized bed without magnets. The addition of these magnetic particles stabilized the bed height and minimized particle elutriation. The refluidization of the magnetically processed SiO_2 powder achieved similar results as fluidization of SiO_2 without magnetic assistance.

The settled bed height, height of the bed when without gas flow, initially expands with magnetically assisted fluidization processing. This is due to the largest agglomerates being broken down first and being dispersed within the bed. The number of smaller agglomerates increases and the total volume and surface area of powders increases. After the first moments of expansion, the settled bed height starts to decrease in height. The more magnets present increases the rate of decrease in the settled bed height. The decrease can be caused by a combination of effects. With the shearing taking places in the impaction zone, the voidage of the agglomerates are decreasing, creating denser powders. The powder densities increase with increasing processing time

and magnet-to-sample ratio. The denser powders will change the behavior of the fluidized powders from APF to ABF. ABF fluidization requires higher flow rates and less bed expansion is achieved. Another contributing factor to the bed decrease can be due to the weight of the magnets compacting the powders into a cake on top of the distributor.

Homogeneity of mixing results indicates that MAFB mixing is a drastic improvement from conventional fluidization mixing. The better mixed samples coincide with the decreased bed height. The lower the bed height decreases, the more homogeneous the mixing becomes. This is due to a higher percentage of agglomerates located in the impaction zone leading to better mixing. A side effect of the declined bed height is that the powders start caking at the distributor plate and further increasing the rate of decrease in bed height.

The results clearly suggest viability of magnetically assisted impaction mixing methods to many industrial applications requiring nanocomposite powders. Results also show that unlike previous reports stating ineffectiveness of MAIM for nanoparticle mixing, MAIM may be used to achieve not only mixing quality as good as other environmentally benign methods but also a desired level of mixing, i.e., Homogeneity of Mixing, through adjusting the number of magnets and processing time. Magnetically assisted mixing methods showed comparable Homogeneity of Mixing to sonication in supercritical carbon dioxide and better than rapid expansion of supercritical and high pressure solutions, sonication in deionized water, homogenizer shearing, supercritical stirring and conventional fluidized bed mixing. The MAIM process is simple, and a potentially scalable method that can be used on a wide variety of nano-materials.

APPENDIX A

SAMPLING SITES

Figures A.1 to A.9 show secondary electron and x-ray mapping images for different homogeneity of mixing.

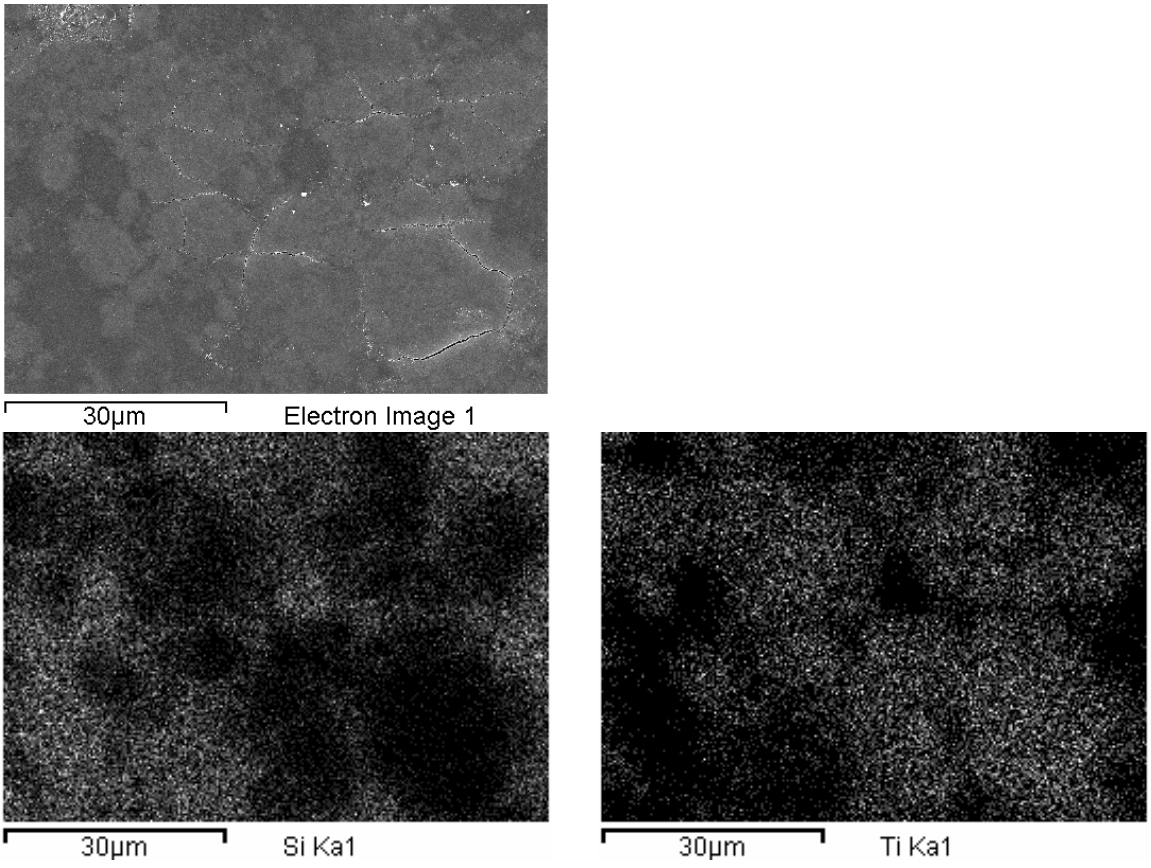

Figure A.1 SEM and EDS Images. For a sample with an intensity of segregation of 0.45. Secondary electron image (top), silicon elemental mapping (left), titanium elemental mapping (right).

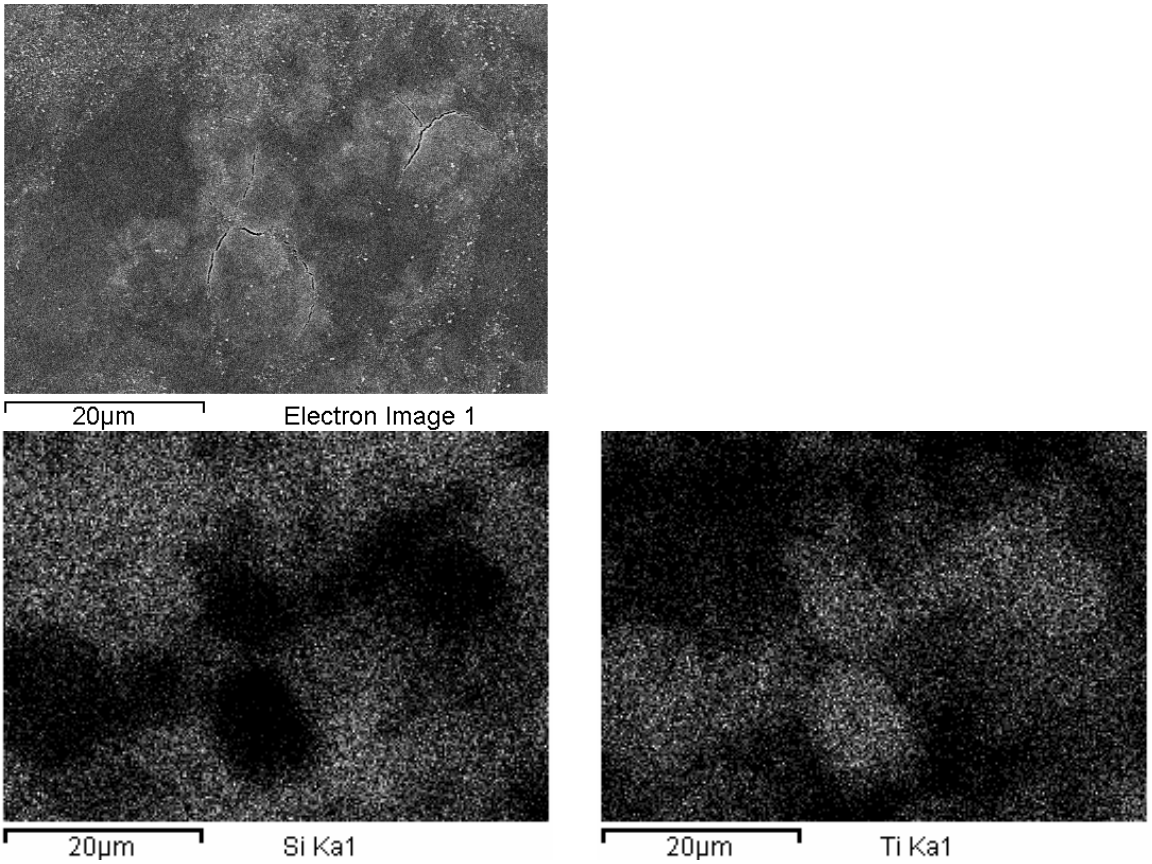

Figure A.2 SEM and EDS Images. For a sample with an intensity of segregation of 0.27. Secondary electron image (top), silicon elemental mapping (left), titanium elemental mapping (right).

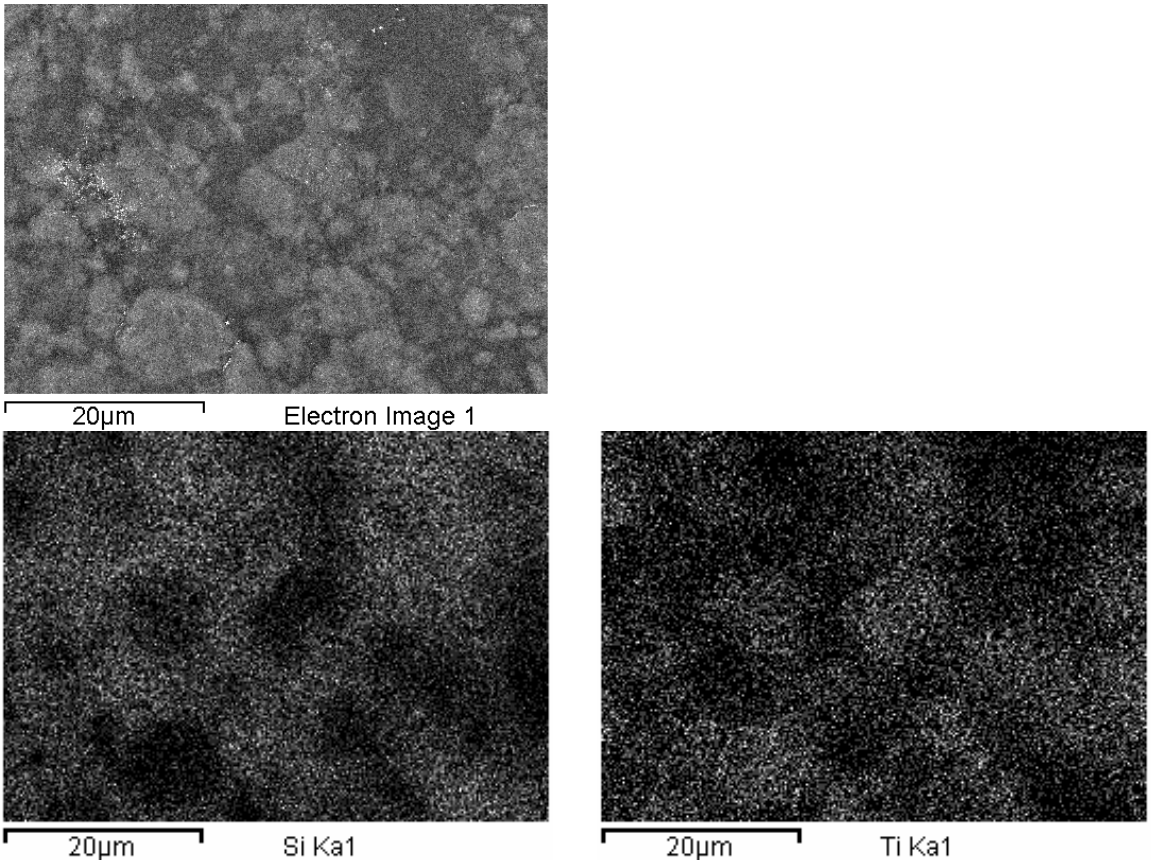

Figure A.3 SEM and EDS Images. For a sample with an intensity of segregation of 0.197. Secondary electron image (top), silicon elemental mapping (left), titanium elemental mapping (right).

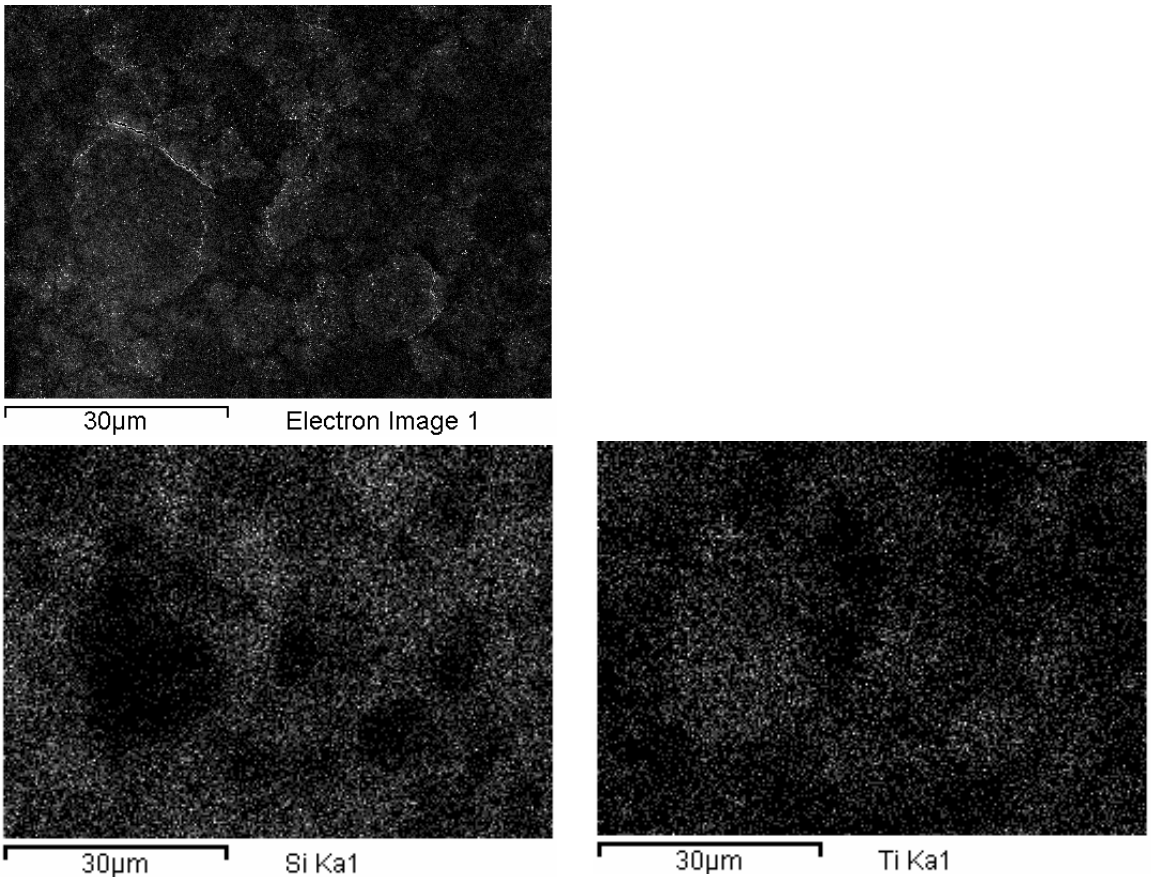

Figure A.4 SEM and EDS Images. For a sample with an intensity of segregation of 0.161. Secondary electron image (top), silicon elemental mapping (left), titanium elemental mapping (right).

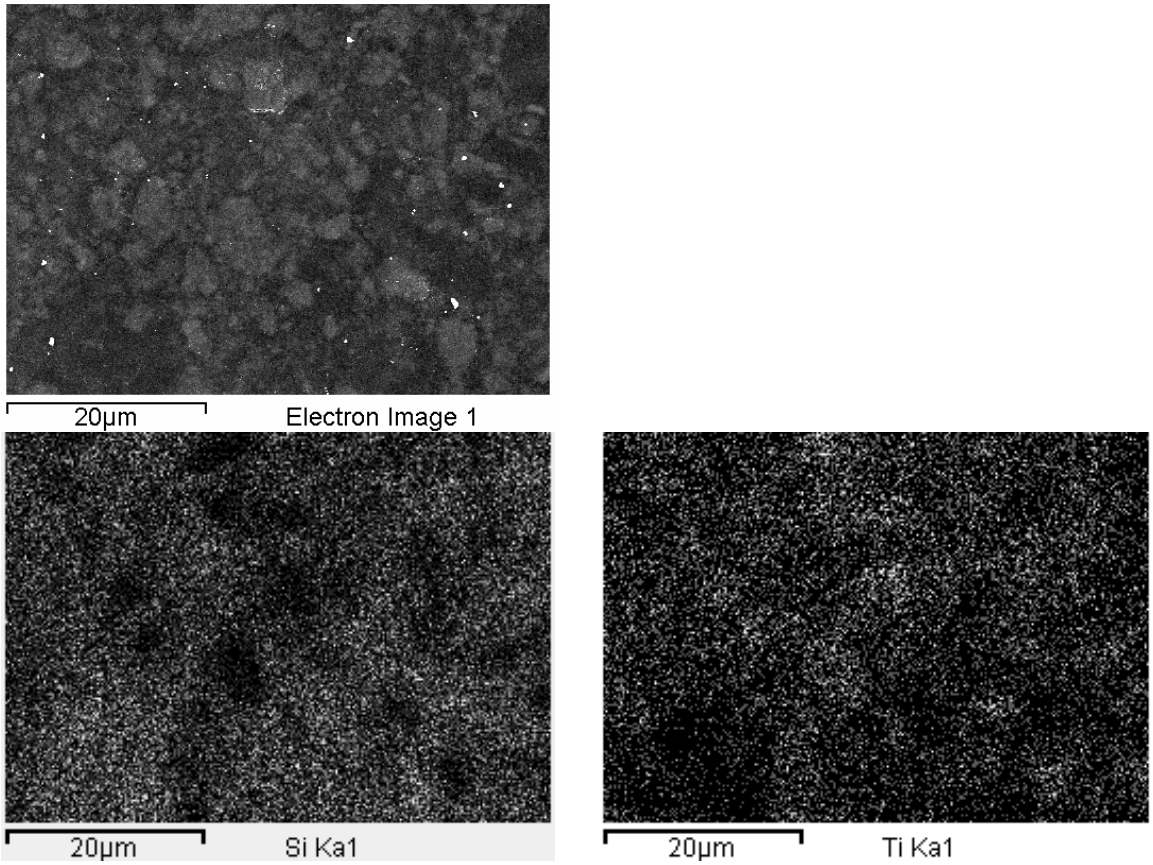

Figure A.5 SEM and EDS Images. For a sample with an intensity of segregation of 0.128. Secondary electron image (top), silicon elemental mapping (left), titanium elemental mapping (right).

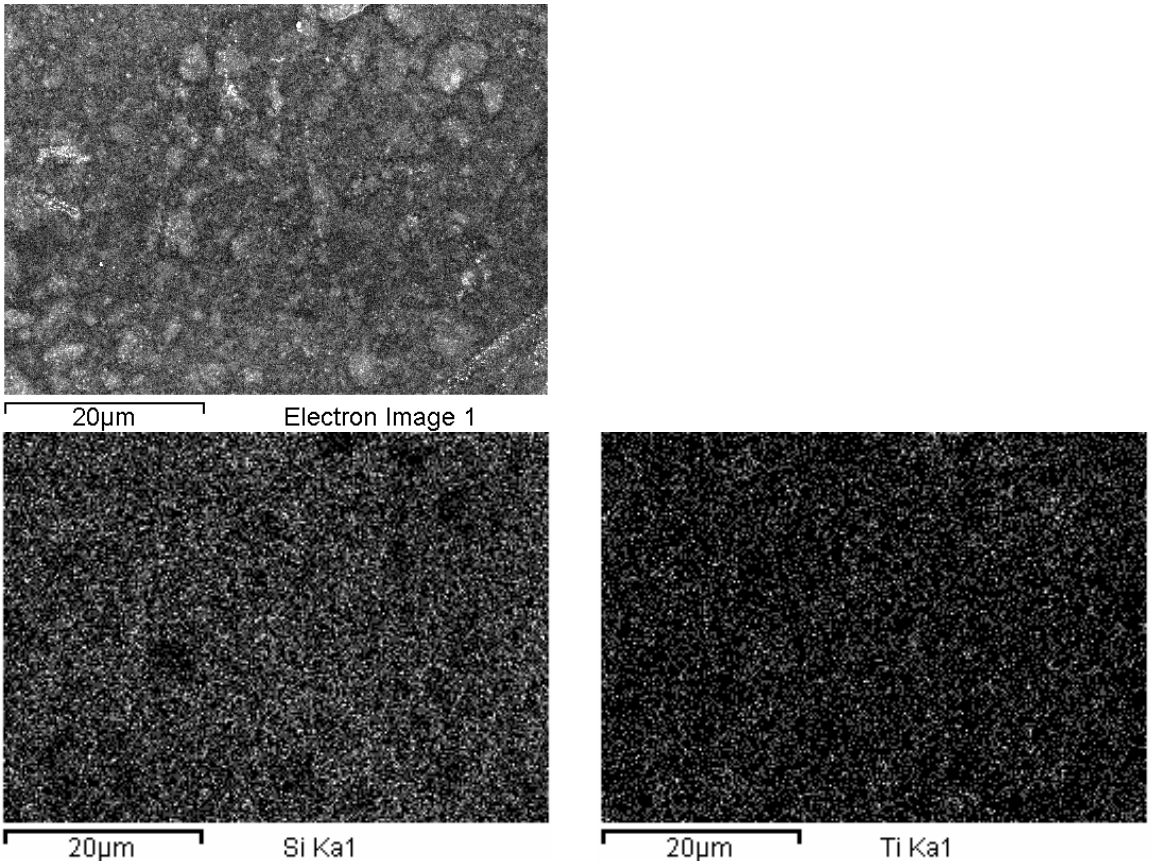

Figure A.6 SEM and EDS Images. For a sample with an intensity of segregation of 0.07. Secondary electron image (top), silicon elemental mapping (left), titanium elemental mapping (right).

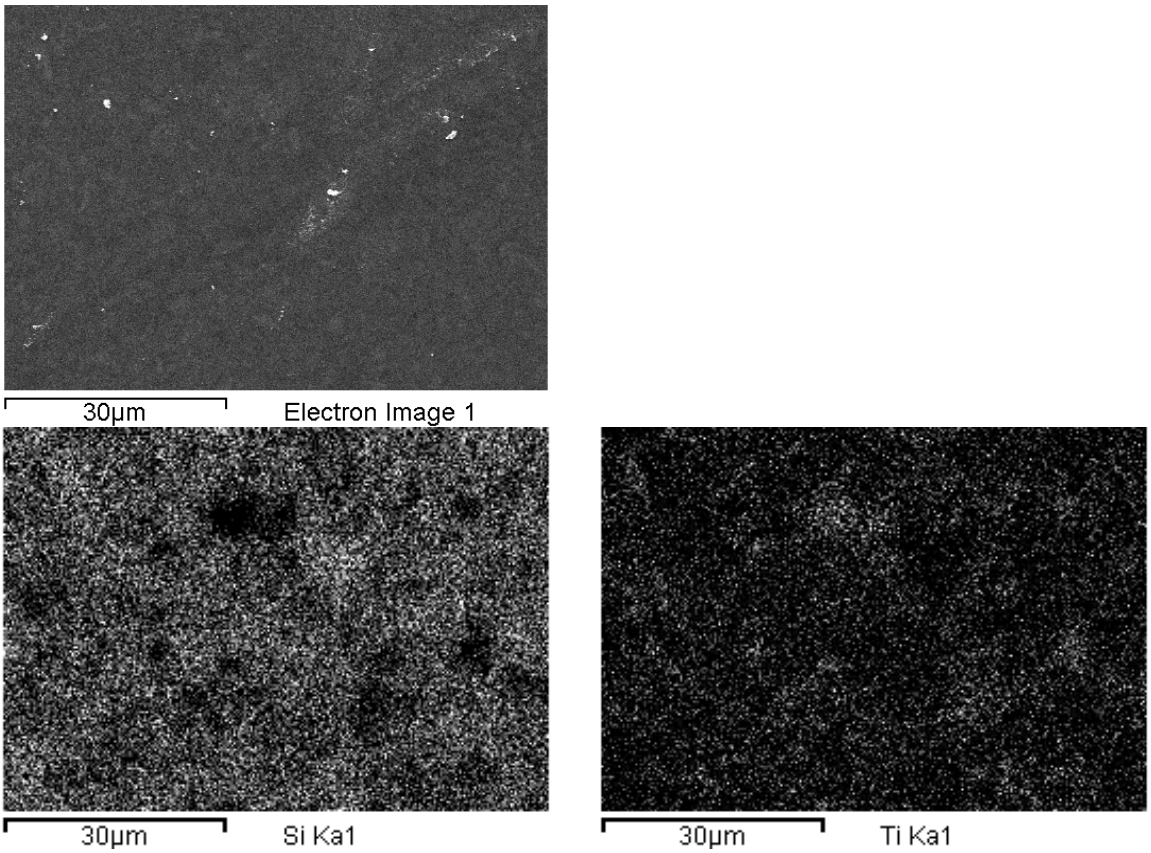

Figure A.7 SEM and EDS Images. For a sample with an intensity of segregation of 0.035. Secondary electron image (top), silicon elemental mapping (left), titanium elemental mapping (right).

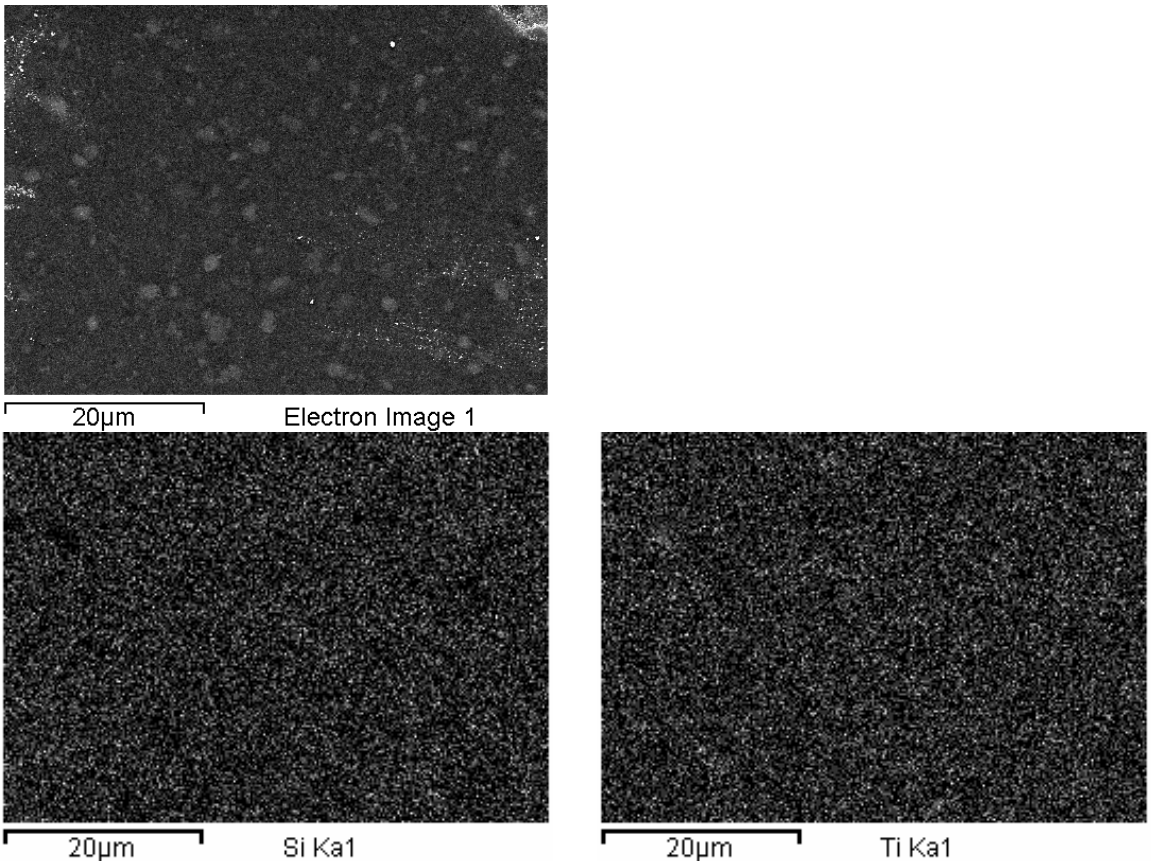

Figure A.8 SEM and EDS Images. For a sample with an intensity of segregation of 0.007. Secondary electron image (top), silicon elemental mapping (left), titanium elemental mapping (right).

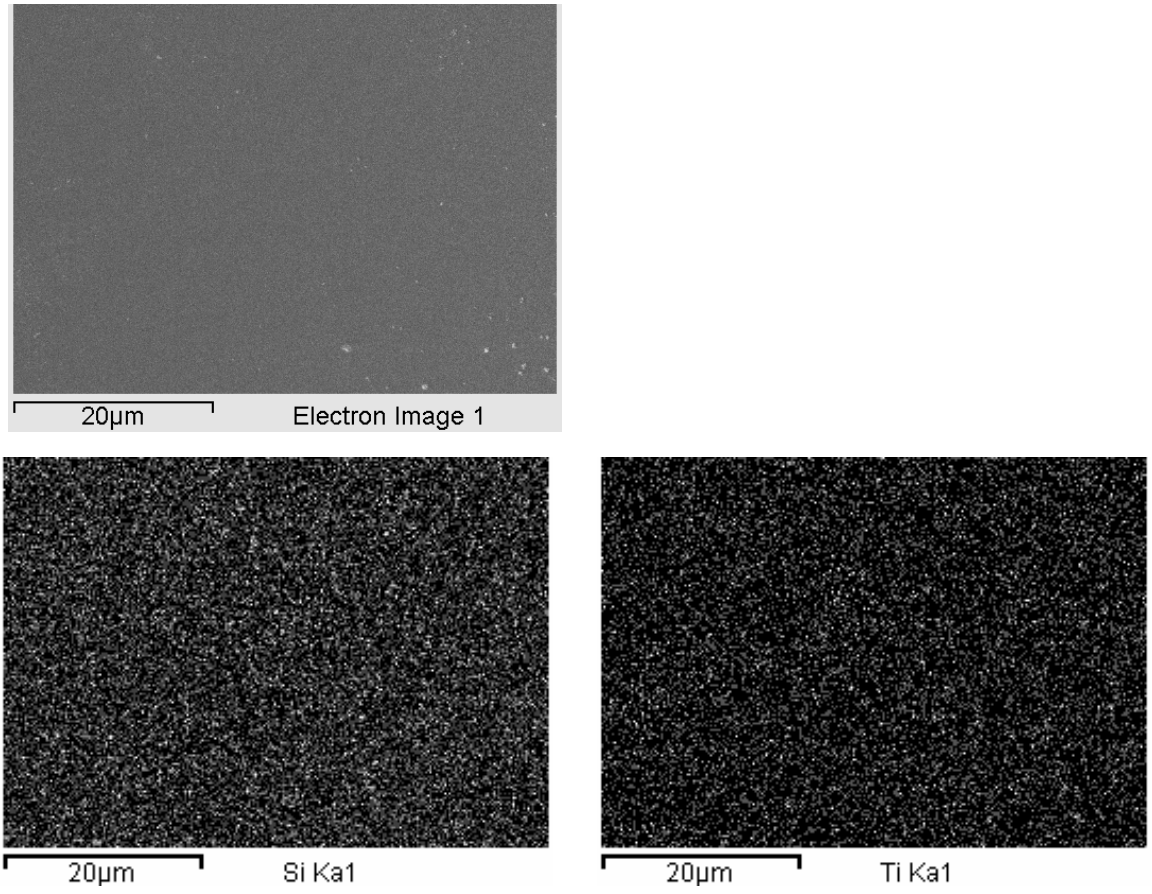

Figure A.9 SEM and EDS Images. For a sample with an intensity of segregation of 0.0009. Secondary electron image (top), silicon elemental mapping (left), titanium elemental mapping (right).

APPENDIX B

TRANSMISSION ELECTRON MICROSCOPY IMAGES

Figures B.1 to B.9 contains EFTEM images, titania elemental mappings, and EELS spectrums for mixtures of silica R974-titania and silica A200-titania. Figures B.1-B.4 are collected using a LEO 1530 VP Field Emission Scanning Electron Microscope equipped with an Oxford UTW X-ray detector using a beam energy of 15kV and a Zeiss Libra120 EFTEM equipped with a LaB6 filament using a beam energy of 120 kV and a JEOL 2010F TEM with a 2Kx2K GATAN imaging filter (GIF) electron energy loss spectrometer (EELS) and energy filtered transmission electron microscopy (EFTEM) is used to image nanoparticle mixtures in Figures B.5-B.10.

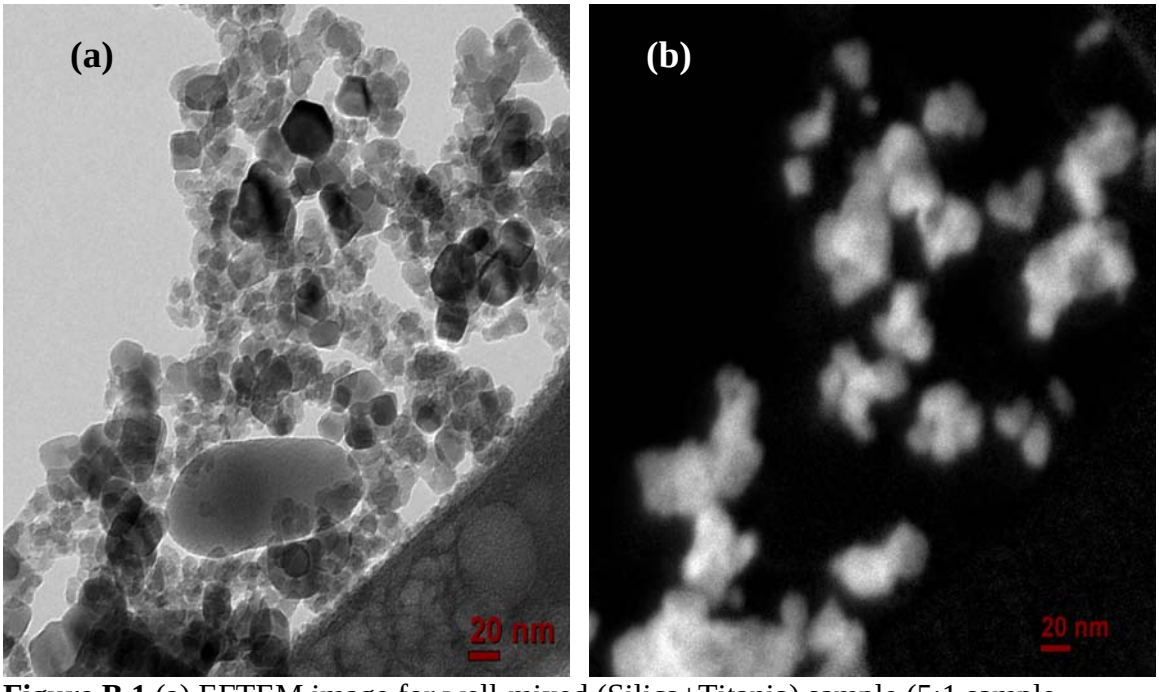

Figure B.1 (a) EFTEM image for well-mixed (Silica+Titania) sample (5:1 sample-magnet weight ratio, 120 minutes, 1400-850 μm magnet size) and the corresponding (b) titanium elemental mapping.

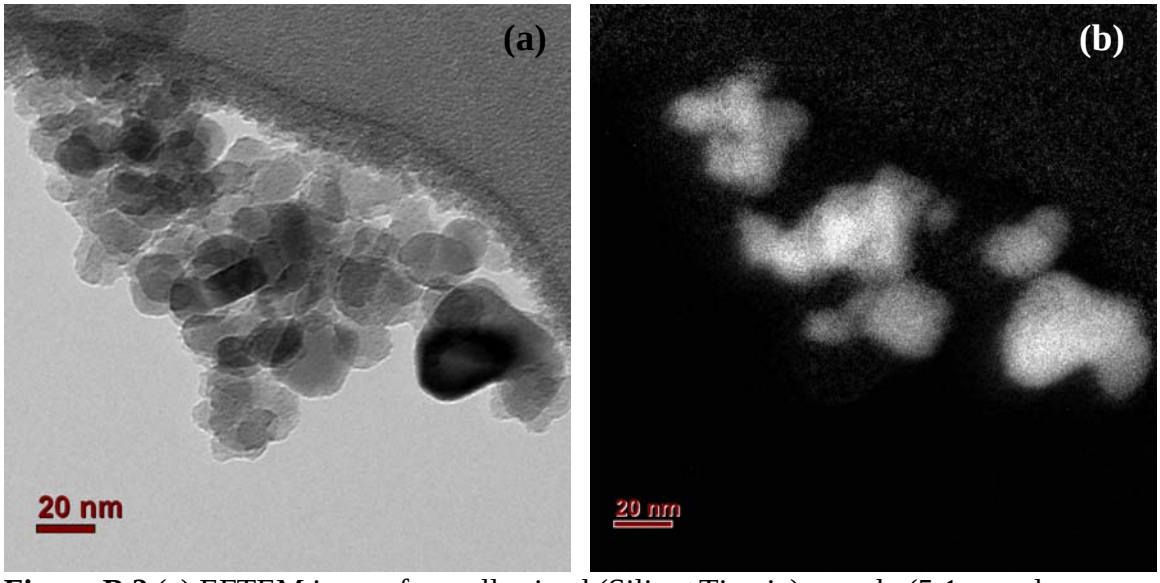

Figure B.2 (a) EFTEM image for well-mixed (Silica+Titania) sample (5:1 sample-magnet weight ratio, 120 minutes, 1400-850 µm magnet size) and the corresponding (b) titanium elemental mapping.

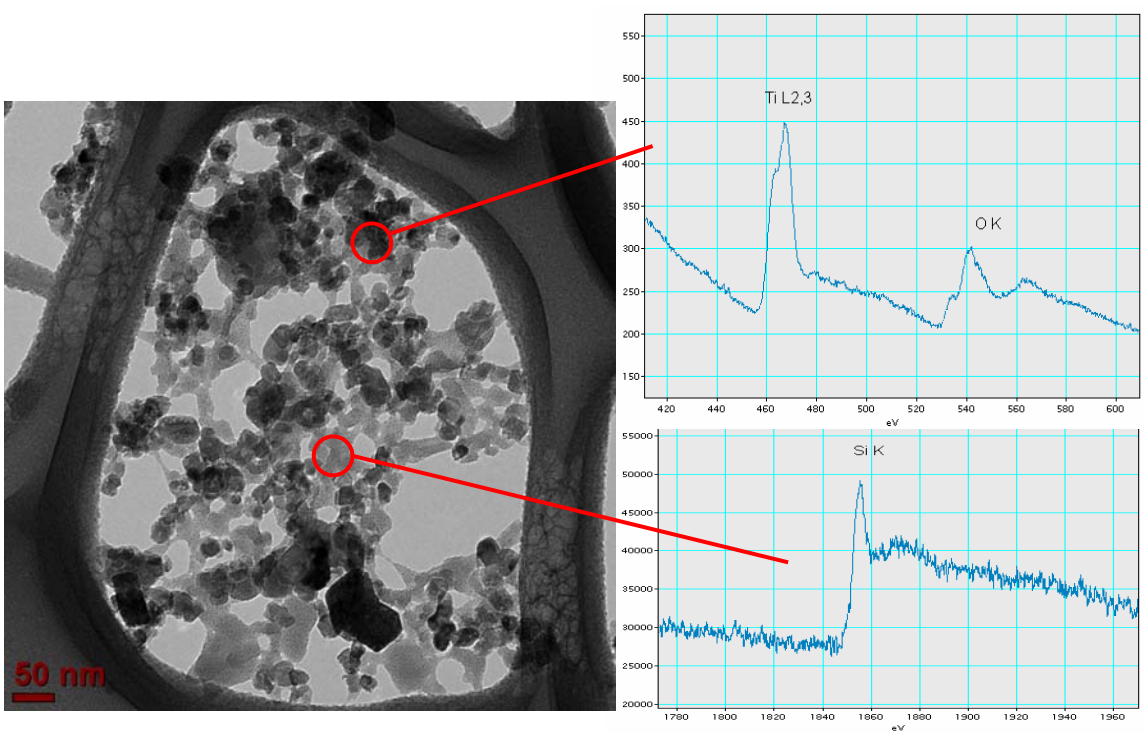

Figure B.3 EELS spectrum of an agglomerate of silica R974 and titania P25 showing the ionization edges around 455, 530 and 1850 eV, corresponding to the $L_{2,3}$ ionization edge of titanium and the K-shell ionization edges of oxygen and silicon, respectively. 5:1 sample-magnet weight ratio, 120 minutes, 1400-850 µm magnet size.

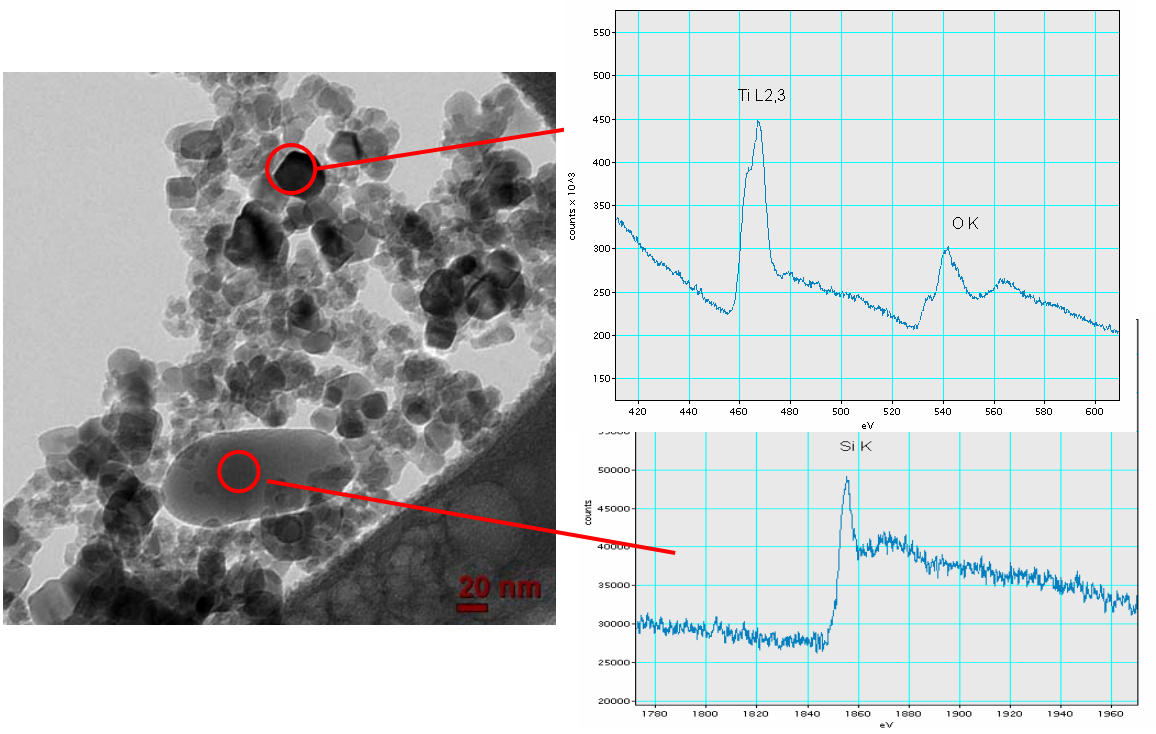

Figure B.4 EELS spectrum of an agglomerate of silica R974 and titania P25 showing the ionization edges around 455, 530 and 1850 eV, corresponding to the $L_{2,3}$ ionization edge of titanium and the K-shell ionization edges of oxygen and silicon, respectively. 5:1 sample-magnet weight ratio, 120 minutes, 1400-850 µm magnet size.

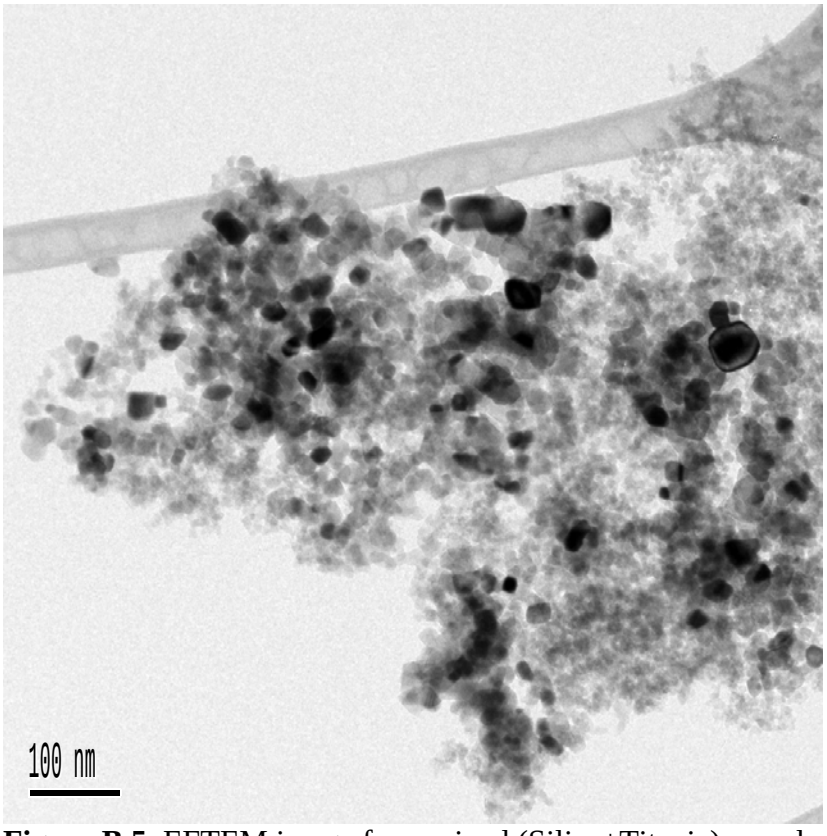

Figure B.5 EFTEM image for a mixed (Silica+Titania) sample (2:1 sample-magnet weight ratio, 60 minutes, 1400-850 μm magnet size).

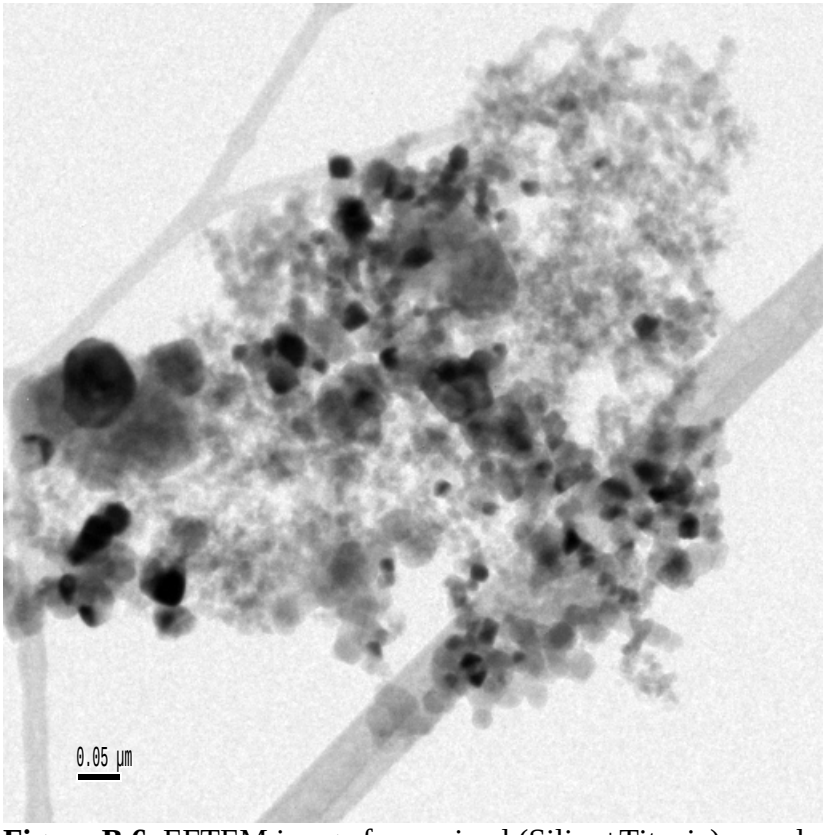

Figure B.6 EFTEM image for a mixed (Silica+Titania) sample (2:1 sample-magnet weight ratio, 60 minutes, 1400-850 µm magnet size).

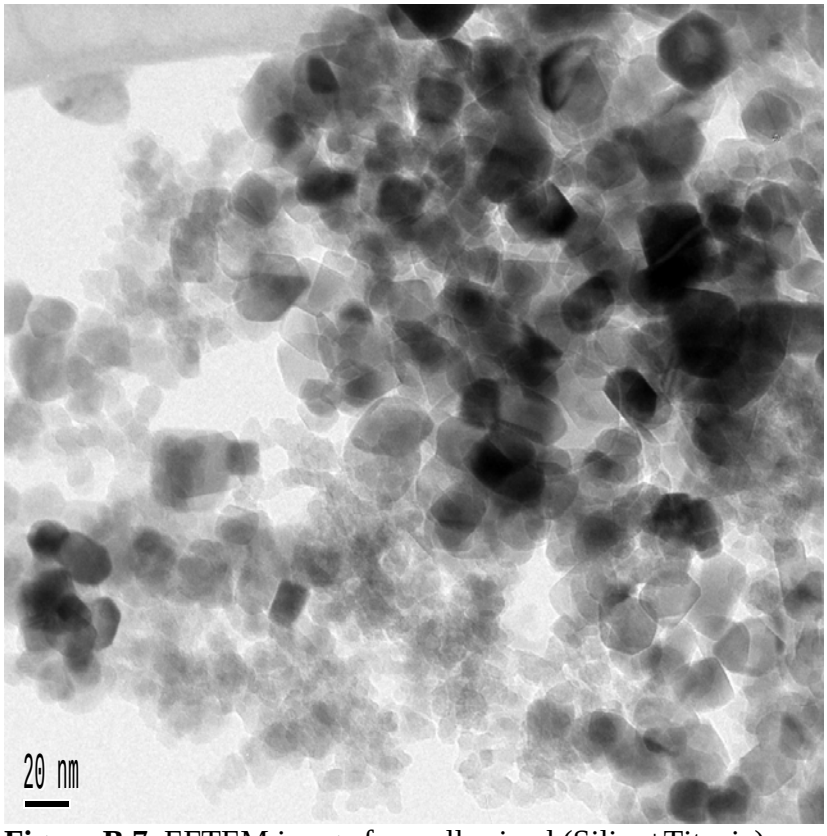

Figure B.7 EFTEM image for well-mixed (Silica+Titania) sample (2:1 sample-magnet weight ratio, 60 minutes, 1400-850 μm magnet size).

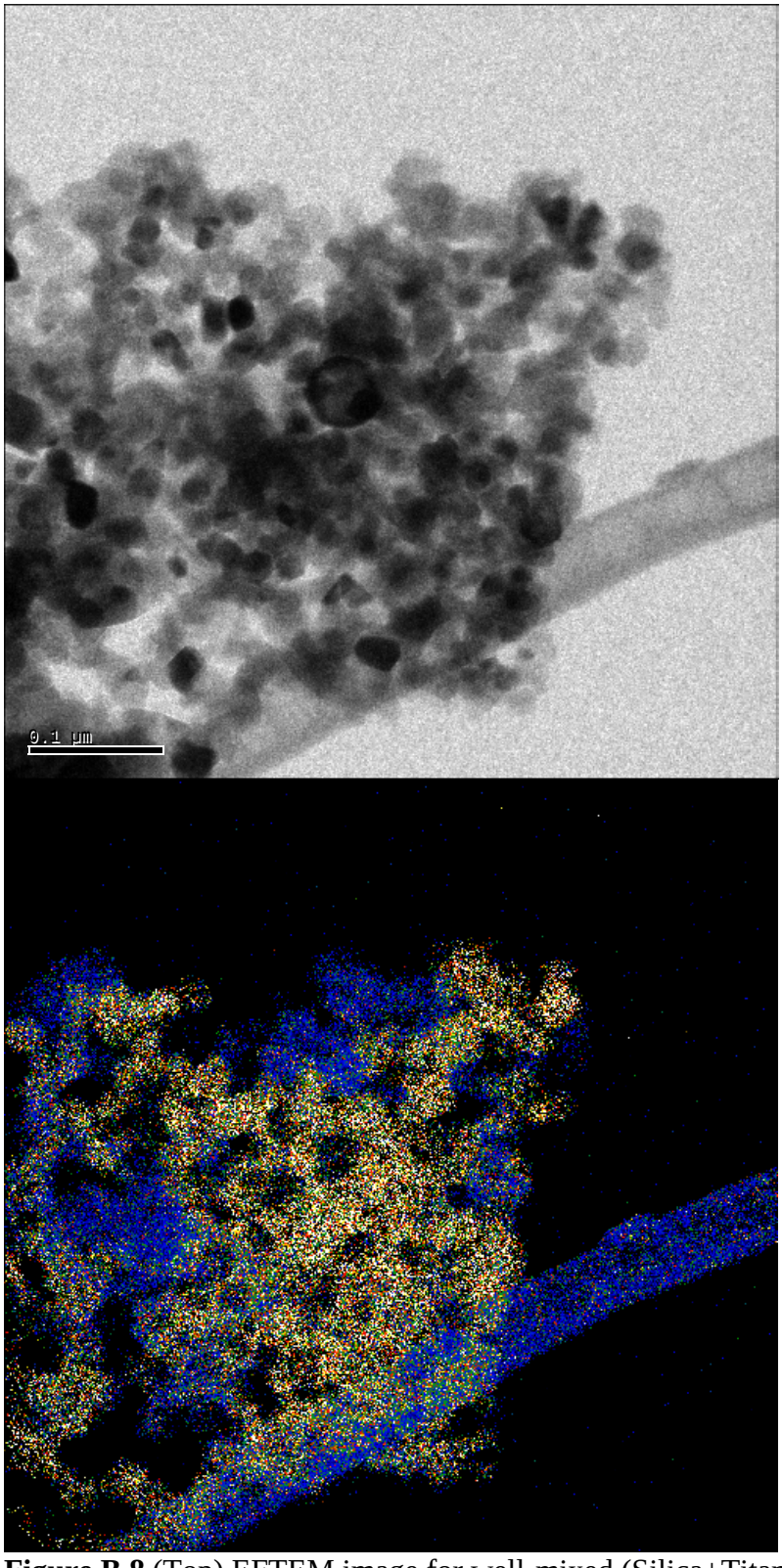

Figure B.8 (Top) EFTEM image for well-mixed (Silica+Titania) sample (2:1 sample-magnet weight ratio, 60 minutes, 1400-850 µm magnet size) and the corresponding (bottom) titanium elemental mapping.

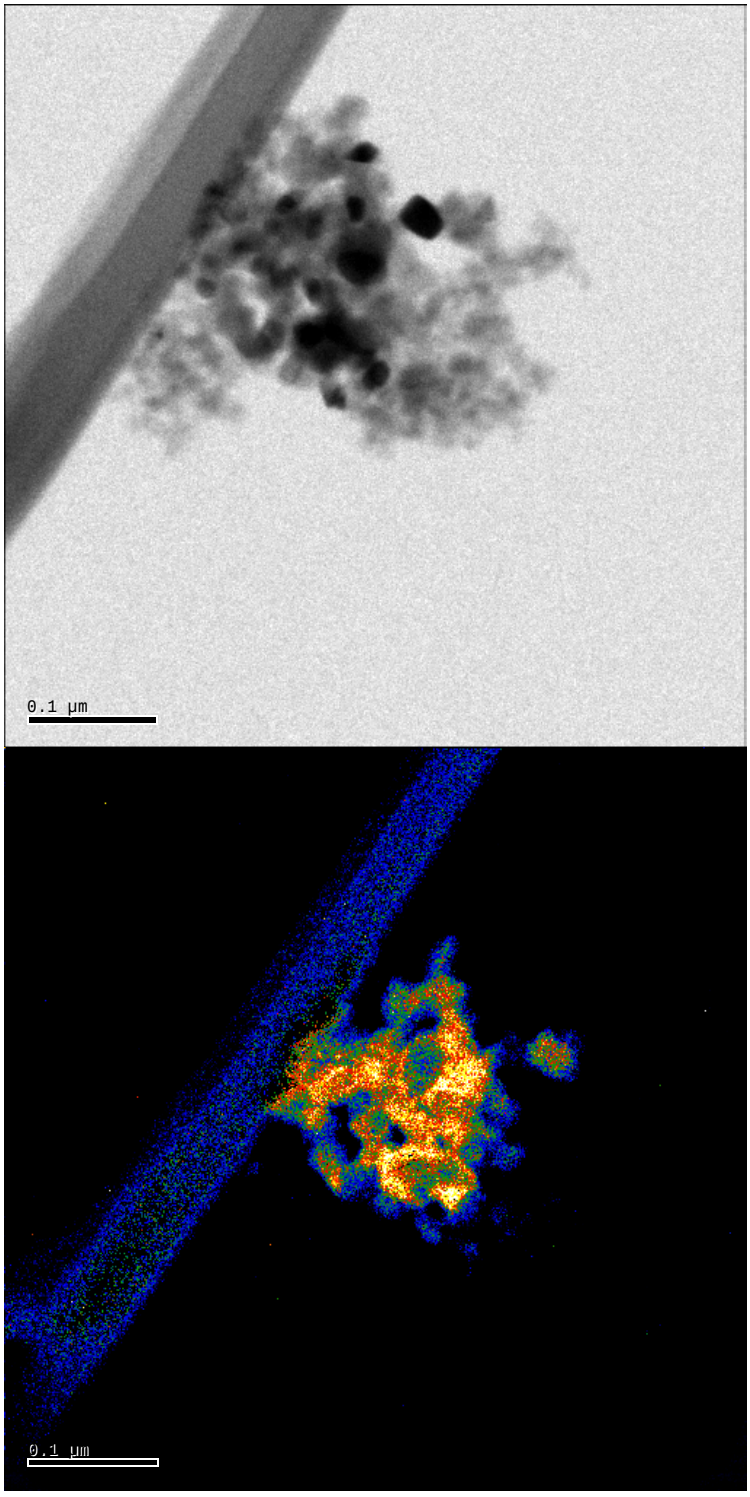

Figure B.9 (Top) EFTEM image for well-mixed (Silica+Titania) sample (2:1 sample-magnet weight ratio, 60 minutes, 1400-850 µm magnet size) and the corresponding (bottom) titanium elemental mapping.

APPENDIX C

CONTROLING HOMOGENEITY OF MIXING FOR MAIM MIXTURES

To further understand dependencies on the Homogeneity of Mixing, jar size and powder loading are studied. The first study maintains a constant bed height for three jars with different diameters: 2.15 cm, 4.7 cm and 5.6 cm (Figure C.1). The bed height is maintained at 2.3 cm (H1) and 3 cm (H2). The previous MAIM studies are performed with the 4.7 cm jar. The magnet per volume density of 23 magnets per mL is constant for each study. When the HoM values are plotted versus time, Figure C.2, similar trends for each case is observed. Higher values of HoM are obtained for the larger the size of the jar for a given mixing time. The higher value is obtained because there are more magnets present in the larger jars (to maintain a constant magnet density). Similar to Chapters 3 and 4, the next step is to account for the magnets. The time*number of magnets results, Figure C.3, show that for the HoM values of the regular and small jars overlap while the large jar is a separate trend.

The magnets are spinning, setting up a shear flow in the immediate vicinity of each magnet and this shear is responsible for the mixing. If this is correct, then the HoM should be proportional to time multiplied by (Number density of magnets), Figure C.4. The HoM values for the three jars seem to follow an overlapping trend with some scatter. The trend observed for time*number density shows a dependency of HoM on single magnets. The magnets are also undergoing magnet-magnet collisions and they contribute to crushing of the agglomerates. If this is true, then HoM will be

proportional to time multiplied by (number density of magnets)^2, Figure C.5, and be independent of the jar diameter and bed height. Since there is more scatter in Figure C.5, the results show that HoM has a greater dependency on shear by individual magnets oppose to magnet-magnet collisions. The third method by which the magnets interact with nanopowders are when they collide with the wall. During this collision, the nanoagglomerates get crushed and lead to mixing. If this is true, then the HoM should be proportional to the product of time* number density of magnets *jar radius * bed height, Figure C.6. The results, in Figure C.6, show the best trend of the interactions between magnets and nanopowders is most dependant on magnet-powder-wall collisions.

In order to determine where most of the wall collisions occur, promoting the mixing of nanopowders, HoM values are plotted versus the product of time, number density of magnets and surface area. The HoM results plotted versus total surface area (side walls and bottom of jar) and versus the surface area of the sides of the jar are shown in Figures C.7 and C.8, respectively. The HoM trends for the total surface area separate based on jar sizes, while the HoM trends for the data plotted versus the surface area of the jar sides show overlapping results with less scatter. The collapse of the trends indicates that the collisions between the magnets and the sides of the jars (driven by the alternating magnetic field) are the driving force promoting the mixing of nanopowders.

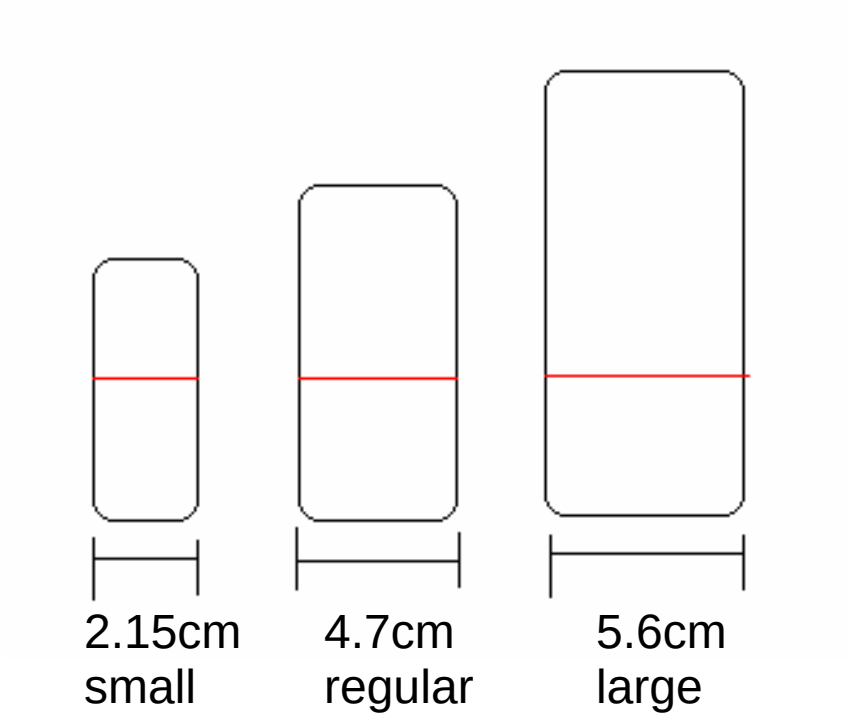

Figure C.1 Diagram of three different sized jars with a maintained powder bed height.

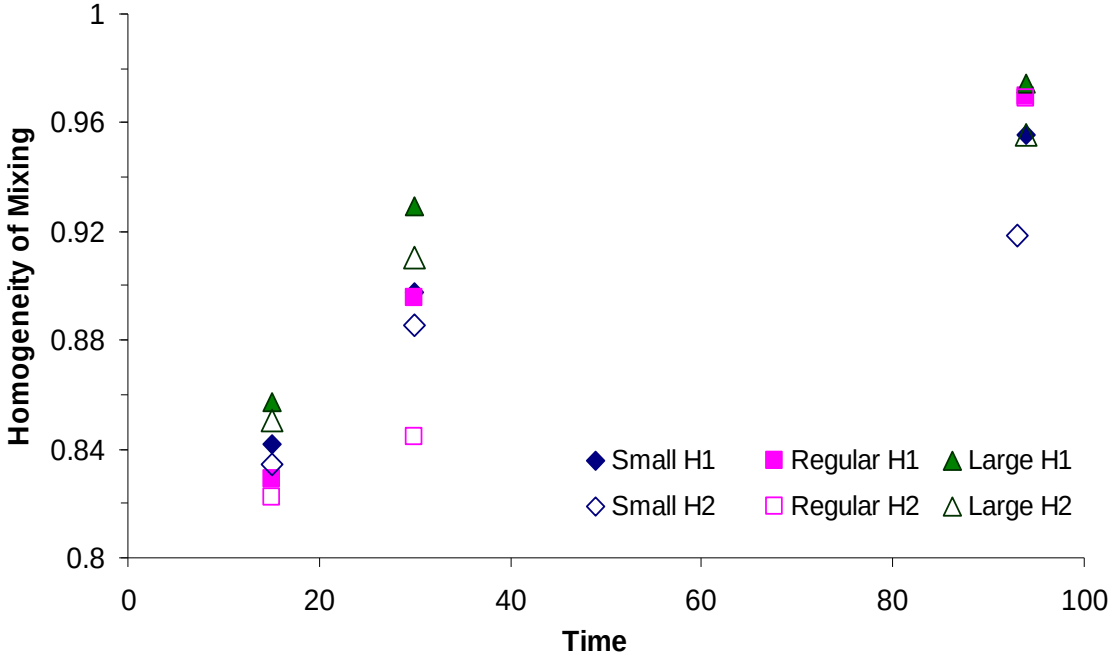

Figure C.2 HoM versus time for small (D = 2.15 cm), regular (D = 4.7 cm) and large jars (D = 5.6 cm) with maintained bed heights of H1 (2.3 cm) and H2 (3cm).

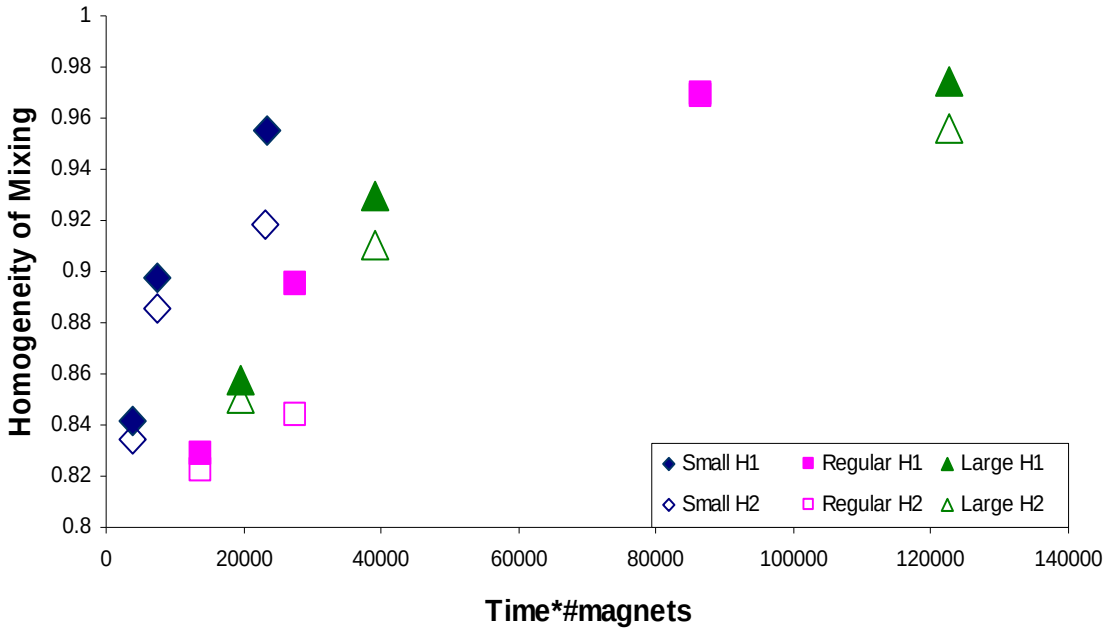

Figure C.3 HoM versus time*number of magnets for small (D = 2.15 cm), regular (D = 4.7 cm) and large jars (D = 5.6 cm) with maintained bed heights of H1 (2.3 cm) and H2 (3cm).

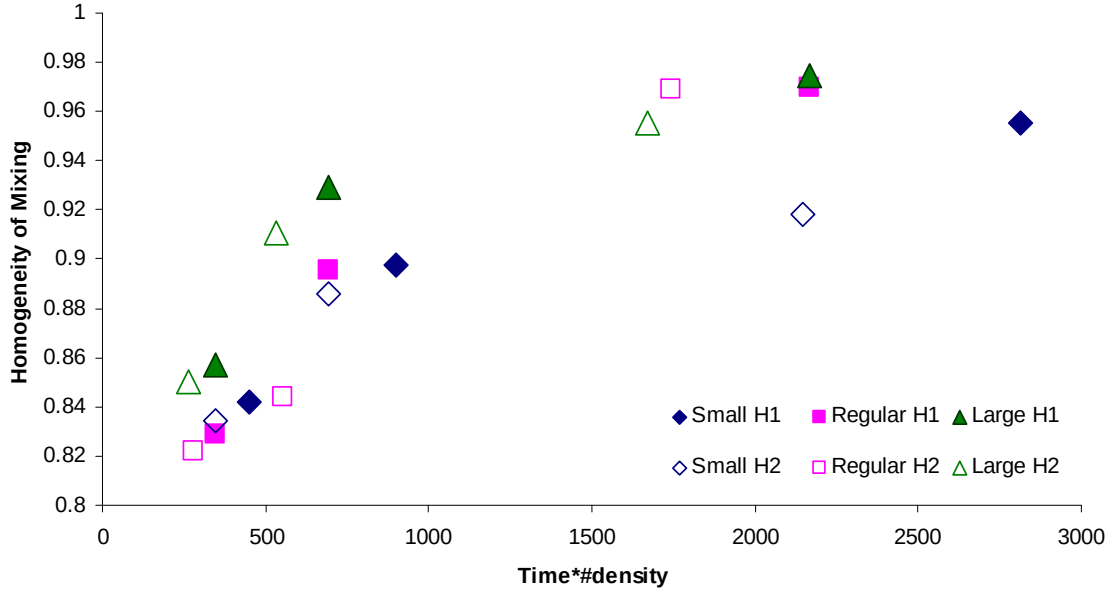

Figure C.4 HoM versus time*number density of magnets for small (D = 2.15 cm), regular (D = 4.7 cm) and large jars (D = 5.6 cm) with maintained bed heights of H1 (2.3 cm) and H2 (3cm).

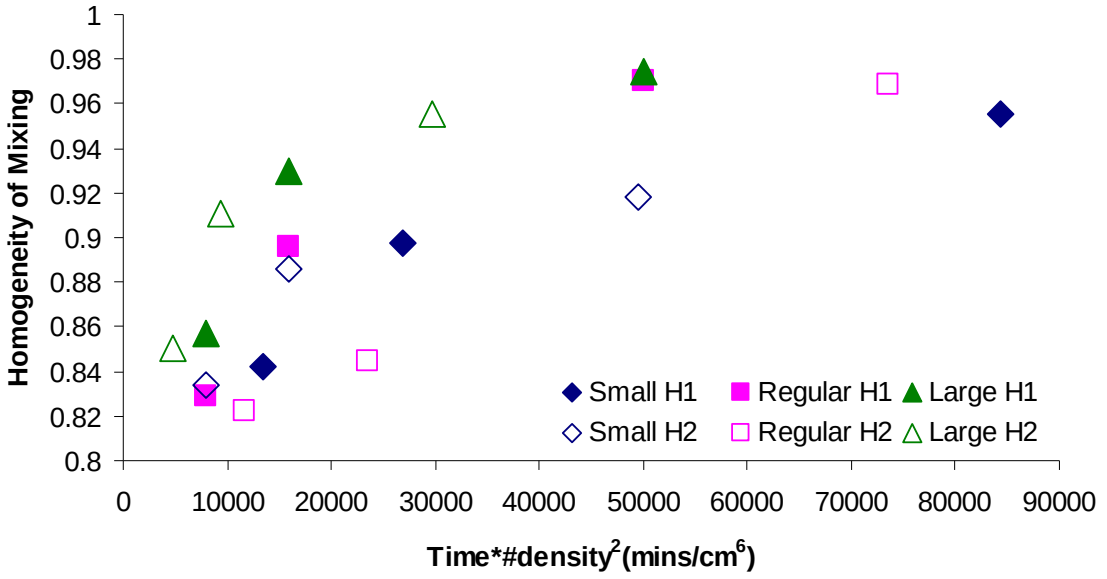

Figure C.5 HoM versus time*square of number density of magnets for small (D = 2.15 cm), regular (D = 4.7 cm) and large jars (D = 5.6 cm) with maintained bed heights of H1 (2.3 cm) and H2 (3cm).

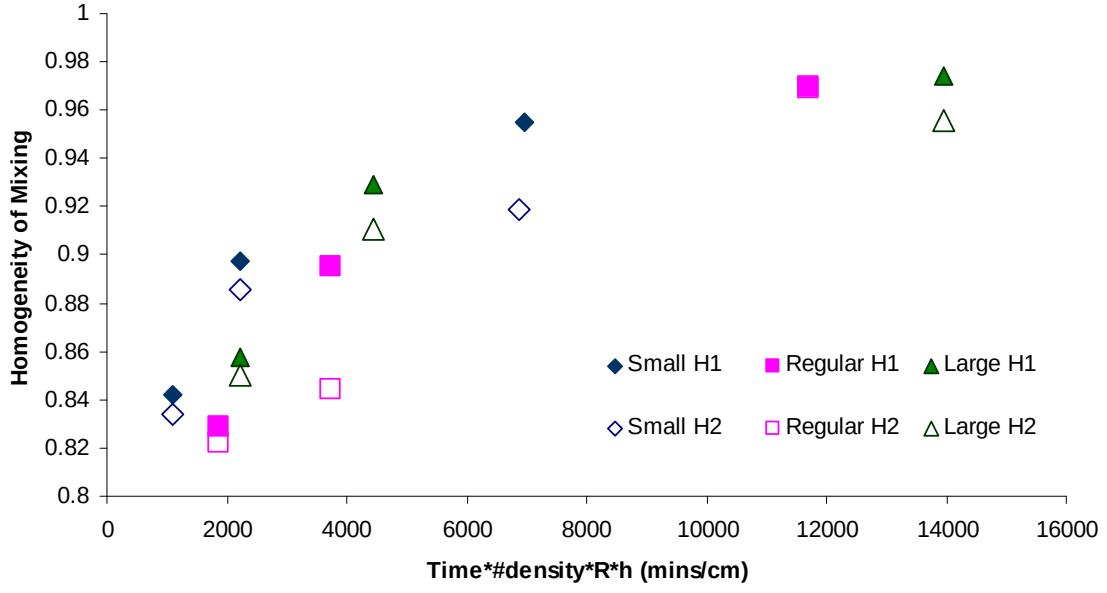

Figure C.6 HoM versus time*number density of magnets*radius*bed height for small (D = 2.15 cm), regular (D = 4.7 cm) and large jars (D = 5.6 cm) with maintained bed heights of H1 (2.3 cm) and H2 (3cm).

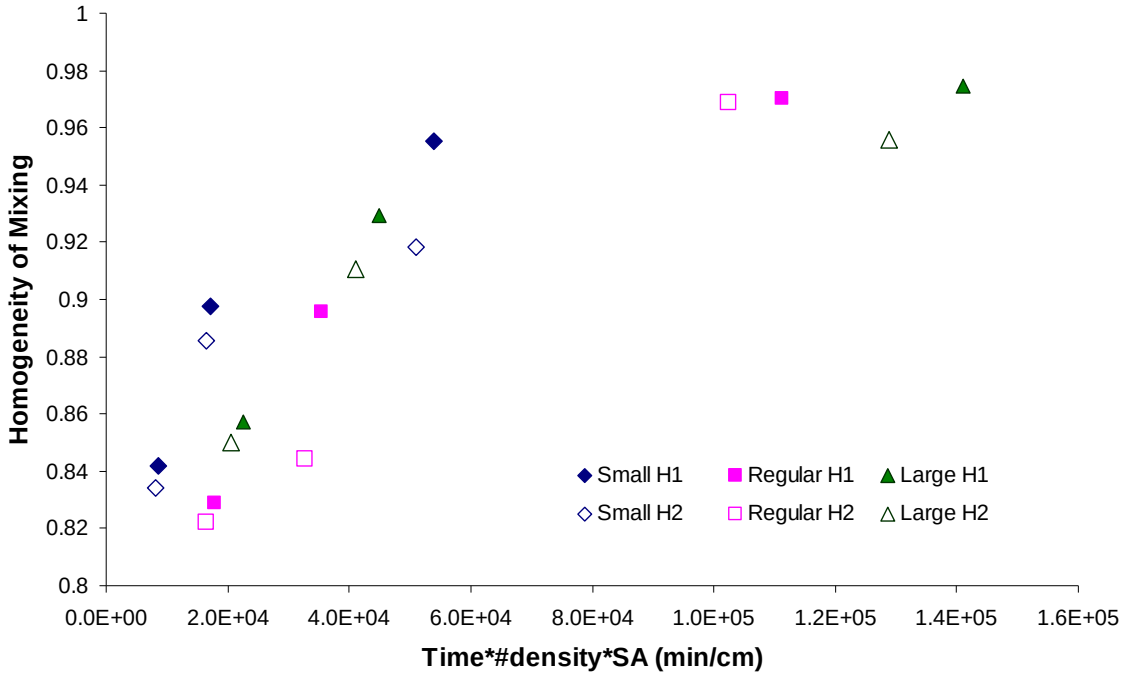

Figure C.7 HoM versus time*number density of magnets*total surface area for small (D = 2.15 cm), regular (D = 4.7 cm) and large jars (D = 5.6 cm) with maintained bed heights of H1 (2.3 cm) and H2 (3cm).

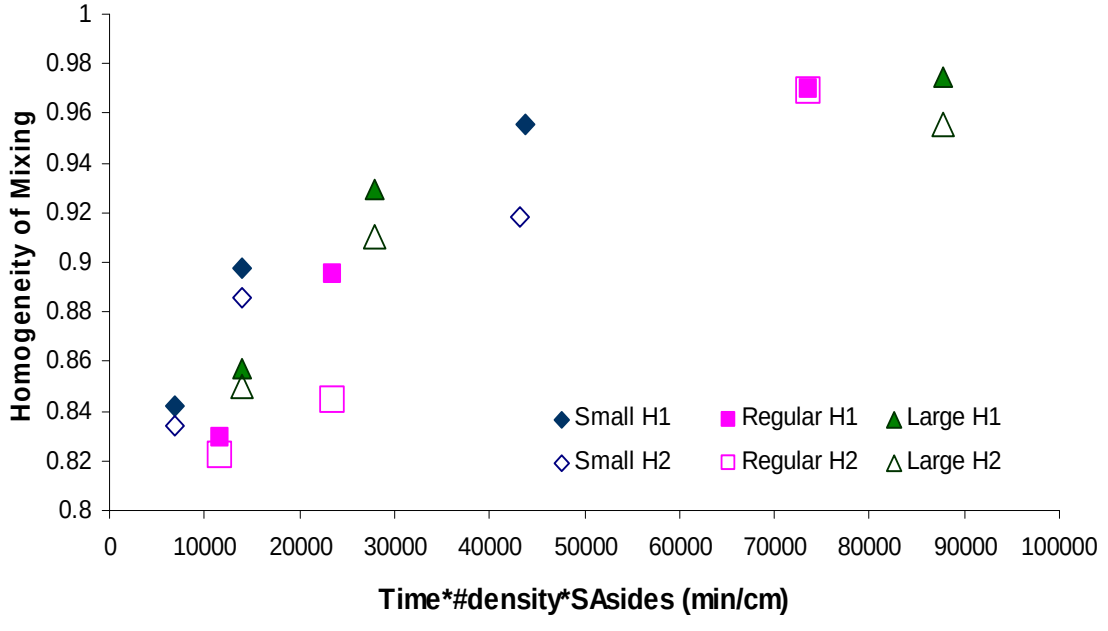

Figure C.8 HoM versus time*number density of magnets*surface area of the side of the walls for small (D = 2.15 cm), regular (D = 4.7 cm) and large jars (D = 5.6 cm) with maintained bed heights of H1 (2.3 cm) and H2 (3cm).

APPENDIX D

ADDITIONAL RESEARCH: SPRAY DRYING AND DEAGGLOMERATION BY SONICATION

D.1 Spray Drying and Drug Release

This section details the research performed during the student exchange to the University of Wollongong. Spray drying technique is used to create particles drug particles coated by polymer. Spray drying is the process in which dry powders are collected from a liquid suspension by the rapidly drying using hot gas flow. Spray drying is widely used for its ability to produce uniform particle distribution. The liquid suspension or solvent flow is sprayed out a nozzle into a hot gas stream, vaporizing the liquid. The solid can then be colleted and the liquid condenses and can be reused. Spray drying can be used in pharmaceutical and food industries for encapsulation[1] and dehydration.[2] Dexamethasone, an anti-inflammatory, is the drug used in the study. The base polymer used is sodium alginate along with crosslinking agents of calcium chloride and chitosan.

D.1.1 Procedure

A Buchi Mini Spray Dryer, similar to Figure D.1, is used to create the particles. Figure D.2 demonstrates a flow diagram of the spray dryer. A literature search is used to investigate the optimal operating conditions.[3-6] A solution of 1.5% $^{w}/_{v}$ alginate (80,000-120,000 g/mol) is prepared (2.25g/150mL). The spray dryer is run with an inlet temperature of 140˚C, 100% aspiration, pump rate of 25% (~12cm/s) and the outlet temperature varied between 80˚C to 73˚C during the run. 70mL of the solution is sprayed to test the system. 0.205 grams of dexamethasone 21 phosphate (Dex21) is added to the

remaining 80mL of solution (18% $^{w}/_{w}$). Approximately 0.75 grams of particles are collected. 0.4031 grams of sample is weighed out and mixed with 7.5 molar solution of $CaCl_2$.

Figure D.1 Buchi Mini Spray Dryer.

Dr. Joselito Razel, who has worked with alginate, suggested up to 30 minutes is an adequate time for crosslinking, but as low as 5 minutes could also work. When using longer crosslinking times, the loss of dexamethasone can become an issue. A longer time is decided to be used because the high concentration of Ca^{+2} ions can limit the loss of dexamethasone into solution. A crosslinking time of 20 minutes is used. During crosslinking, the solution is agitated intermittently.

After the 20 minutes the samples are placed in a centrifuge and spun until as much of the sample possible had settled. The solution is siphoned off and ethanol is used to rinse the sample. Ethanol is chosen for its volatility and it is unlikely to damage the product. The particles are collected together and dried with low heat (around 50˚C). The procedure is reproduced with dexamethasone (Dex-Base). Ultraviolet visible spectrum is run at varying concentrations of Dex-Base and Dex21 to obtain a fitted trend to relate peak intensity to concentration. Alginate particles with Dex21 and the particles with Dex-Base are individually massed to a value of 0.01 grams and 1 mL of artificial cerebral spinal fluid (ACSF) is added. The samples are then placed in a water bath. The crosslinked versions are also prepared. The particles should obtain a maximum concentration of 3.371 mM of the respective versions of dexamethasone.

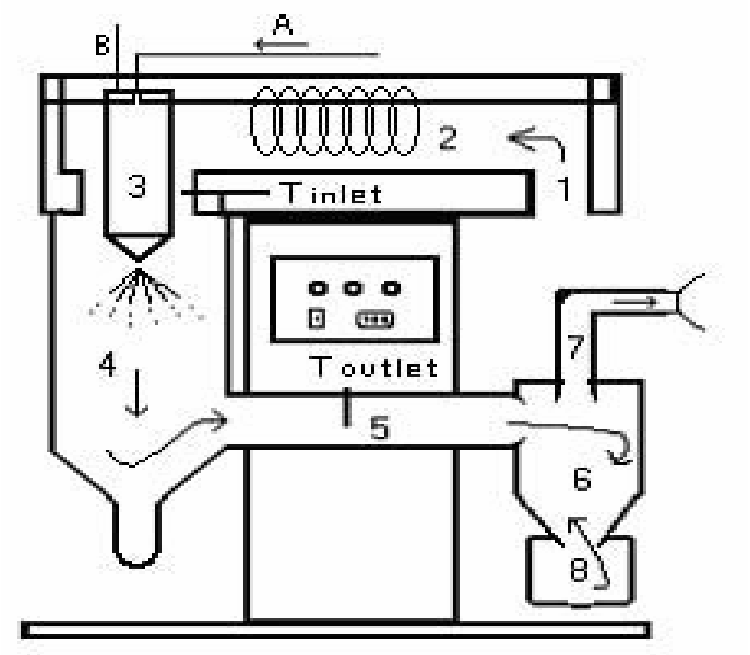

Figure D.2 Flow diagram of gas and solution in a spray dryer. A: Suspention; B: Atomization Gas; 1: Drying Gas; 2: Heating coil; 3: Spraying of suspension; 4: Drying chamber; 5: Outlet Tempurature; 6: Cyclone; 7: Exhaust flow; 8: Collection chamber.

Source: http://en.wikipedia.org/wiki/Spray_Drying; September 2009

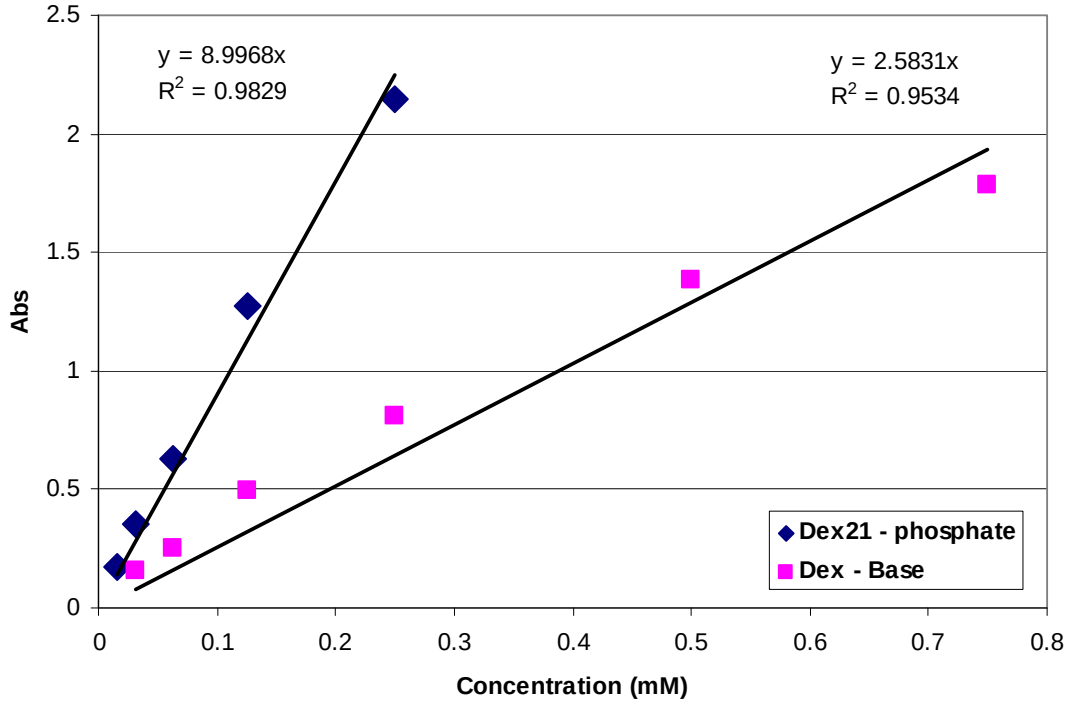

Figure D.3 The concentration versus absorption peak for Dex21 and DexBase.

D.1.2 Eighteen Percent Weight Loading of Dexamethasone in Alginate

From the data collected, Figure D.4 and Figure D.5, it can be observed that Dex21 is released quickly, with approximately 100% of expected release in 8 hours. When the alginate is crosslinked, the release of the Dex21 is slowed down. The Dex-Base and Dex-Base crosslinked seem to respond similarly. More data is desired, so more samples are prepared at lower concentration of particles. The results show the trend continues for the crosslinked samples; however, the Dex-Base results have shown a much higher concentration in the results. Points are repeated for a comparison, yet the new results are within observed error. To rule out any degradation of the Dex-Base, Dex-Base is added to ACSF and placed in a water bath to determine if the peak changes. Another standard test is run with ACSF in the bath to see if there could be any other peak attributing to a

higher concentration obtained. Both results showed no significant difference around the 230-250 nm range, with the dexamethasone peak at 242.5 nm.

Scanning electron microscopy is used to analyze the morphology and size of the particles. It is observed, Figures D.6-D.9, that there is a very large particle size distribution for all the particles obtained. The SEM showed that the crosslinked versions of the alginate samples appear to be melted or sintered together. Smaller particles could be observed within the larger particles but they seemed largely interconnected. This could have possibly attributed to the separation and drying process. Either the heat or the use of ethanol could have played a role. Alternate separation processes are contemplated.

To try and control the particle size within a narrower particle size distribution, the alginate concentration is lowered to 0.75% w/v and the pump rate is lowered to 5%. The temperature is also increased to 150˚C. With less sample being pumped into the spray nozzle, and with a higher temperature, smaller particles should be obtained. Unfortunately the SEM analysis did not show significant difference in particle size distribution. The new procedure used to collect the crosslinked particles is that of using filter paper. The particles are further allowed to dry overnight in a vacuum filled with desiccant. The results proved that filtering the particles is a more efficient method of collecting the particles.

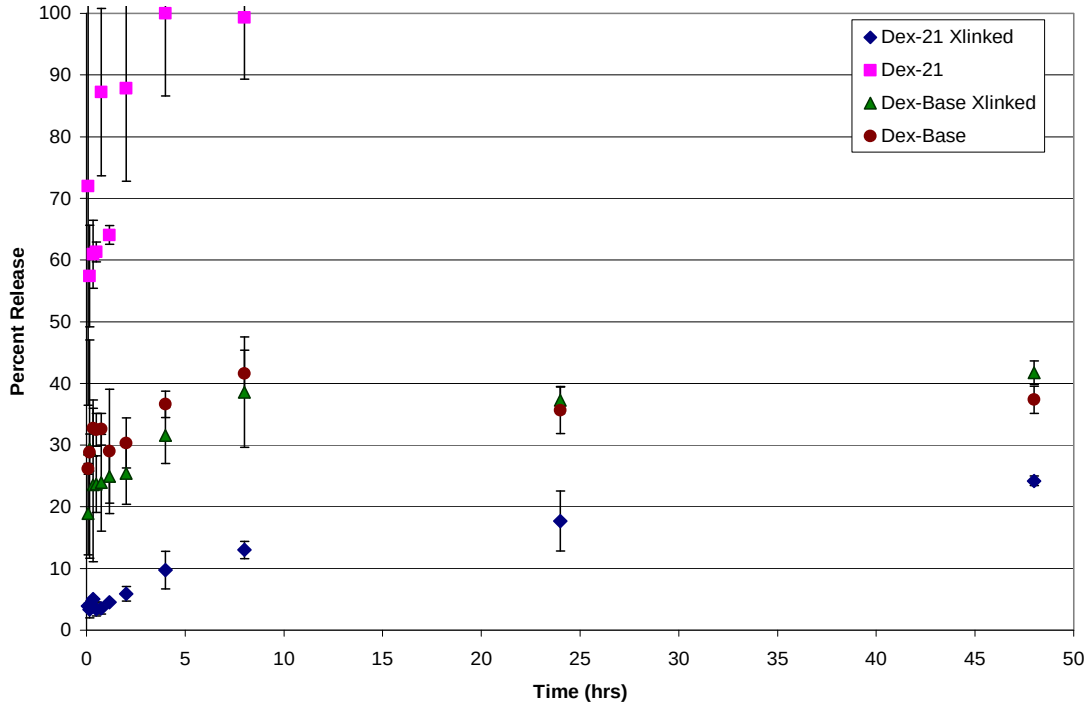

Figure D.4 Two day release study of dexamethasone from alginate spray dried particles.

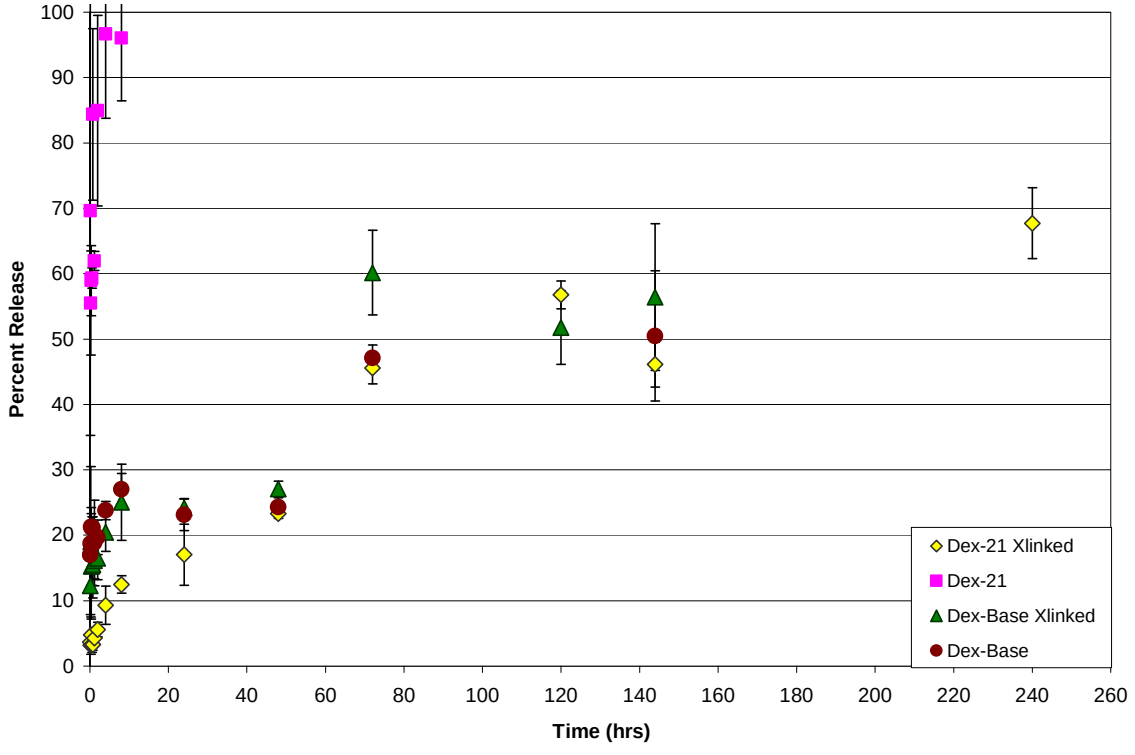

Figure D.5 Release of dexamethasone from alginate spray dried particles. Experiments carried out over 10 days.

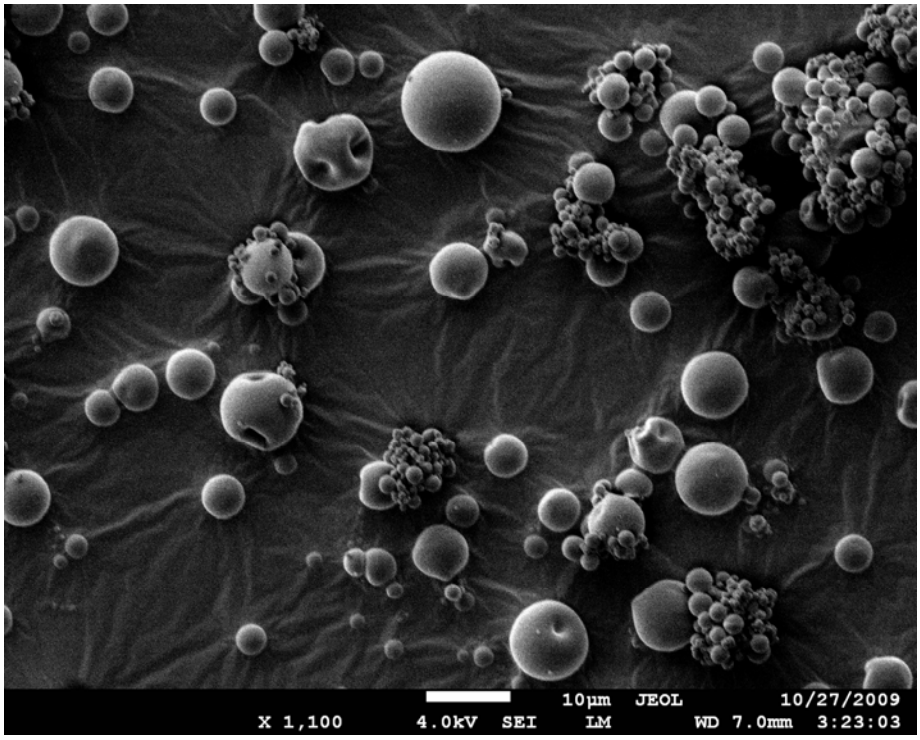

Figure D.6 SEM image of alginate particles with dexamethasone 21 phosphate (Dex-21).

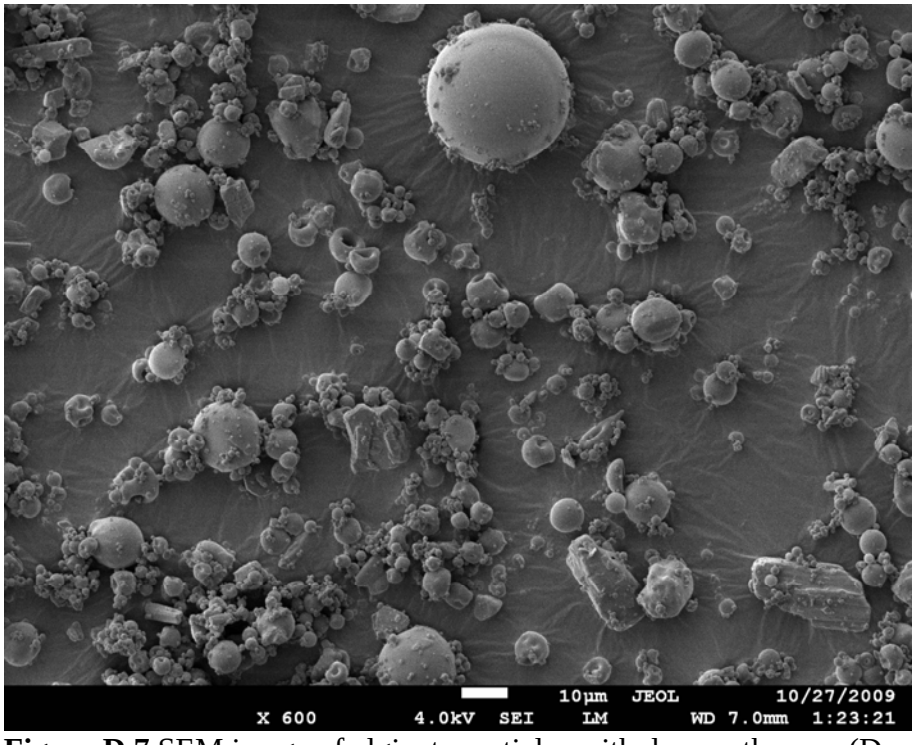

Figure D.7 SEM image of alginate particles with dexamethasone (Dex-Base).

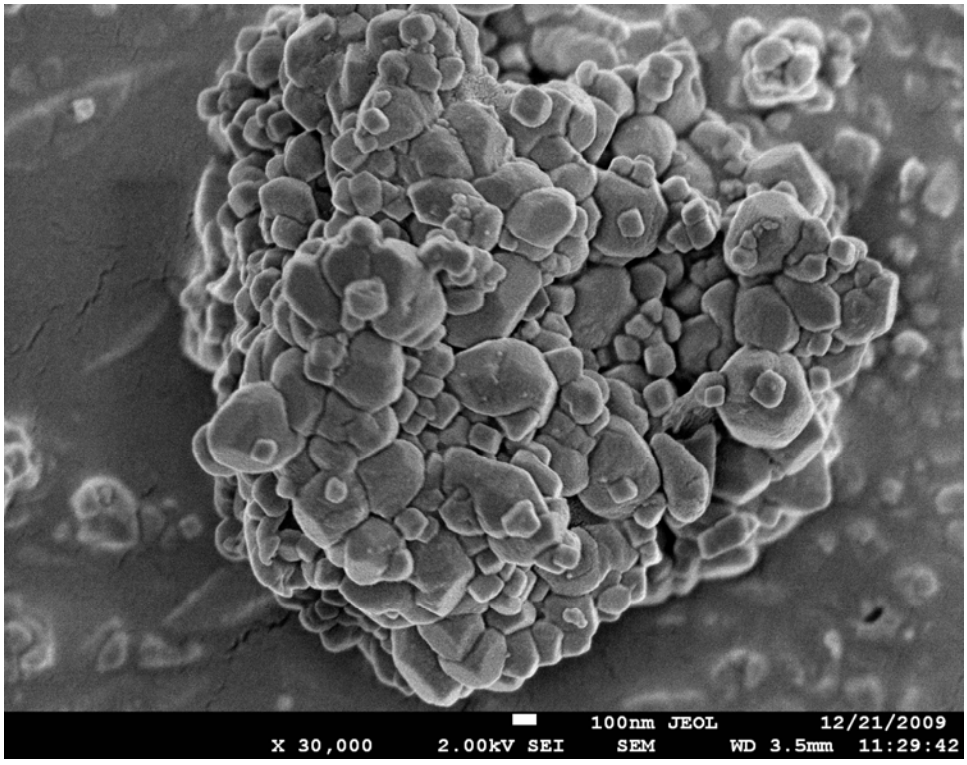

Figure D.8 SEM image of crosslinked alginate particles with dexamethasone 21 phosphate (Dex-21).

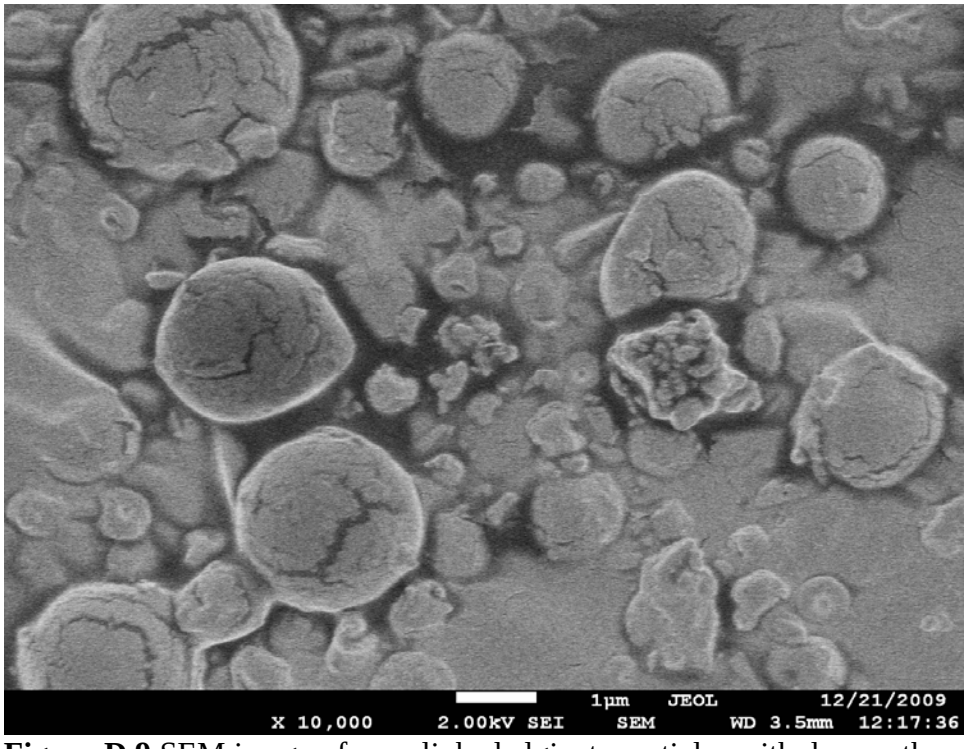

Figure D.9 SEM image of crosslinked alginate particles with dexamethasone (Dex-Base).

When running the spray dryer, a thin film builds up on the spray column over time. Over a long enough processing time, the film does build up and in some sections able to be pealed off, however since most of the film is a thin coating, an accurate measurement cannot be obtained. A known sample of the film that is thick enough to peal off is completely dissolved in ACSF to determine the dexamethasone concentration found in the film. Per milligram of film, 0.788 mM of Dex21 and 0.535 mM of DexBase are obtained.

D.1.3 Six Percent Weight Loading of Dexamethasone in Alginate

To try and control the particle size within a narrower particle size distribution, the alginate concentration was lowered to 0.75% w/v and the pump rate was lowered to 5%. The inlet temperature was set to 150˚C. With less solution pumped into the spray nozzle, and with a higher inlet temperature, smaller particles should be obtained. 6% $^{w}/_{w}$ drug loaded was chosen as a more suitable drug loading because the 18% drug loading samples required diluting for analysis with the UV visible spectrometer. New samples were run with the lower pump rate (5%) and the increase of the inlet temperature to 150˚C, the corresponding outlet temperature ranged between 101-96˚C. Solutions of 0.75% $^{w}/_{v}$ alginate and 6%$^{w}/_{w}$ of drug were used for both dexamethasone and dexamethasone-21-phosphate. Since SEM showed melting occurred during the drying process, the alginate particles were separated from the calcium chloride solution by paper filtration. The samples were then dried overnight in a vacuum with desiccant. SEM images show that no melting occurred by filtering and vacuum drying.

For the 6% dexamethasone samples, crosslinking time and $CaCl_2$ concentration are altered to determine the effect of crosslinking on the drug release. For both Dex-Base

and Dex21, crosslinking was performed in 5 molar calcium chloride solutions for both 20 minutes and 2 hours. The results, Figure D.10, show that the longer exposure to the calcium chloride delayed the drug release for Dex21; however, with the longer exposure time, the Dex-Base released quicker from the alginate particle. The longer exposure to the crosslinking agents did not seem to have significant changes in the amount of dexamethasone leaching into solution.

The effect of calcium chloride concentration on the drug release is studied closer. Results from the 5 molar calcium chloride crosslinked for 20 minutes, Figure D.10, are compared to the 20 minute crosslinking in 7.5 molar solutions, Figure D.5. The results, Figure D.11, show significant differences in the drug release profiles for both Dex-Base and Dex21. It is observed that the drug release sooner for samples crosslinked in 5M $CaCl_2$ than the samples crosslinked in 7.5M concentration, over a ten day period.

There is much research using chitosan to crosslink alginate.[4,7-11] A solution containing $0.25^{w}/_{v}$ of chitosan, $0.25^{v}/_{v}$ acetic acid and $5\%^{w}/_{v}$ calcium chloride is used to crosslink alginate with Dex21 for 20 minutes. The acetic acid was used to thoroughly disperse the chitosan into the calcium chloride solution. The drug release profile of the Dex21 showed a rapid release of the drug into the ACSF, Figure D.12. At the concentration used, the chitosan did not prove to provide any addition benefit in the crosslinking. From the results, the most important consideration when crosslinking the alginate particles is to have the highest concentration of calcium ions in solution.

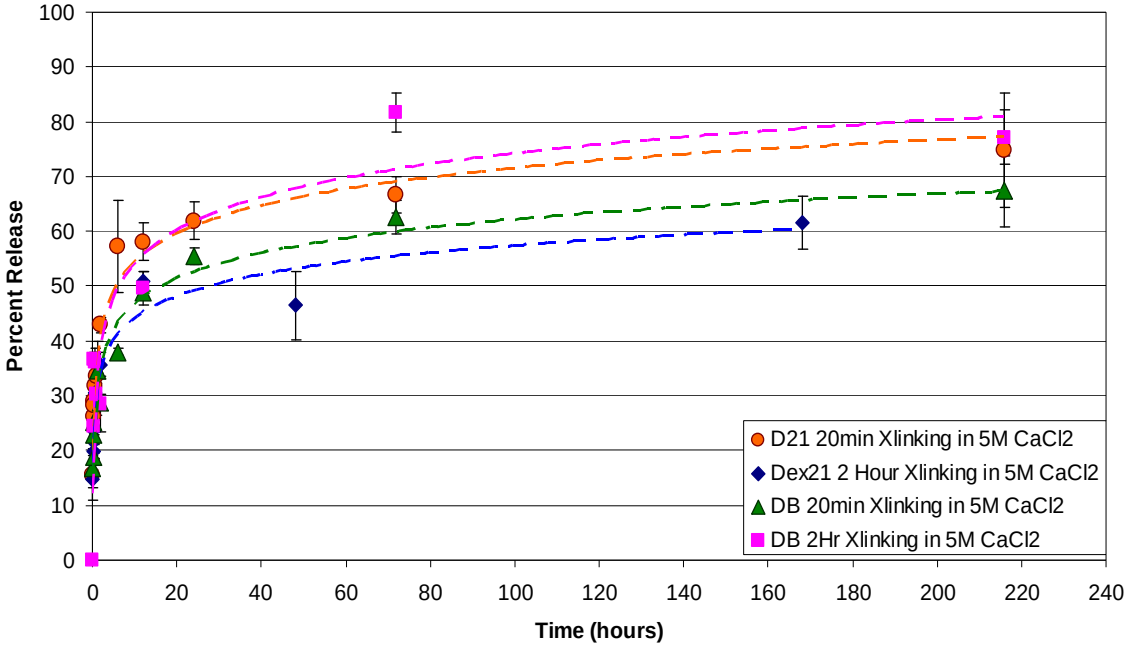

Figure D.10 Ten day release study of dexamethasone from alginate spray dried particles. Samples are of both dexamethasone and dexamethasone-21-phosphate. Crosslinked samples were placed in 5M solution of $CaCl_2$ for either 20 or 120 minutes.

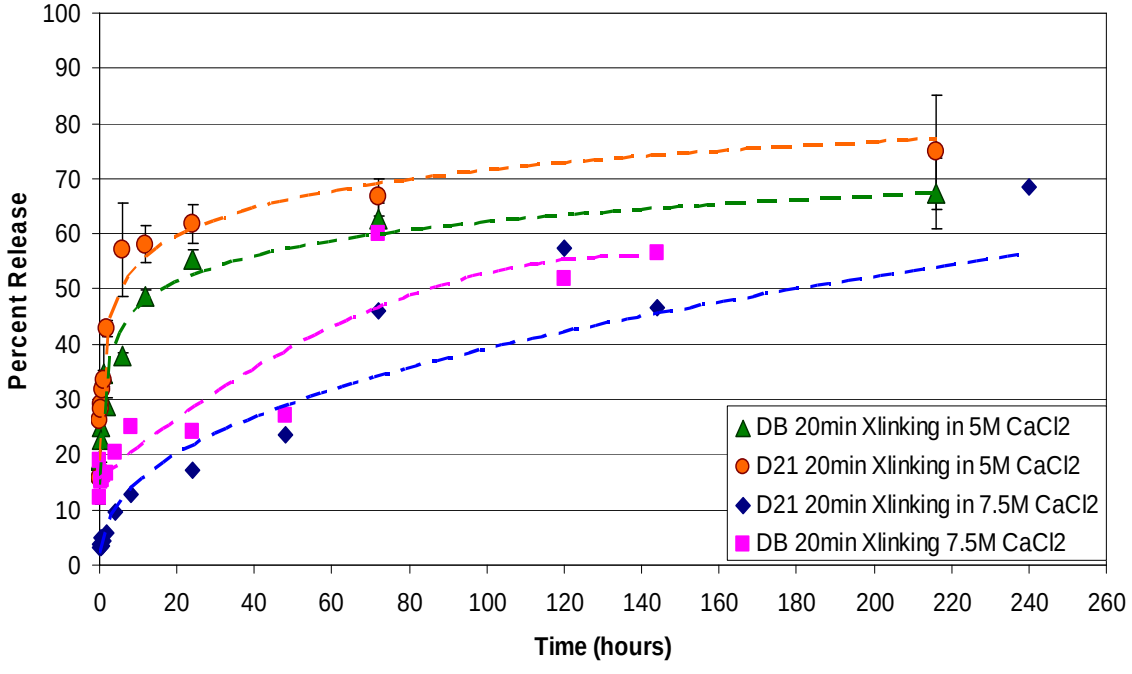

Figure D.11 Ten day drug release of dexamethasone from alginate spray dried particles. Samples are of both dexamethasone and dexamethasone-21-phosphate. Crosslinked samples were placed in 5M solution or 7.5M of $CaCl_2$ for 20.

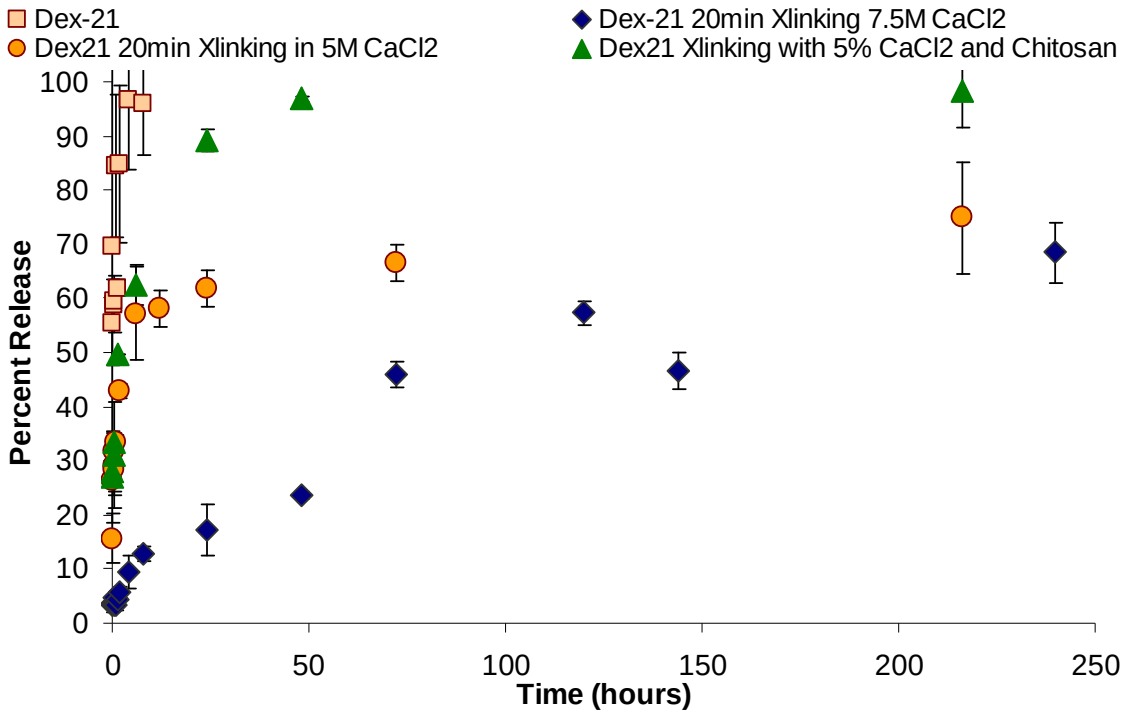

Figure D.12 Ten day release study of dexamethasone from alginate spray dried particles with and without crosslinking.

D.2 Titania Deagglomeration and Particle Sizing

Nanoparticles are sized between 1 and 100 nanometers and form nanopowders from agglomerates of nanoparticles. Nanoparticles are of currently of interest as they bridge molecular structures and bulk materials. Bulk materials usually have constant physical properties, however, nanoparticles are observed to have size dependent properties. Therefore, with the use of nanoparticles, the properties of materials can change. This is due to the higher percentage of atoms on the surface of the material in relation to the atoms found in the bulk material. For bulk materials, of particles larger than a few microns, the percentage of atoms is much less signification in relation to the total atoms in the material. However, there are serious challenges faced in handling and

homogeneous mixing due to high cohesion and tendency to form large, difficult to break agglomerates that form due to strong inter-particle forces. The titania nanoparticles used in this study are produced at the ETH University using flame pyrolysis. The primary particle size formed is around 70 nanometers.

Nanopowders are deagglomerated using a sonic horn in a solvent and the particles are sized. NanoSight LM20 uses ultramicroscopy to count, size, and visualize nanoparticles in a solvent suspension. A laser light is used to illuminate nanoparticles within a few hundred microliters. Nanoparticles are tracked individually and sized based on Brownian motion calculations. Based on preliminary lab work researched by the group, isopropanol is chosen as the solvent. The effects of surfactants are studied in order to ascertain a system which will produce the most stable suspension.

Initial tests are performed on the compatibility of the surfactants with isopropanol. Surfactants are individually added to approximately 5 mL of isopropanol and slightly agitated at room temperature. The systems where the surfactants were soluble in isoproanol are then combined with approximately 2 milligrams of titania are added to each of the systems. Once the titania is added a sonic horn is used at 50% amplitude, a cycle of 100 and a processing time of 20 seconds. The systems are then monitored to see when the titania would precipitate out of solution. Five surfactants kept the titania suspended after 24 hours. These systems were scaled up to 20mL. One gram of titania and 100 mg of surfactant is added to the isopropanol. The surfactant that performs the best with the isopropanol and titania is the Byk 9077 by BYK Additives & Instruments. Byk 9077 is a high molecular weight copolymer with pigment affinic groups. The recommended use of Byk 9077 is 1 – 3 percent of the titania used in the suspensions.

The next step is to optimize the conditions to run the sonic horn. Amplitude and cycling (off – on) are varied and particle size is measured. Titania particle loading of 1% $^{w}/_{v}$ is used with a surfactant concentration of 10% $^{w}/_{w}$. Each experiment was run for 7 minutes and particle size was collected 2, 3, 7 and 10 days after sonication. For the amplitude study, Figure D.13, the cycle is kept at 55%. For the cycle study, Figure D.14, the amplitude remains at 55. Surfactant concentration is examined closer in Figure D.15. The sonic horn is run for 7 minutes, cycle of 55% and amplitude of 55. It is not uncommon to see particle size decrease versus time as larger particles tend to precipitate out of solution and settle to the bottom, leaving the smaller particles still in suspension.

A major problem with the NanoSight is that it only analyzes particles near the surface of the solution. Since smaller particles tend to remain suspended longer, the NanoSight's analysis of particle size will result in a smaller size distribution than the actual result. These results show that the particle size on day 3 tends to be smaller than day 2. Days 7 and 10 tend to have larger particle sizes. The excess amount of surfactant in solution did not provide sufficient benefits in keeping the particle size smaller versus time.

The sonication time is examined next. Based on previous data, a cycle of 70% and amplitude of 70% are chosen because the results showed the most variability making it easier to see trends from the data. The samples are sonicated for 30, 60 and 150 minutes and particle size analysis was collected right after sonication, then on day 1, 2 and 3. Lower sonication times showed more consistency, versus time, in the data than the 150 minute sonication.

The results show that deagglomeration can occur close to the primary particle range, sizes are about twice the size of primary particles; however, the NanoSight is not adequately sufficient to analyze the particles in suspension. Additional particle size analysis should be collected when using a NanoSight to obtain the larger and more accurate particle size distribution.

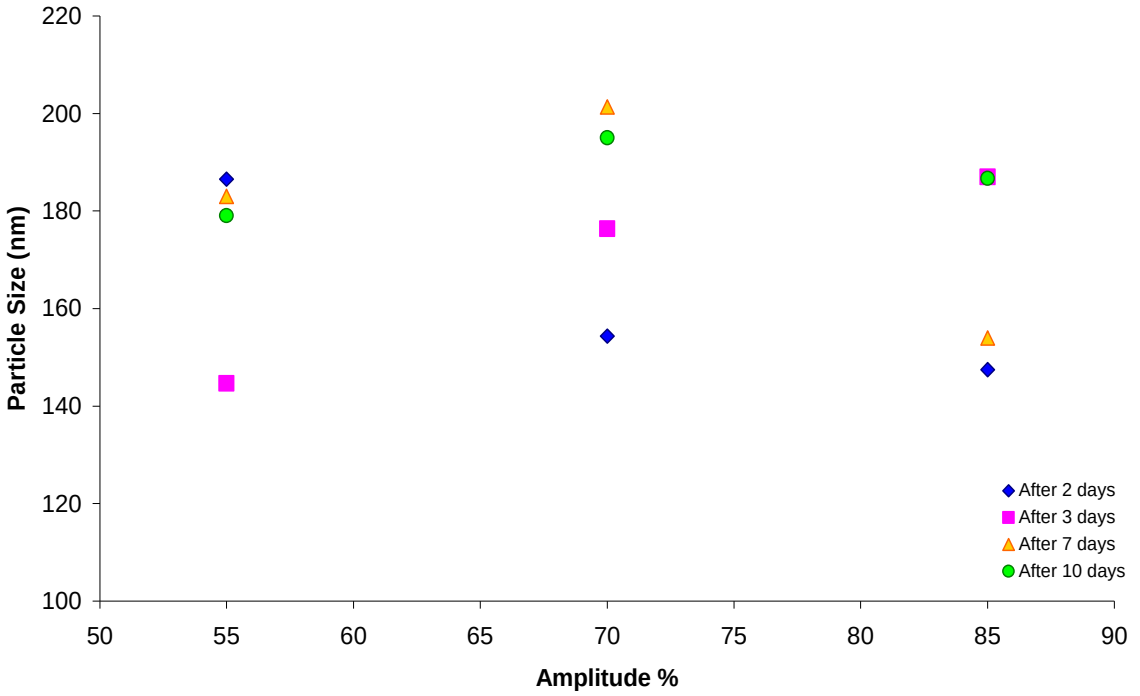

Figure D.13 Titania particle size versus sonication amplitude, collected at different times after sonication.

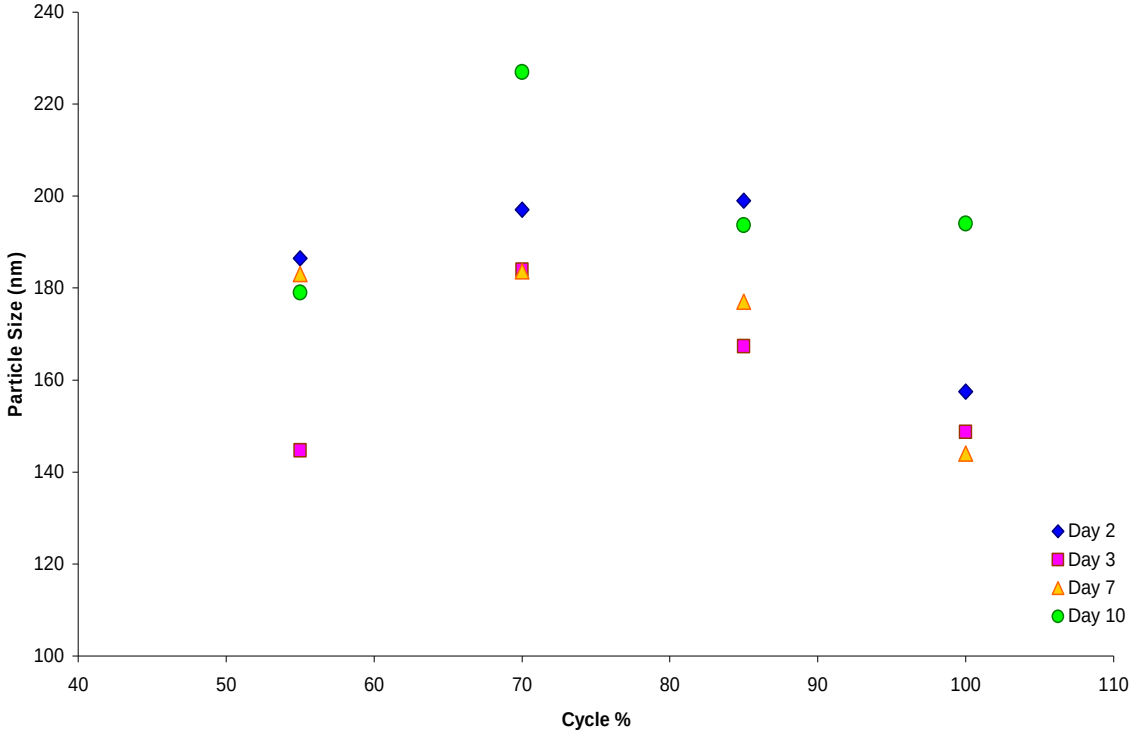

Figure D.14 Titania particle size versus cycling percent, collected at different times after sonication.

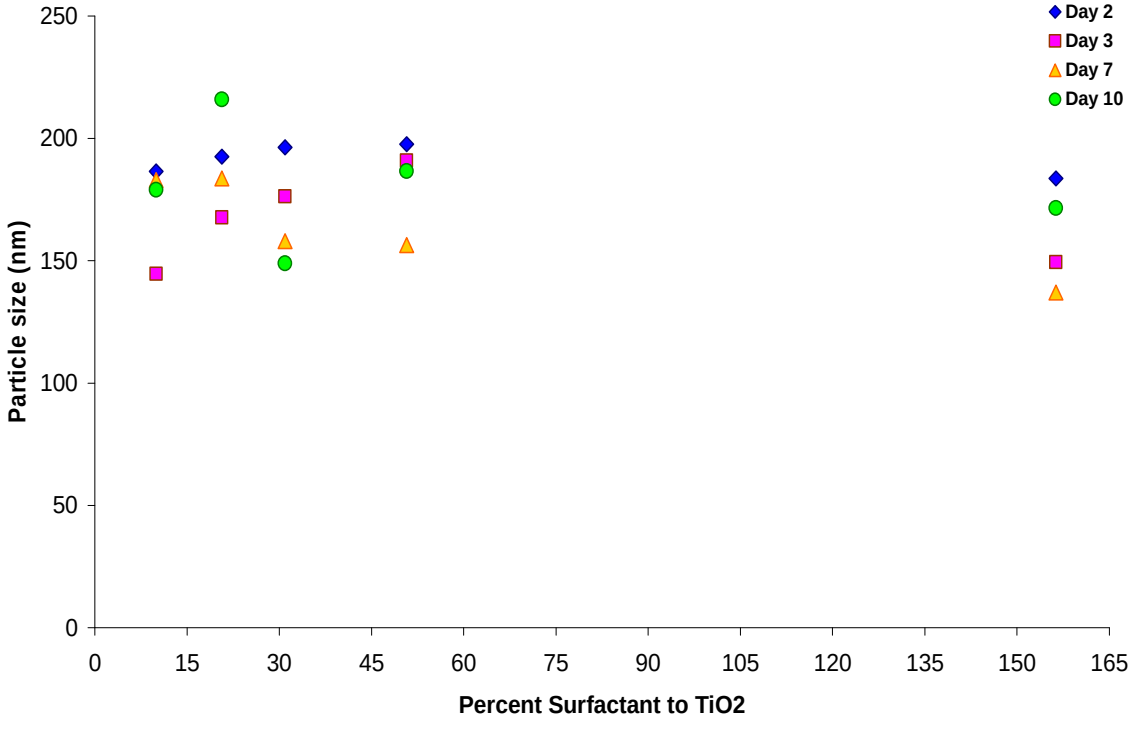

Figure D.15 Titania particle size versus percent surfactant, collected at different times after sonication.

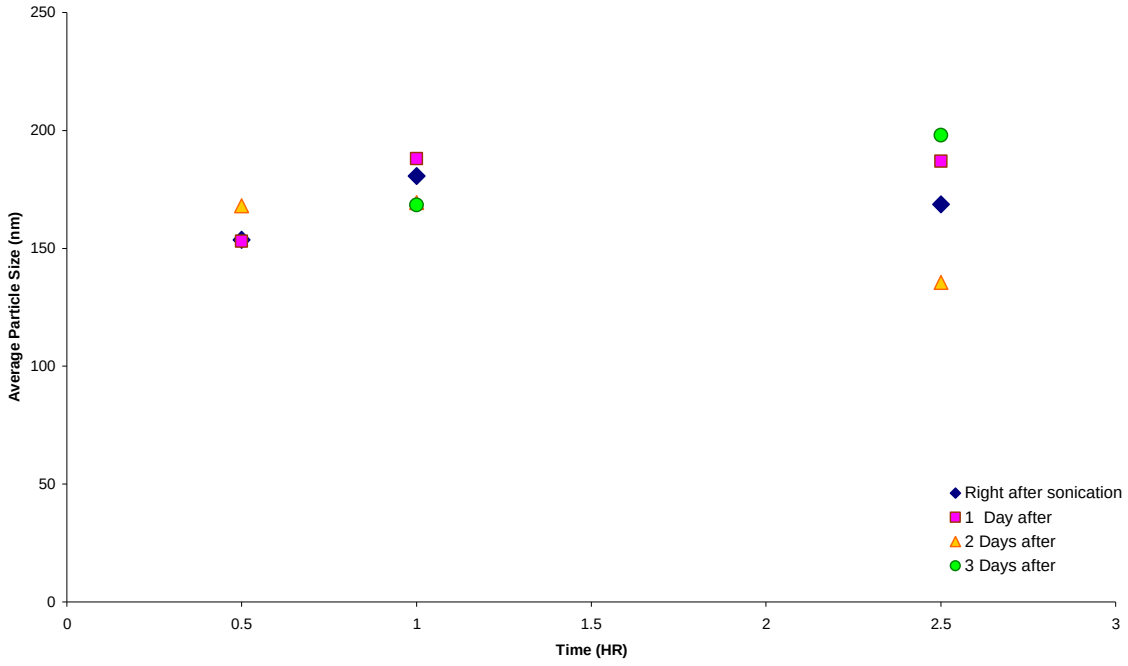

Figure D.16 Titania particle size versus sonication times, collected at different times after sonication.

REFERENCES

[1] Wei D, Dave RN, Pfeffer R. Mixing and characterization of nanosized powders: An assessment of different techniques. Journal of Nanoparticle Research. 2002; 4:21-41.

[2] Yang J, Wang Y, Dave RN, Pfeffer R. Mixing of nano-particles by rapid expansion of high-pressure suspensions. Advanced Powder Technology. 2003;14:471-493.

[3] Berthiaux H, Marikh K, Gatumel C. Continuous mixing of powder mixtures with pharmaceutical process constraints. Chemical Engineering and Processing*:* Process Intensification. 2008;47:2315-2322.

[4] Tallon S, Davies C. In-situ monitoring of axial particle mixing in a rotating drum using bulk density measurements. Powder Technology. 2008;186:22-30.

[5] Doucet J, Hudon N, Bertrand F, Chaouki J. Modeling of the mixing of monodisperse particles using a stationary DEM-based Markov process. Computers and Chemical Engineering. 2008;32:1334-1341.

[6] Lu L, Hsiau H. Mixing in a vibrated granular bed: Diffusive and convective effects. Powder Technology. 2008;184:31-43.

[7] Portillo P, Ierpetritou M, Muzzio F. Characterization of continuous convective powder mixing processes. Powder Technology. 2008;182:368-378.

[8] Hardy E, Hoferer J, Kasper G. The mixing state of fine powders measured by magnetic resonance imaging. Powder Technology. 2007;177:12-22.

[9] Hsiau S, Lu L, Chen J, Yang W. Particle mixing in a sheared granular flow, Int. J. of Multiphase Flow. 2005;31:793-808.

[10] Hogg R. Characterization of relative homogeneity in particulate mixtures. Int. J. Miner. Process. 2003;72:477-487.

[11] Venables H, Wells JI. Powder mixing. Drug Development and Industrial Pharmacy. 2001;27:599-612.

[12] Huang C, Wang Y, Wei F. Solids mixing behavior in a nano-agglomerate fluidized bed. Powder Technology. 2007;179:229-236.

[13] Siegel RW. In: Siegel RW, Hu E. Reco MC eds. Nanostructure Science and Technology: A Worldwide Study. WTEC, Loyola College in Maryland. 1999:1-14.

[14] Roco MC. Nanoparticles and nanotechnology research. Journal of Nanoparticle Res. 1999;1:1-6.

[15] Carter SA, Scott JC, Broack PJ. Enhanced luminance in polymer composite light emitting device, Appl. Phys. Lett. 1997; 71:1145-1147.

[16] Maser WK, Lukyanchuk I, Bernier P, Molini P, Lefrant S, Redlich P, Ajayan PM. Superconducting RNi2B2C (R = Y, Lu) nanoparticles: size effects and weak links Adv. Mater. 1997;9:503-522.

[17] Imanaka N, Kohler J, Toshiyuki M. Inclusions of nanometer-sized Al2O3 particles in a crystalline (Sc,Lu)2(WO4)3 matrix. Journal of Am. Ceram. Soc. 2000;83:427-429.

[18] Lines MG. Nanomaterials for practical functional uses. J Alloys Comp. 2008; 449:242-245.

[19] Steyer P, Mege A, Pech D, Mendibide C, Fontaine J, Pierson J-F, Esnouf C, Goudeau P. Influence of the nanostructuration of PVD hard TiN-based films on the durability of coated steel. Surface and Coating Technology. 2008; 202:2268-2277.

[20] Yu Q, Dave RN, Zhu C, Quevedo JA, Pfeffer R. Enhanced fluidization of nanoparticles in an oscillating magnetic field. *AIChE J*. 2005; 51:1971-1979.

[21] Friedlander SK. Smoke, Dust, and Haze: Fundamentals of Aerosol Dynamics. New York, NY: Oxford University Press, 2000.

[22] Nam CH, Pfeffer R, Dave RN, Sundaresan S. Aerated vibrofluidization of silica nanoparticles. AIChE J. 2004; 50:1776-1785.

[23] Kurkela JA, Brown DP, Raula J, Kauppinen EI. New apparatus for studying powder deagglomeration. Powder Technol. 2008; 180:164-171.

[24] Yao W, Suangsheng G, Fei W, Jun W. Fluidization and agglomerate structure of SiO2 nanoparticles. Powder Technol. 2002; 124:152-159.

[25] Song YS, Youn JR. Influence of dispersion states of carbon nanotubes on physical properties of epoxy nanocomposites. Carbon. 2005; 43:1378-85.

[26] Marioth E, Kroeber H., Loebbecke S, Fuhr I, Krause H. Deagglomeration and mixing of nanoparticles using rapid expansion of supercritical dispersions. PARTEC. 2007; Nuremberg, Germany.

[27] Chen CC, Yu CK. Two-dimensional image characterization of powder mixing and its effects on the solid-state reactions. Mater Chem Phys. 2004; 227-37.

[28] Van der Wel, Peter G.J. Powder Mixing. Powder Handling Process. 1999; 11:83-86.

[29] Peciar M. Mixing of finely powdered materials. Chem. Prum. 1992;42:124-126.

[30] Naganuma N. Mixing powder with liquid. Netsu Shori. 1991; 31:95-99.

[31] Vaizoglu O. Assessment of the degree of mix of powder mixtures. Turk. J. Phys. 1999; 23:97-104.

[32] Kaye BH. Powder Mixing. Powder Technology Series, Chapman & Hall., 1997; 19-35: 77-131.

[33] Laitinen N. and A. M. Juppo. Measurement of pharmaceutical particles using a time-of-flight particle sizer. European Journal of Pharmaceutics and Biopharmaceutics. 2003; 55(1): 93-98.

[34] Reddy V. Getting from wet to dry. Manufacturing Engineering. 1989; 102:83-86.

[35] Paul EL, Midler M, Sun Y. "Mixing in the Fine Chemicals and Pharamcuetical Industries." Handbook of industrial Mixing: Science and Practice. Ed. Edward L. Paul, Victor A. Atiemo-Obeng, and Suzanne M. Kresta. Hoboken: John Wiley & Sons, Inc., 2004. 1027-1069

[36] Baldyga J, Orciuch W, Makowski L, Malik K, Oezcan-Taskin G, Eagles W, et al. Dispersion of nanoparticle clusters in rotor-stator mixer. Ind Eng Chem Res. 2008.

[37] Ding P, Pacek AW. De-agglomeration of silica nanoparticles in the presence of surfactants. J Dispersion Sci Technol. 2008; 29:593-9.

[38] Wengler R, Nirschl H. Turbulent hydrodynamic stress induced dispersion and fragmentation of nanoscale agglomerates. J Colloid Interface Sci. 2007; 306:262-73.

[39] Xie L, Rielly CD, Ozcan-Taskin G. Break-up of nanoparticle agglomerates by hydrodynamically limited processes. J Dispersion Sci Technol. 2008; 29:573-9.

[40] Seekkuarchchi N, Kumazawa H. Aggreagation and disruption mechanisms of nanoparticulate aggregates. 2. Dispersion of aggregates using a motionless mixer. *Ind Eng Chem Res*. 2008; 47:2401-2413.

[41] Aoki M, Ring TA, Haggerty JS. Analysis and modeling of the ultrasonic dispersion technique. Adv Ceram Mater. 1987; 2:209-212.

[42] Ding P, Pacek AW. De-agglomeration of goethite nanoparticles using ultrasonic comminution device. Powder Technol. In Press.

[43] Uhland SA, Cima MJ, Sachs EM. Additive-enhanced redispersion of ceramic agglomerates. J Am Ceram Soc. 2003; 86:1487-1492.

[44] Ding P, Pacek AW. Effect of pH on deagglomeration and rheology/morphology of aqueous suspension of goethite nanopowder. J Colloid Interface Sci. In Press. AQ1

[45] Le Bars N, Levitz P, Messier A, Francois M, Van Damme H. Deagglomeration and dispersion of Barium Titanate and alumina particles in an organic medium. J Colloid Interface *Sci*. 1995; 175: 400-410.

[46] Harnby N. An engineering view of pharmaceutical powder mixing. Pharm Sci Technol Today. 2000; 3:303-9.

[47] Sanganwar GP, Ermoline A, Scicolone JV, Dave RN, Gupta RB. Environmentally Benign Nano-mixing by Sonication in Supercritical CO_2. Journal of Nanoparticle Research. 2009; 11:405-419.

[48] Scicolone J, Sanganwar G, To D, Ermoline A, Dave RN, Gupta RB, Pfeffer R. Deagglomeration and mixing of nanoparticles. Proceedings of PARTEC 2007 Meeting, paper 36218, pp 1-4, Nuremburg, Germany, March 27-29, 2007.

[49] Dave RN, Gupta R, Pfeffer R, Sundaresan S, Tomossone MS. Environmentally Benign Mixing of Nanoparticles. Proceedings of 2008 NSF Engineering Research and Innovation Conference, Knoxville, Tennessee, January 7-9, 2008.

[50] Barrow R, Yang J, Dave RN, Pfeffer R. Dry-mixing of sub-micron B and BaCrO4 particles for use in a time delay composition. SAFE *J*. 2007; 35:7-13, 2007.

[51] Geldart D, Types of gas fluidization. Powder technology. 1973; 7:285-292.

[52] Zhu C, Liu G, Yu Q, Pfeffer R., Dave R., Nam C. Sound assisted fluidization of nanoparticle agglomerates. Powder Technology. 2004; 141:119-123.

[53] Guo Q, Li Y., Wang M, Shen W., Yang C. Fluidization characteristics of SiO2 nanoparticles in an acoustic fluidized bed. Chemical Engineering Technology. 2006; 29:78-86.

[54] Levy EK, Celeste B. Combined effects of mechanical and acoustic vibrations on fluidization of cohesive powders. Powder Technology, 2006; 163:41-50.

[55] Hakim F, Portman JL, Casper M.D., Weimer A.W. Aggregation behavior of nanoparticles in fluidized beds. Powder Technology. 2005; 160:149-160.

[56] Coulaloglou C. (1979). Fluidization of Permanently Magnetic Particle Beds. US Patent 4132005.

[57] Thivel P-X, Gonthier Y, Boldo P, Bernis A. Magnetically stabilized fluidization of a mixture of magnetic and non-magnetic particles in a transverse magnetic field. Powder Technology. 2004; 139 (3), pp. 252-257

[58] Hristov J. Gas Fluidization of Ferromagnetic Granular Materials in an External Magnetic Field, PhD Thesis, UCTM, Sofia, Bulgaria (1994).

[59] Hristov J. Magnetic Field Assisted Fluidization—A Unified Approach. Part 1. Fundamentals and Relevant Hydrodynamics, Rev. Chem. Eng. 18, 295-509 (2002).

[60] Hristov J. Magnetic Field Assisted Fluidization—A Unified Approach. Part 2. Solids Batch Gas-Fluidized Beds: Versions and Rheology, Rev. Chem. Eng. 2003; 19:1-132.

[61] Hristov J. Magnetic Field Assisted Fluidization—A Unified Approach. Part 4. Moving Gas-Fluidized Beds, Rev. Chem. Eng. 2004; 20:377-550.

[62] Hristov J. Magnetic Field Assisted Fluidization: Dimensional Analysis Addressing the Physical Basis, China Particuol. 2007a; 5:103-110.

[63] Hristov J. Magnetic Field Assisted Fluidization—A Unified Approach. Part 6. Topics of Gas-Liquid-Solid Fluidized Bed Hydrodynamics, *Rev. Chem. Eng*. 2007b; 23, 373-526.

[64] Hristov J. Magnetically assisted gas-solid fluidization in a tapered vessel: First report with observations and dimensional analysis. Canadian Journal of Chemical Engineering. 2008; 86: 470 - 492.

[65] Zeng P, Zhou T, Chen G, Zhu Q. Behavior of mixed ZnO and SiO nano-particles in magnetic field assisted fluidization. China Particuology. 2007; 5 (1-2), 169-173.

[66] Lu X, Li H. Fluidization of CaCO and FeO particle mixtures in a transverse rotating magnetic field. Powder Technology. 2000; 107 (1-2), 66-78.

[67] Zhu Q, Li H. Study on magnetic fluidization of group C powders. Powder Technology.1996; 86 (2), 179-185.

[68] Quevedo J. (2004). Fluidization of agglomerates of nanoparticles under different force fields. NJIT Master Thesis.

[69] Hakim LF, Blackson J, George SM, Weimer AW. Nanocoating individual silica nanoparticles by atomic layer deposition in a fluidized bed reactor. Chem Vapor Deposition. 2005;11:420-425.

[70] Mangold H, Kerner D, Kleinschmit P. (1999) Pyrogenic silica, process for the production thereof and use. US Patent 5976480

[71] Goldstein J, Newbury D, Joy D, et al. Scanning Electron Microscopy and X-Ray Microanalysis. 3rd Ed. New York: Springer Science + Business Media, Inc., 2003.

[72] Danckwerts PV. The definition and measurement of some characteristics of mixtures. Appl. Sci. Res. 1952;A3, 279-296.

[73] van Herk D, Castano P, Quaglia M, Kreutzer M, Makkee M, Moulijn J. Avoiding segregation during the loading of a catalyst-inert powder mixture in a packed micro-bed. Applied Catalysis A: General, 2009; 365, 110-121

[74] Rollins D, Faust D, Jabas D. A superior approach to indices in determining mixture segregation. Powder Technology. 1995;84:277-282.

[75] Lee CS, Lee JS, Oh ST. Dispersion control of Fe2O3 nanoparticles using a mixed type of mechanical and ultrasonic milling. Materials Letters. 2003; 57, pp. 2643-2646.

[76] Sato K, Li JG, Kamiya H, Ishigaki T.Ultrasonic dispersion of TiO2 nanoparticles in aqueous suspension. Journal of the American Ceramic Society, 2008; 91, pp. 2481-2487.

[77] Sauter C, Emin MA., Schuchmann HP, Tavman S. Influence of hydrostatic pressure and sound amplitude on the ultrasound induced dispersion and de-agglomeration of nanoparticles Ultrasonics Sonochemistry. 2008; 15, pp. 517-523

[78] Dave RN, Wu C-Y, Chaudhuri B, Watano S. Magnetically mediated flow enhancement for controlled powder discharge of cohesive powders. *Powder Technology*. 2000; 112:111-125.

[79] To D, Yin X, Sundaresan S, Davé RN. Investigation of Nano-particle Aggregate Deagglomeration via the Rapid Expansion of High-Pressure Suspensions in Carbon Dioxide Through an Orifice, *AIChE Journal*, 55 (2009) 2807-2826.

[80] Wang Y, Gu G, Wei F, Wu J. Fluidization and agglomerate structure of SiO2 nanoparticles, Powder Technology. 2002, 124:152-159

[81] Guo Q, Liu H, Shen W, Yan X, Jia R. Influence of sound wave characteristics on fluidization behaviors of ultrafine particles. Chem Eng J. 2006;119:1-9.

[82] Levy E, Celeste B. Combined effects of mechanical and acoustic vibrations on fluidization of cohesive powders. Powder Technol. 2006;163:41-50.

[83] Zhu C, Yu Q, Dave R, Gas fluidization characteristics of nanoparticle agglomerates, AIChE J. 51 (2) (2005) 426-439.

[84] Zhou T, Ge Z, Dave R, et al., Characteristics of non-magnetic cohesive particles by adding coarse magnets in magnetic fluidized beds, Chem. Reaction Eng. Technol. (China) 21 (1) (2005) 22-25.

[85] Quevedo JA, Omosebi A, Pfeffer R. Fluidization Enhancement of Agglomerates of Metal Oxide Nanopowders by Microjets. AIChE, 2010; 56:1456-1468.

[86] Valverde JM, Quintanilla MAS, Castellanos A, Mills P. The Settling of Fine Cohesive Powders, Europhysics Lett. 2001; 54, 3, 329.

[87] Seinfeld JH. Atmospheric Chemistry and Physics of Air Pollution, Wiley, New York. 1986; p. 317.

[88] Park A-H, Bi H, Grace J. Reduction of electrostatic charges in gas-solid fluidized beds. Chem. Eng. *Sci.* 2002; 57, 153-162.

[89] Mehrani P, Bi HT, Grace J. Electrostatic charge generation in gas-solid fluidized beds. J. Electrostatics 2005; 63, 165-173.

[90] Quevedo J, Pfeffer R. In Situ Measurements of Gas Fluidized Nanoagglomerates. Ind. Eng. Chem. Res. 2010; 49, 5263-5269.

[91] Elversson J, Millqvist-Fureby A, In situ coating - An approach for particle modification and encapsulation of proteins during spray drying. International Journal of Pharmaceutics. 2006; 323, 1-2, 12, p52-63.

[92] Vega-Mercado H, Góngora-Nieto MM, Barbosa-Cánovas GV. Advances in dehydration of foods. Journal of Food Engineering. 2001; 49, 4, p271-289.

[93] Takeuchi H, Yasuji T, Yamamoto H. Spray-dried lactose composite particles containing an ion complex of alginate-chitosan for designing a dry-coated tablet having a time-controlled releasing function. Pharmaceutical Research. 2002; 17, pp. 94-99.

[94] Mi FL, Sung HW, Shyu SS, Drug release from chitosan-alginate complex beads reinforced by a naturally-occuring cross-linking agent. Carbohydrate Polymer. 2002; 48, pp. 61-72.

[95] Coppi G, Iannuccelli V, Leo E, Bernabei MT, Cameroni R. Chitosan-alginate microparticles as a protein carrier Drug Development and Industrial Pharmacy. 2001; 27 (5), pp. 393-400.

[96] Coppi, G, Iannuccelli, V. Alginate/chitosan microparticles for tamoxifen delivery to the lymphatic system. International Journal of Pharmaceutics. 2009; 367 (1-2), pp. 127-132.

[97] Chen SC, Wu YC, Mi FL, Lin YH, Yu LC, Sung HW. A novel pH-sensitive hydrogel composed of *N*,*O*-carboxymethyl chitosan and alginate cross-linked by genipin for protein drug delivery, J. Control. Release 2004; 96, pp. 285-300

[98] Wan LS, Heng PW and Chan LW. Drug encapsulation in alginate microspheres by emulsification. J. Microencapsulation 1992; 9, pp. 309-31C.

[99] Xu Y, Zhan C, Fan L, Wang L, Zheng H. Preparation of dual crosslinked alginate-chitosan blend gel beads and in vitro controlled release in oral site-specific drug delivery system, Int J Pharm 2007; 336, pp. 329-337.

[100] George M, Abraham TE. Polyionic hydrocolloids for the intestinal delivery of protein drugs: alginate and chitosan, J Controlled Release 2006; 114, pp. 1-14.